

2023-07

Spatial, temporal, and circuit-specific activation patterns of basolateral amygdala projection neurons during stress

Aukema, Robert

Aukema, R. (2023). Spatial, temporal, and circuit-specific activation patterns of basolateral amygdala projection neurons during stress (Doctoral thesis, University of Calgary, Calgary, Canada). Retrieved from <https://prism.ucalgary.ca>.

<https://hdl.handle.net/1880/116771>

Downloaded from PRISM Repository, University of Calgary

UNIVERSITY OF CALGARY

Spatial, temporal, and circuit-specific activation patterns of basolateral amygdala
projection neurons during stress

by

Robert Aukema

A THESIS

SUBMITTED TO THE FACULTY OF GRADUATE STUDIES
IN PARTIAL FULFILMENT OF THE REQUIREMENTS FOR THE
DEGREE OF DOCTOR OF PHILOSOPHY

GRADUATE PROGRAM IN NEUROSCIENCE

CALGARY, ALBERTA

JULY, 2023

© Robert Aukema 2023

Thesis Abstract

In humans and rodents, the amygdala is rapidly activated by stress and hyperactivated in conditions of pathological stress or trauma. However, there is a striking lack of information of the anatomical specificity of amygdala subregions and circuits explicitly activated by stress, and of its role in governing typical responses to stress such as hypothalamic-pituitary-adrenal (HPA) axis activation. The overarching aim of this thesis was to conduct a systematic investigation of the spatial, temporal, and circuit-specific activation patterns of basolateral amygdala (BLA) projection neurons during exposure to acute stress. Additionally, we explicitly tested the role of the BLA in activation of the HPA axis, as this remains a poorly understood process. *Chapter 1* describes how the BLA is anatomically well-situated for cognitive evaluation of emotional stimuli and describes the role of the BLA in diverse behavioural and physiological processes via efferent projections to many different brain structures. *Chapter 2* identifies a common BLA subregion that is responsive to stressful stimuli, albeit with distinct temporal activation patterns, and which bidirectionally influences HPA axis activity. *Chapter 3* maps the topographical distribution of six different populations of projection neurons throughout the BLA, and demonstrates that, although widely activated by stress exposure, inhibition of isolated populations does not influence HPA axis activity. *Chapter 4* investigates the topographical distribution and stress-induced activation of BLA neurons expressing corticotropin-releasing hormone receptor type I (CRHR1), which, just like discrete circuits, does not influence HPA axis activity on its own. Together, this emphasizes the heterogeneity of BLA projection populations, while providing evidence that a large, diverse population of BLA projection neurons are activated by exposure to acute psychological stress.

Preface

This thesis contains three manuscripts in preparation. None are currently published.

Research done in *Chapter 2, 3, and 4* were conducted in the Hill lab at the University of Calgary, and in accordance with the approved animal protocols (AC20-0090).

1. Robert J Aukema, Gavin N Petrie, Benjamin K Lau, Samantha L Baglot, Lauren T Seabrook, Leo Molina, Tamás Füzesi, Sandra Kadhim, Andrei S Nastase, Morena M, Jaideep S Bains, Stephanie L Borgland, Matthew N Hill. "Identification of a stress-integratory subregion of the basolateral amygdala". *2023, in preparation – Chapter 2.*

RA designed and conducted experiments, analyzed data, prepared figures, and wrote the manuscript. GP designed and conducted experiments and reviewed the manuscript. BL and LS designed and conducted electrophysiology experiments and LS reviewed the manuscript. LM developed photometry analysis tools and reviewed the manuscript. TF developed optogenetic and photometry analysis tools. SL Baglot, MM, SK, and AS conducted experiments. SL Borgland and JB provided advice. MNH developed and supervised the project and wrote the manuscript.

2. Robert J Aukema, Gavin N Petrie, Lauren T Seabrook, Benjamin K Lau, Maria Morena, Jaideep S Bains, Stephanie L Borgland, Matthew N Hill. "Topographical distribution and projection-specific activation of basolateral amygdala projection neurons". *2023, in preparation – Chapter 3.*

RA designed and conducted experiments, analyzed data, prepared figures, and wrote the manuscript. GP conducted experiments. LS designed and conducted electrophysiology experiments and reviewed the manuscript. BL designed and conducted electrophysiology experiments. MM conducted experiments and provided advice. JC provided viral construct. JB and SB provided advice. MNH developed and supervised the project and wrote the manuscript.

3. Robert J Aukema, Andrei S Nastase, Gavin N Petrie, Samantha L Baglot, Nick Gilpin, Matthew N Hill. "Topographical and circuit-specific characterization of corticotropin-releasing hormone receptor type I -expressing neurons in the basolateral amygdala during stress. 2023, *in preparation – Chapter 4*.

RJA designed and conducted experiments, analyzed data, prepared figures, and wrote the manuscript. ANS designed, conducted, and analyzed experiments. GNP conducted experiments. SB conducted experiments and provided technical advice. NG provided animals and technical advice. MNH developed and supervised the project and wrote the manuscript.

Thesis Acknowledgements

This work was completed on Traditional Territories of the people of the Treaty 7 Region in Southern Alberta, which includes the Blackfoot Confederacy (including the Siksika, Piikuni, Kainai First Nations), the Tsuut'ina and the Stoney Nakoda (including the Chiniki, Bearspaw, and Wesley First Nations). The City of Calgary is also home to Metis Nation Alberta, Region III. As a settler and guest to the Southern Alberta Traditional Territories I have directly benefited from being on this land as it is where I have pursued my PhD. It is also where I have lived, worked, and played the past six years, and for which I am grateful.

Work in this thesis would be impossible without the technical expertise from Hotchkiss Brain Institute (HBI) core facilities. I want to thank the ARC staff for taking care of the animals used in this research, particularly Brittany Munro, Krista Jensen, Vince, Onilea, and Mario; I want to thank Frank Visser from the HBI Molecular Core for providing expertise in genotyping tissue; I want to thank Vincent Ebacher, Kelvin Poon, and David Elliott from the HBI Advanced Microscopy Platform for providing expertise in imaging and analyses; and I want to acknowledge the expertise and help from the CSM Optogenetics Platform - I greatly admire the incredible expertise of Tamás Füzési and Leo Molina and their constant willingness to help.

I am incredibly grateful to come to work every day in a lab environment that surrounds me with such collaborative, supportive, fun, and intelligent people. Many of these experiments could not have been done without their advice and expertise, and their constant support has been essential in managing the highs and lows of science. As such, I would like to thank all current and former Hill Lab members: Cat Hume, Gavin Petrie, Georgia Balsevich, Haley Vecchiarelli, Jess Scheufen, Maria Morena, Martin Sticht, Min Qiao, Sabin Nastase, Sam Baglot, Sandra Kadhim,

and Savannah Lightfoot. I will miss our frequent lunches together as a lab. I want to especially thank my supervisor Matt Hill, whose unwavering support, encouragement, and guidance has helped me maintain excitement for science despite countless experiments that did not get the result we hoped. You have taught me so much and I have seen the growth of myself as a scientist from your influence, to which I am deeply grateful.

The HBI is filled with many impressive and supportive trainees, post-docs, staff, and faculty members, both as scientists and individuals. I want to specifically acknowledge Benjamin Lau for his critical thinking towards my project and his passion for science; Laurie Wallace for all her immunohistochemistry advice and unrelenting positivity; Abhi Kumar for his stability as the most easy-going roommate one could ever ask for; Dion Kelly for giving me a place to live in a pinch as I wrote my thesis; and my committee members Jaideep Bains and Stephanie Borgland for their insightful feedback and interest in my project. I also want to acknowledge Gavin Petrie; I can't picture a more supportive person to have "grown up" in grad school with, and who has spent countless hours reading drafts of grant proposals and debating science as well as distract me from the lows of grad school.

Finally, I want to acknowledge my dad for always giving me the freedom and support to pursue whatever I am passionate about, and I want to thank Lauren Seabrook for her endless support and stability throughout the unpredictability of grad school, who has always expressed excitement for my projects, kept life's challenges in perspective, and edited almost every section of this thesis.

Table of Contents

<i>Thesis Abstract.....</i>	<i>II</i>
<i>Preface</i>	<i>III</i>
<i>Thesis Acknowledgements.....</i>	<i>V</i>
<i>List of Tables.....</i>	<i>X</i>
<i>List of Figures.....</i>	<i>XI</i>
MAIN FIGURES.....	XI
SUPPLEMENTARY FIGURES.....	XI
<i>List of Abbreviations.....</i>	<i>XII</i>
<i>Chapter 1. Introduction.....</i>	<i>1</i>
1.1 THE STRESS RESPONSE: ADAPTIVE ROLE AND UNDERLYING CIRCUITRY	1
1.2 ANATOMY OF THE BASOLATERAL AMYGDALA	3
1.3 ROLE OF THE BASOLATERAL AMYGDALA IN THE STRESS RESPONSE	9
1.4 ROLE OF EFFECTOR REGIONS IN STRESS.....	13
1.5 ROLE OF DISCRETE BASOLATERAL AMYGDALA PROJECTION NEURON POPULATIONS	17
1.6 MOLECULAR AND RECEPTOR IDENTITY OF BLA PROJECTION NEURONS.....	19
1.7 CONCLUSIONS	21
1.8 THESIS OBJECTIVES AND HYPOTHESES.....	22
<i>Chapter 2. Identification of a stress-integratory subregion of the basolateral amygdala.....</i>	<i>24</i>
2.1 ABSTRACT	24
2.2 INTRODUCTION	24
2.3 METHODS	27
Stereotaxic surgery.	27
Blood collection and corticosterone analysis.....	28
Brain collection.	28
FOS immunohistochemistry	29
Histology	29
Electrophysiology.....	30
Exposure to novel stimuli.....	31
Topographical mapping and quantification of FOS+ cells.....	33
Fiber photometry.....	35
Chemogenetic inhibition.....	41
Optogenetic stimulation.....	42
Statistics.....	45
2.4 RESULTS	46

Aversive stimuli induce a common spatial activation pattern in the basolateral amygdala	46
Distinct novel stimuli elicit distinct temporal patterns of activation in the medial basal amygdala.....	49
Systemic administration of propranolol blunts stress-induced response of BLA projection neurons.....	53
mBA projection neurons bidirectionally influence corticosterone release.....	55
2.5 DISCUSSION	60
2.6 ACKNOWLEDGEMENTS	66
2.7 FUNDING.....	66
2.8 AUTHOR CONTRIBUTIONS	67
2.9 SUPPLEMENTARY FIGURES.....	68
<i>Chapter 3. Topographical distribution and projection-specific activation of basolateral amygdala projection neurons.....</i>	<i>77</i>
3.1 ABSTRACT	77
3.2 INTRODUCTION	78
3.3 METHODS	80
Animals.....	80
Blood collection and corticosterone analysis	80
Brain collection.....	80
FOS immunohistochemistry	81
Stereotaxic surgery	81
Anterograde tracing	82
Optogenetic stimulation	83
Retrograde tracing and colocalization with FOS	85
Electrophysiology.....	88
Projection-specific chemogenetic inhibition	89
Statistics.....	92
3.4 RESULTS.	93
BLA projection neurons innervate a wide range of downstream targets.....	93
Optogenetic stimulation of BLA projection neurons leads to activation of downstream brain regions.....	94
Topographical distribution of BLA projection neurons.....	97
BLA projection populations are broadly activated by stress and with a common bias towards the medial basal amygdala	102
Individual effect of BLA projection populations on stress-induced CORT release	106
3.5 DISCUSSION	111
3.6 ACKNOWLEDGEMENTS	119
3.7 FUNDING.....	119
3.8 AUTHOR CONTRIBUTIONS	119
<i>Chapter 4. Topographical and circuit-specific characterization of corticotropin-releasing hormone receptor type I-expressing neurons in the basolateral amygdala.....</i>	<i>121</i>

4.1 ABSTRACT	121
4.2 INTRODUCTION	121
4.3 MATERIALS AND METHODS	124
Animals.....	124
Genotyping	124
Brain collection.....	125
Tilescan imaging for topographical mapping.....	126
Topographical mapping and quantification of CRHR1+ cells	126
Stereotaxic surgery	128
Retrograde Tracing with cholera toxin subunit B.....	129
Restraint Stress	129
Histology	129
Confocal imaging for colocalization of CTB-488, FOS, and tdTomato.....	130
Analysis of CTB-488, FOS, and tdTomato	130
Chemogenetic inhibition	131
4.4 RESULTS	135
Topographical distribution of CRHR1 neurons in the basolateral amygdala.....	135
CRHR1 and BLA-NAc neurons are activated by restraint stress	139
Functional contribution of BLA:CRHR1 neurons	144
4.5 DISCUSSION	149
4.6 ACKNOWLEDGEMENTS	154
4.7 FUNDING.....	155
4.8 AUTHOR CONTRIBUTIONS	155
4.9 SUPPLEMENTARY DATA.....	156
<i>Chapter 5. Discussion</i>	<i>157</i>
5.1 SUMMARY OF MAIN FINDINGS.....	157
5.2 MODELS OF ACUTE STRESS.	159
5.3 FOS MAPPING.....	161
5.4 FIBER PHOTOMETRY.	164
5.5 DREADDS AND OPTOGENETICS.	166
5.6 ANATOMICAL MAPPING OF PROJECTION POPULATIONS AND CRHR1+ CELLS	170
5.7 SEX AS A BIOLOGICAL VARIABLE.....	174
5.8 FUTURE DIRECTIONS AND CONCLUSION	175
<i>References.....</i>	<i>179</i>

List of Tables

Supplementary Table 2.1 – Standardized Dimensions.....	34
Table 3.1 – BLA Projection Targets.....	93
Table 3.2 – Regional distribution of projection populations.....	102
Supplementary Table 4.1 – Standardized Dimensions.....	127

List of Figures

MAIN FIGURES

Figure 2.1 – Aversive stimuli induce a common spatial pattern in the basolateral amygdala.....	47
Figure 2.2 – Distinct novel stimuli elicit distinct temporal patterns of activation in the mBA.....	51
Figure 2.3 – Propranolol reduces stress-induced activation of BLA.....	55
Figure 2.4 – BLA projection neurons bidirectionally influence HPA activation and corticosterone release.....	58
Figure 3.1 – BLA projection neurons innervate a wide range of downstream targets.....	94
Figure 3.2 – Optogenetic stimulation of BLA projection neurons leads to activation in downstream brain regions.....	96
Figure 3.3 – Topographical distribution of BLA projection neurons.....	99
Figure 3.4 – BLA projection populations are broadly activated by stress and with a common bias towards the medial basal amygdala.....	104
Figure 3.5 – Individual effect of BLA projection populations on stress-induced CORT release....	110
Figure 4.1 – Topographical distribution of CRHR1 neurons in the basolateral amygdala.....	137
Figure 4.2 – CRHR1 and BLA-NAc projection neurons are activated by stress.....	141
Figure 4.3 – Functional contribution of BLA:CRHR1 neurons.....	146
Figure 5.1 – Summary.....	176

SUPPLEMENTARY FIGURES

Supplementary 2.1 – Methods & Rostral-caudal distribution of BLA FOS expression.....	68
Supplementary 2.2 – BLA response to stimulus termination & overview of experimental procedures.....	71
Supplementary 2.3 – Systemic administration of propranolol prior to stress.....	73
Supplementary 2.4 – In vivo and in vitro validation of hM4Di.....	74
Supplementary 4.1.....	156

List of Abbreviations

AAV adeno-associated virus
aBST bed nucleus of the stria terminalis, anterior subdivision
AChE acetylcholinesterase
ACSF artificial cerebrospinal fluid
ANOVA analysis of variance
AP anterior-posterior
AUC area-under-the-curve
BA basal amygdala
BLA basolateral amygdala
BLA basolateral amygdala
BST bed nucleus of the stria terminalis
Ca²⁺ calcium
CaMKIIa calcium/calmodulin-dependent protein kinase II
CeA central amygdala
CNO clozapine-n-oxide
CNO.2HCl clozapine-n-oxide dihydrochloride
CORT corticosterone
CRE cre recombinase enzyme
CRH corticotropin-releasing hormone
CRHR1 corticotropin-releasing hormone receptor type I
DMSO dimethyl sulfoxide
DREADD designer receptor exclusively activated by a designer drug
DV dorsal-ventral
eCB endocannabinoid
GABA gamma-aminobutyric acid receptor A
GABAA gamma-aminobutyric acid receptor A
Gi inhibitory G alpha protein subunit
HBI Hotchkiss Brain Institute
HPA hypothalamic-pituitary-adrenal
i.p. intraperitoneal
kg kilogram
LA lateral amygdala
LAv ventral lateral amygdala
LED light-emitting diode
LH lateral hypothalamus
mBA medial basal amygdala
mg milligram
ML medial-lateral
ml millilitre
ms millisecond
NAc nucleus accumbens
NE norepinephrine
nm nanometer
PBS phosphate buffered saline
Ppp1r1b protein phosphatase 1 regulatory inhibitor subunit 1B
PrL prelimbic cortex
PROP propranolol
PVN paraventricular nucleus of the hypothalamus
Rspo2 R-spondin 2
RM repeated measures

SAM sympatho-adreno-medullary
um micron
VEH vehicle
VH ventral hippocampus

Chapter 1. Introduction

1.1 THE STRESS RESPONSE: ADAPTIVE ROLE AND UNDERLYING CIRCUITRY

In response to a real or perceived threat, the body mounts a collective stress response (Schneiderman et al., 2005). This involves multiple behavioural and physiological processes intended to promote short-term survival needs and prepare for subsequent challenges. Increased arousal facilitates the identification of incoming threat and promotes consolidation of emotionally salient memories (Schwabe et al., 2022), mobilization of energy stores prepares for anticipated energetic demand (Rabasa & Dickson, 2016), increased sympathetic tone supports cardiovascular requirements necessary for confrontation or escape (Ulrich-Lai & Herman, 2009), and generation of defensive or avoidance behaviours minimize the likelihood of physically encountering the threat at hand (Mobbs et al., 2020). This is a complex and widely encompassing biological process and as such, the stress response involves activation and coordination of many different brain regions.

All stressors lead to activation of the major neuroendocrine and sympathetic systems, the hypothalamic-pituitary-adrenal (HPA) and sympatho-adreno-medullary (SAM) axes, respectively. The mediators of the stress response include the effector molecules corticosterone (CORT), corticotropin-releasing hormone (CRH), and norepinephrine (NE) (Ulrich-Lai & Herman, 2009). Activation of these biological axes, however, can be initiated through convergence of differential brain circuits governing these responses, as different stressors represent unique challenges and are thus identified and interpreted by discrete neural pathways. Indeed, distinct stressors can produce activation of very different patterns of brain regions (Emmert & Herman, 1999; Herman et al., 2003), which has led to two broad classifications of stressors: physiological and psychological (Herman & Cullinan, 1997).

Physiological stressors involve very real and immediate homeostatic challenges such as pain, inflammation, or alterations in fluid volume or osmolality, and directly activate the HPA axis, typically through hindbrain or local hypothalamic circuits sensitive to alterations in internal physiological states. In contrast, psychological stressors are stimuli or environments that predict the *potential* for threat (Herman et al., 2003, 2016). This includes environments that are uncertain due to their novelty, unpredictability, or that have previously been paired or are predictive of harm (i.e., through classical conditioning). As such, psychological stressors involve much greater cognitive evaluation of stimuli via processing within corticolimbic circuits prior to activation of the HPA axis.

Many brain regions classically involved in motivation are critical for the response to psychological stressors, including the prefrontal cortex, ventral hippocampus, amygdala, and nucleus accumbens (Daviu et al., 2019; Herman et al., 2003; McEwen, 2007). However, despite this understanding, stress-related psychiatric disorders remain highly prevalent, debilitating, and often resistant to treatment (Calhoun & Tye, 2015), and few pharmacological targets have successfully been translated to human treatment (Griebel & Holmes, 2013). One critical gap in our understanding is the underlying circuits (Griebel & Holmes, 2013) and cell types (McCullough, Morrison, et al., 2016) driving stress-related behaviour, and specifically the stress response. Recent technological advances have since allowed for real-time imaging and manipulation of discrete cell types and circuits through the use of fiber photometry (Gunaydin et al., 2014), optogenetics (Boyden et al., 2005), and chemogenetics (Armbruster et al., 2007). Likewise, innovation and refinement in anatomical techniques has increased precision in mapping cells based on their projection target (Beyeler et al., 2018) or molecular phenotype (O'Leary et al., 2020). As such, the resolution we can identify, characterize, and manipulate circuits activated during stress has dramatically improved in recent years

This thesis is particularly focused on the basolateral amygdala (BLA). The BLA is reliably activated by psychological stress in both humans and rodents (Ipser et al., 2013; Reznikov et al., 2008; van Marle et al., 2009), and amygdala hyperactivity has been implicated in stress disorders such as post-traumatic stress disorder and generalized anxiety disorder (K. S. Blair et al., 2016; Engel et al., 2009; Etkin & Wager, 2007; Rauch et al., 2000). Additionally, symptoms of post-traumatic stress disorder correlate with amygdala activity in emotional memory tasks, suggesting that attenuated amygdala activity during remission may act as a functional marker of current symptom severity (Dickie et al., 2011). The BLA is well-positioned anatomically for cognitive evaluation of psychological stress; it receives sensory inputs from all modalities, which it can then integrate with cognitive information encoding memory and motivational drive (Sah, Faber, Lopez De Armentia, et al., 2003). The BLA then targets many structures capable of affecting diverse behavioural and physiological outcomes. That being said, the BLA is clearly not a unitary structure as pharmacological, optogenetic, chemogenetic, and lesion experiments in the BLA suggest that discrete circuits or cell types exert diverse – and sometimes opposing – influences (Janak & Tye, 2015). Collectively, this emphasizes the importance in clearly identifying BLA cell types and circuits activated by stress and characterizing how individual circuits may contribute to the stress response.

1.2 ANATOMY OF THE BASOLATERAL AMYGDALA

Structure. The BLA is bound by two major fiber tracts medially and laterally, and can be broadly divided into two major regions largely based on acetylcholinesterase (AChE) staining: the dorsally-located lateral amygdala (LA), which only mildly stains for AChE, and the ventrally-located basal amygdala (BA), which has comparatively rich AChE staining (Girgis, 1980). We have further subdivided the BA into medial (mBA) and lateral (LBA) subregions, as has been done

recently by others for anatomical mapping (Beyeler et al., 2018). The mBA largely corresponds with the magnocellular (often referred to as “anterior”) and intermediate subregions of the basolateral nucleus, and the LBA largely corresponds with the parvicellular (“posterior”) subregion of the basolateral nucleus, as described by Savander *et al.* (1995) and Paxinos & Watson (2007).

Cell types. The BLA is predominantly comprised (70-80%) of excitatory, glutamatergic projection neurons (McDonald, 1982; Millhouse & DeOlmos, 1983). Although this is consistent across the entire structure, there are subtle differences throughout, with the largest pyramidal cells (regarding size of soma, thickness of dendrites, and extent of dendritic branching) located in the rostral BA, and the smallest pyramidal cells located in the LA (J. Kim et al., 2016; Millhouse & DeOlmos, 1983). These neurons resemble cortical projection neurons, with similar morphology and use of glutamate as a neurotransmitter (Carlsen & Heimer, 1988; McDonald et al., 1989; Sah, Faber, Armentia, et al., 2003), although organization is not columnar and layered like the cortex (Nikolenko et al., 2020). Many projection neurons target extra-amygdala structures, although substantial collateralization is often observed locally (Sah, Faber, Armentia, et al., 2003; Y. Smith & Paré, 1994), and a large number of projection neurons in the LA send direct projections to the BA (Krettek & Price, 1978). Although dendritic branching is extensive throughout individual subregions of the BLA, there is little spread into adjacent (extra-BLA) brain structures at the ventral, medial, and lateral borders (McDonald, 1984). Perhaps more notably, there is little dendritic branching between the LA and BA, further supporting clear delineation between these two regions; although, it should be noted there is substantial overlap between medial and lateral areas of the BA (McDonald, 1984).

The remaining neurons in the BLA (20-30%) are a wide range of GABAergic, local circuit interneurons that act to tightly constrain activity of nearby projection neurons (Krabbe et al., 2018; Woodruff & Sah, 2007). Unlike our rather homogenous understanding of projection neurons in

the BLA, there is substantial and well-documented diversity of interneurons in the BLA (Hájos, 2021), including differences in local connectivity, molecular expression, and functional role (Katona et al., 2001; Krabbe et al., 2018; Muller et al., 2003).

Inputs. The BLA receives abundant and heterogenous inputs from diverse brain structures, and inputs can be broadly classified into five major groups: sensory, integrative, contextual, neuromodulatory, and miscellaneous (L. Huang et al., 2021). The majority of sensory input arrives into the LA, while integrative, contextual, and neuromodulatory inputs preferentially target the BA (LeDoux, 2007)

The BLA receives **sensory input** from all modalities (Sah, Faber, Lopez De Armentia, et al., 2003), with the majority of sensory input entering the LA where it then gets relayed to other amygdala subregions (Pitkänen et al., 1997). Olfactory inputs arrive at a relatively early stage of cortical processing, such as from the piriform cortex, while the majority of other sensory inputs arrive at a relatively later stage (McDonald, 1998) from regions such as the posterior internuclear nucleus, insular cortex, perirhinal cortex, parabrachial nucleus, infralimbic cortex, and various thalamic nuclei (McDonald, 1998; Sah, Faber, Lopez De Armentia, et al., 2003). As such, the LA is classically considered the “sensory interface” of the amygdala (LeDoux et al., 1990). In contrast to the closely connected central amygdala, the BLA receives minimal physiological inputs from the hypothalamus and brainstem (Herman et al., 2003; Sah, Faber, Lopez De Armentia, et al., 2003), and thus it is not surprising that it is particularly attuned to psychological rather than physiological stressors.

The basal amygdala and ventral regions of the LA (LAv) receives more complex, polymodal inputs conveying **integrative and contextual information**, such as those arising from regions such as the prefrontal cortex, entorhinal cortex, hippocampus, perirhinal cortex, and infralimbic cortex (Bloodgood et al., 2018; Canteras & Swanson, 1992; L. Huang et al., 2021;

McDonald et al., 1996; McDonald, 1998; McDonald & Mascagni, 1997; Sah, Faber, Lopez De Armentia, et al., 2003; Shi & Cassell, 1999). Many of these regions are implicated in memory processing and may thus be critical in retrieving contextual information (L. Huang et al., 2021). While there is a relatively clear separation between the organization of LA and BA inputs, many structures broadly target both the mBA and LBA subdivisions of the BA, including the orbitofrontal cortex and piriform cortex (McDonald, 1998). However, the LBA receives a preferentially strong input from the insular cortex and dorsolateral entorhinal cortex (McDonald, 1998), and the mBA receives stronger inputs from temporal association areas, hippocampal CA1 region, ventral subiculum, ventrolateral entorhinal cortex, prelimbic cortex and anterior cingulate cortex (McDonald, 1998).

The densest ***neuromodulatory inputs*** to the BLA are from cholinergic projections from the basal forebrain (Wilson & Fadel, 2017), primarily targeting the entire basal subregion (Muller et al., 2011). However, although there is moderate to dense inputs throughout the entire BLA, the dorsal raphe nucleus (Asan et al., 2013), and ventral tegmental area and substantia nigra (Asan, 1997; Pinard et al., 2008; Taylor et al., 2014) especially target the LBA. Precise anatomical tracing of BLA inputs has been less described for other modulatory structures such as the locus coeruleus (Fallon et al., 1978; McCall et al., 2017).

Intra-amygdala signaling. The BLA involves strong intra-amygdala connectivity. Short, excitatory projections allow for substantial and repeated modulation of information from other inputs as information flows within and across different subregions (Pitkänen et al., 1997). Encoding generally follows a dorsal-to-ventral pattern from the LA to BA (LeDoux, 2007), although there is some evidence of axons projecting from the BA back to the LA (Savander et al., 1997). Within the BA, there is widespread connectivity between the medial and lateral aspects (Savander

et al., 1995). Most apical dendrites of projection neurons face rostrally (McDonald, 1984), suggesting a rostral-to-caudal flow, and perhaps separation (or gradient) of information.

In addition, a heterogeneous population of GABAergic, local interneurons are widely distributed throughout the BLA, acting to tightly constrain activity of nearby projection neurons (Krabbe et al., 2018; Woodruff & Sah, 2007). Activity of interneurons is heavily regulated via inputs from the medial prefrontal cortex (Hájos, 2021), local interneurons (Muller et al., 2005), or collaterals from neighbouring BLA projection neurons (Beyeler et al., 2018), and can therefore strongly influence BLA output (Wolff et al., 2014). Notably, dense clusters of GABAergic neurons surround the BLA in the intercalated cell masses; the lateral cluster gates flow into the BLA (Krabbe et al., 2018), while the medial cluster plays an important role in gating out-flow to the CeA (Asede et al., 2015; Ehrlich et al., 2009).

Outputs. Nearly all BLA projection neurons are excitatory, glutamatergic pyramidal neurons that express calcium/calmodulin-dependent protein kinase II (CaMKII α) (McDonald et al., 2002). Just as the BLA exhibits diversity of inputs, the BLA also projects widely throughout the brain. This includes vast projections to **cortical regions**, including to the prelimbic and infralimbic cortex (Manoocheri & Carter, 2022), orbitofrontal cortex (Lichtenberg et al., 2021), insular cortex (Gehrlach et al., 2020), and anterior cingulate cortex (Fillinger et al., 2017), **motor output regions** such as the bed nucleus of the stria terminalis (Hintiryan et al., 2021), central amygdala (Beyeler et al., 2018), caudate putamen (McDonald, 1991), and ventral striatum (Brog et al., 1993), **sensory relay regions** such as the thalamus (Aizenberg et al., 2019), **hippocampal memory systems** such as the perirhinal cortex (Petrovich et al., 2001) and ventral hippocampus (Beyeler et al., 2018), and **arousal centres** such as the substantia innominata (Russchen et al., 1985) and claustrum (Niu et al., 2022).

The majority of projections, including those to the mPFC (Hoover & Vertes, 2007), nucleus accumbens (Brog et al., 1993), hippocampus (Roozendaal et al., 1999), and central amygdala (T.-N. Huang et al., 2019) are ipsilateral, although there is evidence of some direct projections to the contralateral BLA (T.-N. Huang et al., 2019). The extent of collateralization of projection populations is unclear. Many experiments suggest that projections are largely non-overlapping (Beyeler et al., 2018; Klavir et al., 2017; Lichtenberg et al., 2021; Senn et al., 2014), with less than 5% of any two populations exhibiting collateralization (L. Huang et al., 2021). However, several experiments suggest high amounts of collateralization, particularly in those projecting to the prelimbic cortex (Shinonaga et al., 1994) or the nucleus accumbens (Beyeler et al., 2016). Thus, findings may be highly dependent on the anatomical tracing techniques used and remains an important gap in our understanding of BLA anatomy.

There are two notable omissions in BLA output regions, especially given its importance in memory and emotional behaviour. First, the BLA does not send any direct projections to the dorsal hippocampus, and thus modulation of this region likely occurs via indirect projections to ventral or parahippocampal regions of the hippocampus (McDonald & Mott, 2017). Second, with the exception of the lateral hypothalamus (Reppucci & Petrovich, 2016), there are only very light BLA projections throughout the hypothalamus (McDonald, 2020), and virtually no direct projections to the paraventricular nucleus of the hypothalamus (PVN) (Petrovich et al., 1996). As such, it remains unclear how activity of the BLA could influence HPA axis activation (Herman et al., 2020).

Although recent work has begun to identify topographical organization of BLA projection neurons (Beyeler et al., 2018; L. Huang et al., 2021; J. Kim et al., 2016; McGarry & Carter, 2017; O'Leary et al., 2020; Reppucci & Petrovich, 2016), clear spatial organization of BLA projection neurons based on their primary output target is not well understood (J.-Y. Zhang et al., 2019a). Functionally, it appears that populations are heterogeneously mixed, with neurons responding to positive and aversive stimuli largely intermingled throughout the BLA (Gore et al., 2015; Shabel

& Janak, 2009). As such, the spatial organization of discrete projection populations remains an important gap in our understanding of BLA structure and function.

Summary and functional implications of anatomical organization. The anatomical structure of the BLA makes it extremely well-suited for the cognitive evaluation of emotional-laden stimuli and subsequent initiation of diverse behavioural and physiological responses. It receives sensory input from all sensory modalities, primarily into the LA subregion. This information gets integrated with cognitive information, memory, and motivational drive through intra-amygdala processing, inhibitory regulation by local interneurons, and convergence with higher-order cortical and mnemonic regions. Activity in the BLA can then drive behavioural, physiological, and cognitive changes through projections to a wide array of effector regions via CaMKii+ glutamatergic projection neurons. In the following sections, we will outline the functional role in stress of the BLA and its projection targets and highlight any findings specifically investigating discrete BLA efferents.

1.3 ROLE OF THE BASOLATERAL AMYGDALA IN THE STRESS RESPONSE

Operationalization of terms. Stressful environments often elicit a fear or anxiety-like response. Generally consistent with terminology in the field, within this thesis I operationalize fear as a rapid and transient response to a distinct, known, and present acute sensory stimulus that represents an immediate threat; in contrast, anxiety is a prolonged, generalized response, typically characterized by risk assessment, heightened arousal, and avoidance in anticipation of an ambiguous, potential, or unknown threat (Davis et al., 2010). As such, fear typically induces an organized behavioural reaction to threat, while anxiety is often characterized by a state of heightened vigilance and generalized physiological arousal lacking organized behaviour (Lang et

al., 2000). A well-differentiated example of this separation has been described previously, wherein fear is the emotional state, and behavioural response, that occurs when an individual encounters an aggressive dog, while anxiety is the emotional state, and behavioural response, that occurs when we will visit a friend which has an aggressive dog that we may encounter (Daviu et al., 2019).

Anxiety. Since early work demonstrating that lesions of the amygdala greatly reduces fear in monkeys (Bucy & Klüver, 1955; Weiskrantz, 1956), a large body of work has since implicated the BLA in also driving anxiety-like behaviour. Human imaging has demonstrated that the amygdala is hyperactive in states of pathological anxiety and is hyperactive to social cues in individuals with generalized anxiety disorder and social anxiety disorder (Martin et al., 2009). A wide range of optogenetic (Tye et al., 2011; Yin et al., 2019) and pharmacological approaches in rodents (Di et al., 2016; J. M. Gray et al., 2015) widely support the broad anxiogenic role of the BLA in regulating anxiety. Further, it is apparent that the influence of the BLA extends beyond classic avoidance behaviours such as those measured in the open field test (Choleris et al., 2001), elevated plus maze (Pellow et al., 1985), or light-dark box (Chaouloff et al., 1997). Indeed, the BLA has been widely implicated in ancillary stress behaviours such as feeding (Jochman et al., 2005), social interaction (L. L. Wellman et al., 2016), self-grooming (Felix-Ortiz & Tye, 2014; Folkes et al., 2020), cognitive function (Yin et al., 2019), decision-making (Orsini et al., 2015), and struggling behaviour (N. Grissom et al., 2008).

Endocrine response. There is not nearly as much understanding of the contribution of the BLA to endocrine activation, likely because the BLA does not send any direct projections to the PVN (Petrovich et al., 1996). However, there is widespread, and at times contradictory, evidence that the BLA can influence HPA function. Gross lesions of the BLA reduce stress-induced CORT

(Bhatnagar et al., 2004; Coover et al., 1973; Goldstein et al., 1996). This is supported by intra-BLA pharmacological manipulations targeting orexin (Yaeger et al., 2022), endocannabinoid (Hill et al., 2009) and corticotropin-releasing hormone signaling (J. M. Gray et al., 2015), collectively supporting the idea that excitation of the BLA leads to a net drive on the HPA axis. However, many other pharmacological manipulations have no effect, including those targeting the ghrelin (M. Jensen et al., 2016), dopamine type II (de Oliveira et al., 2017), neuropeptide Y (T. J. Sajdyk et al., 2008), and GABAA receptors (Bhatnagar et al., 2004). Further, electrical stimulation of the BLA can increase (Feldman et al., 1982; Matheson et al., 1971; Rubin et al., 1966; Vouimba & Richter-Levin, 2013), decrease (Slusher & Hyde, 1961), or have mixed effects on HPA activation (Dunn & Whitener, 1986). There is also evidence that activation of GABAergic interneurons (Morena et al., 2019; Qin et al., 2022) or astrocytes (Xiao et al., 2020) inhibits HPA activation. It is therefore unclear how, exactly, the BLA contributes to HPA activation, and may be a result of the vast heterogeneity of BLA projection neurons (Herman et al., 2020). However, the role of individual BLA projection populations or molecularly distinct neurons on HPA axis activity has not been investigated.

Sympathetic activation. Activation of the BLA can drive heart rate and blood pressure (T. J. Sajdyk & Shekhar, 1997; S. K. Sanders & Shekhar, 1991; Soltis et al., 1997) and respiratory rate (Sugita et al., 2015). However, analogous to mixed findings of BLA influence on endocrine function, manipulation of discrete cells or subregions may exert an opposite effect (Gore et al., 2015), although evidence is limited.

Fear and Emotional Memory. Most of this thesis is in the context of exposure to acute, single episode stressors. Thus, it is difficult to make conclusions on our findings in the context of expression of learned behaviours such as fear, as we never explicitly test fear recall or return

animals to environments that they have learned as aversive. There is a large body of evidence, however, demonstrating the importance of the BLA in emotional memory. This includes consolidation and expression of fear (S. A. Jimenez & Maren, 2009; Paré, 2003; Roozendaal et al., 2009) as well as fear extinction (Tovote et al., 2015).

Reward. There is significant evidence for the role of the BLA in processing of reward, although it is not as well-established or defined as its role in fear, anxiety, and stress (Wassum & Izquierdo, 2015). Neurons in the BLA fire in response to reward-predictive cues (Beyeler et al., 2018; Shabel & Janak, 2009) and projections from the BLA-NAc are readily self-stimulated (Namburi et al., 2015; Stuber et al., 2011). However, lesions of the BLA do not reliably affect simple Pavlovian and instrumental appetitive learning (Wassum & Izquierdo, 2015). Rather, the BLA may be more heavily involved in updating representations of value (Morrison & Salzman, 2010), possibly through reciprocal connections with the orbitofrontal cortex (Seabrook & Borgland, 2020). For example, disruption of opioid signaling in the BLA prevents food deprivation-induced increases in responding for food reward (Wassum et al., 2009), and lesions of the BLA prevent both sensory-specific satiation and LiCl conditioned taste aversion (A. W. Johnson et al., 2009). This may have an important influence for stress-related changes in reward responding. For example, BLA connections with the NAc and VH are necessary for stress-enhanced nicotine self-administration (G. Yu & Sharp, 2015), and opioid signaling within the BLA is important in stress-induced reinstatement of extinguished drug cues (G. Yu & Sharp, 2015). Finally, it must be noted that the BLA is implicated in many other behaviours, including decision-making (Winstanley et al., 2004), attention (Roozendaal & McGaugh, 2011; X. Yu et al., 2020), and sleep (Hasegawa et al., 2022; Machida et al., 2021).

1.4 ROLE OF EFFECTOR REGIONS IN STRESS

Overview. The BLA likely exerts its functional influence via projections to many downstream regions. Here, we highlight six specific regions chosen based on their dense innervation by the BLA and large body of evidence implicating them in the stress response.

Bed Nucleus of Stria Terminalis (BST). The BST is an important effector region of the amygdala via strong outputs to hypothalamic and brainstem regions. As such, it has significant influence on autonomic, neuroendocrine, and behavioural responses to stress (Crestani et al., 2013). The BST may be particularly important in driving a sustained stress response during exposure to aversive environments (Davis et al., 2010; Lebow & Chen, 2016; Radke, 2009; Sullivan et al., 2004). For instance, lesions or pharmacological inactivation of the BST disrupt light-enhanced startle (Walker & Davis, 1997) and reduce behavioural responses to unpredictable threats (Goode et al., 2019), suggesting its role in facilitating a stress response in unpredictable environments. Indeed, electrical (Casada & Dafny, 1991), optogenetic (S.-Y. Kim et al., 2013), or pharmacological stimulation (Lee et al., 2008; Lungwitz et al., 2012; Mazzone et al., 2018; T. Sajdyk et al., 2008) of the BST increases anxiety-like behaviour, and gross lesions of the BST reduce HPA activity (Feldman et al., 1990; T. S. Gray et al., 1993; Zhu et al., 2001). This collectively suggests an overall stress-facilitatory role of the BST.

However, the BST has rich functional and anatomical heterogeneity of many distinct subregions (Ch'ng et al., 2018), and as such, distinct subregions of the BST may have opposing roles in stress (Choi et al., 2007). Anatomical tracing and lesion studies have demonstrated the anterior BST (aBST) as a critical inhibitory relay of the HPA axis from other brain regions such as the PrL and VH (Cullinan et al., 1993; Radley et al., 2009; Radley & Sawchenko, 2011). The aBST may additionally have an important role in dampening stress-enhanced consolidation of aversive memory (Lingg et al., 2020) and inhibiting passive coping responses during stress (S. B. Johnson

et al., 2019). Likewise, optogenetic stimulation of discrete BST subregions (S.-Y. Kim et al., 2013) or efferent projections, including those from the BLA (Crowley et al., 2016), reduce anxiety-like behaviour. Collectively, this suggest that discrete subregions of the BST, specifically the aBST, may drive independent effects.

Ventral hippocampus. The ventral hippocampus is also activated by exposure to psychological stressors (Úbeda-Contreras et al., 2018) and appears to have somewhat paradoxical roles in the stress response. Specifically, the VH has an inhibitory influence over the HPA axis (Cullinan et al., 1993; Radley & Sawchenko, 2011, but see Kjelstrup et al., 2002), which is primarily thought to facilitate termination of the stress response via glucocorticoid negative feedback (Jacobson & Sapolsky, 1991). Despite inhibitory influence on the HPA axis, broad evidence supports the role of the VH in driving anxiety-like behaviour and fear expression (Bannerman et al., 2003; Deacon et al., 2002; Fanselow & Dong, 2010; Kjelstrup et al., 2002; McHugh et al., 2004; Parfitt et al., 2017). In particular, stimulation of BLA inputs to the VH significantly increases anxiety-like behavior (Felix-Ortiz et al., 2013) and social avoidance (Felix-Ortiz & Tye, 2014), and enhances consolidation of aversive memory (Huff et al., 2016).

Prelimbic cortex (PrL). The prelimbic cortex is activated in response to psychological stressors (Moghaddam, 1993). Lesions or pharmacological inhibition of the PrL potentiates acute stress-induced HPA activation (Radley et al., 2009; Spencer et al., 2005) and tachycardia (Tavares et al., 2009), suggesting an inhibitory influence on physiological responses to stress. This may be particularly notable in the context of chronic stress, as inactivation of the PrL interferes with HPA axis habituation observed during exposure to a repeated homotypic stressor (Weinberg et al., 2010). Indeed, repeated stress leads to structural remodeling of the PrL (McEwen, 2006; McEwen

et al., 2016; C. L. Wellman et al., 2020), and restoration of some of these changes ameliorates stress-induced behavioural deficits (Wei et al., 2018).

Behaviourally, the PrL is critical for expression of learned fear (Blum et al., 2006; Corcoran & Quirk, 2007), and pharmacological stimulation increases anxiety-like behaviour (Saitoh et al., 2014). In particular, BLA-PrL circuits are activated by stress exposure (Marcus et al., 2020) and drive anxiety-like behaviour (Felix-Ortiz et al., 2016; Marcus et al., 2020) and fear expression (Tovote et al., 2015). Given the importance in learned fear, the PrL may thus play a particularly important role in mediating a physiological and behavioural response to previously experienced stressors.

Nucleus Accumbens (NAc). The NAc has a likely role in driving behavioural responses to salient stimuli. Although the NAc is classically implicated in mediating appetitive learning and reward processing (Floresco, 2015), it is also activated by exposure to stress (Perrotti et al., 2004; Úbeda-Contreras et al., 2018). However, its precise role in stress is less studied than other structures. Pharmacological depletion of dopaminergic signaling in the NAc impairs conditioned avoidance behaviour (Wadenberg et al., 1990) and conditioned freezing during fear conditioning (Wendler et al., 2014). In particular, the NAc core is involved in a variety of fear-related processes (Haralambous & Westbrook, 1999; Ray et al., 2020). Additionally, the NAc can drive avoidance behaviour (Al-Hasani et al., 2015), particularly via stimulation of the BLA-NAc projection (Folkes et al., 2020; Shen et al., 2019). As such, it has been proposed that the NAc plays a critical role in biasing behaviour towards a response by assigning “motivational salience” to important cues (Floresco, 2015; J. Jensen et al., 2003). Supporting this, progressively greater intensity of footshock leads to matching increases in dopaminergic release in the NAc (Sorg & Kalivas, 1991), while milder stressors such as brief air puffs (Mirenowicz & Schultz, 1996), gentle handling, or

mild tail pinches (Cenci et al., 1992) do not elicit a response, collectively suggesting the NAc signal may act to scale intensity, or “salience”, of threat (Horvitz, 2000; Ray et al., 2020)

Alternatively, activation of the NAc may counteract negative effect of stress or encode relief upon termination of a stressor. Indeed, BLA-NAc projections are inherently self-stimulated (Namburi et al., 2015; Stuber et al., 2011) and promote resilience to chronic stress-induced behavioural deficits (Bagot et al., 2015), and as such, activation may counteract maladaptive stress-induced behavioural changes.

Lateral hypothalamus (LH). The lateral hypothalamus also plays a role in mediating physiological and behavioural responses to emotional stressors (Gomes-de-Souza et al., 2021). However, due to heterogenous expression of glutamatergic, GABAergic, and peptidergic neurons, it is difficult to make an overarching conclusion on its role in stress (Ulrich-Lai & Herman, 2009). For example, inhibition of the LH has different effects on stress-induced sympathetic response depending on which neurotransmitter system is targeted (Deolindo et al., 2013; Iwata et al., 1986; Pugliesi & De Aguiar Corrêa, 2004). Similarly, optogenetic and chemogenetic studies also demonstrate seemingly both a stress-promoting and stress-protective effect on behavior; specifically, stimulation of the LH promotes anxiety-like behavior (J. C. Jimenez et al., 2018) but is also shown to reduce stress-induced anhedonia (Campbell et al., 2017). Collectively, this suggests that, through complex activation of heterogenous cell types, the LH has an important general role in mediating arousal and motivated behavior.

Central amygdala (CeA). The central amygdala is the major output region of the amygdala (Pitkänen et al., 1997) to drive behavioural and physiological responses to emotionally important events (Gilpin et al., 2015). This includes effector regions such as the paraventricular nucleus of the hypothalamus (T. S. Gray et al., 1989), periaqueductal gray (W. Han et al., 2017), locus

coeruleus (Cedarbaum & Aghajanian, 1978), lateral hypothalamus (Reppucci & Petrovich, 2016), and nucleus of the solitary tract (Saha et al., 2000). As a result, the CeA has been implicated in a wide range of stress-related effects, including stress-induced hypophagia (Petrovich et al., 2009), HPA axis activation (Herman et al., 2005), defensive behaviours (W. Han et al., 2017), sympathetic tone (Ikegame et al., 2022), and expression of fear and anxiety (Davis, 1992).

However, there is growing evidence (Fadok et al., 2018) that discrete subregions and circuits of the CeA can be reinforcing (Ross et al., 2016), drive appetitive behaviors (Hardaway et al., 2019), and even reduce anxiety-like behaviour (Tye et al., 2011). The BLA may have discrete roles depending on which CeA circuits are activated. Indeed, the BLA-CeA is necessary for expression of fear (S. A. Jimenez & Maren, 2009) and aversive learning (Beyeler et al., 2018), yet discrete projections can also drive reward (X. Zhang et al., 2020) and reduce anxiety-like behaviour (Tye et al., 2011).

Implications. It is apparent that major projection targets of the BLA can drive a wide range of behavioural and physiological changes associated with the stress response. However, many of these structures are heterogenous in anatomy and function, and it is therefore difficult to predict how individual BLA circuits may influence their response to afferent activation from stress.

1.5 ROLE OF DISCRETE BASOLATERAL AMYGDALA PROJECTION NEURON POPULATIONS

Disconnection studies have proven useful to explore the function of discrete circuits. In this case, pharmacological inactivation or lesion of the unilateral BLA and a contralateral other structure (e.g., lesion of BLA on left hemisphere, lesion of mPFC on right hemisphere) functionally

disconnects two structures while still preserving their individual function. As such, disconnection studies clearly demonstrate the importance of BLA connectivity with the CeA in expression of learned fear (S. A. Jimenez & Maren, 2009), and connectivity with the VH in consolidating inhibitory avoidance learning (Wang et al., 2017). Additionally, BLA/mPFC connectivity is important in mediating stress-induced impairments in learning (Maeng et al., 2010) and driving active coping behaviours (Andolina et al., 2013), and connectivity between the BLA and NAc is important in stress-enhanced reacquisition of nicotine self-administration (G. Yu & Sharp, 2015). However, most of these experiments focused on learning processes, and further, directionality of connectivity cannot be tested. This is especially true for structures such as the VH and mPFC that involve reciprocal BLA circuits. As such, it was not until the advent of viral approaches such as optogenetics or chemogenetics that circuit-level control of behaviour could easily be tested in acute environments.

Recent circuit-specific manipulation of BLA circuits is extensively described in a seminal review paper by (Janak & Tye, 2015), and emphasize strong functional diversity of BLA circuits. For instance, optogenetic stimulation of BLA projection neurons can increase (Felix-Ortiz et al., 2013, 2016; Felix-Ortiz & Tye, 2014) or decrease (Crowley et al., 2016; Tye et al., 2011) anxiety-like behaviour depending on which brain regions they target. This heterogeneity is apparent even within individual circuits; whereas BLA-NAc projections are inherently self-stimulated (Namburi et al., 2015; Stuber et al., 2011) and promote resilience to chronic stress-induced behavioural deficits (Bagot et al., 2015), they can also drive anxiety-like behaviour (Folkes et al., 2020; Shen et al., 2019). Likewise, the BLA-CeA is necessary for expression of fear (S. A. Jimenez & Maren, 2009) and aversive learning (Beyeler et al., 2018), yet discrete projections can also drive appetitive responding (X. Zhang et al., 2020). Individual divergence of discrete circuits may be separated on the basis of discrete molecular markers (J. Kim et al., 2016; Shen et al., 2019), although work on this is only just emerging.

This heterogeneity extends beyond anxiety, as manipulation of discrete circuits influences many other behaviours including feeding, social behaviour, and appetitive/aversive learning (Janak & Tye, 2015), and in this respect, the influence of a given BLA projection pathway is difficult to predict. As such, functional mapping (i.e., identifying which circuits are activated by specific behaviours) may be particularly useful for guiding our understanding of the role of discrete projection populations.

1.6 MOLECULAR AND RECEPTOR IDENTITY OF BLA PROJECTION NEURONS

Overview. Along with circuit identity, BLA neurons can be characterized by expression of specific receptors or molecular markers. These “molecular signatures” may be particularly informative for identifying potential pharmacological targets to treat stress-related disorders (McCullough, Morrison, et al., 2016).

Molecular Identity. While molecular and functional heterogeneity has been well-described in BLA interneurons (Hájos, 2021; Krabbe et al., 2018), BLA projection neurons have largely been classified into only two subtypes: parvicellular and magnocellular (Savander et al., 1995); these have since been shown to uniquely express protein phosphatase 1 regulatory inhibitor subunit 1B (*Ppp1r1b*) and R-spondin 2 (*Rspo2*), respectively (J. Kim et al., 2016). However, recent work has revealed that BLA projection neurons exhibit wide heterogeneity in molecular expression (O’Leary et al., 2020).

These developments establish a new avenue for exploring amygdala anatomy. Molecularly distinct projection populations in the BLA have been shown to mediate opposing appetitive vs. aversive learning in the BLA (J. Kim et al., 2016). Further, *Ppp1r1b*⁺ neurons are activated by reward, and driving their activity inhibits expression of fear during extinction learning

(X. Zhang et al., 2020), suggesting overlapping circuitry of distinct, but perhaps related, processes. Likewise, BLA projection neurons that express *Thy1* drive fear inhibition (Gilman et al., 2018; Jasnow et al., 2013). Notably, this projection population exhibits specificity in projection targets, with dense projections to the NAc and BST, and an absence of projection to the CeA (McCullough, Choi, et al., 2016).

Most of this work has been performed in the context of learning, and thus it is unclear which cell types are engaged during exposure to acute stress. Further, to the best of our knowledge, no work has investigated the molecular identity of BLA projection populations driving HPA axis or sympathetic activity, and this remains a critical gap in our understanding of BLA anatomy.

Receptor Identity. The BLA expresses a heterogeneous mix of receptors. Among many others, this includes receptors for feeding peptides such as ghrelin (Alvarez-Crespo et al., 2012) and leptin (Z. Han, 2003), arousal signals such as orexin (Flores et al., 2017) and acetylcholine (Aittah et al., 2018; Unal et al., 2015), neuromodulators such as dopamine (Pickel et al., 2006) and serotonin (McDonald & Mascagni, 2007), and stress signals such as corticotropin-releasing hormone (J. M. Gray et al., 2015) and glucocorticoids (Morimoto et al., 1996). These represent exciting potential molecular markers for stress-responsive neurons. Of note are receptors for the endocannabinoid, CRH, and NE systems.

The **endocannabinoid (eCB) system** is implicated in most brain and body functions (Piazza et al., 2017) and has a particularly strong regulatory influence on activation of stress circuits (Morena et al., 2016). Activation of the endocannabinoid system generally reduces anxiety-like behaviour and suppresses activation of the HPA axis, and the BLA appears to be particularly involved in this process (Hill, Patel, et al., 2010; Petrie et al., 2021; Steiner & Wotjak, 2008). Indeed, intra-BLA pharmacological manipulations demonstrate that endocannabinoids

largely act in the BLA to constrain both HPA activity (J. M. Gray et al., 2015; Hill et al., 2009; Hill, McLaughlin, et al., 2010) as well as both fear and anxiety-like behaviour (J. M. Gray et al., 2015; Gunduz-Cinar et al., 2013).

The **CRH receptor Type I (CRHR1)** is widely expressed across limbic regions (Weera et al., 2022) and global pharmacological inhibition or genetic deletion of CRHR1 dramatically reduces both anxiety-like behaviour and HPA responses to stress 2023-07-19 7:04:00 PM. CRHR1 expression is evident in BLA projection neurons (Agoglia et al., 2020; Y. Chen et al., 2000; Van Pett et al., 2000) and may have a particularly important role during stress, as it is readily released into the amygdala during acute stress (Merlo Pich et al., 1995). Indeed, administration of CRH directly into the BLA amplifies the HPA response to stress and drives anxiety-like behaviour (J. M. Gray et al., 2015).

Norepinephrine (NE) is readily released peripherally during stress to drive sympathetic activation (Tank & Wong, 2014). However, there is also substantial central release from the locus coeruleus during stress to various projection targets including the BLA (Galvez et al., 1996; McCall et al., 2017). The Gs-coupled β -noradrenergic receptor is widely expressed through the BLA (Qu et al., 2008), and administration of β -noradrenergic antagonists blunt stress-induced activation of the BLA (Giustino et al., 2020). Specifically, NE action in the BLA drives anxiety-like behaviour (McCall et al., 2017) and enhances consolidation for aversive memory (LaLumiere et al., 2003).

1.7 CONCLUSIONS

The BLA is heavily implicated in the stress response. It is reliably activated by psychological stress, and through anatomical connections to a diverse array of sensory inputs and motor and cognitive outputs, is well-situated to drive widespread changes in anxiety-like

behaviour, HPA activation, and sympathetic tone. However, it is a heterogeneous structure, and discrete cell types and circuits can mediate diverse (and even opposing) effects on anxiety-like behaviour. Circuit- and subregion- specificity remains a critical gap in our understanding of how the BLA contributes to the stress response, and further, relatively little research has been conducted on the contribution of the BLA to the HPA response to stress. It is therefore essential to map distinct topographical subregions, circuits, and molecular phenotypes of BLA neurons explicitly activated by stress, and with a particular focus on how they may contribute to HPA activation.

1.8 THESIS OBJECTIVES AND HYPOTHESES.

Objective. The objective of this thesis is to conduct a systematic investigation of the spatial, temporal, and circuit-specific activation patterns of BLA projection neurons during stress, as this is a brain region highly involved in processing emotional stimuli that are both stressful and rewarding. Additionally, we wanted to clarify the role of the BLA in activation of the HPA axis.

Overarching hypothesis. The overarching hypothesis is that stress uniquely activates discrete BLA subregions, circuits, and molecularly defined projection populations to drive stress-related increases in HPA axis activation. This hypothesis will be tested in three related but distinct aims:

Aim 1 (Chapter 2): What subregions of the BLA are activated by stress, and does activation contribute to stress induced HPA axis activation?

Hypothesis: Distinct subregions of the BLA are differentially activated by stress and that temporarily increasing or decreasing the activity of BLA projection neurons will bidirectionally influence HPA axis activity.

Aim 2 (Chapter 3): How are projection neuron populations organized in the BLA and which projection populations are activated by stress? Do individual projection populations contribute to stress-induced activation of the HPA axis?

Hypothesis: Projection neuron populations are heterogeneously distributed throughout the BLA, as expressed by differences in subregion-specific density. Discrete populations are activated by exposure to acute stress. Temporary inhibition of isolated populations will reduce stress induced HPA axis activity.

Aim 3 (Chapter 3): How are CRHR1+ neurons organized in the BLA, and are they activated by stress? Do they contribute to behaviours associated with an aversive state?

Hypothesis: CRHR1 neurons are heterogeneously distributed throughout the BLA, as expressed by differences in subregion-specific density. BLA:CRHR1 cells are activated by stress and may be a molecular marker for stress-responsive cells. Temporary inhibition of CRHR1 cells will reduce fear learning, anxiety-like behaviour, and stress-induced HPA axis activation.

Chapter 2. Identification of a stress-integratory subregion of the basolateral amygdala

2.1 ABSTRACT

In humans and rodents, the amygdala is rapidly activated by stress and hyperactive in conditions of pathological stress or trauma. However, there is a striking lack of information of the anatomical specificity of amygdala subregions and of its role in governing typical responses to stress such as HPA axis activation. Using c-fos mapping and fiber photometry in male rats, we identified the medial basal amygdala (mBA) as a distinct subregion that is specifically activated by a range of stressors. Using restraint stress as a prototypical model for stress, we found that systemic administration of propranolol, a β -adrenoceptor antagonist, reduced the magnitude of calcium-related response to restraint stress. Further, chemogenetic inhibition of mBA projection neurons dampened stress-induced HPA activity, and optogenetic stimulation drove HPA activity in non-stress conditions. These data identify the mBA as a subregion that is robustly and specifically recruited by stress exposure to contribute to activation of the HPA axis.

2.2 INTRODUCTION

In response to a real or perceived threat, the body mounts a multi-level response which is collectively referred to as a “stress response”. This is a complex and widely encompassing biological process, involving diverse behavioural and physiological changes including activation of the endocrine and sympathetic systems, enhanced vigilance, and avoidance behaviours. Despite differences in the nature and temporal dynamics of psychological stressors, all aversive, stressful stimuli induce a relatively comparable stress response (Chaaya et al., 2019; Fendt et al., 2003; Morrow et al., 2002; Ong et al., 2014). In particular, all stressors reliably and consistently lead to activation of the paraventricular nucleus of the hypothalamus (PVN), the main driver of

the hypothalamic-pituitary-adrenal (HPA) axis and subsequent release of the glucocorticoid hormone corticosterone (CORT) (Herman et al., 2016). Despite a similar response, differing modalities or intensity of stressors elicit varying magnitude of the stress response (Armario et al., 1986; Kant et al., 1983). Thus, an essential question is how the brain coordinates and regulates a response to psychological stressors.

The basolateral amygdala (BLA) is anatomically well-situated as a stress-regulatory region. It receives sensory input from all sensory modalities (LeDoux, 2007; McDonald, 1998), where it can then integrate it with cognitive information encoding memory and motivational drive and subsequently modulate physiological processes and behavioural responses through widespread projections to effector brain regions via CaMKII+ glutamatergic projection neurons (Sah, Faber, Lopez De Armentia, et al., 2003). Indeed, psychological stressors robustly increase activity in the BLA of both rodents and humans (Reznikov et al., 2008; van Marle et al., 2009), and preclinical research has demonstrated that the BLA is strongly involved in many stress-related processes, including avoidance behaviour, sympathetic activation, and memory (Felix-Ortiz et al., 2016; McCall et al., 2017; Paré, 2003; Petrovich et al., 2002; Soltis et al., 1997; Tye et al., 2011)

Collectively, this has established the BLA as a critical stress “hub” (Herman et al., 2020; van Marle et al., 2009). Supporting this, gross lesions of the amygdala, including the BLA, have been found to inhibit stress-induced HPA activity (Bhatnagar et al., 2004; Goldstein et al., 1996). Additionally, certain intra-BLA pharmacological experiments alter stress-induced CORT, including manipulations targeting the orexin, endocannabinoid, corticotropin-releasing factor, and neuropeptide S systems (Cohen et al., 2018; J. M. Gray et al., 2015; Hill et al., 2009; Yaeger et al., 2022). However, many other intra-BLA manipulations – such as those targeting GABA-A, dopamine type II, neuropeptide Y, or ghrelin receptors – have no effect on HPA activity (Bhatnagar et al., 2004; de Oliveira et al., 2017; M. Jensen et al., 2016; T. J. Sajdyk et al., 2008). Collectively,

this suggests that as a structure, the BLA is integral to the stress response, but distinct subregions or neuromodulators may play a more influential and specific role in driving the stress response.

Although most cells in the BLA are excitatory projection neurons (~80-85%), a small population are GABAergic interneurons that regulate output activity of the BLA and may thus act to counteract stress-promoting roles of BLA projection neurons (Morena et al., 2019; Qin et al., 2022). Additionally, there is some evidence that astrocytes may also dampen stress-induced output of the BLA (Xiao et al., 2020). Thus, variation in the impact of BLA manipulations to drive changes in the endocrine response may result from specific differences in the cell types or signaling molecules involved. Additionally, regional differences in the BLA have also been proposed, including rostral-caudal and circuit-specific projections in BLA activation by learned rewarding vs aversive stimuli (Beyeler et al., 2018; J. Kim et al., 2016; X. Zhang et al., 2020). More notably, various experiments in several animal species and human epilepsy patients have demonstrated that electrical stimulation of the BLA can increase COR release, however these effects are variable and seem to depend on the exact region of the BLA the electrode was targeted (Dunn & Whitener, 1986; Feldman et al., 1982; Matheson et al., 1971; Rubin et al., 1966; Slusher & Hyde, 1961; Vouimba & Richter-Levin, 2013). Together, these data support our hypothesis that distinct BLA subregions and neurotransmitter systems are involved in the stress response.

We used a rodent model to allow for systematic, specific, and high-resolution investigation of how the BLA responds to a range of aversive and non-aversive novel stimuli. First, we characterized the spatial and temporal patterns of activity in the BLA during exposure to several different stressors or non-aversive stimuli, to determine if there is a common activation pattern in response to stress. Our goal was to identify if there was a specific “stress-sensitive” sub-region of the BLA. Secondly, using chemo- and optogenetic approaches, we tested the necessity and sufficiency of BLA projection neurons within stress-sensitive sub-regions to modulate stress-induced release of CORT. Collectively, we identified the medial basal amygdala (mBA) as a

distinct subregion of the amygdala that is robustly and specifically recruited by wide range of psychological stressors to drives changes in HPA axis activity.

2.3 METHODS

Animals. All animal protocols were approved by the University of Calgary Animal Care Committee and followed guidelines from the Canadian Council on Animal Care. Adult male Sprague Dawley rats were obtained from Charles River Laboratories (175-225g upon arrival) and maintained under a 12h light-dark cycle (lights on at 8am) with food and water available ad libitum. Unless otherwise specified, animals were pair-housed and all experiments were performed during the light phase of the cycle between 8am and 2pm. Cage-mates were always in identical treatment groups and underwent all aspects of experimentation at the same time, including intraperitoneal injections, blood collection, stimulus exposure, and sacrifice.

Stereotaxic surgery. Rats were maintained under isoflurane anesthesia and analgesic treatment (meloxicam (2mg/kg, subcutaneously)) in a stereotaxic apparatus during surgical injection of viruses or implantation of fibre optic cannulas. To deliver viral vectors, a glass capillary containing viral vector was lowered into the brain and pressure injected using a NanoInject II apparatus (Drummond Scientific). Coordinates targeting the BLA were relative to bregma and the surface of the skull: -2.8mm anterior-posterior (AP), ± 4.9 to 5.0mm medial-lateral (ML), and -8.4 to -8.7mm dorsal-ventral (DV). To implant fibre optic cannulas used in photometry or optogenetic experiments, 2 weeks were allowed for recovery before implantation of a 600 μ m diameter mono fiber optic cannula (Doric Lenses, MFC_600/630/0.48_8.6mm_MF2.5_FLT) 0.1mm above the injection site, and secured with Metabond, dental cement, and four anchoring screws.

Optogenetic and chemogenetic experiments involved bilateral injections, and fiber photometry experiments involved unilateral injections targeting the right BLA.

Blood collection and corticosterone analysis. Animals were gently placed into clear Plexiglas restraint tubes and blood samples were collected into ice chilled, EDTA treated microvettes (Sarstedt AG & Co. KG; #16.444.100) from a small nick over the lateral tail vein. Tail blood was centrifuged at 10,000 rpm for 20min at 4°C to separate plasma, which was stored at –20°C until corticosterone analyses. Plasma samples were analyzed with an enzyme-linked immunosorbent assay kit (Arbor Assays; #K014-H5) by following the manufacturer’s instructions and as performed previously (DeVuono et al., 2020). Standards were run in triplicate, and samples were tested in duplicate and diluted 1:100 to ensure levels fit the standard curve. Groups were compared at individual time points or as an area-under-the-curve (AUC). The following formulas for AUC were used: for comparison of different stimuli: $[(t_{30} + t_{90}) * 60\text{min}] / 2$; and for comparison following optogenetic stimulation: $[((t_{30} + t_{60}) * 30\text{min}) / 2] + [((t_{60} + t_{90}) * 30\text{min}) / 2]$ (Pruessner et al., 2003).

Brain collection. Brains were collected and processed identically for all experiments. For perfusion, animals were anesthetized with an overdose of sodium pentobarbital and transcardially perfused with 0.9% saline (~60mL per rat, 30 mL/min) followed by 3.8% paraformaldehyde in 0.01M PBS (~120mL per rat, 30 mL/min). Following perfusion, brains were removed and immersed in 3.8% paraformaldehyde in 0.01 M PBS overnight before being switched to a 20% sucrose solution in PBS for 48-72 hours, and then transferred to a 30% sucrose solution in PBS for cryoprotection. Coronal sections of 40um were cut in four series’ on a Leica SM 2010R sliding microtome and collected in antifreeze (30% wt/vol sucrose, 1% wt/vol polyvinylpyrrolidone-40, 30% vol/vol ethylene glycol, 0.0065% wt/vol sodium azide, in PBS; adapted from (Butler et al., 2012)) and stored at -20 C until processing.

FOS immunohistochemistry. Free-floating sections of the BLA were rinsed 3x10min in PBS, followed by 3x10min in PBS + Triton X-100 (0.1%). Sections were then blocked for 1h at room temperature with gentle agitation in 5% normal donkey serum in PBS and incubated for 23h at 4°C with anti-cFos antibody raised in rabbit (cFos, #2250s, Cell Signaling Technology, 1:400) in an antibody blocking solution (0.1% vol/vol Triton X-100, 0.1% wt/vol BSA, 0.05% wt/vol sodium azide, 0.04% wt/vol sodium EDTA in PBS). Following a 3x10min wash in PBS + Triton X-100 (0.1%), sections were incubated for 2h at room temperature with a donkey anti-rabbit AlexaFluor 647-conjugated secondary antibody (Alexa-647, #711-605-152, Jackson ImmunoResearch, 1:125) in antibody blocking solution. Finally, sections were rinsed 3x10min in PBS + Triton X-100 (0.1%) and 2x10min in PBS, mounted onto charged slides, and cover-slipped using Fluoroshield with DAPI mounting medium (Sigma Aldrich).

Histology. To verify viral expression or cannula tract location following fiber photometry, optogenetic, or chemogenetic experiments, free floating sections of the BLA were rinsed 3x10min in PBS, mounted onto charged slides, and cover-slipped using Fluoroshield with DAPI mounting medium (Sigma Aldrich). For imaging of GCaMP6s in Figure 2 or hM4D(Gi), images were acquired with a Leica DM4000 B LED microscope using a 2.5X / 0.07 NA PLAN (Leica 556036) or 5X / 0.12 N PLAN EPI (Leica 566076) objective. For imaging of ChR2 or GCaMP6s in Figure 3, images were acquired using an Olympus VS120 slide scanner using a 10X / 0.4 NA air objective. Each construct had distinct imaging parameters which remained consistent throughout each experiment. Notably, the mCherry expression was observed to have substantially greater fluorescent intensity than hM4D(Gi), and therefore required lower intensity and exposure settings. Location of maximal expression of virus and/or location of cannula tips were plotted onto coronal images adapted from an atlas (Swanson, 2004). Animals were excluded if there was no

expression in at least one hemisphere, significant expression outside of the BLA, significant damage at the injection site, or placement of the cannula tip was outside of the BLA.

Electrophysiology. For slice experiments, animals were deeply anaesthetised with isoflurane, decapitated and coronal slices (250 μ m) containing the BLA were cut using a vibratome (VT1200, Leica Microsystems) in room temperature, NMDG-based artificial cerebrospinal fluid (ACSF). Slices were then briefly transferred to a submerged chamber containing NMDG ACSF of the following composition: 93 mM NMDG, 2.5 mM KCl, 1.2 mM NaH_2PO_4 , 30 mM NaHCO_3 , 20 mM HEPES, 25 mM glucose, 2 mM thiourea, 5 mM Na-ascorbate, 3 mM Na-pyruvate, 0.5 mM $\text{CaCl}_2 \cdot 4\text{H}_2\text{O}$ and 10 mM $\text{MgSO}_4 \cdot 7\text{H}_2\text{O}$, where they were maintained at 32°C for 10-12 mins to allow for protective recovery of tissue. Finally, slices were transferred to a holding chamber containing regular ACSF of the following composition: 126mM NaCl, 2.5mM KCl, 1.4 mM NaH_2PO_4 , 1.2 mM MgCl_2 , 2.4 mM CaCl_2 , 11 mM glucose and 25 mM NaHCO_3 ; equilibrated with 95% O_2 and 5% CO_2 . When time to record, slices were individually transferred to a chamber on an upright microscope (Olympus BX51) and superfused continually with ACSF (32°C, flow rate: 2.0 ml min⁻¹). Neurons were visualised with a 40X water-immersion objective using infra-red Dodt-tube gradient contrast optics.

Functional DREADD expression and blue light photostimulation in BLA pyramidal neurons was confirmed using in-vitro patch clamp electrophysiology. Using fluorescence, neurons expressing CaMKII-hM4DI were identified by the presence of an mCherry reporter. Whole-cell current-clamp recordings (Axopatch 700B, Molecular Devices) were then conducted in labelled neurons using a K-Gluconate-based internal solution containing: 130 mM K-Gluconate, 10 mM HEPES, 10 mM KCl, 4 mM Mg_2ATP , 0.3 mM Na_2GTP and 10 mM $\text{Na}_2\text{-Phosphocreatine}$ (pH 7.3). Neurons were maintained at a membrane potential of -70 mV by DC current injection via the patch-electrode. To confirm DREADD functionality, cell excitability was assessed by examining

the current-voltage relationship (range: -25 - +400 pA) before and during application of Clozapine-N Oxide (CNO, 10 μ M). Furthermore, evoked firing rate was assessed over time by application of series of 5 current pulses (250 ms in duration, 5-25 pA apart, every 60 secs), where the current amplitude was set for each cell so that ~ 3-4 action potentials were elicited during the 2nd-4th steps. To confirm that blue light photostimulation *in vitro* reliably excited BLAChR2 cells, single pulses and trains were elicited using a 470 nm Light Emitting Diode (LED) (405 mW: Thor Labs) through the 40x microscope objective. Responses to a single pulse of blue light (3ms) in current and voltage clamp mode, light pulses delivered at 20Hz for 1s in current and 10s in voltage clamp mode, and a 500ms light pulse in voltage clamp was reliably repeated in several different brain slices from BLAChR2 expressing rats.

Exposure to novel stimuli.

Groups. To assess the impact of different novel stimuli on plasma corticosterone response and spatial activation patterns in the BLA, animals were randomly pre-assigned to one of 7 experimental conditions (citral odour, n=8; bobcat urine, n=8; crackers, n=8; restraint stress, n=10; swim stress, n=10; mild foot shock, n=8; naïve, n=8). Cage-mates were assigned to the same condition and experienced stimulus exposure at the same time. The experiment was run across multiple days, but all immunohistochemistry and imaging were performed together and all ELISAs were performed over two days.

Handling and habituation. All animals were habituated for 7 consecutive days prior to experimental day with two daily handlings. In the mornings, animals were carted to an adjacent experimental room for 30min and handled for 1min each before being returned to their colony room. Animals remained pair-housed and in their home cage during habituation, except for animals who would be subject to cracker, bobcat urine, or citral odour exposure on the

experimental day; in this case, they were placed alone into empty cages with no enrichment, food, or water access for the 30min habituation. For afternoon handlings, animals remained in the colony room and were handled for 1min each. This was to ensure that the endocrine and FOS response to each stimulus was largely reflective of the stimulus rather than handling stress.

Stimulus exposure. On experimental day (Day 8), animals were carted to their testing rooms and immediately exposed to their pre-assigned stimulus for 30min. For odour exposure, rats were placed alone into an empty cage with a sponge soaked in citral odour (Sigma-Aldrich; 1% in mineral oil (Abraham et al., 2012; Slotnick, 2004)) or bobcat urine (Maine Outdoor Solutions; (Whitaker & Gilpin, 2015)). For cracker exposure, rats were placed alone into an empty cage with unlimited access to goldfish crackers (Pepperidge Farm). For restraint, animals were placed into a clear Plexiglas restraint tube. For mild foot shock, animals were placed alone into fear conditioning chambers equipped with metal stainless-steel rod flooring connected to a shock generator (Med Associates) and were exposed to 7 equally spaced shocks (0.65 mA, 1s long) over 30min. For swim, animals were placed into an opaque plastic bucket (40cm internal diameter filled with 25 ± 2 °C water for 15min, and then immediately removed, gently dried off with a towel, and returned to their home-cage with their cage-mate. In the naïve condition, animals remained untouched in the colony room until time of sacrifice.

Blood and brain collection. Blood was collected 30min (t30) and 90min (t90) following stimulus-onset, except for the naïve condition in which only a single blood sample was collected, occurring immediately prior to sacrifice. Perfusion occurred 90min following stimulus onset, and brains were removed for processing to perform immunohistochemistry for c-fos.

Imaging for stimulus-induced c-fos topography. Immunohistochemistry for FOS expression was performed and 20X tilescan images of the BLA from AP -2.12 to AP -3.60 (Paxinos & Watson atlas) were acquired from each animal using an Olympus VS110 Slidescanner with a 20X (0.75 NA air) objective. Only images with tissue undamaged throughout processing, sectioning, and immunohistochemistry were included (number of animals and slices per group: naïve=7/96; citral=8/93; crackers=8/113; bobcat=7/86; shock=5/73; swim=7/103; restraint=10/121). All imaging parameters (e.g., exposure, light intensity) remained identical between all images, and the experimenter was blinded to experimental condition. All images were saved as a virtual slide image (.vsi) for further analyses using Imaris software.

FOS Exclusions. Animals were excluded if there were not at least 5 BLA images to count from (N=4; swim=1, shock=2, naïve=1) or human error resulting in different imaging parameters for that animal (N=4; swim=2, shock=1, bobcat=1).

CORT Exclusions. Animals were excluded if there was not sufficient plasma to run the ELISA (n=3 at t90; restraint=1; shock=2).

Topographical mapping and quantification of FOS+ cells. The experimenter remained blinded to the conditions of each animal during plotting and counting. Analyses were largely guided by work from (Beyeler et al., 2018). Given that the BLA shape and size varies due to changes in AP position and imperfections in mounting and slicing tissue, we normalized all FOS+ neurons to a standardized shape of the BLA to accurately compare density gradients in the BLA.

Identification of FOS. Images were pseudo-colored blue for DAPI and magenta for FOS. DAPI staining was used to visually identify the shape of the BLA based on contours provided by the

surrounding fiber tracts. We automatically identified all FOS+ neurons of a standardized size and minimum quality using the spot detection tool. These parameters remained identical across all images in the experiment. The experimenter visually observed the spots detected and manually removed any spots located outside of the BLA or within fiber tracts. Coordinates of FOS+ cells were localized relative to the most dorsal point of the BLA using the position reference frame tool (Supplementary Fig. 1A; “o”) and exported to an excel sheet for further analyses.

Normalization. First, we established the average width and height of the BLA at 7 anterior-posterior (AP) positions. For every image, we identified its approximate AP position according to the Paxinos & Watson atlas (-2.12, -2.30, -2.56, -2.80, -3.14, -3.30, -3.60; (Paxinos & Watson, 2007)) and measured the height, width, and triangular area of the BLA (Supplementary Fig. 1A-D) using Imaris Cell Imaging Software (Oxford Instruments). The formula for triangular area was: $[(\text{height} \times \text{width}) / 2]$. Any image with a triangular area exceeding two times the standard deviation of the mean for the chosen AP position was re-assigned to a more appropriate AP position. We then calculated the average width (medial-lateral axis) and height (dorsal-ventral axis) from all slices at each of these 7 AP positions, which was then rounded to the nearest 25um for standardization (Supplementary Table 2.1).

AP	Width (um)	Height (um)
-2.12	700	1500
-2.30	825	1775
-2.56	900	1950
-2.80	1175	2200
-3.14	1275	2350
-3.30	1375	2425
-3.60	1475	2650

Supplementary Table 2.1
(A) Standardized width (medial-lateral axis) and height (dorsal-ventral axis) at each AP position.

Next, we normalized coordinates of FOS+ neurons from each image according to these standardized dimensions. For each raw coordinate, the x-coordinate was normalized to the average width of the BLA at that AP position, and the y-coordinate to the average height of the BLA at that AP position. This established new x,y coordinates that maintained their original relative position in the BLA but could now be directly compared to images with a BLA of different raw dimensions.

To subdivide the BLA into the LA, LBA, and mBA subdivisions and to account for the curvature of the BLA along the medial fiber tract, a template shape was first created by manually fitting a standardized shape of the BLA derived from the Paxinos & Watson atlas (Paxinos & Watson, 2007) to all normalized FOS+ neurons in each plane, and then excluding FOS+ points outside of this template (Supplementary Fig. 1E-G). In total, the standardized shape fit 85.39% (41,111 of 48,146) of labelled cells. This established a standardized template comprised of 25um x 25um “pixels” used for representation and quantification.

Quantification. To visually represent gradients of density across the BLA, the average density of FOS+ neurons were calculated per 25um x 25um bin and represented in heatmaps using a custom MATLAB script. Each pixel value represents average density per image, averaged across animals in the same group. To compare group differences, we calculated FOS density for each animal individually and then compared group means. The total area of a subregion was calculated as: [(number of 25umx25um pixels comprising the subregion of interest) * 25um * 25um]. The density was then calculated as: [total # of FOS+ cells detected in all pixels comprising the subregion of interest / total area of subregion of interest]. As multiple images were often collected from each AP plane for each animal, data were analyzed as average density per image: [(total # of cells from all pixels comprising the subregion of interest, from all slices) / (total area of subregion of interest * number of slices)]. These calculations were streamlined using a custom MATLAB script that can be accessed at the authors’ request (mnhill@ucalgary.ca and robert.aukema1@ucalgary.ca).

Fiber photometry.

Viral vectors and fiber optic cannula. Viral vectors were injected unilaterally into the right basolateral amygdala to express the calcium-sensitive protein GCaMP6s, to allow recording of

calcium transients from CaMKII neurons in the BLA of freely moving rats. GCaMP6s was selectively expressed under the CaMKII promoter to restrict expression to BLA projection neurons. AAV.CaMKII.GCaMP6s.WPRE.SV40 (7.0×10^{12} GCs/mL) was a gift from James M. Wilson (Addgene viral prep #107790-AAV9; <http://n2t.net/addgene:107790> ; RRID:Addgene_107790). A final volume of 322nL was delivered in 32.2nL boluses every 30sec, and the capillary remained in place for 10min following delivery of the final bolus to allow for diffusion of the virus. Approximately 2 weeks were allowed for recovery before a 600- μ m diameter mono fiber optic cannula (Doric Lenses, MFC_600/630/0.48_8.6mm_MF2.5_FLT) was implanted 0.1mm above the injection site.

Handling and habituation. Following surgical implantation of the fiber optic cannula, rats were single-housed and given a minimum of 1 week to recover before undergoing experiment 1 or 2. Animals then underwent 6 days of handling and habituation. On days 1-3, animals were carted to their testing room and placed into an empty cage with only bedding for 1h, and then handled by the experimenter for 2min before returning to the colony room. On days 4-6, the same procedure occurred but animals were habituated to the optic fiber in an empty cage for 20min in the testing room. Habituation and testing cages had a lid with a small slit cut in it to allow for entry of the fiber. This occurred for all conditions except for shock, which were treated similarly except for being habituated to fear conditioning chambers equipped with metal stainless-steel rod flooring connected to a shock generator (Med Associates) rather than a testing cage.

Experiment 1: GCaMP6s Response to different stimuli. Experiments were performed during the light phase of the cycle between 8am and 6pm. On test day, animals were exposed to one of 4 conditions: crackers (n=5), shock (n=4), pickup followed by either restraint (n=5) or swim (n=5), and citral followed by bobcat urine exposure (n=7). We recorded ~15min of baseline activity in

the habituation cage immediately before animals were exposed to a stimulus (in the shock condition, baseline was recorded in the fear conditioning chamber). Some animals were exposed to multiple conditions, but testing was separated by a minimum of 5 days (which included 2 days of habituation), and the least stressful stimulus was always presented first. For cracker exposure (Supplementary Fig. 2R), rats were provided unlimited access to goldfish crackers (Pepperidge Farm) for 15min in their testing cage. For shock (Supplementary Fig. 2T), animals were exposed to 5 equally spaced shocks (0.65 mA, 1s long) over 14min. For pickup (Supplementary Fig. 2S, V), animals were briefly picked up by the experimenter for ~15sec and returned to their testing cage before repeating the pickup 15min later. After 5min of being untouched in their testing cage following the second pickup, animals were exposed for 15min to either swim (Supplementary Fig. 2S), by placing them into an opaque plastic bucket (40cm internal diameter) filled with 25 ± 2 °C water, or restraint (Supplementary Fig. 2V), by gently wrapping the animal in a towel that restricted all bodily movement. For odor exposures (Supplementary Fig. 2U), a sponge soaked in citral odor (Sigma-Aldrich; 1% in mineral oil; (Abraham et al., 2012; Slotnick, 2004)) was placed into the cage for 15min; it was then removed, and the animal remained undisturbed for 5min before placing a different sponge soaked in bobcat urine into the cage (Maine Outdoor Solutions; (Whitaker & Gilpin, 2015)). Following removal of the stimulus, recordings continued for a minimum of 5min. All animals were euthanized, perfused, and brains were collected and processed for imaging on a separate day.

Recordings. A fiber photometry system with recording parameters similar to that described in (Daviu et al., 2020) was used for experiment 1. Briefly, two excitation light-emitting diodes (LEDs, 470nm M470F3 and 405nm M405F1 from Thorlabs) were controlled by a RZ5P (Tucker-Davis Technology) processor running Synapse software (Tucker-Davis Technology). The LEDs were modulated at 211Hz (470nm) and 531Hz (405nm) to avoid contamination from room lighting. Both

LEDs were connected to a Doric Mini Cube filter set (FMC4_AE(405)_E(460–490)_F(500–550)_S) and the excitation light was directed to the animal via a mono fiber optic patch cord (Doric MFP_600/630/3000-0.48_2m_FC_MF2.5). The power of the LEDs was adjusted to provide 5-7 μ W at the end of the patch cord. The resulting signal was detected by a photoreceiver (NewPort model 2151) and demodulated by a RZ5P processor.

Exclusions. Recordings were excluded if substantial broken signal was observed such as from a broken or disconnected patch cord (n=11), missed placements of cannula outside the BLA (n=9), absence of viral expression (n=6), variable signal during the baseline epoch (n=1), or absent signal (n=1). Any noticeable artifacts in sampling regions were replaced with linear interpolation and the section was excluded from analysis (n=8 of 40 recordings). To further control for artifacts, we excluded animals displaying a significant outlier value in analyses, according to the Grubb's test (Bobcat: n=1; Citral: n=1).

Experiment 2: GCaMP6s Response to different stimuli. Experiments were performed during the light phase of the cycle between 8am and 6pm. On test day, animals were administered propranolol (Sigma Aldrich; 2mg/kg or 10mg/kg) or vehicle (0.9% saline; 2 or 5mg/ml). 10min after injections, fibers were attached to the implanted ferrules and photometry recording began. We recorded ~15min of baseline activity in the habituation cage immediately before animals were exposed to restraint or shock stress (in the shock condition, baseline was recorded in the fear conditioning chamber). Animals were gently wrapped in a towel that restricted all bodily movement to induce restraint stress. After 15min, animals were returned to the testing cage and recordings continued for a minimum of 5min. All animals were euthanized, perfused, and brains were collected and processed for imaging.

Recordings. A Doric fiber photometry system with recording parameters similar to that described in (Daviu et al., 2020) was used for experiment 2. This system consists of two excitation LEDs (465nm and 405nm from Doric) controlled by an LED drive and console running Doric Studio software (Doric Lenses). The LEDs were modulated and the resulting signal demodulated using lock-in amplification. Both LEDs were connected to a Doric Mini Cube filter set (FMC4_AE(405)_E(460-490)_F(500-550)_S) and the excitation light was directed to the animal via mono fiber optical patchcord (Doric MFP_400/460/900-0.48_2m_FC/MF2.5). The power of the LEDs was adjusted to provide 9-13 μ W at the end of the patch cord. The resulting signal was detected by a photoreceiver (NewPort model 2151).

Exclusions. Recordings were excluded if substantial broken signal was observed such as from a broken or disconnected patch cord (n=3, all during shock), missed placements of cannula outside the BLA (n=2 in all groups), or absence of signal due to no viral expression (n=4). Sections of individual traces with significant motion artifacts were excluded from analysis (first restraint: n=1 (PROP); second restraint: n=3 (VEH), n=1 (PROP)).

Data analysis. Analysis was conducted for both experiment 1 and 2. Fluorescent signal data were processed in real time and acquired at a sampling rate of 1 kHz. Data were then exported to MATLAB (MathWorks) for offline analysis using custom-written scripts (Molina, 2021) and similar to (Daviu et al., 2020). Data were first downsampled to 100 Hz. Photobleaching was modeled by fitting an exponential decay on a smoothed portion of the data (low-pass filter at 0.1Hz) and subtracted from the 470nm and 405nm signals. Fast oscillations were removed with a low-pass filter (10Hz). The 405nm signal was then fitted to the 470nm using a robust polynomial regression. The change in fluorescence (ΔF) was then calculated by subtracting the 405nm Ca²⁺-independent baseline signal from the 470nm Ca²⁺-dependent signal at each time point. Within-

animal analyses were performed on the resulting z-score calculation using the following equation: $z=(F-F_0)/\sigma F$, where F is the test signal, F_0 and σF are the mean and standard deviation of the baseline signal. All photometry recordings were TTL-linked to a camera to allow precise time-locking of stimulus onset and termination. This was necessary as the length of time required to initiate or terminate a stressor was variable (for example, placing an animal into restraint). Thus, for recordings where the stimulus exceeded 15min, a section of the trace was deleted 120sec prior to stress termination, to ensure the total duration was exactly 15min. For recordings where the stimulus was less than 15min, a section of the trace was shifted 120sec prior to stress termination (leaving a gap in data for those time-points), to ensure the total duration was exactly 15min.

For experiment 1, the baseline epoch was determined as the 120sec immediately prior to stimulus onset. To compare average activity patterns upon onset of stimulus exposure, the average z-scores of each of the first 3 5min epochs were calculated among animals exposed to the same condition, and then compared between groups (Fig. 2L-R). To compare the average magnitude of initial response, the average z-score change from baseline was calculated for each animal, averaged among animals exposed to the same condition, and then compared to the “pickup” condition (Fig. 2K). To compare the average peak z-score, the average z-score in a 10sec rolling window was calculated for each animal, averaged among animals exposed to the same condition, and then statistically compared to the “pickup” condition (Fig. S2W).

For experiment 2, the baseline epoch was determined as the 120sec immediately prior to stimulus onset. To compare average activity between PROP- or VEH-treated animals in the first 1min or entire 15min following stress onset, or the 25min following stress termination, the average z-score of was calculated for each animal for that epoch and then compared between groups (Fig. 3C-E).

Chemogenetic inhibition.

Viral vectors. Viral vectors were injected bilaterally into the basolateral amygdala to express either the control fluorophore mCherry or the G_i-coupled receptor hM4D(Gi), which inhibits neural activity upon activation with a designer drug (cite). mCherry or hM4D(Gi) were selectively expressed under the CaMKII promoter, to restrict expression to BLA projection neurons. AAV8.CaMKII.hM4Di.mCherry ($1.6\text{--}2.5 \times 10^{13}$ GCs/mL) was a gift from Bryan Roth (Addgene viral prep # 50477-AAV8 ; <http://n2t.net/addgene:50477> ; RRID:Addgene_50477) and AAV8.CaMKii.mCherry (1.3×10^{13} GCs/mL) was a gift from Université Laval. Constructs were diluted in 0.01M of sterile PBS to reach desired titer. A final volume of 220.8–276nL was delivered in 27.6nL boluses every 30sec, and the capillary remained in place for 10min following delivery of the final bolus to allow for diffusion of the virus. A minimum of 3 weeks were allowed for recovery and sufficient viral expression before experiments began.

Handling and habituation. Animals were habituated to the test room for 1 hour each morning for 3 days prior to experiment day, and each animal was handled by the experimenter for 2min in the position used for injections on test day.

Experimental testing. On experimental day, animals were injected intraperitoneally (*i.p.*) with either CNO (Cayman Chemical; 3mg/kg at 1mg/ml), to activate hM4D(Gi), or vehicle (0.2% DMSO in 0.9% saline), and 30min later were moved to a separate room and immediately placed into clear Plexiglas restraint tubes for 30min. The experimenter was blinded to viral condition of the animal (mCherry vs hM4D(Gi)). Blood samples were collected immediately at initiation (t0) and termination (t30) of restraint stress. Following stress exposure, animals returned to their home cage and remained in the testing room. 90min following stress onset, animals were anesthetized, perfused, and brains were collected and processed.

cFos colocalization with hM4D(Gi) or mCherry. A sample of hM4Di/VEH (n=4) and hM4Di/CNO (n=3) animals were randomly chosen for confocal imaging on a Leica TCS SPE II confocal microscope using a 20X / 0.55 NA HC PL FLUOTAR (Leica 5065190) objective. Only slices with expression in the BLA were included for analysis (hM4Di/VEH n=39 from 4 animals; hM4Di/CNO n=40 from 3 animals), and location of imaging within the BLA occurred in regions with maximal hM4D(Gi)-mCherry expression. cFos, hM4Di-mCherry, and DAPI signals were acquired independently and exported to ImageJ for quantification. Number of cells expressing cFos, hM4D(Gi)-mCherry, or colocalization of both signals were counted manually. Colocalization was determined as a cFos signal bound by expression of hM4D(Gi)-mCherry. The experimenter was blinded to the condition of each animal, and all imaging and threshold parameters remained identical across image acquisition and quantification.

Exclusions. Animals were excluded from statistical analysis if there was significant expression outside of the BLA (Experiment cohort: n=5 hM4Di/CNO, n=5 hM4Di/VEH; Control Cohort: n=1 hM4Di/VEH, n=1 mCherry/CNO), no expression in at least one hemisphere (Experiment cohort: n=5 hM4Di/CNO, n=2 hM4Di/VEH; Control cohort: n=1 hM4Di/VEH), or sufficient plasma was not available to perform ELISA for corticosterone analyses (Experiment cohort: n=1 hM4Di/VEH; Control cohort: n=2 hM4Di/VEH, n=1 mCherry/CNO)

Optogenetic stimulation.

Viral vectors. Viral vectors were injected bilaterally into the basolateral amygdala to express either the control fluorophore mCherry or the excitatory opsin ChR2, which increases neural activity upon activation with 473nm light (cite). mCherry or ChR2 were selectively expressed under the CaMKII promoter, to restrict expression to BLA projection neurons. AAV5-CaMKII-

hChR2(H134R)-mCherry (4.6×10^{12} GCs/mL) was a gift from Karl Deisseroth (Addgene viral prep #26975-AAV5; <http://n2t.net/addgene:26975>; RRID:Addgene_26975) and AAV8.CaMKii.mCherry (6.7×10^{12} GCs/mL) was a gift from Université Laval. A final volume of 828.0nL was delivered in 69nL boluses every 45sec, and the capillary remained in place for 10min following delivery of the final bolus to allow for diffusion of the virus. Approximately two weeks later a 600- μ m diameter mono fiber optic cannula (Doric Lenses, MFC_600/630/0.48_8.6mm_MF2.5_FLT) was implanted 0.1mm above the injection site.

Handling and habituation. Following surgical implantation of the fiber optic cannula, rats were single-housed and given a minimum of 4 days before handling and habituation began. Animals then underwent 10 days of habituation and handling. On days 1-6, animals were carted to the testing room each morning and handled for 1min each, and then placed into an empty cage with only bedding for ~90min. On days 7-10, the same procedure occurred but animals were also habituated to the optic fiber (no light) attached to their heads while exploring their test cage. Habituation and testing cages had a lid with a slit cut in it to allow for entry of the fiber.

Experimental testing. On experimental day, animals were carted to the testing room 1 hour prior to testing. The light source (for ChR2: 473nm, Laserglow Technologies LRS-0473-GFM-00100-05 LabSpec 473nm DPSS Laser System connected to Laser Power Supply PSU-III-LED) was connected to the implanted ferrules with a fiber optic cable (600um core diameter, Doric Lenses) attached to a beam splitter. The lasers were controlled using the open-source programmable pulse generator Pulse Pal (J. I. Sanders & Kepecs, 2014). Blue light (5ms long pulses; 10 mW laser intensity measured at the tip) was shone at 20 Hz for 15min. Light intensity was measured using a Standard Photodiode Power Sensor (ThorLabs S120C) connected to a Compact Power and Energy Meter Console (ThorLabs PM100D). The experimenter was blinded to viral condition

(mCherry vs ChR2) of the animal. The animal remained connected to the fiber for an additional 15min (30min total) and then removed and returned to their home cage. In the first experiment (mCherry n=7; ChR2 n=7), blood samples from the lateral tail vein were collected to measure plasma corticosterone 30, 60, and 90min following onset of 473nm stimulation. Animals were anesthetized, perfused, and brains were collected for verification of viral expression. In the second experiment (mCherry n=5, ChR2 n=6), no blood samples were collected; rather, 90min following onset of 473nm stimulation animals were anesthetized, perfused, and brains were to verify viral expression and perform immunohistochemistry for cFos.

cFos colocalization with ChR2 or mCherry in the BLA. After immunohistochemistry for cFos, images were acquired for each animal on a Leica TCS SPE II confocal microscope using a 20X / 0.55 NA HC PL FLUOTAR (Leica 5065190) objective. Only slices with expression in the BLA were included for analysis (n=3-9 images per animal), and location of imaging within the BLA occurred in regions with maximal mCherry or ChR2 fluorophore expression. cFos, ChR2 or mCherry fluorophore, and DAPI signals were acquired independently and exported to ImageJ for quantification. Number of cells expressing cFos were counted automatically, and ChR2-mCherry, mCherry, or colocalization of either signal with cFos were counted manually. Colocalization was determined as a cFos signal bound by expression of ChR2-mCherry. The experimenter was blinded to the condition of each animal, and all imaging and threshold parameters remained identical across image acquisition and quantification.

cFos quantification in the PVN. After immunohistochemistry for cFos, a 1-in-4 series of 40um thick sections was collected and images were acquired for each animal on a Leica DM4000 B LED microscope using a 20X objective / 0.55 NA HC PL FLUOTAR (Leica 5065190) objective. DAF and L5 filter cubes were able to detect expression of DAPI and Alexa488 (to label anti-cFos),

respectively. Images were acquired bilaterally in defined regions of interest across the anterior-posterior axis of the PVN (Figure S4N). Only images from slices with an intact region-of-interest were acquired (mCherry n= 31 images from 17 slices from 5 animals; ChR2 n=61 images from 32 slices from 6 animals).

Exclusions. Animals were excluded from statistical analysis if the cannula tip or significant viral expression was outside of the BLA (Experiment 1 (CORT): n=2 mCherry, n=4 ChR2; Experiment 2 (FOS): n=1 mCherry, n=4 ChR2), animals required euthanasia due to surgical complications (Experiment 1 (CORT): n=2 ChR2; Experiment 2 (FOS): n=1 mCherry), or cFos or CORT values were considered a statistical outlier (Experiment 1 (CORT): n=1 mCherry, n=1 ChR2; Experiment 2 (FOS): n=1 ChR2). An outlier was defined as cFos or CORT values being twice the standard deviation of the mean of that group at any time-point.

Statistics. GraphPad Prism 9 software was used for all statistical analyses. When comparing differences between group means of a single data point, an ordinary one-way ANOVA was used. Dunnett's multiple comparisons test was followed when comparing to the naïve condition; Tukey's multiple comparisons test followed when comparing between all groups. When comparing differences between groups at multiple points (e.g., time), a 2Way ANOVA was used followed by Sidak's multiple comparison's test. When data points were missing or excluded, a mixed-effects ANOVA was used after performing the Greenhouse-Geisser correction. When comparing within-subjects differences at multiple points, we used repeated measures one-way ANOVA followed by Dunnett's multiple comparisons test to the baseline epoch. When comparing within-subjects differences at two points, we used a two-tailed paired t-test. When comparing differences between two group means, a two-tailed unpaired t-test was used.

2.4 RESULTS

Aversive stimuli induce a common spatial activation pattern in the basolateral amygdala.

All stressors lead to activation of the HPA axis (Herman et al., 2003). However, the magnitude of this response is known to differ across stressors of varying modalities (Armario et al., 1986; Kant et al., 1983), and novel stimuli, which are not aversive, also have the capacity to both activate the BLA and drive an HPA response. Thus, we first characterized the HPA response to six novel stimuli in adult male rats, including four aversive stimuli (stressors): restraint (Di et al., 2016), shock (Morena et al., 2019), swim (Masaki & Nakajima, 2005), and bobcat urine (Whitaker & Gilpin, 2015); and two stimuli which are not aversive, but are novel and mildly appetitive: crackers (Modlinska et al., 2015) and citral odour (Saraiva et al., 2016) (Figure 2.1A). Compared to the naïve condition, plasma CORT was increased 30min following exposure to shock, swim, and restraint, and remained elevated 90min following shock (Figure 2.1B-C). To compare the magnitude of the HPA response to different stimuli, we also calculated the area-under-the-curve (AUC). Restraint and swim exhibited a larger AUC than crackers, citral odour, shock, and bobcat urine; and shock exhibited a greater AUC than crackers or citral odour (Figure 2.1D).

Psychogenic stressors reliably activate neurons in the BLA (Herman et al., 2003). However, the BLA is highly heterogenous in anatomy (Sah, Faber, Lopez De Armentia, et al., 2003), connectivity (Beyeler et al., 2018; Reppucci & Petrovich, 2016), and function (Janak & Tye, 2015). As such, we hypothesized that the BLA is not uniformly activated by stress, but rather, exhibits biased activation towards distinct subregions that mediate appropriate behavioural and physiological outcomes.

We therefore used immunohistochemistry to map spatial patterns of activation within the BLA using the activity-responsive protein FOS following exposure to different stressors (Figure 2.1E). As predicted, all stimuli significantly increased overall FOS density within the BLA compared to the naïve condition (Figure 2.1F). To visualize patterns of FOS expression, we

localized each FOS+ cell relative to the most dorsal point of the BLA and normalized its position according to the average size and shape of the BLA at each anterior-posterior (AP) plane (Supplementary Figures 2.1A-D); we then created heatmaps for each stimulus representing density of FOS+ cells (Figure 2.1G). This visually identified a regional activation bias for each

Figure 2.1

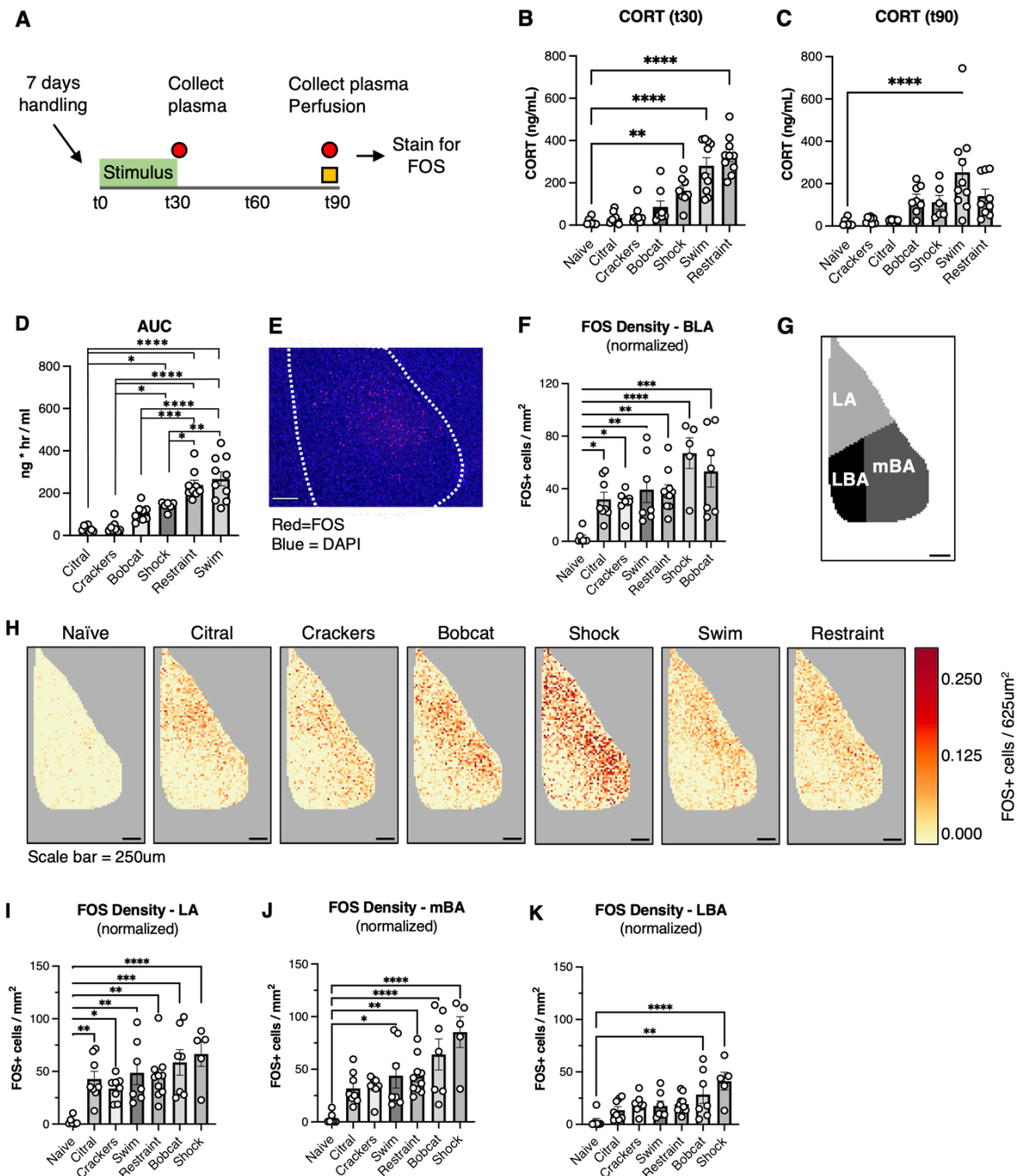


Figure 2.1. Aversive stimuli induce a common spatial activation pattern in the basolateral amygdala.

(A) Overview of experimental procedures.

(B) Plasma CORT 30min following stimulus onset (n=8-10 per group; $F_{6,53}=24.99$, $p<0.0001$).

(C) Plasma CORT 90min following stimulus onset (n=6-10 per group; $F_{6,50}=6.376$, $p<0.0001$).

(D) t30 to t90 area-under-the-curve (AUC) of plasma CORT from t30 to t90 (n=6-10 per group; $F_{5,43}=24.98$, $p<0.0001$).

(E) Representative image of FOS+ neurons following exposure to restraint; scalebar=150um.

(F) Density of FOS+ neurons in the BLA following exposure to each novel stimulus (n=5-10 per group; $F_{6,45}=6.571$; $p<0.0001$).

(G) Heatmaps representing density of normalized FOS+ expression in 25umx25um bins at AP -2.80. Darker colours represent higher FOS density, as shown on colour bar.

(H) BLA subdivisions at AP -2.80: lateral amygdala (LA), lateral basal amygdala (LBA), and medial basal amygdala (mBA). Scalebar=250um

(I-K) Normalized FOS density in each BLA subdivision (n=5-10 per group; LA: $F_{6,45}=5.530$, $p=0.0002$; mBA: $F_{6,45}=7.581$, $p<0.0001$; LBA: $F_{6,45}=5.096$, $p=0.0005$).

All comparisons were performed using Ordinary One-Way ANOVA; post hoc comparisons were performed using Dunnett's multiple comparisons test to the naïve condition except in Fig. 1D, which used Tukey's multiple comparison's test.

FOS+ neurons were quantified across the entire BLA (AP -2.12 to AP -3.60) and normalized according to average BLA dimensions at each AP position and number of slices. Error bands represent mean +/- SEM. * $p<0.05$, ** $p<0.01$, *** $p<0.001$, **** $p<0.0001$.

stimulus. To quantify the expression bias observed at a gross anatomical level, the BLA was divided into lateral (LA), medial basal (mBA), and lateral basal (LBA) subdivisions (Figures 2.1H; Supplementary Figure 2.1E-G) and average density of FOS for each stimulus was compared to the naïve condition.

This identified a subtle but important difference between aversive and non-aversive stimuli. Specifically, exposure to any novel stimulus (aversive or non-aversive) significantly

increased FOS+ density in the LA (Figure 2.1I). Conversely, only aversive stimuli – restraint, swim, shock, and bobcat urine – significantly increased FOS+ density in the mBA (Figure 2.1J), and only shock and bobcat urine significantly increased FOS+ density in the LBA (Figure 2.1K). There were no significant differences in expression of FOS across the rostral-caudal axis in any condition (Supplementary Figures 2.1H-N). Collectively, these data suggest that although the BLA is responsive to novel stimuli primarily through activation of the LA, activation of the mBA is selectively responsive to aversive, stressful stimuli. This positions the mBA in a central role in processing of stressful stimuli that is distinct from general encoding of novelty by the LA.

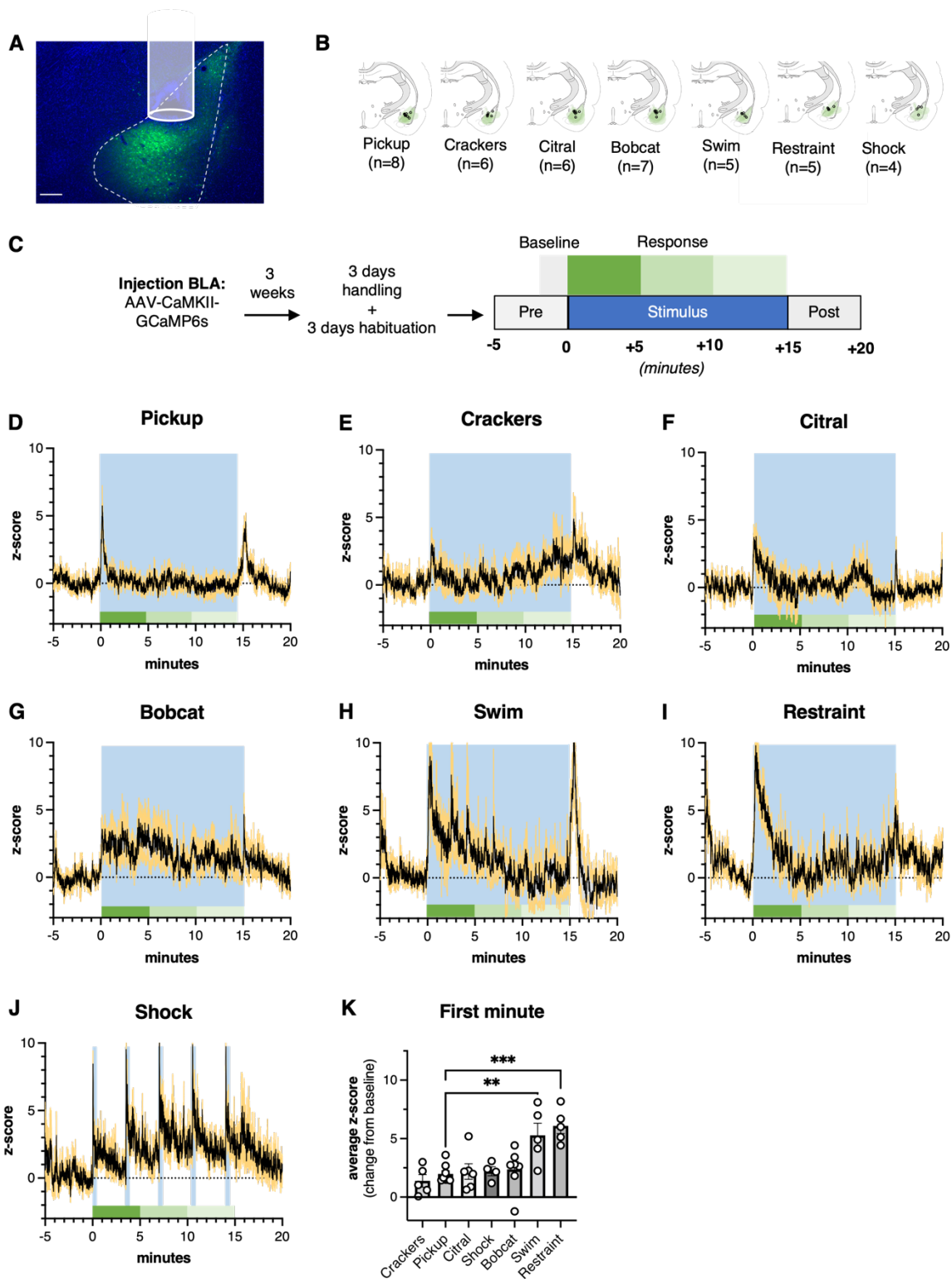
Distinct novel stimuli elicit distinct temporal patterns of activation in the medial basal amygdala.

FOS mapping provides an excellent description of spatial, anatomical patterns of activation but cannot adequately detect rapid differences in temporal patterns of coordinated activity. Stress typically drives peak activation of the BLA within the first 30min of exposure (Cullinan et al., 1995) and activation decreases with repeated presentation of homotypic, anticipatory stressors (N. M. Grissom & Bhatnagar, 2011). However, very little is known precisely when, how long, and in what temporal patterns activation is occurring acutely throughout a single, acute exposure to novelty. Further, we had not identified specific cell types that expressed FOS, an important caveat given that many different cell types in the BLA are activated in response to stress including parvalbumin- and calbindin-positive interneurons (Mineur et al., 2022; Reznikov et al., 2008). To address both these questions, we used fiber photometry to record neuronal Ca^{2+} transients specifically in excitatory CaMKII+ projection neurons in real time (Gunaydin et al., 2014). GCaMP6s was virally expressed in CaMKII+ neurons and an optic fiber was implanted directly above the mBA, the subregion we identified as particularly responsive to stressful stimuli,

and habituated animals to their testing environment and fiber for 3 days prior to testing. We then recorded Ca^{2+} -associated fluorescence upon exposure to either restraint, bobcat urine, shock, swim, citral odour, crackers, or a brief pickup by the handler (Figures 2.2A-C, Supplementary Figures 2.2Y-CC). To control for changes in fluorescence unassociated with neural activity, we simultaneously recorded Ca^{2+} -insensitive GCaMP fluorescence using 405nm light and then subtracted this signal from the Ca^{2+} -associated signal (465nm) after scaling it to fit using robust polynomial regression. This provided a motion-corrected Ca^{2+} signal that was then normalized to a z-score to compare across animals (Martianova et al., 2019; Reed et al., 2018) (Supplementary Figures 2.2A-C).

Distinct temporal patterns of Ca^{2+} -associated fluorescence were observed following presentation of each stimulus (Fig. 2.2D-J; Supplementary Figures 2.2D-J) without any significant changes in Ca^{2+} -independent fluorescence (Supplementary Figures 2.2K-X). Exposure to pickup, bobcat urine, swim, restraint, or shock all significantly increased average GCaMP6s fluorescence in the first 5min immediately following stimulus onset relative to baseline (Figures 2.2L, O-R). There was no significant increase in GCaMP6s fluorescence in animals exposed to the non-aversive stimuli: citral odour or crackers (Figures 2M-N), again supporting that the mBA is selectively and rapidly sensitive to stressful stimuli. However, even among stressors, there were clear differences in the temporal dynamics of activation between stimuli. To quantify this, we used the response to pick-up as a reference, which all animals had been habituated to prior to testing. Only animals exposed to restraint or swim had significantly greater GCaMP6s fluorescence in the first 60sec than those picked up (Figure 2.2K). Additionally, only these two groups also had a significantly greater sustained 10sec peak than those picked up (Supplementary Figure 2.2DD).

Figure 2.2



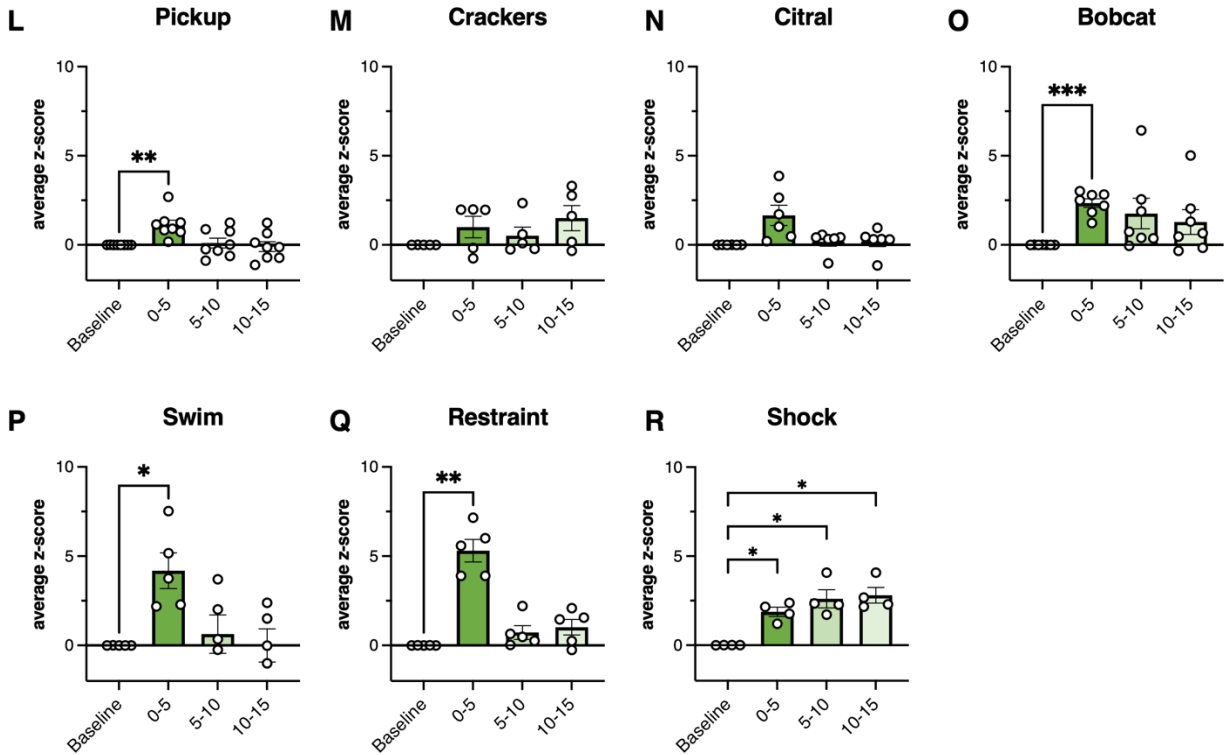


Figure 2.2. Distinct novel stimuli elicit distinct temporal patterns of activation in the mBA

(A) Representative image of GCaMP6s expression and ferrule placement. Scalebar=250um; dashed lines delineate BLA.

(B) Representative images of GCaMP6s expression (green) and locations of ferrule tips (o) for each group.

(C) Overview of experimental procedures. Blue represents exposure to stimulus; gray epoch indicates 120sec baseline recording; green epochs indicate 60sec epochs following stimulus onset analyzed in Fig 2k-q.

(D-J) Temporal patterns of GCaMP6s fluorescence in BLA CaMKIIa+ neurons following novel exposure to each stimulus (n=4-8 per group). Values are normalized to the mean z-score of the 120sec baseline epoch immediately preceding stimulus onset. Blue band indicates stimulus exposure; green blocks indicate 5min epochs used for analyses; black line represents mean z-score of all animals in that condition; gray bands represent SEM.

(K) Change from baseline of average z-score in the first minute following stimulus onset (n=4-8 per group). Data were analyzed using ordinary one-way ANOVA ($F_{6,33} = 7.736$, $p < 0.0001$ followed by Dunnett's multiple comparisons test).

(L-R) Average z-score of baseline vs. 3x5min epochs following stimulus onset (n=4-8 per group). Data were analyzed using a RM one-way ANOVA (pickup: $F_{2,155, 15.08} = 5.616$, $p = 0.0137$;

crackers: $F_{1,815,7.262}=3.005$, $p=0.1143$; citral: $F_{1,100,5.501}=4.211$, $p=0.0888$; bobcat: $F_{1,138,6.827}=4.776$, $p=0.0633$; swim: $F_{2,388,9.544}=7.799$, $p=0.0081$; restraint: $F_{1,719,6.877}=37.62$, $p=0.0002$; shock: $F_{1,433,4.328}=22.33$, $p=0.0062$; followed by Dunnett's multiple comparison's test to the baseline epoch. Error bars represent mean \pm SEM. * $p<0.05$, ** $p<0.01$, *** $p<0.001$, **** $p<0.0001$.

Thus, swim and restraint induced the largest initial GCaMP6s response, and while shock and bobcat odor did not mount as robust initial responses as swim and restraint they did exhibit more prolonged elevations in GCaMP6s fluorescence. Interestingly, swim and restraint stressors evoked the largest corticosterone response (Figure 2.1D), while shock and bobcat produced the largest FOS responses (Figure 2.1F). This suggests that a large, initial coordinated activation in the mBA may relate to the HPA response to stress, while more moderate, but sustained, changes in calcium signaling may relate to elevations in FOS within the mBA, consistent with the calcium dependence of the activation of this protein.

Systemic administration of propranolol blunts stress-induced response of BLA projection neurons.

Next, we tested the contribution of neuromodulators that may influence activation within the mBA. We specifically investigated the role of the β -noradrenergic receptor, a Gs-coupled receptor that is widely expressed throughout the BLA (Qu *et al*, 2008). Importantly, the main ligand for this receptor, norepinephrine, is readily released in the BLA during stress exposure (Galvez *et al*, 1996) and is known to drive stress-related processes such as increased anxiety-like behaviour (McCall *et al*, 2017) and memory enhancement (LaLumiere *et al*, 2003).

Therefore, we tested if we could influence the response of mBA projection neurons to stress by systemically administering propranolol, a β -noradrenergic receptor antagonist, 30min prior to stress exposure. We virally expressed GCaMP6s in mBA CaMKii neurons (Figure 2.3A),

and then animals were tested over two sessions, separated by two weeks, and randomly assigned to a treatment group (VEH vs PROP) each session (Supplementary Figure 2.3A). Pre-treatment with a low dose of propranolol (2mg/kg, *i.p.*) had no effect on stress-induced changes in GCaMP6s fluorescence in BLA CaMKii+ neurons during restraint stress (Supplementary Figure 2.3B). However, two weeks later, pre-treatment with a high dose of propranolol (10mg/kg, *i.p.*) 30min prior to restraint stress significantly reduced average GCaMP6s fluorescence in BLA CaMKii+ neurons during both the first 1min and entire 15min restraint episode, without influencing average GCaMP6s fluorescence upon termination of the stressor (Figures 2.3B-E). This suggests that noradrenergic signaling contributes to activation of the mBA during stress exposure, and systemic administration of propranolol reduces stress-induced activation of mBA projection neurons.

Figure 2.3

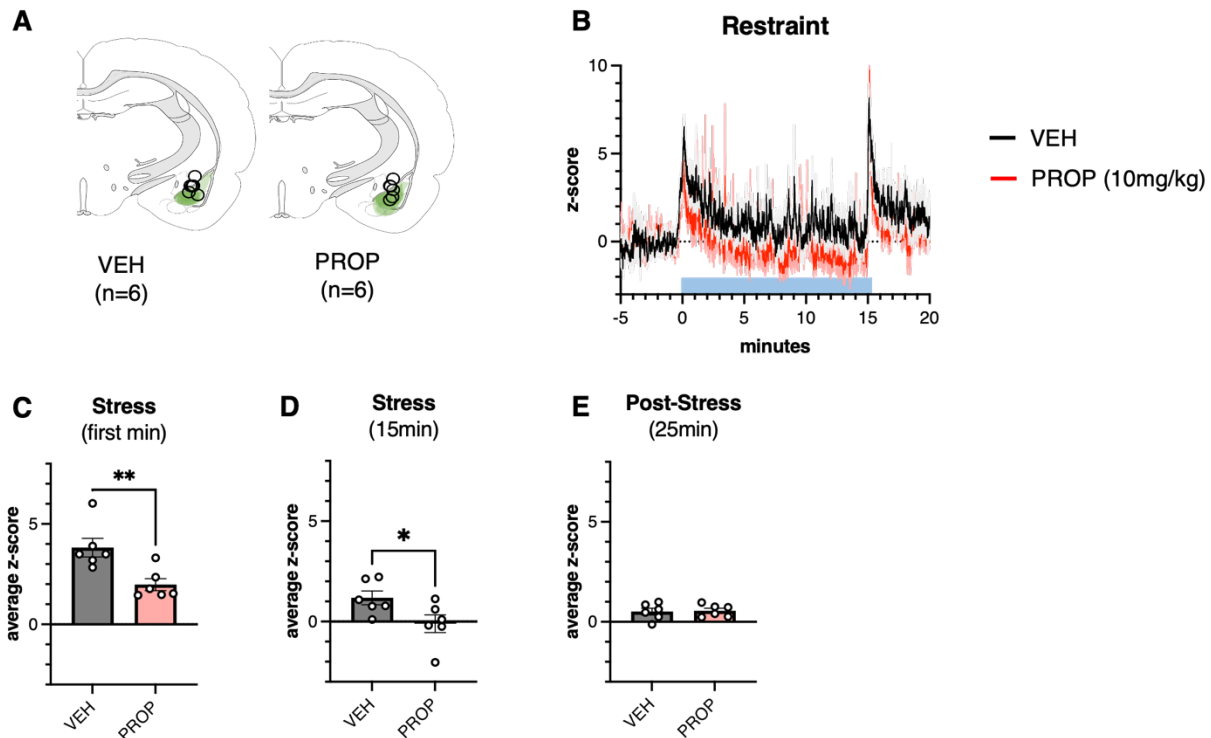


Figure 2.3. Propranolol reduces stress-induced activation of the basolateral amygdala

(A) Representative images of GCaMP6s expression (green) and locations of ferrule tips (o) for each group.

(B) GCaMP6s fluorescence in BLA CaMKIIa+ neurons following exposure to restraint stress, with either saline or propranolol (10mg/kg *i.p.*) administered 30min prior to stress exposure (n=6 per group). Blue block indicates stress exposure.

(C-E) Average z-score in VEH vs. PROP treated animals (n=6 per group) in first 1min or 15min of stress, or 25min immediately following stress termination. Data were analyzed using an unpaired t-test (First Min: $t_{10}=3.342$, $p=0.0075$; First 15min: $t_{10}=2.309$, $p=0.0436$; First 25min following stress: $t_{10}=0.2108$, $p=0.8373$).

Error bars represent mean \pm SEM. * $p<0.05$, ** $p<0.01$, *** $p<0.001$, **** $p<0.0001$.

mBA projection neurons bidirectionally influence corticosterone release.

To test if activation of mBA projection neurons is necessary or sufficient for release of CORT, we measured plasma CORT following chemogenetic inhibition during stress, or optogenetic activation under non-stress conditions, of CaMKII+ neurons in this subregion. First,

we expressed an inhibitory Gi DREADD (hM4Di (Armbruster et al., 2007)) or a control protein (mCherry) in mBA CaMKii+ neurons (Figure 2.4A-B). Animals were tested 3 weeks later to allow for sufficient viral expression. In slice, CNO led to Gi-mediated neural inhibition in hM4Di+ but not mCherry+ cells (Supplementary Figures 2.4A-C), confirming its specificity on only transduced cells. Prior to behavioural testing, animals were handled for 3 days to habituate to the experimenter and testing environment. On test day, VEH or CNO (3mg/kg, 1mg/ml *i.p.*) was administered 30min prior to a 30min restraint stress episode and we then collected plasma at initiation and termination of stress to measure circulating corticosterone (Figure 2.4C). We selected restraint as our stressor as it had reliably and consistently induced strong CORT release.

We first established that CNO reliably reduced activation of hM4Di+ cells *in vivo* by quantifying stress-induced FOS expression in the BLA of a subset of animals (Supplementary Figure 2.4D). There were no significant differences between groups in number of hM4Di+ cells in the BLA (Supplementary Figure 2.4E), but there was significantly less number (Supplementary Figure 4F) and percentage (Supplementary Figure 2.4G) of hM4Di+ cells also expressing FOS. Interestingly, CNO led to significantly greater FOS expression in the BLA of hM4Di+ animals (Supplementary Figure 2.4H). Collectively, this confirms that CNO effectively and specifically inhibited hM4Di+ cells in the BLA *in vivo*. We next examined if there was any effect of CNO in the absence of hM4Di expression, given its known off target effects at 5-HT receptors which could influence HPA axis responses to stress (Bærentzen et al., 2019). There was no difference in basal or stress-induced CORT in hM4Di+ animals administered VEH, and mCherry+ animals administered CNO, confirming that CNO at this dose does not influence stress-induced activation of the HPA axis in the absence of hM4Di (Figure 2.4D, Supplementary Figure 2.4I). Thus, we performed all subsequent experiments in hM4Di+ animals using VEH as our control condition and CNO as our experimental treatment.

Indeed, CNO treatment of animals expressing hM4Di in the mBA had significantly lower CORT 30min following stress onset than those expressing the control mCherry protein (Figure 2.4E). These data demonstrate that inhibition of mBA pyramidal neurons reduces stress-induced CORT release.

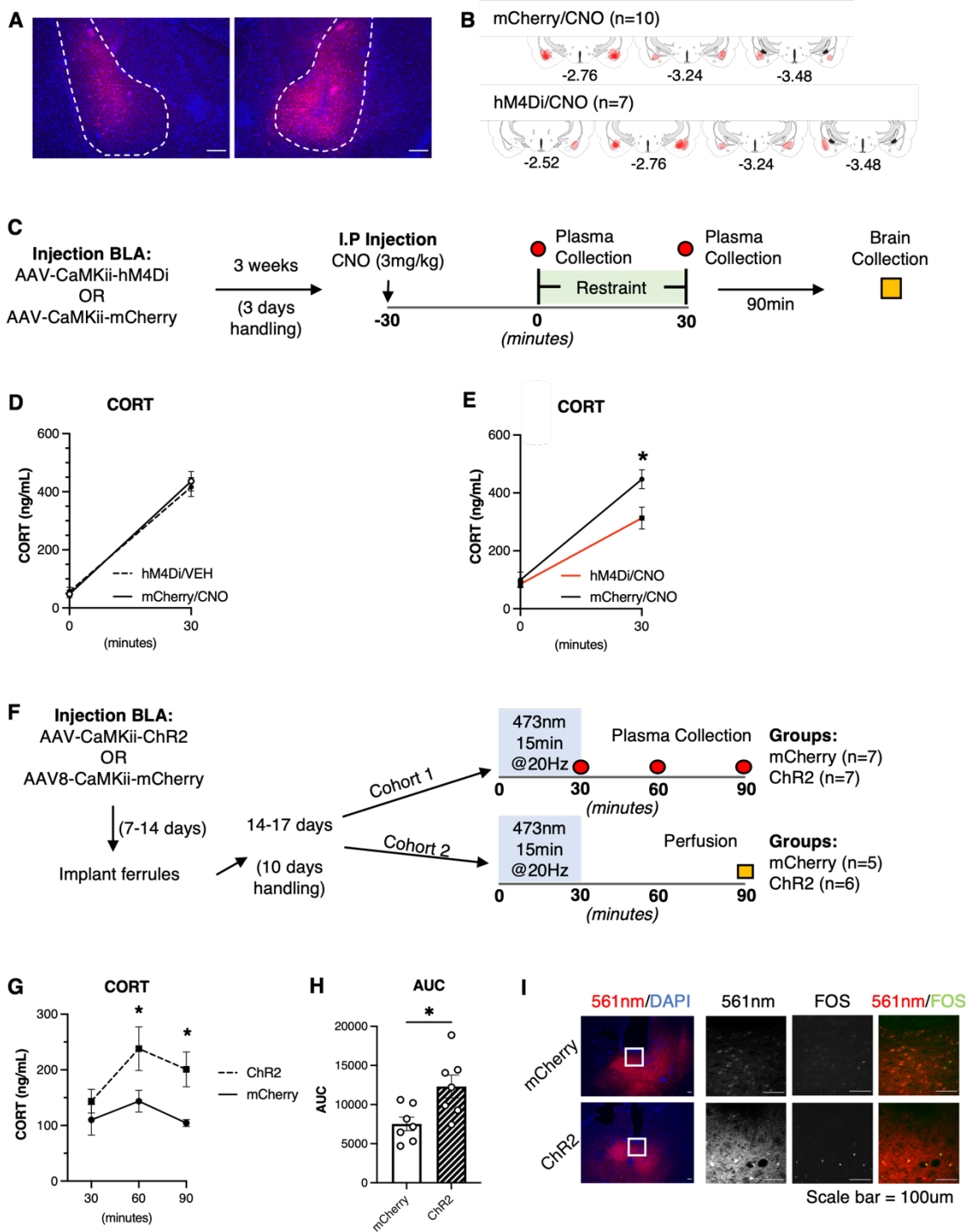
We next tested whether stimulation of mBA CaMKii+ neurons was sufficient to increase plasma corticosterone in the absence of stress. We expressed the light-activated ion channel ChR2 or the mCherry control protein in BLA CaMKii+ neurons using a viral strategy (Supplementary Figures 2.4J-L). Patch-clamp electrophysiology confirmed that stimulation with 473nm light increased firing of BLA neurons expressing ChR2 (Supplementary Figures 2.4M-Q).

We then tested the effects of mBA CaMKii stimulation *in vivo*. Animals were handled and habituated to their fibres and testing cage for 10 consecutive days to ensure maximal habituation to optic fibers and establish appropriate baseline stress levels. On test day, 473nm light was delivered through fibre-optic cannulas for 15min (10mW; 20Hz) and plasma was collected 30, 60, and 90min following the initiation of light delivery (Figure 2.4F, cohort 1). Animals expressing ChR2 had significantly greater plasma CORT following optical stimulation than those expressing mCherry, particularly 60 and 90min following onset of stimulation (Figures 2.4G,H). Together, these data demonstrate that activation of projection neurons in the mBA is sufficient to drive CORT release in the absence of stress.

To confirm that ChR2-mediated activation of mBA projection neurons was also associated with increased activity of PVN neurons, we collected brains 90min following light stimulation in a separate cohort of animals to quantify FOS expression in the BLA and PVN (Figure 2.4F, cohort 2). Predictably, 473nm light increased FOS expression in the mBA of animals expressing ChR2, particularly in fluorescently labelled cells (Figures 2.4I-K). Animals expressing ChR2 in the mBA also exhibited a greater number of FOS+ cells in the PVN than mCherry controls (Figures 2.4L, Supplementary Figure 2.4R), confirming that activation of the mBA leads to activation of the HPA

axis. Collectively, these data strongly support that CaMKii+ neurons in the mBA bidirectionally influence HPA axis activation.

Figure 2.4



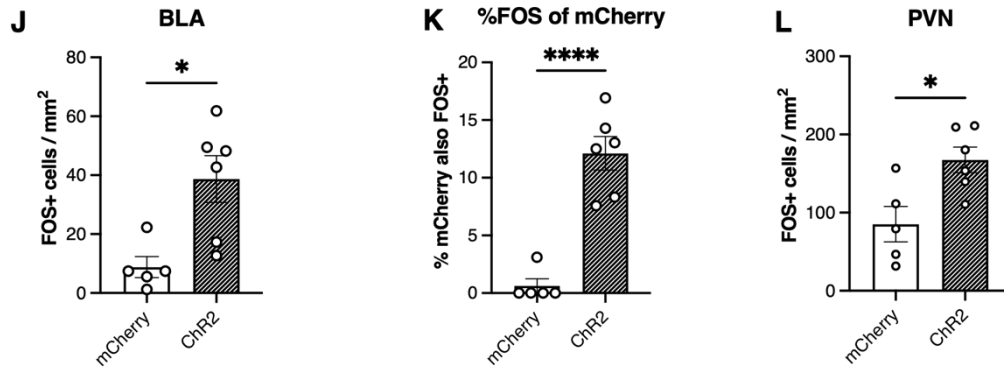


Figure 2.4. BLA projection neurons bidirectionally influence HPA activation and corticosterone release

(A) Representative image of hM4Di expression (red). Dashed lines delineate BLA. Scale bar = 250um

(B) Representative images of hM4Di or mCherry control expression. Red indicates area of maximal expression.

(C) Overview of the experimental procedure.

(D) Average plasma CORT levels in animals expressing mCherry and administered CNO vs animals expressing hM4Di and administered VEH. Data were analyzed using a mixed effects analysis (n=6-7 per group; $F_{1,8}=1.100$, $p=0.3249$).

(E) Average plasma CORT levels in animals expressing mCherry (solid line) or hM4Di (dashed line). Data were analyzed using a 2Way ANOVA (n=7-10 per group; Interaction: $F_{1,15}=7.254$, $p=0.0167$; followed by Sidak's multiple comparisons test).

(F) Overview of experimental procedures.

(G) Plasma CORT in ChR2- vs mCherry-expressing animals following stimulation with 473nm light. Data were analyzed using a 2way ANOVA ($F_{1,12}=9.208$; $p=0.0104$; Sidak's test for multiple comparisons),

(H) Area-under-the-curve (AUC) from t30 to t90 in ChR2- vs mCherry-expressing animals. Data were analyzed using an unpaired t-test ($t_{12}=2.823$, $p=0.0154$).

(I) Representative images of mCherry (top row) or ChR2 (bottom row) expression and co-localization with FOS. Blue=DAPI, green=FOS, red=mCherry control or hM4Di.

(J) Density of FOS expression in the BLA following stimulation with 473nm light in mCherry vs ChR2-expressing animals. Data were analyzed using a two-tailed unpaired t-test ($t_{(9)}=3.203$; $p=0.0108$).

(K) Colocalization of viral proteins with FOS. Data were analyzed using a two-tailed unpaired t-test ($t_{(9)}=6.733$; $p<0.0001$).

(L) PVN FOS expression following stimulation with 473nm light in mCherry vs. ChR2-expressing animals ($t_{(9)}=3.016$; $p=0.0146$).

2.5 DISCUSSION

The BLA is widely considered to be a central stress hub; it is robustly activated by psychological stressors (Reznikov et al., 2008; van Marle et al., 2009) and is involved in many stress-related processes such as anxiety-like behaviour, sympathetic activation, and memory (Felix-Ortiz et al., 2016; McCall et al., 2017; Paré, 2003; Petrovich et al., 2002; Soltis et al., 1997; Tye et al., 2011). However, evidence for the contribution of the BLA to the endocrine response is limited and equivocal, possibly due to the heterogeneity of BLA neurons in responding to stimuli of both positive and negative valence (Herman et al., 2020; Janak & Tye, 2015). Thus, we first characterized spatial and temporal patterns of activation in response to a range of psychological stressors, to determine if there are activation patterns specific to stress. We then used these findings as an anatomical guide for targeting subsequent experiments explicitly testing the role of BLA CaMKII α neurons in the endocrine response to stress. Our results support our central claims that: (1) acute, novel stressors lead to common spatial activation patterns in the BLA, with a particular bias in activation to the medial basal subdivision (mBA); (2) acute, novel stressors elicit distinct temporal patterns of activation of the mBA; and (3) the mBA is both necessary for stress-induced activation of the HPA axis and its activation in the absence of stress is sufficient to activate the HPA axis.

Stress induces a common spatial activation pattern in the BLA

To assess if stress leads to a common activation pattern in the BLA, we mapped expression of the activity-responsive protein FOS following exposure to several different stimuli. We identified that broad activation occurs in the BLA following exposure to a range of novel aversive (bobcat odour, shock, swim, and restraint) and non-aversive stimuli (citral odour and crackers). However, while all stimuli led to significantly greater FOS expression in the LA compared to the naïve condition, only aversive stimuli significantly increased FOS expression in

the mBA. This is not surprising, as most primary sensory afferents terminate in the LA; conversely, the mBA receives more polymodal and cortical inputs (LeDoux, 2007; Sah, Faber, Lopez De Armentia, et al., 2003). Thus, while novelty alone may be sufficient to activate the LA via afferent sensory inputs, activation of the mBA may rely on more complex polymodal or cognitive inputs that may be driven only during exposure to more complex states such as stress exposure. Collectively, this suggests that the LA has a predominant role in responding to novelty (or salient) sensory stimuli, while the mBA has a more explicit role in reacting to aversive stressors. Translationally, it will be essential to continue to investigate differences in the role of the LA and mBA during stress, and, how they may differ in circuit connectivity and receptor expression or molecular signatures. In this way, it may be possible to identify pharmacological treatments that specifically blunt the stress response while still preserving encoding of salience. A similar approach has been utilized to identify neurotensin receptors as a specific pharmacological target for the regulation of fear (Li et al., 2022; McCullough, Choi, et al., 2016)

It is interesting to note that only predator odour and shock significantly increased FOS expression in the LBA. Notably, these two stimuli also readily induce conditioned responses (as measured as conditioned place aversion (Fendt et al., 2003) or conditioned freezing response (Chaaya et al., 2019)), suggesting that this region may be particularly involved in conditioned responses. Indeed, the LBA projects to regions such as the central amygdala, lateral hypothalamus, and ventral hippocampus, all of which are highly involved in encoding aversive or appetitive memory (Beyeler et al., 2018; Hintiryan et al., 2021; Huff et al., 2016; Petrovich et al., 2002; Reppucci & Petrovich, 2016). At the same time, the LBA also receives strong mnemonic and polymodal sensory inputs from the entorhinal cortex and insular cortex (McDonald et al., 1996; McDonald & Mascagni, 1997), as well as intra-amygdala projections from the LA (LeDoux, 2007). Given that the LA is intrinsic to fear memory, it will be important to dissect the differential

contribution of the LA and LBA to conditioning, and how the LBA differs from the LA to facilitate fear-like responses.

Although others have identified a rostral bias in activation patterns to conditioned aversive stimuli (J. Kim et al., 2016), we did not observe this bias. However, our data reflect important differences. First, our stimuli were novel and did not reflect learned responses. It is possible that spatial activation patterns change or become more selective with learning (Jacques et al., 2019; Leake et al., 2021). Secondly, despite having a range of stressful and neutral stimuli, we did not use any truly rewarding stimuli. Although crackers are a palatable food and were readily consumed during experiments, animals are inherently neophobic during the first exposure (Modlinska et al., 2015). Thus, it is likely that a significant proportion of FOS-responsive cells encoded novelty, rather than reward. Thirdly, we did not characterize the very rostral or very caudal sections of the BLA, where biases may have been more apparent.

Stress induces distinct temporal patterns of activation in the BLA

While FOS mapping provides an excellent description of spatial patterns of activation, it has poor temporal resolution and is therefore only capturing one aspect of activation patterns in the BLA. Thus, we recorded calcium responses in CaMKII+ neurons of the mBA using fiber photometry, which therefore allowed for comparisons of spatial and temporal patterns of activation in the BLA in response to a variety of different stressors. Indeed, the GCaMP6s temporal pattern was dissociable from the FOS spatial pattern, exhibiting a significantly greater initial GCaMP6s response to restraint and swim than all other stimuli. Given that GCaMP6s reflects coordinated activity of neurons (Gunaydin et al., 2014), a large initial magnitude such as that observed in response to restraint and swim likely reflects a larger network of neurons being recruited simultaneously. Thus, a more modest response such as that observed during exposure to bobcat urine or shock may instead reflect different populations interchangeably activated, which may

manifest as a larger number of FOS+ cells. Of note, restraint and swim stress also evoked the largest CORT response, suggesting coordinated activity at stress onset (i.e., GCaMP6s response) may be more impactful on HPA activation than total number of neurons activated throughout exposure (i.e., FOS response). Notably, our data agree with findings from others (Úbeda-Contreras et al., 2018) that FOS expression in the BLA is not associated with magnitude of HPA activation. Thus, we hypothesize that predicting the contribution of the BLA to the stress response may best be understood through a combination of identifying (1) *where* activation is occurring (i.e., if activity is particularly within the mBA subregion); and (2) *when* activation is occurring (i.e., if activation is particularly clustered at onset of the stress response).

Our photometry data agrees with that collected from human fMRI demonstrating that the strength of the BLA response at the onset of stressful stimuli is particularly evident early in stress exposure (Wen et al., 2022). However, (Quirk et al., 1995) demonstrated in rodents that different subregions of the LA exhibit different response latencies during conditioned fear, with the ventral LA exhibiting a slightly delayed response from the dorsal LA. Given that information in the BLA generally flows dorsal-to-ventral, it is thus likely that the mBA may exhibit an even greater response latency than in the LA; however, this would be difficult to specifically test using fiber photometry, which lacks the spatial specificity of single-unit recordings. Finally, it would also be informative to test if the magnitude of the initial response is associated with any behavioural or physiological readout, such as a greater release of corticosterone, increased anxiety-like behaviour, or consolidation of memory.

We also identified that systemically blocking B-noradrenergic signaling reduced the average magnitude of the BLA response during exposure to restraint. It is likely these effects are due to inhibition of NE signaling directly in the amygdala, as the BLA widely expresses B-adrenergic receptors (Qu et al, 2008) and NE is known to be released into the BLA during stress exposure and drive anxiety-like responses (Galvez et al., 1996; McCall et al., 2017). However,

given that propranolol is known to dampen the sympathetic system (Andrews & Pruessner, 2013; LeWinter et al., 1975; Rodriguez-Romaguera et al., 2009), this could also be an indirect result of reduced interoceptive stress signals, such as those terminating in the BLA from the insular cortex (Hsueh et al., 2023; Ju et al., 2020). Our findings partially agree with findings from (Giustino et al., 2020) that demonstrated that propranolol reduced shock-induced increases in BLA firing. However, their effect was observed only upon termination of the stressor, while we demonstrated that propranolol reduced BLA activity during the restraint episode without significantly impacting the post-stress period. There are several explanations for these differences. First, (Giustino et al., 2020) performed single-unit recordings and we used fiber photometry, which records from an entire population of cells. Thus, individual effects may have been masked by population-level activity, which may have greater variability of individual cells. Second, recordings by (Giustino et al., 2020) occurred in animals that remained in their stress environment (shock chamber), while our recordings following restraint occurred in animals that were returned to a familiar (non-stressful) environment upon stress termination.

mBA CaMKii projection neurons are necessary and sufficient for activation of the HPA axis.

Chemogenetic inhibition of CaMKii neurons in the BLA reduced stress-induced CORT and conversely, optogenetic stimulation of CaMKii neurons increased CORT in the absence of external stress. There is widespread evidence implicating the BLA in stress-related responses such as avoidance behaviour (Di et al., 2016; Janak & Tye, 2015) and memory (Roosendaal et al., 2009). However, there is a striking lack of investigation towards its contribution to the endocrine response to stress. Indeed, evidence is mixed, depending on which receptors (Bhatnagar et al., 2004; Cohen et al., 2018; de Oliveira et al., 2017; Goldstein et al., 1996; J. M. Gray et al., 2015; Hill et al., 2009; M. Jensen et al., 2016; T. J. Sajdyk et al., 2008; Yaeger et al.,

2022) or subregions are targeted (Dunn & Whitener, 1986; Feldman et al., 1982; Matheson et al., 1971; McGregor & Herbert, 1992; Rubin et al., 1966; Seggie, 1987; Slusher & Hyde, 1961; Vouimba & Richter-Levin, 2013). We thus restricted expression of inhibitory DREADDs or excitatory opsins to excitatory CaMKii+ projection neurons, and specifically targeted the mBA. Thus, while others have shown mixed effects through less specific approaches such as lesions or GABA-A agonists, our effects may have been apparent only by excluding potentially stress-inhibiting cell types such as astrocytes or interneurons (Morena et al., 2019; Qin et al., 2022; Xiao et al., 2020), or by targeting our injection sites to the mBA, which we have indicated as particularly stress-responsive.

However, our approach still lacks specificity, as projection neurons in the BLA exhibit wide heterogeneity in molecular expression (O'Leary et al., 2020). Indeed, discrete populations of CaMKiia neurons actually seem to attenuate stress-related responses, including inhibition of fear (Jasnow et al., 2013; McCullough, Choi, et al., 2016; X. Zhang et al., 2020), and may instead drive approach behaviours such as response to rewarding stimuli (Beyeler et al., 2018; J. Kim et al., 2016). Notably, there are very few known BLA molecular markers which drive stress-related behaviours (Folkes et al., 2020; Shen et al., 2019). This is a critical gap in our understanding of how the BLA responds to stress and will be important to investigate, perhaps using various molecular approaches such as fluorescence-activated cell sorting (FACS) in combination with activity-dependent tagging of neuronal populations (McCullough, Morrison, et al., 2016).

Overall, we have identified that the mBA is a distinct subregion of the BLA that is activated specifically by a wide range of stressors to contribute to the release of corticosterone. Despite a similar spatial pattern, different stressors induce distinct temporal patterns of activation, with responses to restraint and swim particularly robust at initial onset of stress. Blocking norepinephrine signaling in the BLA reduces restraint stress induced activation of BLA projection neurons. Further, chemogenetic inhibition or optogenetic stimulation of BLA projection neurons,

respectively, bidirectionally influenced changes in HPA axis activity. Collectively, this establishes the mBA as a critical organizing and regulatory subregion of the BLA during the stress response.

2.6 ACKNOWLEDGEMENTS

This research was performed at the University of Calgary which is located on the unceded traditional territories of the people of the Treaty 7 region in Southern Alberta, which includes the Blackfoot Confederacy (including the Siksika, Piikuni, Kainai First Nations), the Tsuut'ina, and the Stoney Nakoda (including the Chiniki, Bearspaw, and Wesley First Nations). The City of Calgary is also home to Metis Nation of Alberta, Region III. We would like to acknowledge the Hotchkiss Brain Institute optogenetic core facility and the advanced microscopy facility for their technical support, and Min Qiao for her technical lab support. We also acknowledge the University of Calgary Health Sciences Animal Research Centre, specifically Vincent, Krista Jensen, and Brittany Munro. AAV.CaMKII.GCaMP6s.WPRE.SV40 (Addgene viral prep #107790-AAV9) was a gift from James M. Wilson; AAV8.CaMKII.hM4Di.mCherry (Addgene viral prep # 50477-AAV8) was a gift from Bryan Roth; AAV5-CaMKii-hChR2(H134R)-mCherry (Addgene viral prep #26975-AAV5) was a gift from Karl Deisseroth; AAV8.CaMKii.mCherry and AAV8.CaMKII.EGFP was a gift from Laval Université.

2.7 FUNDING

This research was supported by operating funds to MNH from the Canadian Institutes of Health Research (CIHR). RJA received salary support from the Mathison Centre for Mental Health Research & Education and the Cumming School of Medicine. GNP received salary support from BranchOut Neurological Foundation, CIHR, and the Cumming School of Medicine. LTS received

salary support from a Harley Hotchkiss Doctoral Scholarship in Neuroscience. All authors declare not conflict of interests.

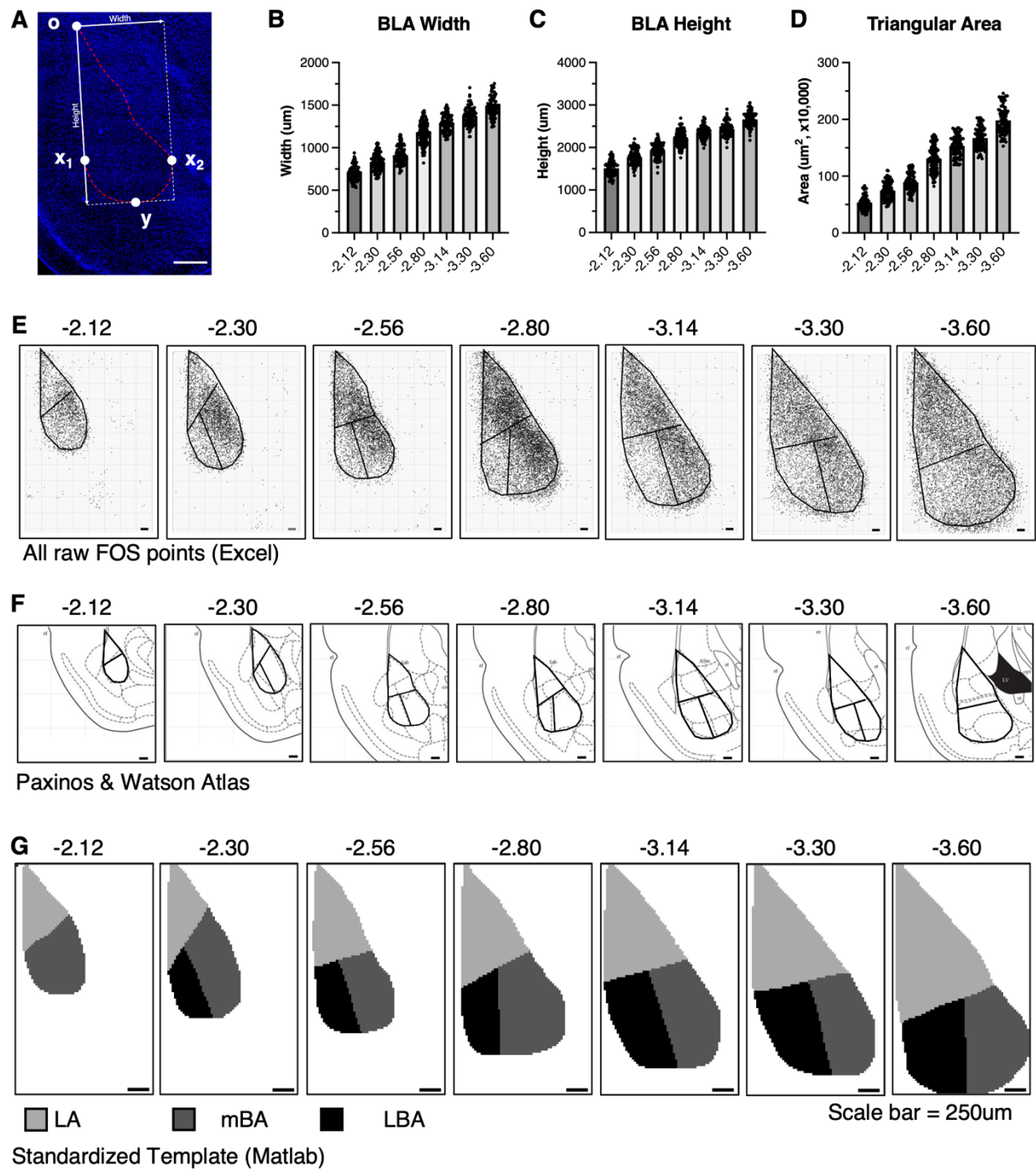
2.8 AUTHOR CONTRIBUTIONS

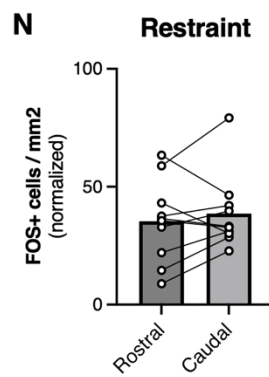
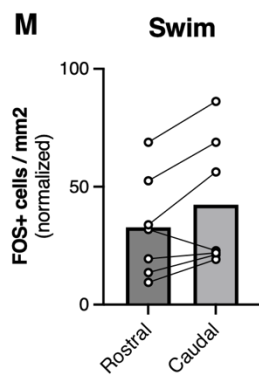
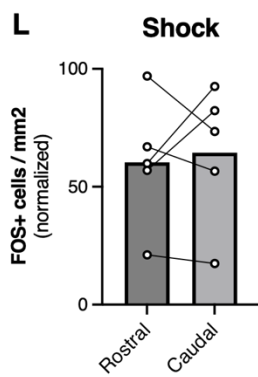
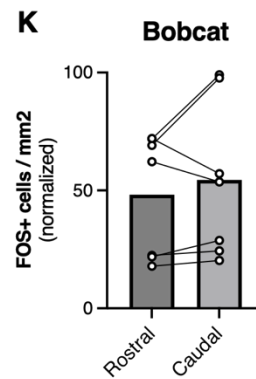
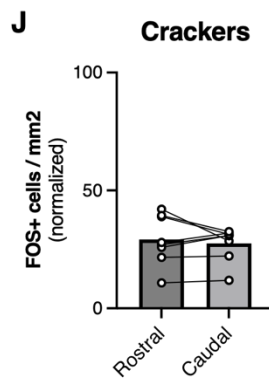
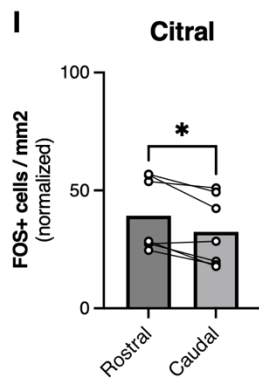
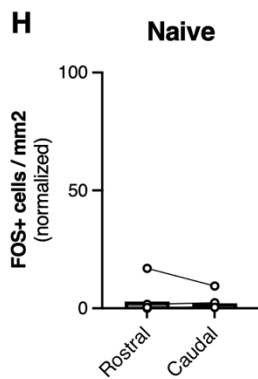
List of authors: Aukema RJ, Petrie GN, Lau BK, Baglot SL, Seabrook LT, Molina L, Füzesi T, Kadhim S, Nastase AS, Morena M, Bains JS, Borgland SL, Hill MN

Contributions: RJA designed and conducted experiments, analyzed data, prepared figures, and wrote the manuscript. GNP designed and conducted experiments and reviewed the manuscript. BL and LS designed and conducted electrophysiology experiments and LS reviewed the manuscript. LM developed photometry analysis tools and reviewed the manuscript. TF developed optogenetic and photometry analysis tools. SL Baglot, MM, SK, and AS conducted experiments. SL Borgland and JB provided advice. MNH developed and supervised the project and wrote the manuscript.

2.9 SUPPLEMENTARY FIGURES

Supplementary Figure 2.1





Supplementary Figure 2.1. Methods & Rostral-caudal distribution of BLA FOS expression

(A) Representative image of the BLA depicting normalization procedure. indicates boundary of BLA as determined by DAPI staining; 'o' indicates point of origin; x_1 indicates most lateral point of the BLA; x_2 indicates most medial point of the BLA; y indicates most ventral point of the BLA;

(B-D) Average calculated width, height, and triangular area of the BLA for each slice at each AP plane.

(E) All normalized FOS+ coordinates (black dots) of every group displayed simultaneously at each AP plane. Grids represent 25um x 25um bins. Solid black lines overlaid on graph indicates boundaries of the BLA and each subregion.

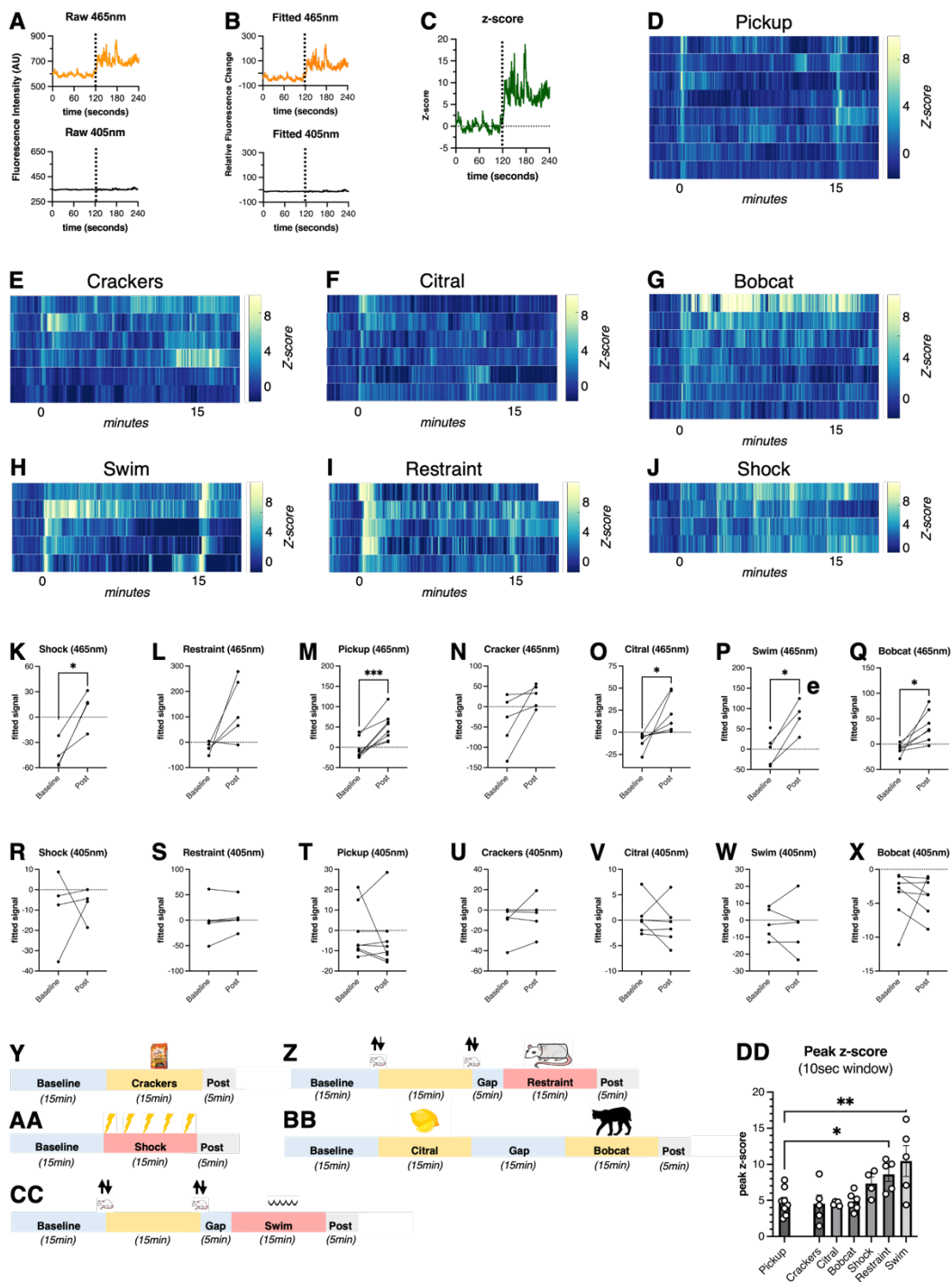
(F) Outline of the BLA and its subdivisions traced from the Paxinos & Watson atlas.

(G) Template of the BLA and its subregions represented as a compilation of 25um x 25um bins.

(H-N) Rostral-Caudal differences in FOS expression between each stimuli. Rostral = AP -2.12 to -2.56; Caudal = AP -3.14 to -3.60. Data were analyzed using a two-tailed paired t-test (Naïve: $t_6=0.6815$, $p=0.5210$; Citral: $t_6=3.601$, $p=0.0114$; Crackers: $t_7=0.7024$, $p=0.5051$; Bobcat: $t_6=0.9985$, $p=0.3566$; Shock: $t_4=0.3845$, $p=0.7202$; Swim: $t_6=2.394$, $p=0.0538$; Restraint: $t_9=0.8555$, $p=0.4145$).

* $p<0.05$, ** $p<0.01$, *** $p<0.001$, **** $p<0.0001$. Error bars represent mean +/- SEM.

Supplementary Figure 2.2



Supplementary Figure 2.2. BLA response to stimulus termination & overview of experimental procedures.

(A) Raw 465nm and 405nm signals during initiation of swim stress (dotted line).

(B) Fitted 465nm and 405nm signals following robust linear regression and correction for photo-bleaching.

(C) Resultant signal after subtracting 405nm reference from 465nm to correct for motion and normalizing as z-score.

(D-J) Heatmap representing z-score for each individual animal during exposure to each stimulus

(K-Q) Difference in average fitted Ca^{2+} -dependent 465nm signal in baseline vs first 60sec following exposure to each stimulus. Data were analyzed using a two-tailed paired t-test (shock: $t(3)=5.039$, $p=0.0151$); restraint: $t(4)=2.554$, $p=0.0631$; pickup: $t(7)=5.671$, $p=0.0008$; crackers: $t(4)=2.464$, $p=0.0694$; citral odour: $t(5)=2.803$, $p=0.0379$; swim: $t(4)=3.603$, $p=0.0227$; bobcat odour: $t(6)=3.444$, $p=0.0137$)

(R-X) Difference in average Ca^{2+} -independent signal in baseline vs. first 60sec following exposure to each stimulus. Data were analyzed using a two-tailed paired t-test.

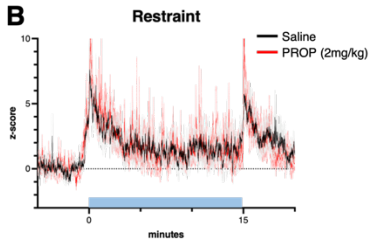
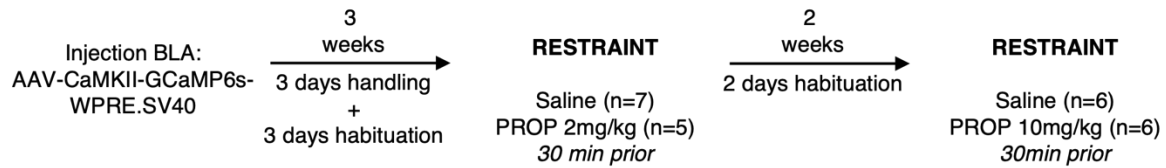
(Y-CC) Overview of experimental procedure. On test day, animals were exposed to one of 5 conditions. In some cases, animals were exposed to multiple conditions with exposures separated by a minimum of 3 days. All animals underwent 15min of baseline recording before exposure to (Y) goldfish crackers (*ad libitum*), (Z) brief pickups by the handler separated by 15min, followed by a 5min washout period and then 15min restraint; (AA) 5 equally spaced 0.65mA shocks over 15min; (BB) a sponge soaked in citral odor for 15min, followed by a 5min washout period prior to 15min exposure to a different sponge soaked in bobcat urine; (CC) brief pickups by the handler separated by 15min, followed by a 5min washout period and then 15min swim exposure.

(DD) Peak average z-score within any 10sec window following stimulus onset for each condition. Data were analyzed using a one-way ANOVA ($F_{6, 31}=5.089$, $p=0.001$) followed by Dunnett's multiple comparisons test.

Error bars represent mean \pm SEM. * $p<0.05$; ** $p<0.01$; *** $p<0.001$; **** $p<0.0001$.

Supplementary Figure 2.3

A

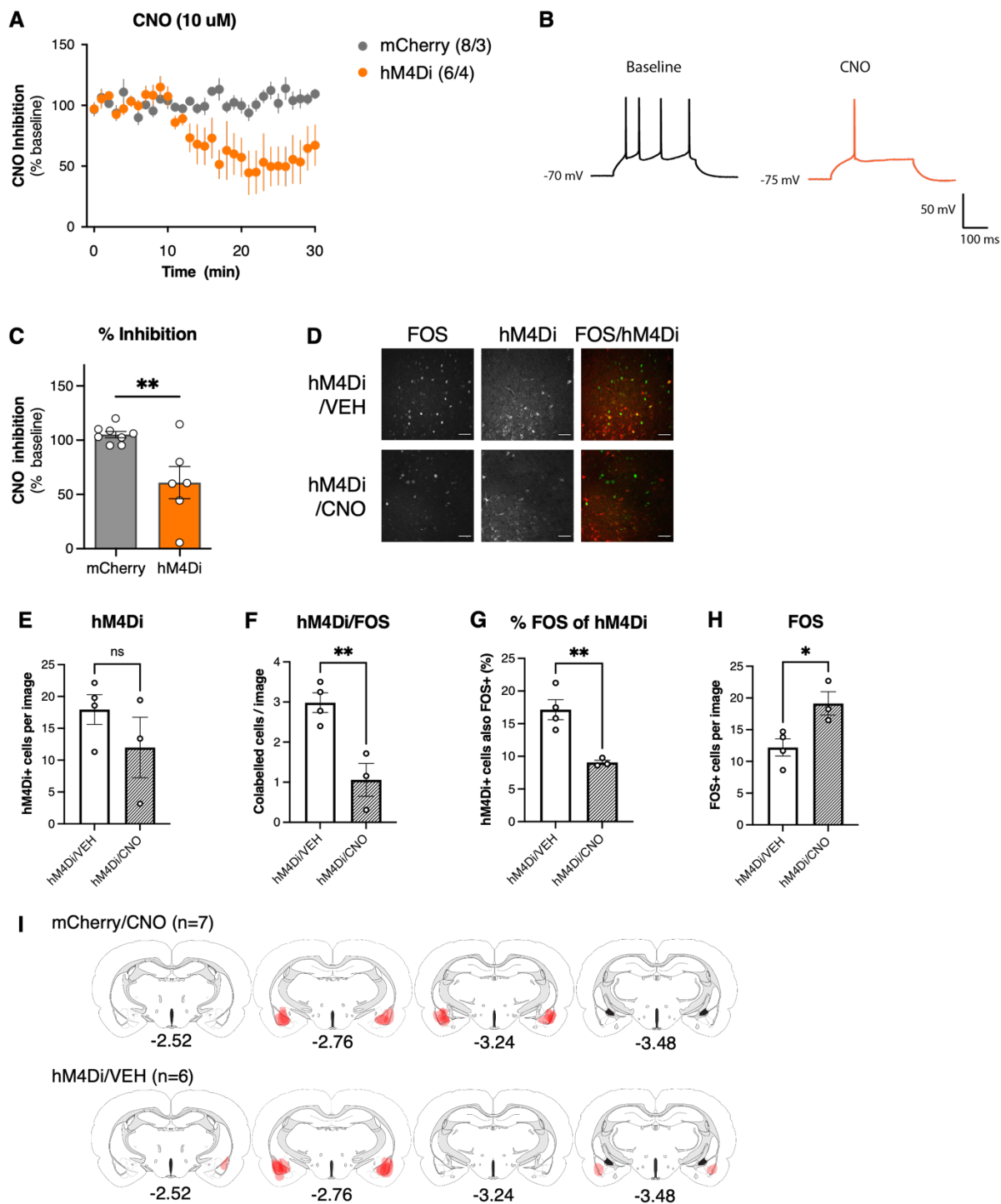


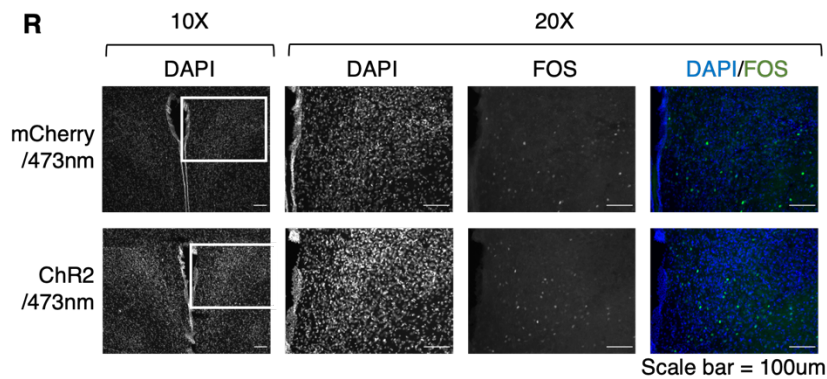
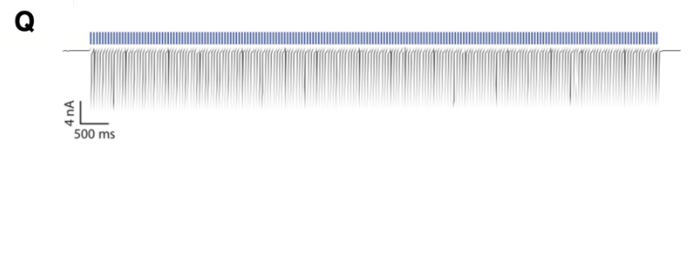
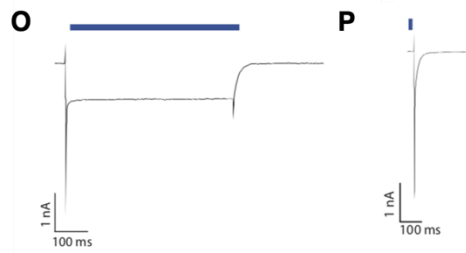
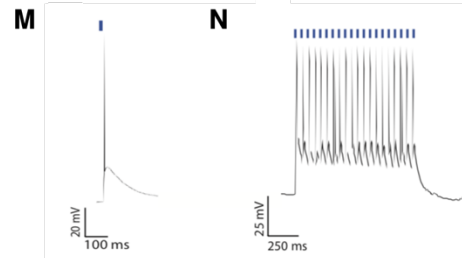
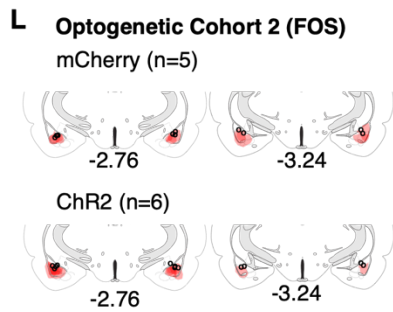
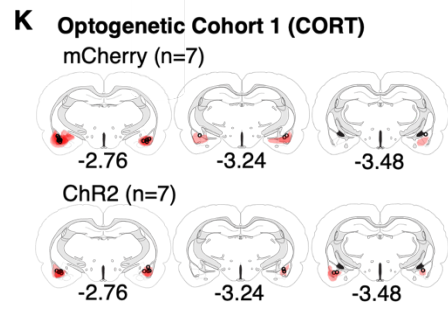
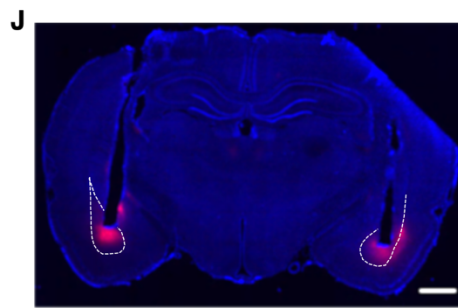
Supplementary Figure 2.3. Systemic administration of propranolol prior to stress.

(A) Overview of experimental procedures.

(B) GCaMP6s fluorescence in BLA CaMKIIa+ neurons following exposure to restraint stress, with either saline (n=7) or propranolol (n=5; 2mg/kg *i.p.*) administered 30min prior to stress exposure. Blue block indicates time of stress exposure.

Supplementary Figure 2.4





Supplementary Figure 2.4. In vivo and in vitro validation of hM4Di

- (A) Time series demonstrating that bath application of CNO (10uM) reduces firing rates in cells expressing hM4Di but not mCherry control (n=6-8 cells from 3-4 animals per group).
- (B) Representative recording of action potentials observed at baseline and after CNO (10uM) wash.
- (C) CNO (10uM) significantly reduced firing rates in cells expressing hM4Di compared to mCherry controls (n=6-8 cells per group; two-tailed unpaired t-test: $t_{(12)} = 3.376$, $p=0.0055$)
- (D) Representative image of FOS, hM4Di, and co-expression following vehicle (VEH; top row) or 3mg/kg CNO (bottom row) administration 30min prior to restraint stress; scalebar=50um
- (E) Average hM4Di+ neurons per slice (n=3-4 animals per group; $t_{(5)}=1.231$, $p=0.2731$)
- (F) Average number of hM4Di+/FOS+ co-labelled cells per slice in CNO- vs VEH-treated animals (n=3-4 animals per group; $t_{(5)}=4.289$, $p=0.0078$). (G) Percentage of hM4Di+ cells also expressing FOS in CNO- vs VEH-treated animals (n=3-4 animals per group; $t_{(5)}=4.395$, $p=0.0071$)
- (H) Average number of FOS+ neurons per slice (n=3-4 animals per group; $t_{(5)}=3.118$, $p=0.0263$)
- (I) Representative images hM4Di or mCherry expression in the BLA (corresponding to data in Figure 4E)
- (J) Representative image of ChR2 expression (red). Dashed lines indicate bounds of BLA.
- (K) Representative images of mCherry or ChR2 expression in the BLA for cohort 1 (CORT)
- (L) Representative images of mCherry or ChR2 expression in the BLA for cohort 2 (FOS). Red indicates site of maximal expression; "o" indicates location of ferrule tip;
- (M) Response of a fluorescent cell to a single pulse of blue light (3ms) in current clamp.
- (N) Response to a train of light pulses delivered at 20Hz for 1sec in current clamp mode.
- (O) Response to a 500ms light pulse in voltage clamp.
- (P) Response to a single pulse of blue light (3ms) in current clamp mode.
- (Q) Response to a train of light pulses delivered at 20Hz for 10sec in voltage clamp
- (R) Representative image of FOS expression in the PVN following optogenetic stimulation of the BLA in animals expressing mCherry (top row) or ChR2 (bottom row). White box in the first column (10X magnification) indicates region-of-interest where cells were counted.
- Error bars are mean +/- SEM; ** $p<0.01$

Chapter 3. Topographical distribution and projection-specific activation of basolateral amygdala projection neurons

3.1 ABSTRACT

The basolateral amygdala (BLA) is reliably activated by psychological stress in both humans and rodents and can influence a wide range of behavioural and physiological changes evoked by stress exposure. However, the BLA is also activated by appetitive and rewarding stimuli. This multi-modal role of the BLA suggests that there is likely a distinct subset of neurons which are activated during exposure to stressful conditions; however, the circuit and functional identity of these neurons remains unknown. First, using optogenetic activation of glutamatergic BLA projection neurons, we confirmed functional connectivity with downstream regions such as the dorsomedial bed nucleus of the stria terminalis and the prelimbic cortex. We then used retrograde tracing to map the topographical distribution within the BLA of six different BLA projection populations targeting the central amygdala (CeA), prelimbic cortex (PrL), nucleus accumbens (NAc), bed nucleus of stria terminalis (BST), lateral hypothalamus (LH), and ventral hippocampus (VH). Distinct projection neuron populations were found to have considerable heterogeneous, and largely non-overlapping, distribution throughout the BLA. Co-expression with the activity-responsive protein FOS revealed that all projection populations were activated, to some degree, during exposure to restraint stress. However, chemogenetic inhibition of discrete BLA populations targeting the CeA, NAc, and BST had no effect on stress-induced corticosterone (CORT) release. In contrast, inhibition of the BLA-PrL enhanced stress-induced CORT, suggesting an inhibitory role over stress-induced neuroendocrine responses mediated by this projection. Collectively, this suggests that BLA circuits are widely activated by stress exposure, but individual circuits do not contribute to driving a hormonal response to stress on their own.

3.2 INTRODUCTION

Exposure to aversive, stressful stimuli leads to a multi-system biological response that prepares an organism for potential harm through physiological, behavioural, hormonal, and autonomic responses. Although adaptive in the short-term, prolonged or unnecessary activation of the stress response can lead to a wide range of health concerns (McEwen, 1998), and stress-related psychiatric disorders are highly prevalent, debilitating, and often resistant to treatment (Calhoun & Tye, 2015; Griebel & Holmes, 2013). To develop more targeted and effective treatment for these conditions, we must better understand precisely which cell types and circuits in the brain are involved in identifying environmental stimuli as stressful.

The basolateral amygdala (BLA) is reliably activated by psychological stress in both humans and rodents (Chapter 2, 2023; Ipser et al., 2013; Reznikov et al., 2008; van Marle et al., 2009), and amygdala hyperactivity has been implicated in stress disorders such as post-traumatic stress disorder and generalized anxiety disorder (K. S. Blair et al., 2016; Engel et al., 2009; Etkin & Wager, 2007; Rauch et al., 2000). Likewise, chronic stress in rodents leads to hyper-excitability of projection neurons in the BLA (Rau et al., 2015; Rosenkranz et al., 2010) which often parallels increases in anxiety-like behaviour (Masneuf et al., 2014; J.-Y. Zhang et al., 2019b). Activation of the BLA is sufficient to drive many stress-related processes, including activation of the hypothalamic-pituitary-adrenal (HPA) axis and subsequent release of corticosterone (Bhatnagar et al., 2004; Chapter 2, 2023; Gray et al., 2015), anxiety-like behaviour (Tye et al., 2011; Yin et al., 2019), sympathetic activation (Soltis et al., 1997), and consolidation of aversive memory (Paré, 2003).

However, apart from aversive and stressful stimuli, the BLA is also activated by appetitive and positive stimuli such as reward (Beyeler et al., 2018; S. Cole et al., 2013; X. Zhang et al., 2020) and safety learning (Herry et al., 2008; McCullough, Choi, et al., 2016; Sangha et al., 2013). Further, distinct “appetitive” vs. “aversive” projection populations in the BLA have been shown to

be mutually inhibitory via intermediate GABAergic interneurons (Beyeler et al., 2018). Together, this suggests that there are distinct subpopulations of projection neurons in the BLA that serve opposing functions. Therefore, it is likely that only a distinct subset of BLA neurons are activated during exposure to stressful conditions, to subsequently coordinate and drive various behavioural and physiological adaptations to stress such as increases in anxiety-like behaviour and release of corticosterone. Specific stress-responsive neurons in the BLA, however, have not been well-identified or characterized.

Although discrete BLA projection neuron populations have been shown to drive anxiety-like behaviour (Felix-Ortiz et al., 2013, 2016; Janak & Tye, 2015; Lowery-Gionta et al., 2018), there has been no investigation regarding if discrete BLA projection neuron populations contribute to HPA responses to stress, despite broad evidence for the BLA in this role (Bhatnagar et al., 2004; Chapter 2, 2023; Cohen et al., 2018; Gray et al., 2015; Yaeger et al., 2022). We have previously demonstrated that a variety of different psychological stressors commonly activates the medial basal amygdala (mBA) subregion of the BLA, and that optogenetic or chemogenetic manipulation targeted at projection neurons in this region bidirectionally drives activation of the HPA axis and release of corticosterone (CORT) (Chapter 2, 2023). However, the projection identity of these stress-responsive neurons, and whether discrete populations of projection neurons are responsible for driving this response, remains unknown.

We therefore had three specific aims: (1) How are projection neuron populations organized within the BLA, and specifically within the mBA; (2) Which BLA projection neuron populations are activated by psychological stress; and (3) Do discrete projection neuron populations contribute to activation of the HPA response to stress?

3.3 METHODS

Animals.

All animal protocols were approved by the University of Calgary Animal Care Committee and followed guidelines from the Canadian Council on Animal Care. Adult male Sprague Dawley rats were obtained from Charles River Laboratories (175-225g upon arrival) and maintained under a 12h light-dark cycle (lights on at 8am) with food and water available ad libitum. All experiments were performed during the light phase of the cycle between 8am and 2pm. Animals were pair-housed, and cage-mates were always in identical treatment groups and underwent all aspects of experimentation at the same time, including intraperitoneal injections, blood collection, stimulus exposure, and sacrifice. For optogenetic experiments, animals were single housed for a minimum of two weeks prior to testing.

Blood collection and corticosterone analysis. While in restraint tubes, blood samples were collected into ice chilled, EDTA treated microvettes (Sarstedt AG & Co. KG; #16.444.100) from a small nick over the lateral tail vein. Tail blood was centrifuged at 10,000 rpm for 20min at 4°C to separate plasma, which was stored at –20°C until corticosterone analyses. Plasma samples were analyzed with an enzyme-linked immunosorbent assay kit (Arbor Assays; #K014-H5) by following the manufacturer's instructions and as performed previously (DeVuono et al., 2020). Standards were tested in triplicate, and samples were tested in duplicate and diluted 1:100 to ensure levels fit the standard curve.

Brain collection. Brains were collected and processed identically for all experiments. For perfusion, animals were anesthetized with an overdose of sodium pentobarbital and transcardially perfused with 0.9% saline (~60mL per rat, 30 mL/min) followed by 3.8% paraformaldehyde in

0.01M PBS (~120mL per rat, 30 mL/min). Following perfusion, brains were removed and immersed in 3.8% paraformaldehyde in 0.01 M PBS overnight before being switched to a 20% sucrose solution in PBS for 48-72 hours, and then transferred to a 30% sucrose solution in PBS for cryoprotection. Coronal sections of 40µm were cut in four series' on a Leica SM 2010R sliding microtome and collected in antifreeze (30% wt/vol sucrose, 1% wt/vol polyvinylpyrrolidone-40, 30% vol/vol ethylene glycol, 0.0065% wt/vol sodium azide, in PB with 0.9% saline; adapted from (Butler et al., 2012) and stored at -20 C until processing.

FOS immunohistochemistry. Free-floating sections of the BLA were rinsed 3x10min in PBS, followed by 3x10min in PBS + Triton X-100 (0.1%). Sections were then blocked for 1h at room temperature with gentle agitation in 5% normal donkey serum in PBS and incubated for 23h at 4°C with anti-cFos antibody raised in rabbit (cFos, #2250s, Cell Signaling Technology, 1:300) in an antibody blocking solution (0.1% vol/vol Triton X-100, 0.1% wt/vol BSA, 0.05% wt/vol sodium azide, 0.04% wt/vol sodium EDTA in PBS). Following a 3x10min wash in PBS + Triton X-100 (0.1%), sections were incubated for 2h at room temperature with a donkey anti-rabbit AlexaFluor 647-conjugated secondary antibody (Alexa-647, #711-605-152, Jackson ImmunoResearch, 1:100) in antibody blocking solution. Finally, sections were rinsed 3x10min in PBS + Triton X-100 (0.1%) and 2x10min in PBS, mounted onto charged slides, and cover-slipped using Fluoroshield with DAPI mounting medium (Sigma Aldrich).

Stereotaxic surgery. Rats were maintained under isoflurane anesthesia and analgesic treatment (meloxicam (2mg/kg, subcutaneously)) in a stereotaxic apparatus during surgical injection of viruses or cholera toxin subunit B (CTb), or implantation of fibre optic cannulas. To deliver viral vectors, a glass capillary containing viral vector was lowered into the brain and pressure injected using a NanoInject II apparatus (Drummond Scientific). Coordinates targeting brain regions are

were relative to bregma and the surface of the skull: basolateral amygdala: -2.8mm anterior-posterior (AP), ± 4.9 to 5.0mm medial-lateral (ML), and -8.4 to -8.7mm dorsal-ventral (DV); prelimbic cortex: AP +3.0, ML ± 0.5 , DV -4.1; ventral hippocampus: AP -5.3, ML ± 5.4 , DV -7.0 to -7.2; nucleus accumbens: AP +1.7, ML ± 1.4 , DV -7.1; central amygdala: AP -2.2, ML ± 4.0 , DV -8.1; lateral hypothalamus: AP -2.7, ML ± 1.5 to 1.7, DV -8.8 to -9.3; bed nucleus of the stria terminalis: AP -0.3, ML ± 1.7 , DV -7.1. For projection-specific chemogenetic experiments, coordinates for the CeA were delivered on a 12-degree inward angle: AP -2.1, ML ± 2.3 , DV -8.6. All experiments involved bilateral injections of virus or anatomical tracers.

Construct	Region	AP	ML	DV
AAV-eGFP AAV-ChR2 AAV-DIO-mCherry AAV-DIO-hM4Di	BLA	-2.8mm	± 4.9 to 5.0mm	-8.4 to -8.7mm
CTB-488 CTB-555	PrL	+3.0mm	± 0.5 mm	-4.1mm
	VH	-5.3mm	± 5.4 mm	-7.0 to -7.2mm
	NAc	+1.7mm	± 1.4 mm	-7.1mm
	LH	-2.7mm	± 1.5 mm	-8.8 to -9.3mm
	BST	-0.3mm	± 1.7 mm	-7.1mm
	CeA	-2.2mm	± 4.0 mm	-8.1mm
AAV-DIO-hM4Di	CeA	-2.1mm	± 2.3 mm (12° angle)	-8.6mm

Anterograde tracing.

Viral vectors. Viral vectors were injected bilaterally into the basolateral amygdala to anterogradely label cells with eGFP. eGFP was selectively expressed under the CaMKII promoter to restrict expression to projection neurons. AAV8.CaMKII.EGFP was purchased from Laval Université. A final volume of 138-207nl was delivered in 69.0nL boluses every 30sec, and the capillary remained in place for 10min following delivery of the final bolus, to allow for diffusion of the virus. A minimum of 3 weeks were allowed for recovery from surgery and sufficient viral expression, before animals were euthanized, perfused, and brains collected for imaging of viral expression throughout the brain.

Imaging. After brains were processed, 40um thick sections in a 1 in 4 series were observed throughout the entire brain (approximately AP +4.00 to AP -8.00) for expression of eGFP. Images were acquired at 2.5X, 5X, and 10X magnification on a Leica DM 4000B LED for select regions with notable GFP expression. Images were exported into ImageJ and brightness and contrast were adjusted for each image to improve image quality. Only animals with expression of cell bodies restricted to the basolateral amygdala were included (n=3).

Analysis. The experimenter noted expression of eGFP-labelled fibers throughout the brain for each case. Only selected regions were imaged for representation.

Optogenetic stimulation.

This tissue was harvested from animals that had undergone optogenetic stimulation in Chapter 2.

Viral vectors. Viral vectors were injected bilaterally into the basolateral amygdala to express either the control fluorophore mCherry or the excitatory opsin ChR2, which increases neural activity upon activation with 473nm light (cite). mCherry or ChR2 were selectively expressed under the CaMKII promoter, to restrict expression to BLA projection neurons. AAV5-CaMKII-hChR2(H134R)-mCherry (4.6×10^{12} GCs/mL) was a gift from Karl Deisseroth (Addgene viral prep #26975-AAV5; <http://n2t.net/addgene:26975>; RRID:Addgene_26975) and AAV8.CaMKII.mCherry (6.7×10^{12} GCs/mL) was a gift from Université Laval. A final volume of

828.0nL was delivered in 69nL boluses every 45sec, and the capillary remained in place for 10min following delivery of the final bolus to allow for diffusion of the virus. Approximately two weeks later a 600- μ m diameter mono fiber optic cannula (Doric Lenses, MFC_600/630/0.48_8.6mm_MF2.5_FLT) was implanted 0.1mm above the injection site and secured with Metabond, dental cement, and four anchoring screws.

Handling and habituation. Following surgical implantation of the fiber optic cannula, rats were single-housed and given a minimum of 4 days before handling and habituation began. Animals then underwent 10 days of habituation and handling. On days 1-6, animals were carted to the testing room each morning and handled for 1min each, and then placed into an empty cage with only bedding for ~90min. On days 7-10, the same procedure occurred but animals were also habituated to the optic fiber (no light) attached to their heads while exploring their test cage. Habituation and testing cages had a lid with a slit cut in it to allow for entry of the fiber.

Experimental testing. On experimental day, animals were carted to the testing room 1 hour prior to testing. The light source (for ChR2: 473nm, Laserglow Technologies LRS-0473-GFM-00100-05 LabSpec 473nm DPsS Laser System connected to Laser Power Supply PSU-III-LED) was connected to the implanted ferrules with a fiber optic cable (600um core diameter, Doric Lenses) attached to a beam splitter. The lasers were controlled using the open-source programmable pulse generator Pulse Pal (J. I. Sanders & Kepecs, 2014). Light intensity was measured using a Standard Photodiode Power Sensor (ThorLabs S120C) connected to a Compact Power and Energy Meter Console (ThorLabs PM100D). Blue light (5ms long pulses; 10 mW laser intensity measured at the tip) was shone at 20 Hz for 15min. The animal remained connected to the fiber for an additional 15min (30min total) and then removed and returned to their home cage. 90min following onset of optogenetic stimulation, animals were anesthetized, perfused, and brains were

collected to verify viral expression and perform immunohistochemistry for cFos. The experimenter was blinded to viral condition of the animal (mCherry: n=5; ChR2: n=6).

FOS quantification in brain regions. After immunohistochemistry for cFos, a 1-in-4 series of 40um thick sections was collected and images were acquired for each animal on a Leica DM4000 B LED microscope using a 20X objective / 0.55 NA HC PL FLUOTAR (Leica 5065190) objective. DAF and L5 filter cubes were able to detect expression of DAPI and Alexa488 (to label anti-cFos), respectively. Images were acquired in defined regions of interest across the anterior-posterior axis of each brain region (Figure 2B-E). Only images from slices with an intact region-of-interest were acquired. Quantified regions included the dmBST and aBST (mCherry n=38 from 5 animals; ChR2 n=43 from 6 animals), PrL (mCherry n=67 from 5 animals; ChR2 n=80 from 6 animals), LH (mCherry n=73 from 5 animals; ChR2 n=106 from 6 animals), CeA (mCherry n=48 from 5 animals; ChR2 n=57 from 6 animals), AcbS and AcbC (mCherry n=48 from 5 animals; ChR2 n=60 from 6 animals), or VH (mCherry n= 34 from 5 animals; ChR2 n=42 from 6 animals). Images from different brain regions were collected over multiple immunohistochemistry runs, but the same brain region was always imaged and analyzed at the same time for all animals.

Exclusions. Animals were excluded from statistical analysis if the cannula tip or significant viral expression was outside of the BLA (mCherry: n=1; ChR2: n=4), animals required euthanasia due to surgical complications (mCherry: n=1), or cFos values were considered a statistical outlier (ChR2: n=1), as defined as being twice the standard deviation of the mean of that group.

Retrograde tracing and colocalization with FOS.

Choleratoxin subunit B. 0.2% dilutions of Alexa-conjugated Cholera Toxin Subunit B in 0.4M PBS (CTB-488 or CTB-555; Invitrogen) were injected bilaterally into one of six target regions: PrL

(303.6nL), VH (303.6nL), NAc (303.6nL), LH (303.6nL), BST (193.2nL), and CeA (151.8 - 193.2nL). 13.8nl boluses were delivered every 30sec until target volume was reached, and the capillary remained in place for 10min to allow for diffusion of the virus. Every animal received injections in two different brain regions using different colors in each region (e.g., CTB-555 delivered bilaterally to CeA and CTB-488 delivered bilaterally to NAc). To eliminate imaging bias for CTB, the color of tracer used to label each projection neuron class was counterbalanced such that a similar number of animals received an injection of CTb-555 or CTb-488 for each region. A minimum of 7 days were allowed for recovery from surgery before experiments began.

Experimental conditions. On experiment day, animals were carted to the adjacent experimental room and placed into a clear Plexiglas restraint tube for 30min. Animals were then returned to their home cage with their cage-mate and remained in the testing room until 90min following stress-onset, where they were anesthetized, perfused, and brains collected. Control animals remained in the colony room immediately until time of sacrifice, when they were anesthetized, perfused, and brains collected.

Histology. To verify that expression of CTB-488 or CTB-555 was constrained to the region of interest at the injection sites, free floating sections of the target region were rinsed 3x10min in PBS, mounted onto charged slides, and cover-slipped using Fluoroshield with DAPI mounting medium (Sigma Aldrich). Images were acquired with a Leica DM4000 B LED microscope using a 2.5X / 0.07 NA PLAN (Leica 556036), 5X / 0.12 N PLAN EPI (Leica 566076), or 10X / 0.30 HCX PL FLUOTAR (Leica 506507) objective. DAF, L5 and RHO filter cubes were used to detect expression of DAPI, CTB-488, and CTB-555, respectively. Location of maximal expression of CTB were plotted onto coronal images adapted from an atlas (Swanson, 2004).

Imaging. A 1-in-4 series of free-floating sections of the BLA (AP -2.30 to AP -3.3) were washed 3x10min in PBS, mounted onto charged slides, and cover-slipped using Fluoroshield with DAPI mounting medium (Sigma Aldrich). Slices were then tile-scan imaged on a Leica DM4000 B LED microscope using a 20X / 0.55 NA HC PL FLUOTAR (Leica 5065190) objective.

Quantification. The experimenter remained blinded to the conditions of each animal during plotting and counting. Analyses were largely guided by work from (Beyeler et al., 2018). Analyses were performed identically as previous work from our group, including division of BLA subregions into the LA, mBA, and LBA_(Chapter 2).

Briefly, we used Imaris software to semi-automatically detect CTB+ and FOS+ cells of a standardized size and quality using the spot detection function. For all images, CTB labeling was detected having an average diameter of 12um, and the quality was manually set for each image until most labelled cells were accurately identified by the software, as determined by the experimenter. Mis-labelled cells were manually removed, and non-labelled cells identified by the experimenter were manually added using the spot detection function. For FOS labeling, the spot detection function identified any FOS labeling averaging 7um diameter. The quality parameters remained identical for images labeling the same projection. However, due to differences in average FOS expression between each experimental run, we adjusted the quality parameters for FOS detection in attempt to keep basal FOS numbers consistent; thus, minimum quality ranged from 8.5-11.5 across the entire experiment, with no limits on maximum quality. All labelled cells were localized to the most dorsal point of the BLA and coordinates were then normalized to standardized BLA templates (width and height) according to the AP position assigned to each image (Chapter 2, 2023). Density quantification was calculated as before (unpublished data), with total number of cells counted in image or region / total area of BLA or subregion on each standardized template. Colocalization experiments were calculated as either: (1) percentage of

total CTB cells for each animal also expressing FOS; or (2) percentage of total FOS cells for each animal also expressing CTB. Anterior-posterior differences were quantified by comparing average density of sections containing slices from AP -2.30 and -2.56 (anterior) to those from AP -2.80 and -3.30 (posterior).

Representation. In figures 3N-S, normalized coordinates for all labelled cells from all animals were plotted as gray onto the same graph, and only those labelling a single projection were labelled black. In figure 3T, normalized coordinates for all labelled cells were plotted onto the same graph, and each individual projection was pseudo-coloured a different colour.

Exclusions. Animals were excluded if the BLA was damaged, there was no CTB expression in at least one hemisphere, or there was significant CTB expression outside of the target region (PrL: naïve (n=2), stress (n=5); VH: naïve (n=10), stress (n=8); NAc: naïve (n=4), stress (n=5); CeA: naïve (n=6), stress (n=6); LH: naïve (n=5), stress (n=6); BST: naïve (n=4), stress (n=4). One animal was excluded in all FOS analyses due to an absence of FOS expression but was included for CTB topography analyses (PrL: stress (n=1). Two animals were excluded when calculating percentage of colocalized cells in each subregion due to having no total colocalized cells (VH: stress (n=1); LH: stress (n=1).

Electrophysiology. For slice experiments, animals were deeply anaesthetised with isoflurane, decapitated and coronal slices (250 μ M) containing the BLA were cut using a vibratome (VT1200, Leica Microsystems) in room temperature, NMDG-based artificial cerebrospinal fluid (ACSF). Slices were then briefly transferred to a submerged chamber containing NMDG ACSF of the following composition: 93 mM NMDG, 2.5 mM KCl, 1.2 mM NaH₂PO₄, 30 mM NaHCO₃, 20 mM HEPES, 25 mM glucose, 2 mM thiourea, 5 mM Na-ascorbate, 3 mM Na-pyruvate, 0.5 mM

CaCl₂·4H₂O and 10 mM MgSO₄·7H₂O, where they were maintained at 32°C for 10-12 mins to allow for protective recovery of tissue. Finally, slices were transferred to a holding chamber containing regular ACSF of the following composition: 126mM NaCl, 2.5mM KCl, 1.4 mM NaH₂PO₄, 1.2 mM MgCl₂, 2.4 mM CaCl₂, 11 mM glucose and 25 mM NaHCO₃; equilibrated with 95% O₂ and 5% CO₂. When time to record, slices were individually transferred to a chamber on an upright microscope (Olympus BX51) and superfused continually with ACSF (32°C, flow rate: 2.0 ml min⁻¹). Neurons were visualised with a 40X water-immersion objective using infra-red Dodt-tube gradient contrast optics.

Functional DREADD expression in BLA pyramidal neurons was confirmed using in-vitro patch clamp electrophysiology. Using fluorescence, neurons expressing CaMKII-hM4Di were identified by the presence of an mCherry reporter. Whole-cell current-clamp recordings (Axopatch 700B, Molecular Devices) were then conducted in labelled neurons using a K-Gluconate-based internal solution containing: 130 mM K-Gluconate, 10 mM HEPES, 10 mM KCl, 4 mM Mg₂ATP, 0.3 mM Na₂GTP and 10 mM Na₂-Phosphocreatine (pH 7.3). Neurons were maintained at a membrane potential of -70 mV by DC current injection via the patch-electrode. Cell excitability was assessed by examining the current-voltage relationship (range: -25 - +400 pA) before and during application of Clozapine-N Oxide (CNO, 10 µM). Furthermore, evoked firing rate was assessed over time by application of series of 5 current pulses (250 ms in duration, 5-25 pA apart, every 60 secs), where the current amplitude was set for each cell so that ~ 3-4 action potentials were elicited during the 2nd-4th steps.

Projection-specific chemogenetic inhibition

Viral vectors. We used a dual-virus cre-dependent approach to restrict hM4Di expression to discrete projection populations. A virus was bilaterally injected into the BLA to cre-dependently express either the control fluorophore mCherry (AAV8-hSyn-DIO-mCherry; 1.6x10¹³ GCs/ml;

Addgene #50459; gift from Bryan Roth) or the G_i -coupled receptor hM4D(Gi) (AAV8-hSyn-DIO-hM4D(Gi)-mCherry; 1.9×10^{13} GCs/ml; Addgene #44362; gift from Bryan Roth), which inhibits neural activity upon activation with a designer drug (Armbruster et al., 2007). At the same time, we bilaterally injected into the target region (CeA, NAc, BST, or PrL) a retrograde virus expressing Cre recombinase (AAV2(retro)-eSYN-EGFP-T2A-iCre-WPRE; $0.9\text{--}1.2 \times 10^{13}$ GCs/ml; gift from John Christianson). In two animals, we only injected AAV8-hSyn-DIO-hM4D(Gi)-mCherry without also delivering AAV2(retro)-eSYN-EGFP-T2A-iCre-WPRE to ensure expression was only achieved with the combination of both viruses. Constructs were diluted in 0.01M of sterile PBS to reach desired titer. A final volume of 515.2n was delivered in 64.4nl boluses every 40sec into the BLA, or 386.4nl (BST, PrL, and CeA) to 579.6nl (NAc) into the target region, and the capillary remained in place for 10min following delivery of the final bolus to allow for diffusion of the virus. A minimum of 3 weeks were allowed for recovery and sufficient viral expression before experiments began.

Handling and habituation. Animals were habituated for 3 days prior to experiment day. This included being carted to the adjacent test room 1 hour each morning and being handled by the experimenter for ~2min in the position used for injections on test day.

Experimental testing. On experimental day, animals were injected intraperitoneally (*i.p.*) with either CNO (3mg/kg at 1mg/ml), to activate hM4D(Gi), or vehicle (0.2% DMSO in 0.9% saline), and 45min later were moved to a separate room and immediately placed into clear Plexiglas restraint tubes for 30min. All animals underwent restraint stress. Blood samples were collected immediately at initiation (t_0) and termination (t_{30}) of restraint stress for analysis of basal and stress-induced plasma corticosterone levels. For chemogenetic validation experiments including expression of the mCherry control virus, animals returned to their home-cage following stress

exposure but remained in the testing room. 90min following stress onset, animals were anesthetized, perfused, and brains were collected and processed. In all other chemogenetic experiments where brains were only necessary to verify viral expression, animals were anesthetized, perfused, and brains collected and processed on a separate day from experiments.

FOS colocalization with hM4D(Gi) or mCherry. Animals expressing hM4Di in the BLA-NAc projection were used for validation of the chemogenetic tools. hM4Di/VEH (n=9) and hM4Di/CNO (n=12) animals were included for confocal imaging on a Leica TCS SPE II confocal microscope using a 20X / 0.55 NA HC PL FLUOTAR (Leica 5065190) objective. Only slices with expression in the BLA and containing a minimum average of 10 RFP+ labelled cells per slice were included for analysis (hM4Di/VEH n=67 slices from 9 animals; hM4Di/CNO n=83 slices from 12 animals), and location of imaging within the BLA occurred in regions with maximal hM4D(Gi)-mCherry expression. cFos and hM4Di-mCherry signals were acquired independently and exported to ImageJ for quantification. Number of cells expressing cFos, hM4D(Gi)-mCherry, or colocalization of both signals were counted manually. Colocalization was determined as a cFos signal bound by expression of hM4D(Gi)-mCherry. The experimenter was blinded to the condition of each animal, and all imaging and threshold parameters remained identical across image acquisition and quantification.

Exclusions. Animals were excluded from statistical analysis if there was substantial DIO-hM4Di or DIO-mCherry expression outside of the BLA or substantial eGFP-iCre expression outside of the target region, or absent DIO-hM4Di or DIO-mCherry expression in at least one hemisphere (BST: n=7 CNO, n=8 VEH; CeA: n=2 CNO, n=2 VEH; PrL: n=2 CNO; NAc: n=7 CNO/hM4Di, n=5 CNO/mCherry, n=4 VEH/hM4Di; NAc+CeA: n=8 CNO, n=7 VEH). One animal was excluded for analyses because a sufficient volume of blood was not collected to perform the ELISA (NAc: n=1

VEH/hM4Di). Four animals were excluded because the t0 CORT value was greater than 150ng/ml, suggesting stress was occurring prior to our experimental manipulation (PrL: n=1 VEH; NAc+CeA: n=3 VEH). One animal was excluded due to pipetting error at the t30 time-point (NAc+CeA: n=1 CNO).

Statistics.

All grouped data and a within-animal design were analyzed using a two-tailed paired t-test (Fig. 3.3W-BB) or

one-way RM ANOVA, followed by Tukey's multiple comparison's test when appropriate (3.4Q-V).

All grouped data and a between-animals design were analyzed using an independent samples t-test or one-way ANOVA (Fig. 3.3CC; 3.4H; 3.4B-G; 3.5F-I). When appropriate, data were analyzed using Tukey's multiple comparison's test. When comparing two or more groups and a within-animal design, and only two levels, a 2Way RM ANOVA was used followed by Sidak's multiple comparisons test (Fig. 3.5J, 3.5K, L, N) or Fisher's LSD (Fig. 3.2G). If samples were missing, a mixed effects model was used (Fig. 3.5M). When comparing two or more groups and a within-animal design, and two or more levels, a 2Way RM ANOVA followed by Tukey's multiple comparison's test was used (Fig. 3.3V).

3.4 RESULTS.

BLA projection neurons innervate a wide range of downstream targets. The BLA is known to project widely to many brain regions involved in motivated behaviour. To replicate these anatomical findings and to guide subsequent experiments, we labelled BLA projection neurons and their fibers by injecting an anterograde virus expressing eGFP under the CaMKii promoter into the BLA of three adult male rats (Figures 3.1A, B) and 3-4 weeks later imaged expression of eGFP throughout the brain. eGFP was expressed widely throughout many brain regions (Table 3.1), replicating many others' previous anatomical work (H.-W. Dong et al., 2001; Hoover & Vertes, 2007; Krettek & Price, 1977; McDonald, 1991; Petrovich et al., 1996; Pitkänen et al., 2002; Reppucci & Petrovich, 2016). Notably we identified strong expression in 6 limbic regions: prelimbic cortex, nucleus accumbens, bed nucleus of the stria terminalis, central amygdala, lateral hypothalamus, and ventral hippocampus (Figures 3.1C-H), all of which are strongly implicated in motivated behaviour.

Table 3.1

Region	Case 1	Case 2	Case 3
Orbitofrontal cortex	x	X	X
Prelimbic cortex	x	X	x
Insular cortex	x	x	x
Anterior cingulate cortex	x	x	x
Infralimbic cortex	x	X	x
M2	x	X	x
Accumbens shell	x	X	x
Accumbens core	x	X	X
Olfactory tubercle / piriform cortex	x	X	x
Dorsal striatum	x	x	x
Bed nucleus of stria terminalis	x	x	x
Clastrum	x	x	x
Paraventricular thalamus	x	x	x
Nucleus of lateral olfactory tract		x	x
Substantia Innominata	x	x	x
Central amygdala		X	x
Medial amygdala		x	x
Lateral hypothalamus	x	X	x
Entorhinal cortex		X	X
Zona incerta		x	
vCA1		X	X

Table 3.1. BLA projection targets.

Presence of eGFP expression in specific brain regions following injection of AAV8-CaMKIIa-eGFP into the BLA, for three different cases

Figure 3.1

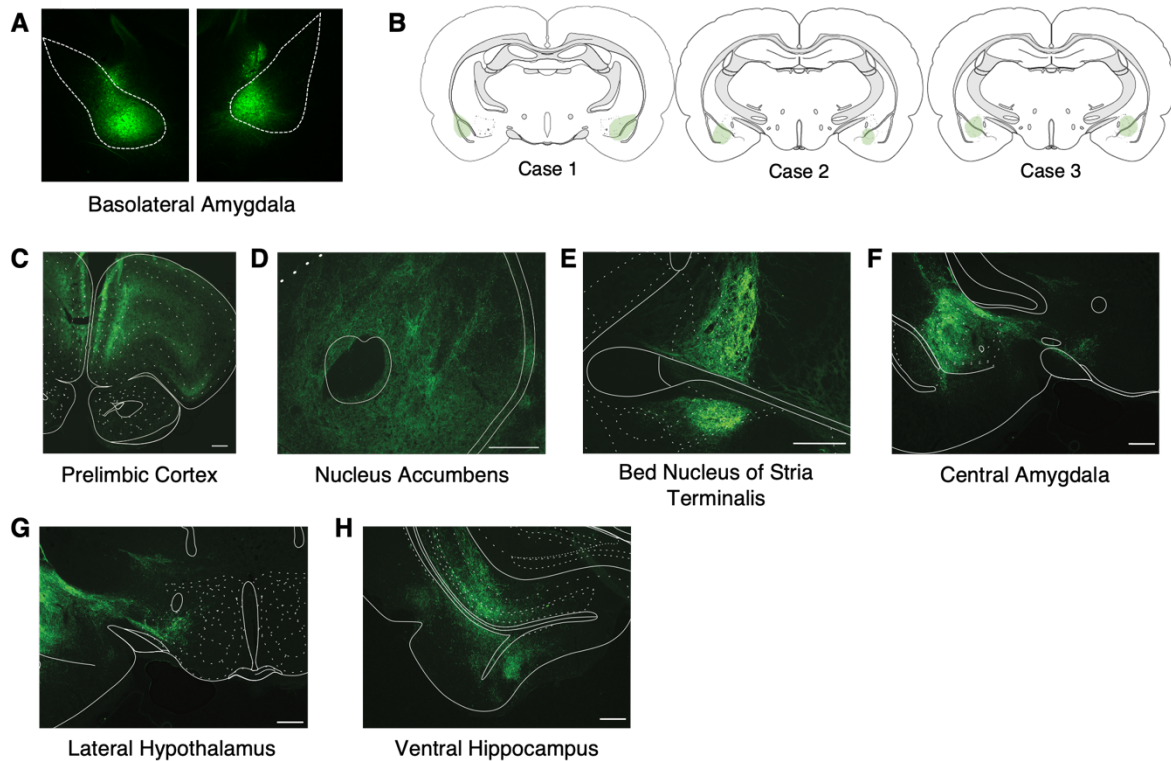


Figure 3.1. BLA projection neurons innervate a wide range of downstream targets

(A) Representative image of GFP expression following injection of AAV8-CaMKIIa-eGFP. Dashed lines delineate BLA;

(B) Representative images of location of viral expression in the BLA for each of the three cases observed.

(C) Representative images of GFP expression in downstream brain regions following injection of AAV8-CaMKIIa-eGFP into the BLA. Images were obtained from different cases.

Optogenetic stimulation of BLA projection neurons leads to activation of downstream brain regions. We have previously demonstrated that optogenetic stimulation of undefined BLA projections from mBA neurons increases plasma corticosterone and FOS-expression in the PVN, in non-stressed animals (Chapter 2). However, the BLA does not send any direct projections to the PVN (Petrovich et al., 1996), a central brain region that initiates activation of the HPA axis and subsequent release of CORT (Herman et al., 2003). To this extent, we wanted to identify candidate brain regions that may relay HPA-activating signals from the BLA to the PVN. Brains

were collected in a previous study (unpublished data), where animals expressing the light-gated excitatory opsin ChR2 or control mCherry protein in BLA projection neurons underwent 15min of 20Hz stimulation with 473nm light targeted at the medial basal amygdala (Figure 3.2A). 473nm light has shown to increase activity of neurons expressing ChR2 compared to mCherry (unpublished data; (Boyden et al., 2005)), thus allowing us to directly test the effect of stimulating BLA projection neurons on activation of downstream targets. Brains were collected and processed 90min following initiation of light to quantify FOS expression in 7 brain regions (Figures 3.2B-E). Two-way RM ANOVA revealed a main effect of region ($F(7,63)=19.83$, $p<0.0001$) but no main effect of condition ($F(1,9)=2.286$, $p=0.1648$) between animals expressing ChR2 vs mCherry. However, we purposely targeted our stimulation towards the mBA. Thus, given our *a priori* hypothesis that a distinct subset of projection neurons would be located here and thus stimulation would lead to activation of selective extra-BLA regions, we proceeded with *post-hoc* comparisons. Fisher's LSD revealed that animals expressing ChR2 displayed significantly greater FOS expression in the PrL ($p=0.0147$) and dmBST ($p=0.0282$; Figure 3.2F-G). Thus, optogenetic stimulation of mBA projection neurons increases activity in several areas innervated by the BLA, particularly in the PrL and dmBST.

Figure 3.2

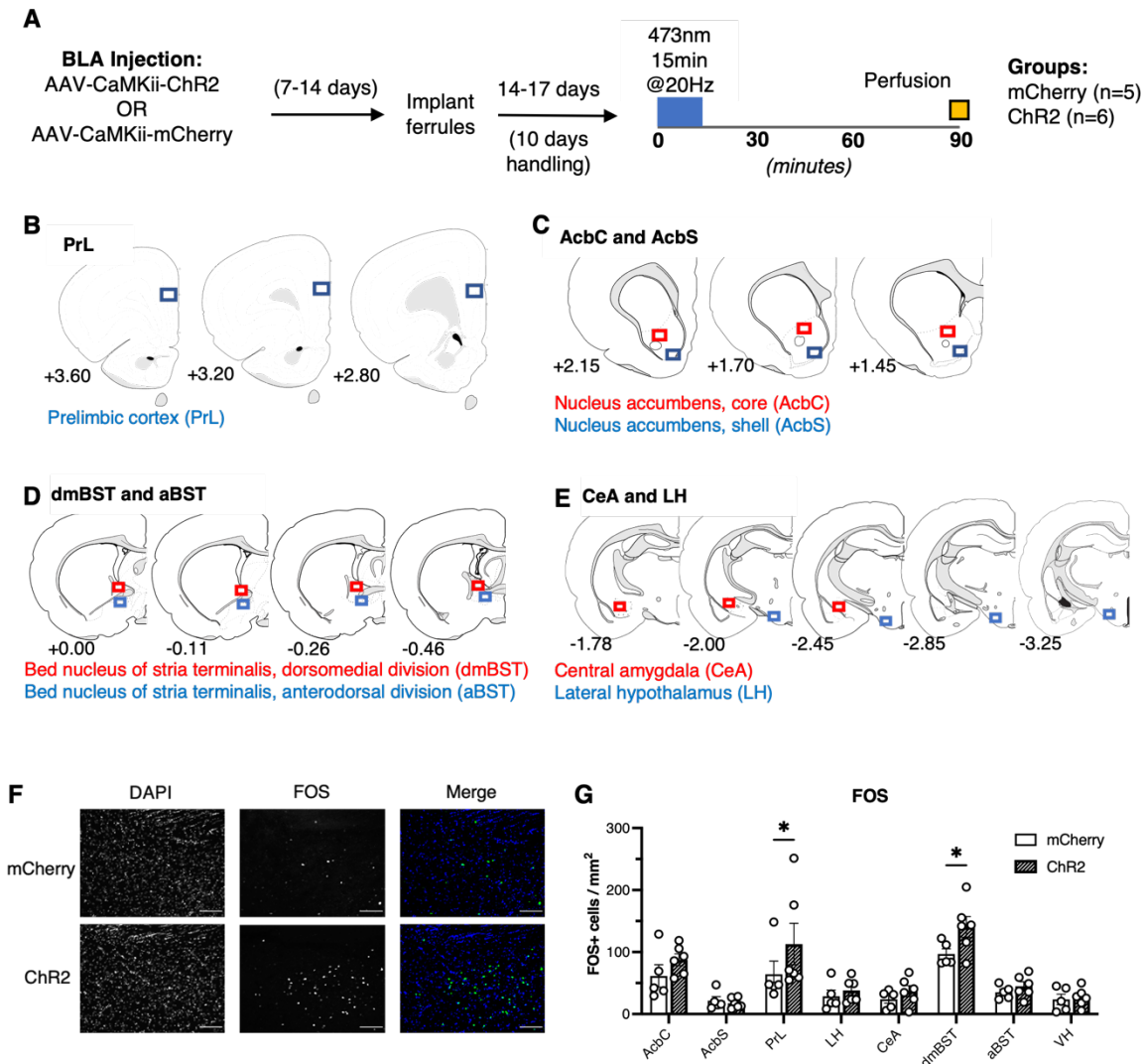


Figure 3.2. Optogenetic stimulation of BLA projection neurons leads to activation in downstream brain regions.

(A) Overview of experimental procedures;

(B-E) Representative regions-of-interest where cells were counted in prefrontal cortex (PrL), nucleus accumbens core (AcbC) and shell (AcbS), dorsomedial bed nucleus of the stria terminalis (dmBST), anterodorsal bed nucleus of the stria terminalis (adBST), central amygdala (CeA), and lateral hypothalamus (LH);

(F) Representative image of FOS expression in the dmBST. Scale bar = 100µm;

(G) FOS expression in BLA projection targets following ChR2 stimulation (n=6) vs mCherry controls (n=5). Data were analyzed using a 2-way ANOVA followed by Fisher's LSD ($F_{1,9}=2.286$; $p=0.1648$; significant differences between conditions in the dmBST ($p=0.0282$) and PrL ($p=0.0147$)). Error bars are mean \pm SEM. * $p<0.05$.

Topographical distribution of BLA projection neurons. The BLA projects to a wide range of brain regions that regulate a diverse, and sometimes competing, array of behavioural processes (Janak & Tye, 2015). We have previously demonstrated that different psychological stressors commonly increase FOS expression in the medial basal subdivision of the BLA (unpublished work). Thus, we hypothesized that projection populations targeting stress-responsive brain regions would be localized in the mBA, the stress-responsive region we had identified. We injected CTB bilaterally into six target regions: PrL, NAc, BST, CeA, LH, and VH (Figures 3.3A-F, n=11-15 per projection). One week later, we exposed animals to stress (n=5-8 per projection) or left them in their home cage (naïve condition; n=6-8 per projection), and then collected brains 90min following stress onset to process for imaging of CTB and FOS.

We mapped the location of projection populations within the BLA innervating the BST, NAc, CeA, PrL, LH, and VH using the retrograde tracer cholera toxin subunit B (CTB; n=11-15 per projection). Bilateral injections of CTB into each target region (Figures 3.3A-F) led to distinct topographical expression, such that isolated projection populations were differentially expressed throughout the BLA (Figures 3.3H-M). We localized the coordinates of every CTB+ cell and then normalized these coordinates to the most dorsal point of the BLA and according to a standardized template for each AP position (Figures 3.3N-T). We then quantified the percentage of each CTB+ cell for each projection localized to the mBA, LBA, or LA subdivisions of the BLA (Figure 3.3U). 2Way ANOVA revealed a significant interaction between population and region (Fig. 3.3V; $F(10, 138)=41.09, p<0.0001$). *Post hoc* tests revealed that there was a significant medial-lateral location bias for each projection population (Table 3.2). Specifically, populations targeting the PrL, BST, and NAc had a significantly greater percentage of CTB-labelled cells in the mBA than either the LA or LBA. In contrast, populations targeting the CeA exhibited a significantly lower percentage of CTB-labelled cells in the mBA than either the LA or LBA. Populations targeting the LH exhibited a significantly greater percentage of CTB-labelled cells in the LBA than the LA or mBA, and

populations targeting the VH exhibited significantly greater percentage of CTB-labelled cells in the mBA than the LBA. We also investigated anterior-posterior biases by comparing the average normalized density of CTB+ cells in anterior (AP= -2.30 and -2.56) vs posterior (AP= -2.80 and -3.30) sections of the BLA using a two-tailed paired t-test. There was significantly greater density in the posterior sections for BST (Figure 3.3W; $t(10)=4.378$; $p=0.0008$) and LH projectors (Figure 3.3AA; $t(12)=8.822$, $p<0.0001$), and a trend towards a posterior bias in CeA projectors (Figure 3.3Y; $t(12)=2.099$, $p=0.0577$). There were no significant anterior-posterior differences in NAc, PrL, or VH projectors (Figures 3.3X, Z, BB).

Finally, we also quantified average density of CTB+ cells for each projection in the BLA. One-way ANOVA revealed a significant difference between projection populations (Figure 3.3CC; $F(5,69)=30.04$, $p<0.0001$). *Post hoc* tests revealed that there was significantly greater CTB+ density in BLA populations targeting the NAc, CeA, and BST than those targeting the LH, PrL, and VH.

Collectively, this suggests that projection populations in the BLA are heterogenous in location bias, with populations targeting the PrL, BST, and NAc largely overlapping and distinct from populations targeting the CeA and LH. Notably, PrL, BST, and NAc projectors had a significant location bias towards the mBA, the region we had identified as being particularly stress responsive. This suggests that these populations may be more likely recruited by psychological stress. Populations targeting the NAc, CeA, and BST contribute to a substantial proportion of BLA projection neurons.

Figure 3.3

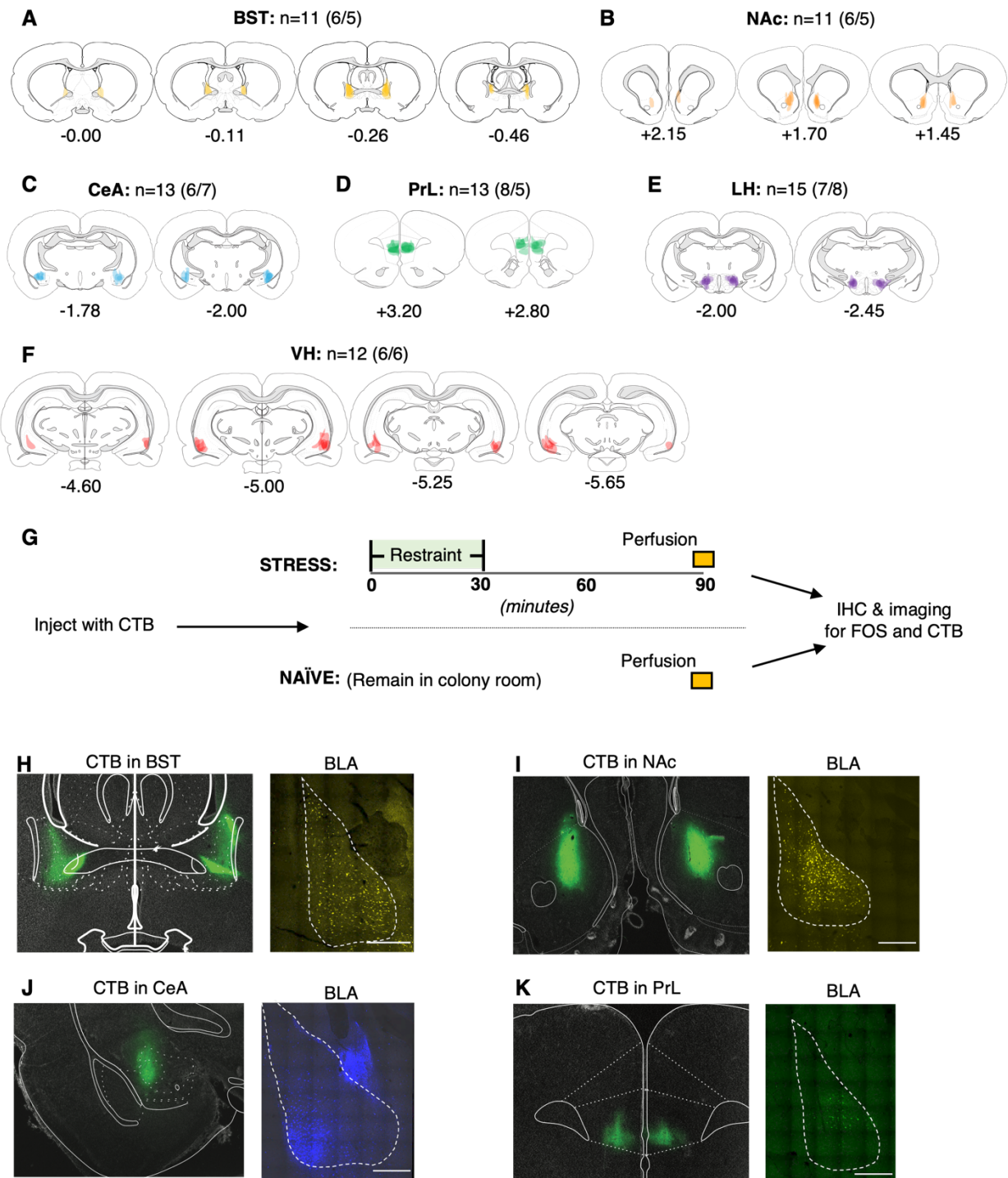


Figure 3.3

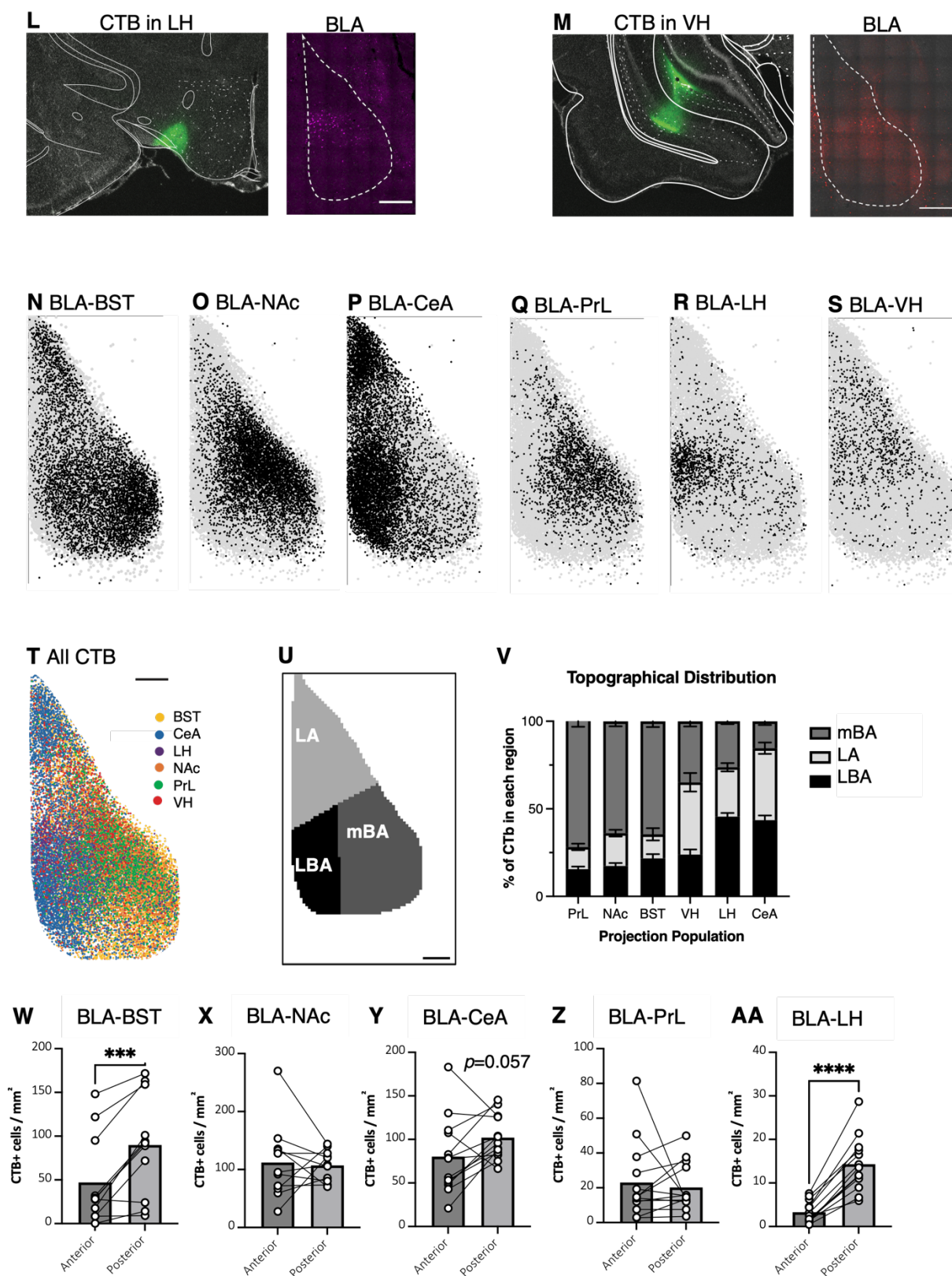


Figure 3.3

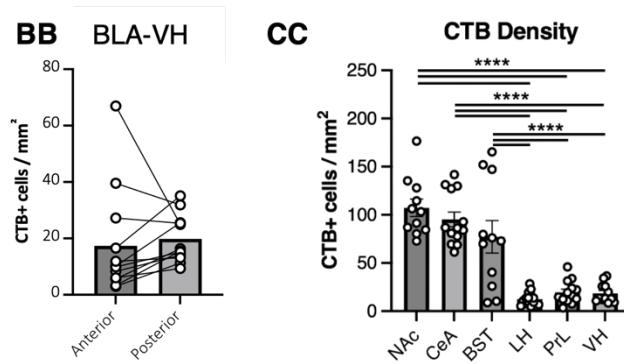


Figure 3.3. Topographical distribution of BLA projection neurons.

(A-F) Representative images of location of CTB injection in the bed nucleus of the stria terminalis (BST; n=11 (6/5)), nucleus accumbens (NAc; n=11 (6/5)), central amygdala (CeA; n=13 (6/7)), prelimbic cortex (PrL; n=13 animals (naïve: n=8; stress: n=5)), lateral hypothalamus (LH; n=15 (7/8)), or ventral hippocampus (VH; n=12 (6/6)). Colored spread indicates area of maximal expression of CTB at the injection site.

(G) Overview of experimental procedures.

(H-M) Representative images of CTB expression in target region (left) and BLA (right).

(N-S) Dot-plots of all CTB+ neurons in the BLA at AP -3.14 following injection of CTB into BST, NAc, CeA, PrL, LH, or VH

(T) Overlay of all dot-plots of CTB+ neurons in the BLA at AP -3.14; yellow =BST; blue =CeA; purple =LH; orange =NAc; green =PrL; red =VH;

(U) BLA subdivisions at AP -3.14: lateral amygdala (LA), lateral basal amygdala (LBA), and medial basal amygdala (mBA). Scale bar=150um.

(V) Percentage of CTB+ cells in each subdivision of the BLA following injection into each target region. Data were analysed using a 2Way ANOVA ($F_{10,138}=41.09$, $p<0.0001$) and differences are displayed in Table 2.

(W-BB) Density of CTB+ cells in anterior (AP -2.30 and -2.56) vs. posterior sections of the BLA (AP -2.80 and -3.30). Data were analysed using a two-tailed paired t-test (BST: $t(10)=4.738$, $p=0.0008$; NAc: $t(10)=0.2717$, $p=0.7914$; CeA: $t(12)=2.099$, $p=0.0577$; PrL: $t(12)=0.4240$, $p=0.6791$; LH: $t(12)=8.822$, $p<0.0001$; VH: $t(11)=0.5354$, $p=0.6030$).

(CC) Density of CTB+ cells throughout the BLA for each population. Data were analyzed using a one-way ANOVA ($F(5,69)=30.04$, $p<0.0001$).

Table 3.2

	% of total CTB+ cells in each subregion		
	mBA (#)	LBA (^)	LA (*)
PrL	71.8 (11.1) ^^^^ ****	15.5 (5.7) #####	12.7 (6.8) #####
NAc	63.9 (9.5) ^^^^ ****	17.4 (5.4) #####	18.7 (6.3) #####
BST	64.5 (11.0) ^^^^ ****	21.7 (7.9) #####	13.7 (11.5) #####
VH	34.8 (10.2)	23.9 (10.1) ##	41.3 (18.3) ^^
LH	26.2 (6.3) ^^^^	45.6 (8.0) ##### **	28.2 (9.3) ^^
CeA	15.4 (7.7) ^^^^ ***	43.6 (9.5) #####	41.0 (11.7) ###

Table 3.2. Regional distribution of projection populations.

Percentage of CTB+ cells in each subdivision of the BLA following injection into each target region. Mean (SEM).

^^ $p < 0.01$, ^^^ $p < 0.0001$ to LBA;

** $p < 0.01$, **** $p < 0.0001$ to LA;

$p < 0.01$, ### $p < 0.001$, #### $p < 0.0001$ to mBA

BLA projection populations are broadly activated by stress and with a common bias towards the medial basal amygdala. To determine if specific populations were activated by restraint stress, we calculated the percentage of CTB+ cells also expressing FOS following restraint stress or the naïve condition (Figure 3.4A). Unpaired t-tests revealed a significant difference between the naïve and stress condition in FOS expression in BLA neurons targeting the BST (Figure 3.4B; $t(9)=9.513$, $p < 0.0001$), CeA (Figure 3.4C; $t(11)=4.393$, $p=0.0011$), LH (Figure 3.4D; $t(13)=4.668$, $p=0.0004$), NAc (Figure 3.4E; $t(9)=10.28$, $p < 0.0001$), and PrL (Figure 3.4F; $t(10)=5.750$, $p=0.0002$). There was a trend towards significance in VH projectors (Figure 3.4G; $t(10)=2.066$, $p=0.0657$). Together, this suggests that a wide range of projection populations in the BLA are activated during stress.

We also normalized the contribution of each population to total FOS activity in the BLA by calculating percentage of FOS+ cells that labelled each projector (Figure 3.4H). A one-way ANOVA revealed a significant difference between projection populations ($F(5,28)=26.57$, $p < 0.0001$). Tukey's post-hoc tests indicated NAc projectors represented significantly more FOS+ neurons on average than any other population, and BST and CeA projectors represented more

FOS+ neurons than populations targeting the PrL or VH. This suggests that stress-induced FOS expression tends to have a bias towards NAc, BST, or CeA projectors.

Given that we had previously demonstrated that stress-induced FOS expression had a bias towards the mBA (unpublished data), we next investigated the anatomical location of CTB+/FOS+ cells to test if there is also a medial bias despite topographical differences for each population. We plotted the normalized coordinates of every co-labelled CTB+/FOS+ cell for each projection population (Figures 3.4I-O). This visually revealed a bias in activation towards the LA or mBA in nearly every population. To quantitatively confirm this bias, we divided the BLA into LA, mBA, and LBA subdivisions (Figure 3.4P) and quantified the proportion of CTB+/FOS+ labelled cells in each region for each projection population (Figure 3.4Q-V). RM One-Way ANOVA revealed a significant difference in percentage of CTB+/FOS+ neurons in each BLA subdivision for populations targeting the BST ($F(1.220,4.881)=28.23$, $p=0.0029$), CeA ($F(1.093,6.556)=14.58$, $p=0.0068$), NAc ($F(1.468,5.870)=41.28$, $p=0.0005$), PrL ($F(1.057,3.172)=27.20$, $p=0.0117$), and VH ($F(1.680,6.720)=14.95$, $p=0.0040$). There was no significant difference in the population targeting the LH ($F(1.753,10.52)=1.085$, $p=0.36411$). *Post-hoc tests* revealed a significant location bias toward the mBA in populations targeting the BST, NAc, PrL, and VH, and a significant location bias towards the LA in populations targeting the CeA. This confirms that, despite differences in topographical organization of discrete projection populations, stress-induced activation of the BLA exhibits a medial bias (Chapter 2). Collectively, these data suggest acute restraint stress activates a diverse array of projection neuron populations that are commonly located in the mBA.

Figure 3.4

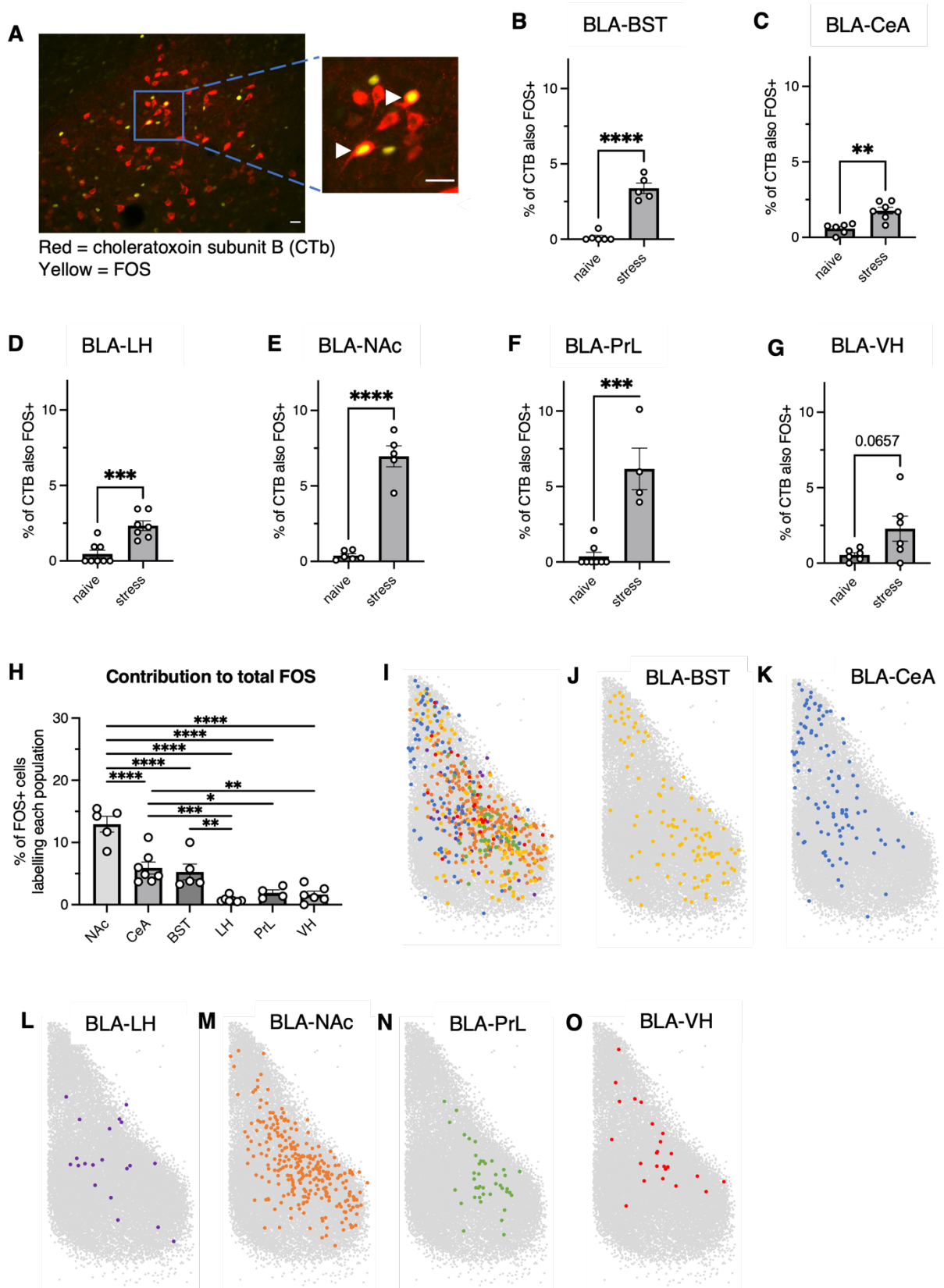


Figure 3.4

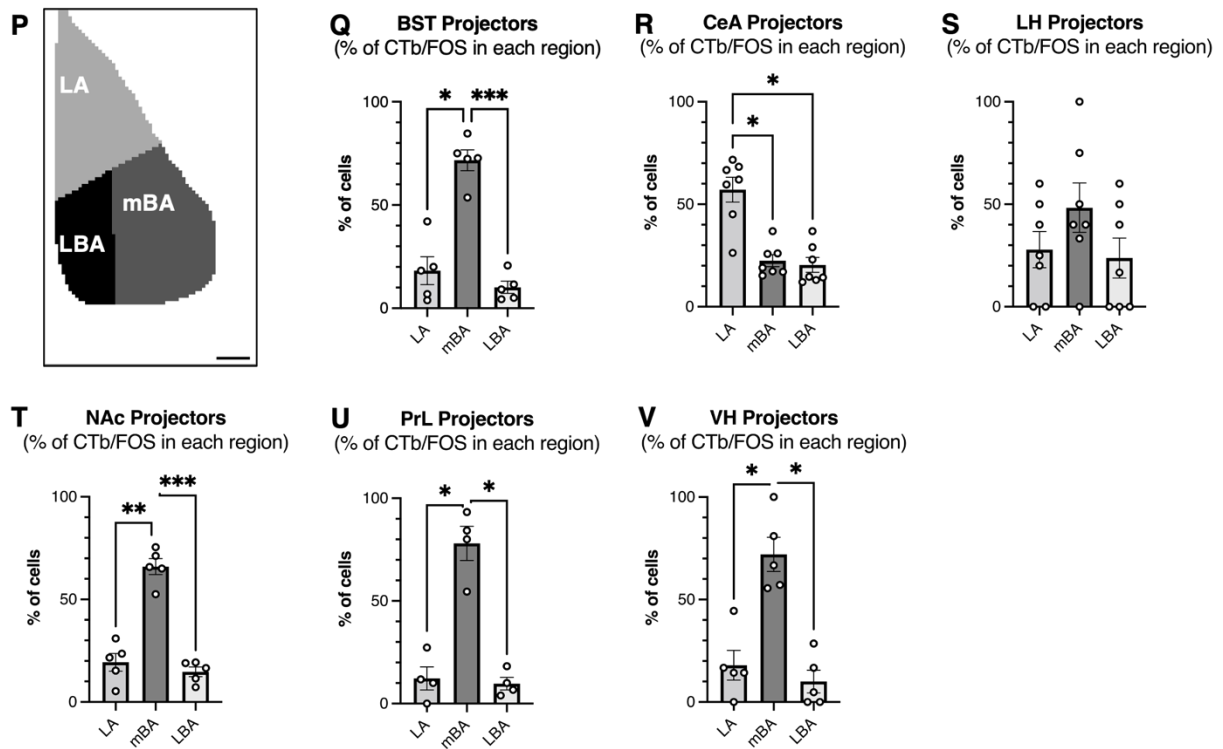


Figure 3.4. BLA projection populations are broadly activated by stress and with a common bias towards the medial basal amygdala

(A) Representative image of expression of FOS (yellow) and CTB (red) in the BLA. White triangle indicates colocalization. Scale bar = 250µm

(B-G) Percentage of CTB labelled cells for each projection population also expressing FOS in the naïve (left, triangles) or stress condition (right, circles). Data were analyzed using an unpaired t-test (BST: $t(9)=9.513$, $p<0.0001$; CeA: $t(11)=4.393$, $p=0.0011$; LH: $t(13)=4.668$, $p=0.0004$; NAc: $t(9)=10.28$, $p<0.0001$; PrL: $t(10)=5.750$, $p=0.0002$; VH: $t(10)=2.066$, $p=0.0657$

(H) Percentage of FOS labelled cells also expressing CTB for each projection population, stress condition only. Data were analyzed using an ordinary one-way ANOVA followed by Tukey's multiple comparison's test ($F(5,28)=26.57$, $p<0.0001$).

(I) Normalized coordinates of all co-labelled CTB+/FOS+ cells for each projection population in the BLA at AP -3.14; stress condition only.

(J-O) Normalized coordinates of all colabelled CTB+/FOS+ cells in the BLA at AP -3.14 following injection of CTB into the J. BST, K. CeA, L. LH, M. NAc, N. PrL, or O. VH; stress condition only.

(P) BLA subdivisions: lateral amygdala (LA), lateral basal amygdala (LBA), and medial basal amygdala (mBA) at AP -3.14. Scale bar=150um.

(Q-V) Percentage of total CTB/FOS co-labelled cells for each projection population in each subdivision of the BLA. Data were analyzed using a RM One-way ANOVA followed by Tukey's multiple comparison's test (BST: $F(1.220,4.881)=28.23$, $p=0.0029$; CeA: $F(1.093,6.556)=14.58$, $p=0.0068$; LH: $F(1.753,10.52)=1.085$, $p=0.36411$; NAc: $F(1.468,5.870)=41.28$, $p=0.0005$; PrL: $F(1.057,3.172)=27.20$, $p=0.0117$; VH: $F(1.680,6.720)=14.95$, $p=0.0040$)).

Error bars represent mean \pm SEM. * $p<0.05$; ** $p<0.01$ *** $p<0.001$; **** $p<0.0001$.

Individual effect of BLA projection populations on stress-induced CORT release. We have previously demonstrated that chemogenetic inhibition of mBA projection neurons reduces stress-induced CORT release and that optogenetic stimulation of mBA projection neurons in non-stressed conditions increases plasma CORT (unpublished data). This agrees with other examples demonstrating that excitotoxic lesions (Bhatnagar et al., 2004; Goldstein et al., 1996) or pharmacological modulation of discrete neurochemical systems within the BLA reduces stress-induced CORT (Cohen et al., 2018; J. M. Gray et al., 2015; Hill et al., 2009; Yaeger et al., 2022). However, each of these manipulations were relatively broad and did not investigate the impact of isolated BLA circuits on this effect. Therefore, it is unknown if this effect is driven by the collective action of multiple projection populations, or if specific BLA projection populations independently contribute to stress-induced HPA axis activation. To test this question, we used an intersectional viral approach to express the inhibitory Gi DREADD hM4Di in discrete BLA projection populations, and then administered the selective hM4Di ligand clozapine-*N*-oxide (CNO; to inhibit hM4Di+ neurons (Armbruster et al., 2007)) or VEH prior to stress exposure.

We first confirmed *in vitro* that CNO selectively reduces activity in neurons expressing hM4Di. We selected the BLA-NAc circuit as it exhibited the greatest density of CTB+ cells of each of the projections we investigated (Fig. 3.3CC) and was robustly activated by restraint stress (Fig. 3.4E). hM4Di was restricted to BLA-NAc neurons by injecting a retrograde virus expressing Cre

into the NAc (AAV2(rg)-eSYN-EGFP-T2A-iCre-WPRE; $1.0\text{--}1.2 \times 10^{13}$ GCs/ml) and injecting a Cre-dependent virus expressing hM4Di into the BLA (AAV8-hSyn-DIO-hM4Di-mCherry; $1.7\text{--}1.9 \times 10^{13}$ GCs/ml; Figure 3.5A). Injections of AAV8-hSyn-DIO-hM4Di-mCherry without the presence of the retrograde Cre virus did not yield any expression of hM4Di-mCherry in the BLA, confirming the cre-dependence of the virus ($n=2$ animals; data not shown). 4-5 weeks after surgery, brains were removed, and we performed whole cell patch clamp electrophysiology by bathing 10uM CNO onto slices expressing hM4Di in BLA-NAc neurons. A paired t-test comparing percentage firing at baseline vs. drug application confirmed that application of CNO reduced firing of cells expressing hM4Di (Figures 3.5B-C; $t(10)=2.477$, $p=0.0327$).

We next confirmed CNO-mediated suppression of hM4Di+ neurons *in vivo*. Along with the dual virus intersectional approach described above, we also injected a Cre-dependent virus expressing mCherry into the BLA (AAV8-hSyn-DIO-mCherry; 1.6×10^{13} GCs/ml) as a secondary control to test off-target effects of CNO. 4-5 weeks later, animals were injected with either CNO (3mg/kg, *i.p.*) or VEH (3ml/kg in 0.2% DMSO) and then all animals were exposed to 30min restraint stress to induce FOS expression in the BLA. Consistent with our previous work (Chapter 2) using chemogenetic approaches to attenuate neuronal activity in the mBA, CNO (to inhibit hM4Di+ cells) or VEH was administered 45min prior to stress onset, and blood was collected at stress onset ($t=0\text{min}$, for baseline levels) and termination ($t=30\text{min}$, for peak stress levels; Figure 3.5D). We also collected brains 90min following stress onset and performed immunohistochemistry to quantify colocalization of FOS expression with hM4Di-mCherry in brains of animals administered CNO or VEH (Figure 3.5E, $n=9\text{--}12$ per group). Animals expressing the control mCherry were not analyzed as this construct produced a substantially stronger intensity of labelling (data not shown) and thus experimenter blinding could not be preserved during quantification. An unpaired t-test revealed no significant differences between CNO- or VEH-treated animals in total number of hM4Di+ (Figure 3.5F) or FOS+ cells per image (Figure 3.5G).

However, there were significantly fewer hM4Di+/FOS+ co-labelled cells per image in animals administered CNO compared to VEH (Figure 3.5H; $t(19)=3.426$, $p=0.0028$), and significantly fewer percentage of hM4Di+ cells also expressing FOS (Figure 3.5I; $t(19)=2.678$, $p=0.0149$). Together, this confirms that CNO reduces activation specifically of hM4Di+ cells in the BLA both *in vitro* and *in vivo*.

We next replicated previous findings that CNO (3mg/kg, *i.p.*) has no effects on basal or stress-induced plasma CORT in the absence of hM4Di (unpublished data). Animals underwent surgery to virally express either mCherry or hM4Di in the BLA-NAc circuit; 4-5 weeks later animals were administered VEH or CNO 45min prior to 30min restraint stress, and blood was collected at stress onset ($t=0$ min, for baseline CORT measure) and termination ($t=30$ min, for peak stress CORT measure). A 2Way ANOVA revealed no significant differences in plasma CORT between animals treated with hM4Di/VEH, mCherry/CNO, or hM4Di/CNO (Figure 3.5J; $F(2,25)=0.2307$, $p=0.7956$). This confirmed there were no off-target effects of CNO on plasma CORT; we therefore performed subsequent experiments with only two groups: hM4Di/VEH and hM4Di/CNO. These experiments also demonstrated that chemogenetic inhibition of BLA-NAc neurons has no effect on stress-induced CORT.

Using the same approach, we then tested the impact of chemogenetic inhibition of three other BLA projection populations. Animals underwent surgery to virally express hM4Di in the BLA-CeA, BLA-BST, or BLA-PrL circuit; 4-5 weeks later animals were administered VEH or CNO 45min prior to 30min restraint stress, and blood was collected at stress onset ($t=0$ min) and termination ($t=30$ min). 2Way ANOVA revealed no significant differences in baseline or stress-induced plasma CORT between animals treated with CNO vs VEH and expressing hM4Di in BLA-CeA (Figure 3.5K; $F(1,14)=1.117$, $p=0.3084$) or BLA-BST projection populations (Figure 3.5L; $F(1,13)=0.1678$, $p=0.6887$). However, a mixed effects analysis revealed a significant difference in plasma CORT between CNO vs. VEH-treated animals when hM4Di was expressed in the BLA-

PrL projection population (Figure 3.5M; $F(1,33)=7.411$, $p=0.0103$). *Post-hoc* tests revealed that animals treated with CNO exhibited significantly greater plasma CORT 30min following stress onset compared to those treated with VEH ($p=0.0116$), suggesting this circuit may actually function to restrain or inhibit HPA activation. Finally, we hypothesized that chemogenetically inhibiting two projection populations in tandem may recapitulate the HPA dampening effects of large-scale inhibition of the mBA. To this extent we chose two projection populations that we had demonstrated were robustly activated by stress and expressed widely throughout the BLA, including the mBA. Thus, we restricted hM4Di to both BLA-NAc and BLA-CeA projections in the same animal by injecting a retrograde virus expressing Cre into the NAc and CeA, and a Cre-dependent virus expressing hM4Di into the BLA. 4-5 weeks later animals were administered VEH or CNO 45min prior to 30min restraint stress, and blood was again collected at stress onset ($t=0\text{min}$) and termination ($t=30\text{min}$). 2Way ANOVA revealed no significant differences between VEH or CNO-treated animals (Figure 3.5N; $F(1,9)=1.328$, $p=0.2789$).

Collectively, these data suggest that chemogenetic inhibition of individual, or even dual, BLA projection neuron populations alone does not recapitulate the HPA-dampening effect of chemogenetic inhibition of projection neurons within the mBA together. Inhibition of the BLA-PrL circuit enhanced stress-induced CORT, suggesting that this projection may endogenously have a stress-dampening role.

Figure 3.5

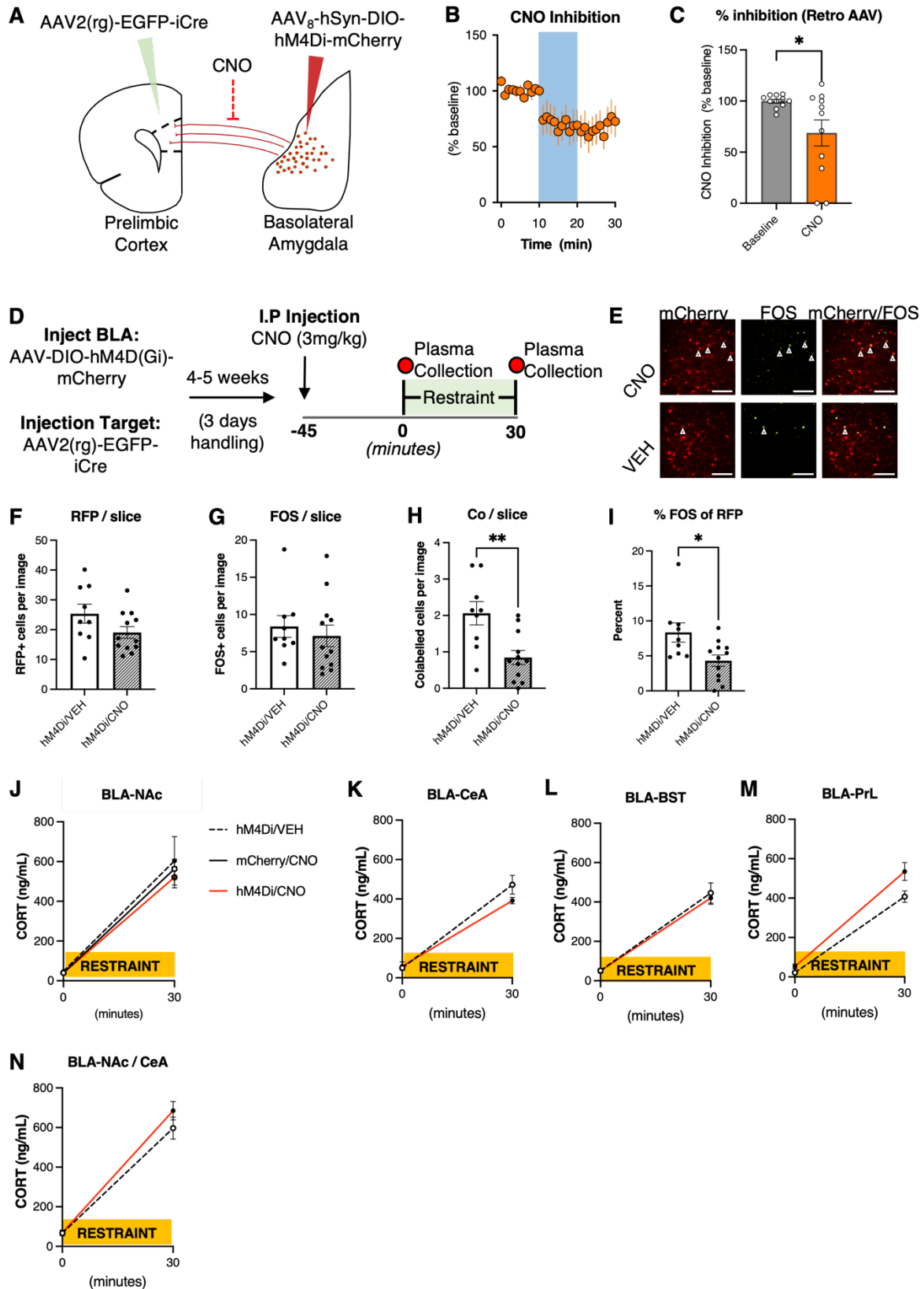


Figure 3.5. Individual effect of BLA projection populations on stress-induced CORT release.

(A) Schematic of dual virus approach to restrict hM4Di expression to discrete projection populations.

(B) Time series demonstrating that bath application of CNO (10uM, blue band) reduces firing rates in cells expressing hM4Di.

(C) Percent firing compared to baseline (gray) of cells expressing CNO (orange). Data were analyzed using a paired t-test ($t(10)=2.477$, $p=0.0327$).

(D) Overview of experimental procedures.

(E) Representative image of expression of mCherry (red) or FOS (yellow) in the BLA of animals expressing hM4Di in BLA-NAc projection neurons and administered CNO (3mg/kg, i.p.) or VEH (saline, 1ml/kg). Scale bar = 100um; white triangles indicate colocalization of FOS and mCherry.

(F) mCherry+ cells per image in animals administered VEH or CNO. Data were analyzed using an unpaired t-test ($t(19)=1.768$, $p=0.0931$).

(G) FOS+ cells per image ($t(19)=0.6030$, $p=0.5537$).

(H) Co-expressing FOS+/mCherry+ cells per image ($t(19)=3.426$, $p=0.0028$).

(I) Percentage of mCherry+ cells also expressing FOS ($t(19)=2.678$, $p=0.0149$).

(J) Plasma CORT levels in animals expressing hM4Di- or mCherry in BLA neurons projecting to the NAc, following injection of CNO or VEH 30min prior to restraint stress ($n=8-11$ per group). Data were analyzed using a 2Way ANOVA followed by Sidak's multiple comparison's test ($F(2,25)=0.2307$, $p=0.7956$).

(K-N) Plasma CORT levels following injection of CNO or VEH in hM4Di-expressing animals that were exposed to restraint stress 30min later, animals with hM4Di expressed in BLA cells projecting to the (K) CeA ($n=6-10$ per group; $F(1,14)=1.117$, $p=0.3084$), (L) BST ($n=6-9$ per group; $F(1,13)=0.1678$, $p=0.6887$), (M) PrL ($n=9-10$ per group; $F(1,33)=7.411$, $p=0.0103$, or (N) both NAc and CeA ($n=4-7$ per group; $F(1,9)=1.328$, $p=0.2789$)). Data were analyzed using a 2Way ANOVA, followed by Sidak's multiple comparison's test. In cases with missing time points from blood samples, a mixed effects model was used.

Error bars represent mean \pm SEM. * $p<0.05$; ** $p<0.01$ *** $p<0.001$, **** $p<0.0001$

3.5 DISCUSSION

It is well-known that psychological stress robustly activates projection neurons in the BLA (Reznikov et al., 2008), however their circuit identity and functional contribution to the stress response remains relatively unknown. We have previously shown that psychological stress leads

to activation of the mBA subregion of the BLA and that BLA projection neurons within the mBA bidirectionally drive stress-induced HPA activation (Chapter 2). Here, we expanded on this to identify and characterize discrete projection neuron populations in the BLA activated by psychological stress. Specifically, we identified that BLA projection neurons are heterogeneously distributed throughout the BLA and that a wide range of projection populations are activated by psychological stress. Optogenetic stimulation of CaMKIIa+ projection neurons in the mBA led to activation in downstream regions such as the dmBST and PrL, confirming functional connectivity with these targets. Specific chemogenetic inhibition of discrete populations targeting the NAc, BST, or CeA had no effect on stress-induced CORT, while inhibition of BLA-PrL neurons increased stress-induced CORT. Together, these data suggest that although BLA projection neurons are heterogeneously distributed throughout the BLA, activation of independent circuits from the BLA are not sufficient to alter stress-induced HPA activation. Thus, while manipulation of discrete BLA circuits may be capable of influencing discrete behavioural processes (Janak & Tye, 2015), it is likely that multiple BLA circuits contribute in tandem to influence stress-induced HPA activation.

Our first two experiments replicated a large body of literature demonstrating anatomical and functional connectivity of BLA projection neurons with multiple downstream regions. Surgical delivery of an anterograde virus expressing eGFP into the BLA led to widespread expression of BLA fibers throughout the brain, including strong axonal expression in the BST, NAc, PrL, LH, CeA, and VH. This supports many classical anatomical experiments (H.-W. Dong et al., 2001; Hoover & Vertes, 2007; Krettek & Price, 1977; McDonald, 1991; Petrovich et al., 1996; Pitkänen et al., 2002; Reppucci & Petrovich, 2016; Sah, Faber, Lopez De Armentia, et al., 2003). We also tested functional connectivity of these circuits to confirm that activation of these circuits led to activation of terminal regions. As others have shown, stimulation of BLA projection neurons increased activity in the PrL and dmBST, which is unsurprising given that these are glutamatergic

projections (Gungor & Pare, 2016; Little & Carter, 2013). We did not see a significant increase in FOS expression in other terminal regions following optogenetic stimulation of BLA projection neurons; however, our optogenetic targeting was aimed at the mBA, and this region is where PrL- and dmBST- projectors were preferentially located.

Indeed, our topographical mapping of projection neurons revealed distinct expression gradients within the BLA for each population. Populations targeting the PrL, NAc, and BST were predominantly located in the mBA, the region we identified as particularly responsive to stressors. In contrast, CeA projectors were more commonly found in the LA and LBA and minimally expressed in the mBA. Finally, VH projectors were predominantly located in the LA. This heterogeneity strongly agrees with previous work mapping topography of projection neurons in rodents (Beyeler et al., 2018; McGarry & Carter, 2017; O'Leary et al., 2020; Reppucci & Petrovich, 2016; Senn et al., 2014), and emphasizes that the BLA is a highly topographically diverse structure and should not be treated as a unitary and homogenous brain region. This heterogeneity likely contributes to the capacity of the BLA to influence a diverse array of behavioural (Janak & Tye, 2015) and physiological outcomes (Bhatnagar et al., 2004; Soltis et al., 1997). It will be informative to further identify if there is also heterogeneity and specificity of inputs to the BLA. For example, previous work has shown that cholinergic (Ben-Ari et al., 1977) and noradrenergic inputs (Fallon et al., 1978) preferentially target the basal amygdala. Thus, it will be important to determine if these inputs synapse onto discrete projection populations or cell types, particularly ones that are responsive to stressors, or if they non-specifically target many different cells in that region.

We only included animals with CTB restricted to target regions. As a result, there were few animals quantified with CTB expressed in two projections. Therefore, we are unable to adequately comment on the degree of collateralization of projection neuron populations. However, others have shown mixed findings depending on the specific projection populations being investigated and the anatomical tracing technique being used (Beyeler et al., 2016, 2018; Klavir

et al., 2017; Lichtenberg et al., 2021; Senn et al., 2014; Shinonaga et al., 1994), and is an important question that warrants further characterization. This is especially critical when performing experiments using projection-specific photometry, optogenetics, or chemogenetics, as it is possible that manipulation of a specific projection population also influences activity of other regions via downstream collaterals.

We have previously identified the mBA as particularly responsive to psychological stress (Chapter 2, 2023). Given that our topographical mapping revealed that this region has dense populations targeting the PrL, NAc, and BST, we hypothesized that these populations would be recruited during stress exposure. Our colocalization experiments revealed stress-induced FOS expression on many CTB-labelled cells, including those targeting the NAc, VH, PrL, CeA, BST, and LH. Activation of VH, PrL, BST, and CeA projectors was not surprising, as many of these populations and targets are known to drive stress-related processes, including anxiety-like behaviour, memory consolidation, and HPA activation (Bruzsik et al., 2021; Davis et al., 2010; Felix-Ortiz et al., 2013, 2016; Huff et al., 2016; J. C. Jimenez et al., 2018; Q. Zhang et al., 2022). We also observed robust activation of BLA-NAc projectors. Activation of this population was somewhat surprising as recent work has shown that this circuit is readily self-stimulated in rodents (Namburi et al., 2015; Stuber et al., 2011) and counteracts stress-induced anxiety (Bagot et al., 2015). Thus, it is unexpected that this projection population would be activated during stress exposure, however given that FOS does not provide any temporal information on when this population was activated, the possibility exists that BLA-NAc neurons may become activated following termination of stress and thus could be involved in stress relief as opposed to having an active role in generating aspects of the stress response. Similarly, this population could be activated during stress to counteract, or buffer, stress induced anxiety, and thus animals with greater activation of this circuit may display greater resilience to maladaptive changes induced by stress (Bagot et al., 2015). Alternatively, this circuit has also been shown to mediate

glucocorticoid-enhancement of memory (Roozendaal et al., 2001), suggesting a potential role in salience encoding. As such, it would be informative to test whether activation of this circuit increases with progressively more salient stimuli, such as increasingly stronger foot shock. Additionally, a distinct subset of BLA-NAc projectors expressing cholecystinin has been demonstrated to facilitate anxiogenic changes following chronic social defeat stress (Folkes et al., 2020; Shen et al., 2019), and thus a subset of this projection population may be involved in aversive behavioural changes. Thus, it is essential to consider that within large projection populations such as the BLA-NAc there may be further heterogeneity dependent on precise anatomical targeting or molecular identity.

Although all populations were activated by stress despite each population having differences in topographical distribution, this still agrees with our previous findings that the mBA is specifically recruited during stress exposure (Chapter 2, 2023). Indeed, the percentage of all CTB/FOS co-labelled cells was overwhelmingly expressed in the mBA for VH-, NAc-, BST-, and PrL- projectors. Additionally, there was not a lateral bias in distribution of LH/FOS or CeA/FOS co-labelled cells despite a lateral topographical bias in these projection populations, demonstrating that despite a lower number of LH- and CeA-projecting cells located in the mBA, these were the cells in those populations that were more likely to be activated stress. It remains to be investigated what biases the more medially localized BLA-CeA projectors for activation by stress, as well as what sort of stimuli lead to activation of the CeA projectors located in the LBA. Given the critical role of the BLA-CeA circuit in expression of learned fear (S. A. Jimenez & Maren, 2009), LBA:BLA-CeA projectors may be preferentially activated with repeated presentation of aversive stimuli to drive a learned response. Indeed, Beyeler and colleagues (2018) have shown that these projection neurons are activated during exposure to learned, aversive stimuli such as quinine, but not to learned, rewarding stimuli. It remains to be tested whether activation of the BLA-CeA projection becomes apparent only with repeated exposure to an aversive stimulus (i.e.,

as learning occurs), and if greater activation of these projection neurons is reflective of enhanced learning. Thus, activation of the LBA:BLA-CeA projection population may not have been apparent in our model, as stress exposure was acute, and activation instead may only have occurred if we had repeatedly presented our stimulus or if there was a stronger component of learning involved.

As mentioned above, FOS provides excellent spatial resolution to map topographical distribution of neurons activated during stress exposure but reflects poor temporal resolution. Thus, despite our finding that many different projection neuron populations are widely activated by stress, they still may exhibit impactful differences in activity patterns based on their temporal dynamics. For instance, Paré *et al*, 2015, demonstrated two classes of projection neurons activated during a foraging task but with different temporal dynamics. Just as different neurons in the BLA respond with different temporal dynamics during the same conditioning task (Kyriazi *et al.*, 2020), it is possible that, at a larger level, different projection populations respond with different temporal dynamics during the same stressor. For instance, ventral LA neurons exhibit a slightly delayed response latency from dorsal LA neurons during fear conditioning (Quirk *et al.*, 1995). Given our heterogenous topographical gradients, this supports the hypothesis that different populations may become active at distinct timepoints of stress, especially as different populations may have different functional roles.

We have previously demonstrated that inhibition of BLA:CaMKii projection neurons reduces stress-induced CORT release (Chapter 2, 2023). However, we did not investigate the circuit identity mediating this effect. Given that the BLA does not send any significant direct projections to the PVN (Petrovich *et al.*, 1996), we hypothesized that this effect may be relayed through intermediary regions such as the CeA, PrL, or BST, each of which have known direct or indirect connections to the PVN (Prewitt & Herman, 1998; Radley *et al.*, 2009; Radley & Sawchenko, 2011). We therefore used a dual-virus cre-dependent approach to restrict expression of an inhibitory DREADD (hM4Di) to each of these discrete projection neuron populations. We

also performed this experiment to inhibit BLA-NAc projection neurons as a negative control, as the NAc is not widely known to influence HPA axis activity (Herman et al., 2003, 2016, 2020).

Inhibition of discrete projection neuron populations in the BLA targeting the CeA, BST, NAc, or a combination of CeA and NAc, had no effect on stress-induced CORT release. Conversely, inhibition of BLA neurons targeting the PrL increased stress-induced CORT, suggesting that role of the PrL may act to constrain HPA activity during stress. Although this seems to counteract the known anxiogenic effect of BLA-PrL projections (Felix-Ortiz et al., 2016), this is not entirely unexpected as lesions of the PrL enhance stress-induced CORT release (Brake et al., 2000; Diorio et al., 1993), supporting this region as HPA-inhibitory. Further, the PrL is known to inhibit HPA activity through a discrete inhibitory circuit via the BST (Radley et al., 2009; Radley & Sawchenko, 2011). Thus, it is possible that the BLA-PrL circuit has a somewhat paradoxical role of driving anxiety-like response while also reducing HPA responses to stress. It remains to be seen if these are two independent pathways or if the same cells mediate these divergent effects. As such, the functional role of the BLA-PrL circuit could be to drive termination of the stress response (Ulrich-Lai & Herman, 2009). It is therefore imperative to determine which cell types the BLA-PrL projection neurons synapse onto in the PrL, and specifically if they are the cells involved in the PrL-BST-PVN inhibitory circuit or an alternative circuit.

While isolated, or dual, inhibition of distinct BLA projection neurons did not reproduce our previous findings that global inhibition of BLA CaMKII neurons within the mBA inhibits stress-induced CORT (Chapter 2), there are several possible explanations. First, we only targeted a select few projection populations in the BLA despite extensive projections throughout the brain (Sah, Faber, Lopez De Armentia, et al., 2003). It is possible that the BLA may mediate its effects on HPA activity through distinct circuits we did not investigate, such as the medial amygdala (Ulrich-Lai & Herman, 2009).

We characterized BLA neurons by projection target rather than molecular identity. While this is one aspect of identifying stress-responsive neurons, further studies should identify specific molecular markers of stress-responsive neurons. Indeed, distinct molecular markers have been shown to promote (Shen et al., 2019; Q. Zhang et al., 2022) or counteract (Jasnow et al., 2013; McCullough, Choi, et al., 2016; X. Zhang et al., 2020) anxiety-like behaviour and fear. It will be worth investigating if these cell types also influence HPA activity and not just behavioural changes. Additionally, pharmacological experiments suggest that activation of certain receptors in the BLA can alter stress-induced CORT, such as those targeting the corticotropin-releasing hormone type 1 receptor (CRHR1; (J. M. Gray et al., 2015)) or orexin type I receptors (Orx1R; (Yaeger et al., 2022)). Thus, an important question is if these receptors are restricted to stress-responsive cells and if they are differentially expressed on specific projection neuron populations. Identification of molecular markers that are unique to stress-responsive cells and circuits in the BLA may thus allow for a greater understanding of stress-responsive neural circuits in the brain which may be involved in the development of stress-related psychiatric disorders. The identification of molecular signatures within discrete circuits emanating from the BLA may in turn allow for pharmacological manipulation of these circuit to influence behavior or hormonal outcomes. In this vein, similar approaches to ours utilizing behavioral responses to aversive and appetitive stimuli have revealed the importance of neurotensin expression within neurons promoting reward and reducing fear (Li et al., 2022; McCullough, Choi, et al., 2016), suggesting that discrete neural circuits can be targeted for therapeutic benefit in stress-related psychiatric conditions. This is therefore an important avenue to continue exploring, as using an anatomical approach in rodents has been effective in identifying a novel pharmacological target for the treatment of stress-related disorders in humans.

3.6 ACKNOWLEDGEMENTS

This research was performed at the University of Calgary which is located on the unceded traditional territories of the people of the Treaty 7 region in Southern Alberta, which includes the Blackfoot Confederacy (including the Siksika, Piikuni, Kainai First Nations), the Tsuut'ina, and the Stoney Nakoda (including the Chiniki, Bearspaw, and Wesley First Nations). The City of Calgary is also home to Metis Nation of Alberta, Region III. We would like to acknowledge the Hotchkiss Brain Institute optogenetic core facility and the advanced microscopy facility for their technical support, and Min Qiao for her technical lab support. We also acknowledge the University of Calgary Health Sciences Animal Research Centre, specifically Vincent, Krista Jensen, and Brittany Munro. AAV8-hSyn-DIO-mCherry (Addgene #50459) and AAV8-hSyn-DIO-hM4D(Gi)-mCherry (Addgene #44362) were gifts from Bryan Roth). AAV2(retro)-eSYN-EGFP-T2A-iCre-WPRE was a gift from John Christianson.

3.7 FUNDING

This research was supported by operating funds to MNH from the Canadian Institutes of Health Research (CIHR). RJA received salary support from the Mathison Centre for Mental Health Research & Education and the Cumming School of Medicine. GNP received salary support from BranchOut Neurological Foundation, CIHR, and the Cumming School of Medicine. LTS received salary support from a Harley Hotchkiss Doctoral Scholarship in Neuroscience. All authors declare not conflict of interests.

3.8 AUTHOR CONTRIBUTIONS

List of authors: Aukema RJ, Petrie GN, Seabrook LT, Lau BK, Morena M, Christianson JP, Bains JS, Borgland SL, Hill MN

Contributions: RJA designed and conducted experiments, analyzed data, prepared figures, and wrote the manuscript. GNP conducted experiments. BL designed and conducted electrophysiology experiments. LS conducted electrophysiology experiments and reviewed the manuscript. MM conducted experiments and provided advice. JC provided viral construct. SL Borgland and JB provided advice. MNH developed and supervised the project and wrote the manuscript.

Chapter 4. Topographical and circuit-specific characterization of corticotropin-releasing hormone receptor type I-expressing neurons in the basolateral amygdala

4.1 ABSTRACT

Although the basolateral amygdala (BLA) and corticotropin releasing hormone receptor type I (CRHR1) signaling are both central to the stress response, the spatial and circuit-specific distribution of CRHR1 has not been identified in the BLA at a high resolution. We used a transgenic CRHR1-Cre-tdTomato rat to topographically map the distribution of BLA:CRHR1+ neurons and test their functional contribution to stress-related behaviours. Additionally, we used the BLA circuit projecting to the nucleus accumbens (NAc) as a model to test circuit-specific expression of CRHR1 in the BLA. As a result, we established several key findings. First, CRHR1 had the strongest expression in the LA, and particularly in the caudal BLA. Second, CRHR1 neurons exhibited an increase in FOS expression following exposure to restraint stress. Third, CRHR1 neurons were expressed on a subset of BLA-NAc projection neurons. Finally, inhibition of CRHR1 neurons did not influence stress-induced CORT release, anxiety-like behaviour, or fear memory.

4.2 INTRODUCTION

The basolateral amygdala (BLA) is a heterogenous structure that is integral to processing emotional stimuli. It is activated by a wide range of psychological stressors (Chapter 2; Úbeda-Contreras et al., 2018) and can drive both anxiety-like behaviour and hypothalamic-pituitary-adrenal (HPA) responses to stress (Bhatnagar et al., 2004; Chapter 2; Tye et al., 2011). These effects are likely mediated through projections to a wide range of limbic regions such as the

prelimbic cortex, ventral hippocampus, bed nucleus of the stria terminalis, and central amygdala (Sah, Faber, Lopez De Armentia, et al., 2003). Indeed, there are multiple lines of evidence that individual BLA projection neuron populations can drive changes in anxiety-like behaviour (Janak & Tye, 2015). However, the BLA also responds to rewarding stimuli (Beyeler et al., 2018; Shabel & Janak, 2009; X. Zhang et al., 2020), and individual projection neuron populations are known to drive a wide range of different, and even competing, behavioural responses (Beyeler et al., 2018; Janak & Tye, 2015; J. Kim et al., 2016). It is unknown, then, precisely which types of cells are active during exposure to stress and what their functional role in the stress response may be. In Chapter 3, we identified that multiple projection neuron populations are activated during exposure to acute restraint stress, including those targeting the prelimbic cortex, central amygdala, ventral hippocampus, lateral hypothalamus, bed nucleus of the stria terminalis, and nucleus accumbens. However, isolated, or even dual inhibition of distinct BLA projection neurons did not reproduce previous work demonstrating the contribution of the BLA in the HPA response to stress (Bhatnagar et al., 2004, Chapter 2, Chapter 3) Thus, perhaps a more effective approach may be to identify and specifically manipulate molecular markers of cells activated during exposure to stress.

Corticotropin-releasing hormone (CRH) is a central regulator of the stress response. The CRH receptor Type I (CRHR1) is widely expressed across limbic regions (Weera et al., 2022), and global pharmacological inhibition or genetic deletion of CRHR1 dramatically reduces both anxiety-like behaviour and HPA responses to stress (Habib et al., 2000b; Müller et al., 2003; G. W. Smith et al., 1998). More specifically, CRHR1 is moderately expressed in the BLA, predominantly in glutamatergic projection neurons (Agoglia et al., 2020; Y. Chen et al., 2000; Van Pett et al., 2000), and CRH is released into the amygdala during acute restraint stress (Merlo Pich et al., 1995). Further, CRH directly into the BLA leads to activation of CaMKII α projection neurons (Rostkowski et al., 2013), enhances memory consolidation (Liang & Lee, 1988; Roozendaal et

al., 2002), drives anxiety-like behaviour, and amplifies the HPA response to stress (J. M. Gray et al., 2015). Thus, release of CRH and activation of CRHR1 during stress likely contributes to aspects of the stress response, perhaps through activation of discrete BLA circuits.

Precise anatomical and circuit mapping of CRHR1 neurons has been difficult due to a lack of reliable anti-CRHR1 antibodies and relatively low protein expression levels, in comparison to other brain regions such as the central amygdala (Refojo et al., 2011; Weera et al., 2022). It is thus poorly understood which specific subregions, and projection populations, of the BLA that CRHR1 is expressed within. Given that distinct subregions of the BLA are differentially responsive to aversive stimuli (Chapter 2, 2023; Kim et al., 2016) and house distinct projection neuron populations (Beyeler et al., 2018; Chapter 3, 2023; McGarry & Carter, 2017; Reppucci & Petrovich, 2016), identifying the topographical distribution of CRHR1 in the BLA will be informative for both establishing which discrete BLA projection circuits CRHR1 is expressed within as well as what behavioural and physiological processes it may contribute to.

Recently, Weera and colleagues (2022) have generated a CRHR1-Cre-tdTomato transgenic rat, thus allowing both the visualization of CRHR1 distribution as well as manipulation of these neurons through genetic tools such as cre-dependent viral constructs (Weera et al., 2022). We therefore used this transgenic line to anatomically map CRHR1 expression throughout the BLA, to determine if there is any bias in expression towards stress-responsive BLA subregions; and establish if CRHR1+ neurons are activated by stress. We then used the BLA projection population targeting the nucleus accumbens (NAc) as a model for interrogating circuit-specific expression of CRHR1. We selected this projection as it is heavily expressed in the BLA and robustly activated by stress (Chapter 3; Huang et al., 2021) and is known to drive both appetitive (Beyeler et al., 2018; Stuber et al., 2011) and aversive behaviours (Birnie et al., 2023; Folkes et al., 2020; Shen et al., 2019).

4.3 MATERIALS AND METHODS

Animals. All animal protocols were approved by the University of Calgary Animal Care Committee and followed guidelines from the Canadian Council on Animal Care. Adult male and female CRHR1-Cre-tdTomato rats on a Wistar background were bred in the facility (10-13 weeks at time of testing). Only animals positive for the presence of transgenic iCre DNA were used after screening with PCR. Rats were maintained under a 12h light-dark cycle (lights on at 8am) with food and water available *ad libitum*. Animals were weaned at 21 days of age, separated by sex, and triple-housed until genotyping via an ear punch was completed. At P28-35 animals were pair-housed with the same cage-mate for the remainder of the study. Cage-mates were always in identical treatment groups and underwent all aspects of experimentation at the same time. All attempts were made to counterbalance pups from each litter into different groups. For tdTomato mapping, 2-3 animals from 4 different litters were used. For stress-induced FOS experiments, no more than 3 animals (and 2 of the same sex) from each litter were used per group, such that a maximum of 30% of animals in each group were from the same litter. For chemogenetic experiments, no more than 2 animals from each litter were used per group, such that a maximum of 12.5% of animals in each group were from the same litter.

Genotyping. Rats were genotyped for the presence of the iCre transgene by extracting DNA from ear notch samples using the Quantabio Extracta DNA prep according to manufacturer's instructions, followed by PCR amplification with Kapa2G Fast Genotyping Mix using the following primers: iCre-F (AGATGCCAGGACATCAGGAACCTG), iCre-R (ATCAGCCACACCAGACACAGAGATC), rROSA26-F (CTTCAGCCACATGGTGGGTC) and rROSA26-R (TTGGCTAACTTACCAGTTATGCTACCT). Rat samples containing the iCre transgene resulted in a specific PCR product of 236 bp whereas the control ROSA26 product

appeared at 826 bp in all samples. Only animals expressing iCre were included for further experimentation.

Brain collection. Brains were collected and processed identically for all experiments. For perfusion, animals were anesthetized with an overdose of sodium pentobarbital and transcardially perfused with 0.9% saline (~60mL per rat, 30 mL/min) followed by 3.8% paraformaldehyde in 0.01M PBS (~120mL per rat, 30 mL/min). Following perfusion, brains were removed and immersed in 3.8% paraformaldehyde in 0.01 M PBS overnight before being switched to a 20% sucrose solution in PBS for 48-72 hours, and then transferred to a 30% sucrose solution in PBS for cryoprotection. Coronal sections of 40um were cut in four series' on a Leica SM 2010R sliding microtome and collected in antifreeze (30% wt/vol sucrose, 1% wt/vol polyvinylpyrrolidone-40, 30% vol/vol ethylene glycol, 0.0065% wt/vol sodium azide, in PBS; adapted from (Butler et al., 2012)) and stored at -20 C until processing.

Immunohistochemistry. Free-floating sections of the BLA were rinsed 3x10min in PBS, followed by 3x10min in PBS + Triton X-100 (0.1%). Sections were then blocked for 1h at room temperature with gentle agitation in 5% normal donkey serum in PBS and incubated for 24-48h in primary antibody at 4°C in antibody blocking solution (0.1% vol/vol Triton X-100, 0.1% wt/vol BSA, 0.05% wt/vol sodium azide, 0.04% wt/vol sodium EDTA in PBS). The primary antibodies used were anti-cFos antibody raised in rabbit (cFos, Cell Signaling Technology #2250s, 1:400, 24h incubation) or anti-RFP antibody raised in goat (RFP, Rockland #200-101-379, 1:1000, 48h incubation). After 24h incubation for FOS, or 48h incubation for RFP, sections were washed 3x10min in PBS + Triton X-100 (0.1%) and then incubated for 2h at room temperature with secondary antibody in antibody solution. The secondary antibodies used were donkey anti-rabbit AlexaFluor 647-conjugated secondary antibody (Alexa-647, #711-605-152, Jackson ImmunoResearch, 1:125) or

Cy3 donkey anti-goat (Cy3, Jackson #705-165-147, 1:500). Finally, sections were rinsed 3x10min in PBS + Triton X-100 (0.1%) and 2x10min in PBS, mounted onto charged slides, and cover-slipped using Fluoroshield with DAPI mounting medium (Sigma Aldrich).

Tilesan imaging for topographical mapping. Following immunohistochemistry against RFP to amplify tdTomato expression (to identify CRHR1+ cells), tilesan images of both the left and right BLA were collected from AP -2.12 to AP -3.60 (Paxinos & Watson atlas) from each animal using an Olympus VS110 Slidescanner with a 20X (0.75 NA air) objective. Only images with tissue undamaged throughout processing, sectioning, and immunohistochemistry were included (number of animals and slices per group: males: 5/36; females: 5/34). Exposure settings remained identical between all images, and the experimenter was blinded to sex of the animal. All images were saved as a virtual slide image (.vsi) for further analyses using Imaris software.

Topographical mapping and quantification of CRHR1+ cells. The experimenter remained blinded to the conditions of each animal during plotting and counting. Analyses were largely guided by work from (Beyeler et al., 2018) and performed identically to Chapter 2 and 2. Given that the BLA shape and size varied due to changes in AP position and imperfections in mounting and slicing tissue, we normalized all RFP+ neurons to a standardized shape of the BLA to accurately compare density gradients in the BLA.

Identification of CRHR1+ cells. We used Imaris software to semi-automatically detect RFP+ cells using the spot detection function. Images were pseudo-colored blue for DAPI and red for RFP. DAPI staining was used to visually identify the shape of the BLA based on contours provided by the surrounding fiber tracts. For all images, positive cells were detected having an average diameter of 8um, and the quality was manually set for each image until most labelled cells were

accurately identified by the software, as determined by the experimenter. Mis-labelled cells were manually removed, and non-labelled cells identified by the experimenter were manually added using the spot detection function. Coordinates of RFP+ cells were localized relative to the most dorsal point of the BLA (Figure 1B; “o”) using the position reference frame tool and exported to an excel sheet for further analyses.

Normalization. First, we established the average width and height of the BLA at 7 anterior-posterior (AP) positions. For every image, we identified its approximate AP position according to the Paxinos & Watson atlas (-2.12, -2.30, -2.56, -2.80, -3.14, -3.30, -3.60; (Paxinos & Watson, 2007)) and measured the average height, width, and triangular area of the BLA (Figure 4.1B) using Imaris Cell Imaging Software (Oxford Instruments). The formula for triangular area was: (height x width) / 2. Any image with a triangular area exceeding two times the standard deviation of the mean for the chosen AP position was re-assigned to a more appropriate AP position. We then calculated the average width (medial-lateral axis) and height (dorsal-ventral axis) at each of these 7 AP positions, which was then rounded to the nearest 25um for standardization (Supplementary Table 4.1).

Table 4.1

AP	Width (um)	Height (um)
-2.12	600	1450
-2.30	700	1650
-2.56	850	1950
-2.80	1075	2000
-3.14	1125	2175
-3.30	1275	2400
-3.60	1300	2450

Supplementary Table 4.1.
Standardized width (medial-lateral axis) and height (dorsal-ventral axis) at each AP position

Next, we normalized coordinates of every RFP+ neurons from each image according to these standardized dimensions. For each raw coordinate, the x-coordinate was normalized to the average width of the BLA at that AP position, and the y-coordinate to the average height of the BLA at that AP position. This established new x,y coordinates that maintained their original relative position in the BLA but could now be directly compared to images with a BLA of different raw dimensions.

To subdivide the BLA into the LA, LBA, and mBA subdivisions and to account for the curvature of the BLA along the medial fiber tract, a template shape was first created by manually fitting a standardized shape of the BLA derived from the Paxinos & Watson atlas (Paxinos & Watson, 2007) to all normalized RFP+ neurons in each plane, and then excluding FRP+ points outside of this template. In total, the standardized shape fit 93.39% (8,302 of 8,890) of labelled cells. This established a standardized template comprised of 25um x 25um “pixels” used for representation and quantification.

Quantification. To visually represent gradients of density across the BLA, the average density of RFP+ neurons were calculated per 25um x 25um bin and represented in heatmaps using a custom MATLAB script. Each pixel value represents average density per image, averaged across animals in the same group. To compare group differences, we calculated RFP density for each animal individually and then compared group means. The total area of a subregion was calculated as: [(number of 25umx25um pixels comprising the subregion of interest) * 25um * 25um]. The density was then calculated as: [total # of RFP+ cells detected in all pixels comprising the subregion of interest / total area of subregion of interest]. As multiple images were often collected from each AP plane for each animal, data were analyzed as average density per image: [(total # of cells from all pixels comprising the subregion of interest, from all slices) / (total area of subregion of interest * number of slices)]. These calculations were streamlined using a custom MATLAB script that can be accessed at the authors' request (mnhill@ucalgary.ca and robert.aukema1@ucalgary.ca).

Stereotaxic surgery. Rats were maintained under isoflurane anesthesia and analgesic treatment (meloxicam (2mg/kg, subcutaneously)) in a stereotaxic apparatus during surgical injection of viruses or implantation of fibre optic cannulas. A glass capillary containing viral vector or CTB-

488 was lowered into the brain and pressure injected using a NanoInject II apparatus (Drummond Scientific). Coordinates were relative to bregma and the surface of the skull, for BLA: anterior-posterior (AP) -2.8mm, medial-lateral (mL) ± 4.9 to 5.0mm, dorsal-ventral (DV) -8.4mm; for NAc: AP +1.8mm, ML -1.4, DV -7.2. Virus was delivered bilaterally in 8 x 64.4nl boluses over 5min (515.2nl total volume), and CTB-488 was delivered to the right hemisphere in 7 x 46nl boluses over 6min (322nl total volume). Following the injection of the last bolus, the glass capillary remained in place for an additional 10min to allow diffusion of CTB-488 or virus. Animals were allowed to recover for a minimum of 1 week before any handling, habituation, or testing began.

Retrograde Tracing with cholera toxin subunit B.

0.2% dilutions of Alexa-conjugated Cholera Toxin Subunit B in 0.4M PBS (CTB-488 or CTB-555; Invitrogen) were injected unilaterally into the NAc. A minimum of 7 days were allowed for recovery from surgery before experiments began.

Restraint Stress. Animals were allowed to recover a minimum of 1 week following CTB-488 injections prior to stress. On experiment day, animals were carted to an adjacent experimental room from the colony room and placed into clear Plexiglas restraint tubes for 30min. Animals were then returned to their home cage with their cage-mate and remained in the testing room until 90min following stress-onset, where they were anesthetized, perfused, and brains collected. Control animals remained in the colony room immediately until time of sacrifice, when they were anesthetized, perfused, and brains collected.

Histology. To verify CTB-488 injection site or viral expression in the BLA, free floating sections of the BLA or NAc were rinsed 3x10min in PBS, mounted onto charged slides, and cover-slipped using Fluoroshield with DAPI mounting medium (Sigma Aldrich). Images were acquired using an

Olympus VS120 slidescanner using a 10X / 0.4 NA air objective for detection of CTB-488 or DIO-hM4Di-mCherry. Imaging parameters (e.g., exposure) remained consistent throughout each experiment. Location of maximal expression of virus or CTB-488 were plotted onto coronal images adapted from an atlas (Swanson, 2004).

Confocal imaging for colocalization of CTB-488, FOS, and tdTomato. After immunohistochemistry for FOS, images of the ventromedial LA (AP -2.76 to AP -3.48) from both hemispheres were collected using a Leica TCS SPE II confocal microscope using a 20X / 0.55 NA HC PL FLUOTAR objective (Leica 5065190). cFos, CTB-488, and raw tdTomato signal were acquired independently and exported to ImageJ for quantification. The experimenter was blinded to condition and sex of each animal, and all imaging parameters remained identical throughout acquisition.

Analysis of CTB-488, FOS, and tdTomato.

Quantification. Number of cells expressing FOS were counted automatically in ImageJ based on minimum size and threshold parameters that remained identical across quantification. Number of cells expressing tdTomato and CTB-488 were counted manually. Double or triple labelling of CTB-488, FOS, and tdTomato were determined as a cFos signal bound by expression of CTB-488 or hM4D(Gi)-mCherry (Jin & Maren, 2015). The experimenter was blinded to condition and sex of each animal, and all imaging parameters remained identical across quantification.

Exclusions. Any animals where CTB-488 injection occurred outside of the NAc were excluded (N=2: n=1 female/stress; n=1 male/naïve). One animal was excluded only for laterality analyses, as the left hemisphere was damaged during brain dissection (n=1 female/naïve). Five animals were excluded due to abnormally low expression of tdTomato, such that there were fewer than

25 tdTomato+ cells counted across all images for each animal (N=5: n=1 female/naïve; n=1 female/stress; n=3 male/stress).

Chemogenetic inhibition.

Viral vectors. Expression of the G_i -coupled receptor hM4D(Gi) inhibits neural activity upon activation with CNO (Armbruster et al., 2007). We used a cre-dependent viral vector in CRHR1-Cre-tdTomato rats to selectively express hM4D(Gi) on CRHR1+ cells. AAV8-hSyn-DIO-hM4D(Gi)-mCherry was a gift from Bryan Roth (1.9×10^{13} GCs/ml; Addgene #44362). Virus was diluted in 0.01M of sterile PBS to reach desired titer. Animals were allowed to recover for a minimum of 4 weeks prior to handling and habituation.

Overview of experimental design. All animals underwent three experimental tests and were randomly assigned to treatment group (CNO vs. VEH) prior to each test, although were always in the same condition as their cage-mate. All animals experienced the same order of tests: restraint stress was followed by light-dark test 5 days later, and shock followed light-dark test 9-22 days later.

Restraint stress. Prior to testing day, animals were habituated to the test room for 1 hour each morning for 3 days prior to experiment day, and each animal was handled by the experimenter for 2min in the position used for injections on test day. On experimental day, animals were injected in their colony room intraperitoneally (*i.p.*) with either CNO-2HCl (HelloBio; 3mg/kg/ml), to activate hM4D(Gi), or vehicle (0.9% saline), and 30min later were moved to the testing room and immediately placed into clear Plexiglas restraint tubes for 30min. Blood samples were collected immediately at stress initiation (t_0 , to measure basal CORT levels) and termination (t_{30} , to measure peak CORT levels) as well as 60 and 90min following stress onset (to measure recovery

of CORT levels). Following stress exposure, animals returned to their home cage with their cage-mate and remained in the testing room. Animals were only removed from their cage to collect blood at t60 and t90.

Blood collection and corticosterone analysis. Animals were gently placed into clear Plexiglas restraint tubes and blood samples were collected into ice chilled, EDTA treated microvettes (Sarstedt AG & Co. KG; #16.444.100) from a small nick over the lateral tail vein. Tail blood was centrifuged at 10,000 rpm for 20min at 4°C to separate plasma, which was stored at –20°C until corticosterone analyses. Plasma samples were analyzed with an enzyme-linked immunosorbent assay kit (Arbor Assays; #K014-H5) by following the manufacturer’s instructions and as performed previously (DeVuono et al., 2020). Standards were run in triplicate, and samples were tested in duplicate and diluted 1:100 to ensure levels fit the standard curve. Groups were compared at individual time points or as an area-under-the-curve (AUC). The following formulas for AUC were used: $[(t_0 + t_{30}) * 30\text{min}] / 2 + [(t_{30} + t_{60}) * 30\text{min}] / 2 + [(t_{60} + t_{90}) * 30\text{min}] / 2$ (Pruessner et al., 2003).

Light-dark test. Prior to testing day, animals were habituated to well-lit and ventilated sound-attenuating chambers in the room for 1 hour each morning for 3 days prior to experiment day. Additionally, each animal was handled by the experimenter for 2min in the position used for injections on test day. On experimental day, animals were injected in their colony room *i.p.* with either CNO-2HCl (HelloBio; 3mg/kg/ml) or vehicle (0.9% saline) and immediately moved to sound-attenuating chambers in the testing room for 30min. After 30-40min, they were then individually placed into the light-dark box. Testing of cage-mates was separated by approximately 11min and performed similar to (Morena et al., 2019). The LD box (Med Associates) was made of white and black opaque Plexiglas (44 × 22 × 30 cm³, l × w × h, light chamber; 44 × 22 × 30 cm³, l × w × h,

dark chamber). The chambers were connected by a 9 × 10 cm² (l × h) door separating the two chambers. Testing was performed in low light conditions (30-40 lux in the light compartment). Animals were placed into the dark compartment and video recording immediately began. The box was cleaned with 70% ethanol solution between each animal. Videos were manually scored by a trained experimenter blinded to the treatment conditions. The parameters included were as follows: percentage of total time spent in light compartment, expressed as [(seconds in light chamber / total seconds spent in LD box) × 100]; total number of entries into the light chamber; and time to first enter the light chamber (latency, in seconds).

Fear conditioning. Fear conditioning and extinction training protocol was performed similar to (Morena et al., 2021) with some modifications. Behavioural testing was conducted in two different contexts within a Fear Conditioning Chamber (Med Associates Inc., St. Albans, VT, USA). Context A consisted of the chamber with clear, transparent front door and ceiling, conductive grid floor, and metal walls. This context was cleaned with 70% EtOH between animals. Context B was produced by placing white, opaque Plexiglas panels over the grid floor and side walls. This context was cleaned with a Virkon solution between animals. Each day, animals were moved into the testing room into sound attenuating, ventilated, and lighted chambers at least 30 minutes before and after exposure to context A or B. Days 1-3 consisted of habituation to the handler and each experimental context: on day 1, animals were handled for 1 minute each by the experimenter; on day 2, animals were handled for 1 minute, then were given 10 minutes to habituate to Context A; and on day 3, animals were again handled for 1 minute, then were given 10 minutes to habituate to Context B. On Day 4, animals underwent auditory fear conditioning. Animals were either injected with a CNO (3mg/kg/ml, HelloBio, CNO.2HCl solution) or VEH (0.9% saline) and immediately taken to the procedural room where they were placed in sound-attenuating chambers for 30 minutes prior to fear conditioning. Conditioning was conducted in context A. After an

acclimatization period of 5 minutes animals were exposed to 7 conditioning trials, each of which consisted of a 30 second conditioned stimulus (CS; 80 dB, 4 Hz tone) that co-terminated with a 1 second unconditioned stimulus (US; 0.65 mA shock). The inter-trial intervals (ITI) between two conditioning trials were 3 minutes. On day 5, extinction training was performed in Context B. This protocol consisted of an acclimatization period of 2 minutes, then 20 CS presentation trials with an ITI of 2 minutes. No shocks were administered. On Day 6, animals were tested for extinction retrieval. This was also performed in Context B and consisted of a 2min acclimatization period followed by 5 CS presentations with an ITI of 2 minutes. Behaviour was video recorded and analyzed for freezing using Video Freeze software (Med Associates Inc., St. Albans, VT, USA).

Exclusions. Animals were excluded from statistical analysis if there was significant expression of hM4Di-mCherry outside of the BLA (n=5). In the stress-induced CORT test, 3 animals were excluded for having baseline CORT values greater than 120ng/ml, suggesting basal stress (n=2 CNO; n=1 VEH). In the LD test, one animal was excluded as a significant outlier, as it never left the dark box for the duration of the test (n=1 CNO).

4.4 RESULTS

Topographical distribution of CRHR1 neurons in the basolateral amygdala.

We used transgenic CRHR1-Cre-tdTomato on a Wistar background to map the pattern of expression of CRHR1 in the basolateral amygdala (n=5 male; n=5 female). Animals were screened for the presence of transgenic iCre DNA using PCR (Supplementary Figure 4.1A). tdTomato was used as a marker for CRHR1 expression as both proteins are expressed as a single polypeptide (iCre-2A-tdTomato) that is cleaved at the 2A site (Weera et al., 2022). Co-expression of *Crhr1* and *iCre* has previously been validated in the BLA (Weera et al., 2022).

TdTomato expression was strongly observed in the lateral amygdala (LA) following anti-RFP immunohistochemistry to amplify the tdTomato signal (Figure 4.1A). To quantify location biases we observed visually, we mapped the location of CRHR1-tdTomato+ neurons within the BLA relative to the most dorsal point of the BLA and normalized each coordinate to the average width and height of the BLA at each AP plane (Figure 4.1B). There was no significant difference between sex in average BLA width (2Way ANOVA; $F_{1,56}=1.451$, $p=0.2335$), height ($F_{1,56}=1.375$, $p=0.2459$) or triangular area ($F_{1,56}=0.007270$, $p=0.9324$) at each AP plane (Supplementary Figure 4.1B-D) and we therefore used coordinates from both sexes to generate a standardized template for each AP plane guided by the Paxinos & Watson atlas (Paxinos & Watson) that subdivided the BLA into three distinct divisions: lateral amygdala (LA), medial basal amygdala (mBA), and lateral basal amygdala (LBA; (Chapter 2, 2023); Figure 4.1C).

We then used these normalized coordinates to quantify differences in density of tdTomato+ neurons across the BLA (Figure 4.1D). An independent-samples t-test revealed no significant difference between males and females in average density of tdTomato+ cells across all sections of the BLA (Figure 1E; $t_8=0.08763$, $p=0.9323$), so we therefore collapsed data from both sexes in further analyses. We next quantified rostral-caudal differences. A paired-samples t-test revealed a significant difference in tdTomato+ density between rostral and caudal sections

(Figure 4.1F; $t_8=5.164$, $p=0.0009$). We then quantified any dorsal-ventral and medial-lateral biases by quantifying tdTomato+ density in each subregion across all sections of the BLA. A RM one-way ANOVA identified a significant difference in average density of tdTomato+ cells between sub-regions ($F_{1.642,14.78}=16.19$, $p=0.0003$; Figure 4.1G), with Tukey's multiple comparison's test revealing significantly greater tdTomato+ density in the LA compared to the LBA ($p=0.0158$) and mBA ($p=0.0008$). Additionally, a RM one-way ANOVA revealed a significant difference in average percentage of tdTomato+ cells in each subregion ($F_{1.777,16}=76.01$, $p<0.0001$; Figure 4.1H), with Tukey's multiple comparison's test revealing a significantly greater percentage of total tdTomato+ cells in the LA compared to both the LBA ($p<0.0001$) and mBA ($p<0.0001$).

Collectively, these data suggest that spatial distribution of CRHR1+ neurons in the BLA is similar between sexes, with strongest expression in the LA subregion and particularly in caudal sections.

Figure 4.1

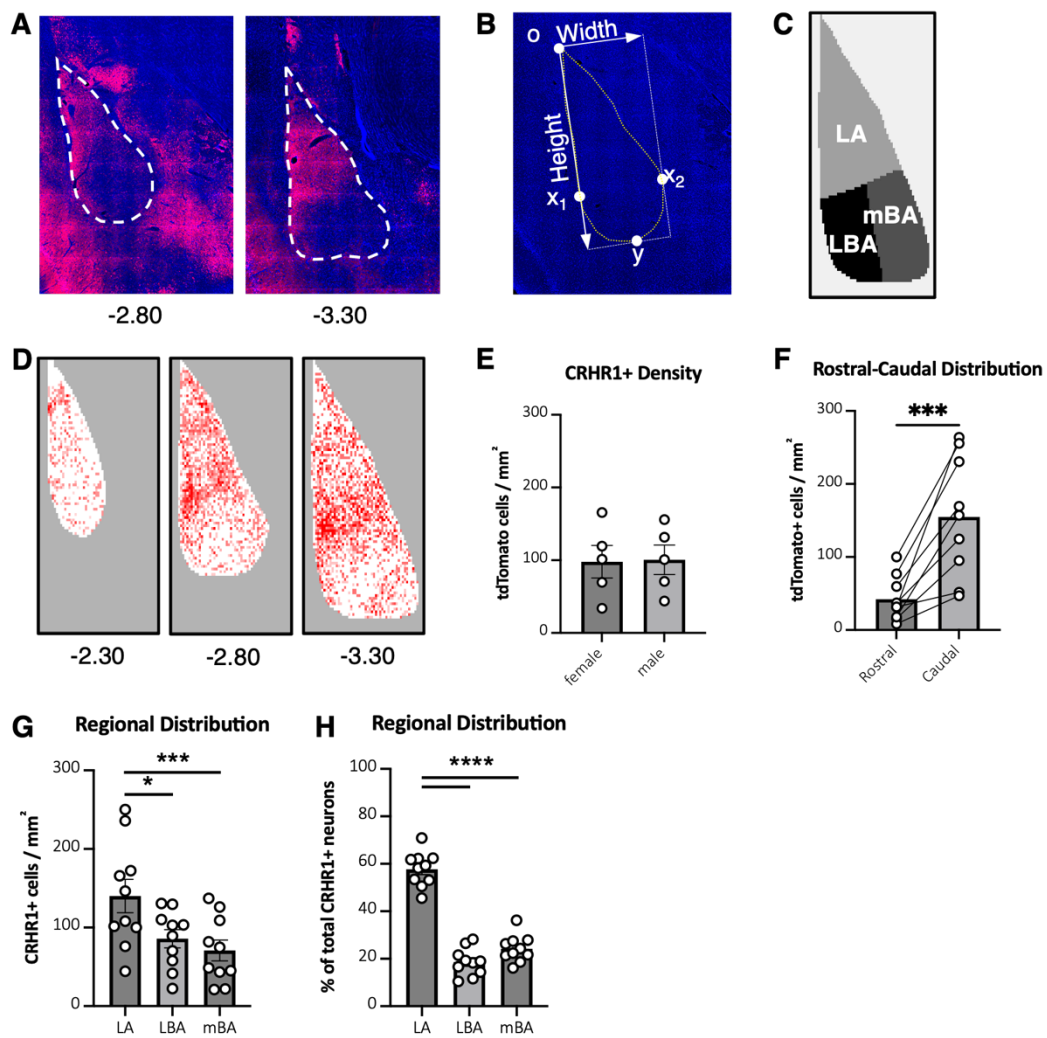


Figure 4.1. Topographical distribution of CRHR1 neurons in the basolateral amygdala

(A) Representative image of CRHR1-tdTomato expression following immunohistochemistry. Dashed lines delineate BLA;

(B) Representative image of the BLA depicting normalization procedure. Curved dashed line indicates boundary of BLA as determined by DAPI staining; 'o' indicates origin of reference frame; x_1 indicates most lateral point of the BLA; x_2 indicates most medial point of the BLA; y indicates most ventral point of the BLA; white arrows indicate measured width and height of the BLA;

(C) BLA subdivisions at AP -3.30: lateral amygdala (LA), lateral basal amygdala (LBA), and medial basal amygdala (mBA).

(D) Heatmaps representing density of normalized FOS+ expression in 25umx25um bins at AP -3.30. Darker colours represent higher density.

(E) Normalized density of CRHR1-tdTomato+ cells in the BLA in males (n=5) vs females (n=5). Data were analyzed using an independent-samples t-test ($t_8=0.08763$, $p=0.9323$)

(F) Normalized density of CRHR1-tdTomato+ cells in the BLA in rostral (AP -2.12, -2.30, -2.56) vs caudal (AP -3.14, -3.30, -3.60) sections. Data were analyzed using a paired t-test and include both sexes ($t_8=5.164$, $p=0.0009$)

(G) Normalized density of CRHR1-tdTomato+ cells in each subdivision of the BLA. Data were analyzed using a RM one-way ANOVA and include both sexes ($F_{1,642,14.78}=16.19$, $p=0.0003$) followed by Tukey's multiple comparison's test (LA vs LBA: $p=0.0158$; LA vs mBA: $p=0.0008$). Data includes both sexes.

(H) Mean percentage of total CRHR1-tdTomato+ neurons in each subdivision of the BLA. Data were analyzed using a RM one-way ANOVA and include both sexes ($F_{1,777,16}=76.01$, $p<0.0001$) followed by Tukey's multiple comparison's test (LA vs LBA: $p<0.0001$; LA vs. mBA: $p<0.0001$). Data includes both sexes.

CRHR1-tdTomato+ neurons were quantified across the entire BLA (AP -2.12 to AP -3.60) and normalized according to average BLA dimensions at each AP position and number of slices. Error bands represent mean +/- SEM. * $p<0.05$, ** $p<0.01$, *** $p<0.001$, **** $p<0.0001$.

CRHR1 and BLA-NAc neurons are activated by restraint stress.

We next investigated projection-specificity of CRHR1+ neurons in the BLA and whether they are activated by restraint stress. Adult male and female CRHR1-iCre-tdTomato rats were surgically injected with the retrograde tracer CTB-488 into the nucleus accumbens (NAc). 7-10 days later animals were immediately anesthetized for perfusion (naïve condition) or exposed to 30min restraint stress and anesthetized for perfusion 90min following stress onset (stress condition; Figure 4.2A). Injection of CTB-488 was largely restricted to the same anatomical location in both males and females (Figure 4.2B). We then quantified expression of CRHR1-tdTomato+, FOS+, and CTB-488+ neurons in the ventral LA of BLA sections ranging from AP -2.76 to AP -3.48 (Figure 4.2C).

We first tested if stress increases FOS expression in the ventral LA. We selected this as a region of interest due to its high expression of CRHR1+ cells, as well as being robustly activated by both novelty and aversive stressors (Chapter 3). An independent-samples t-test including both sexes revealed significantly greater FOS expression in animals exposed to stress than in the naïve condition (Figure 4.2D; $t_{18}=3.805$, $p=0.0013$). There were no significant differences between sex in stress-induced FOS expression (Figure 4.2E; $t_{18}=0.2137$, $p=0.8332$).

We next quantified if stress increases FOS expression in CRHR1+ neurons in the ventral LA (Figure 4.2F). We used tdTomato (termed as red fluorescent protein (RFP)) as a proxy for CRHR1+ cells (Weera et al., 2022). An independent-samples t-test revealed no significant differences between sex in average number of CRHR1-tdTomato+ neurons (Figure 2G; $t_8=1.244$, $p=0.2486$), as previously shown (Figure 4.1E), so we therefore pooled both sexes. There was a significantly greater percentage of tdTomato+ neurons also expressing FOS in the stress condition compared to the naïve condition (Figure 4.2H; $t_{18}=2.109$, $p=0.0492$) without any significant difference between sexes (Figure 4.2I; stress condition only: $t_8=0.9424$, $p=0.3736$).

Next, we quantified if stress increases FOS expression in BLA-NAc projection neurons (CTB+) in the ventral LA (Figure 4.2J) in both males and females. CTB+ expression was significantly greater in the right hemisphere (Supplementary Figure 4.2D; $t_{18}=9.310$, $p<0.0001$). This was not surprising as the BLA-NAc projection is predominantly ipsilateral (Brog et al., 1993), and we restricted our CTB-488 injections to the right NAc. Therefore, we limited further analysis of CTB+ neurons to the right hemisphere only. An independent-samples t-test revealed significantly greater expression of CTB+ neurons in females (Figure 4.2K; $t_{18}=2.661$, $p=0.0159$). Pooled male and female data revealed a significantly greater percentage of CTB+ neurons in the stress condition also expressing FOS, compared to the naïve condition (Figure 4.2L; $t_{18}=3.457$, $p=0.0028$). Females exhibited a marginally significantly lower percentage of CTB+ neurons also expressing FOS compared to males in the stress condition (Figure 4.2M; $t_8=2.306$, $p=0.0500$).

Figure 4.2

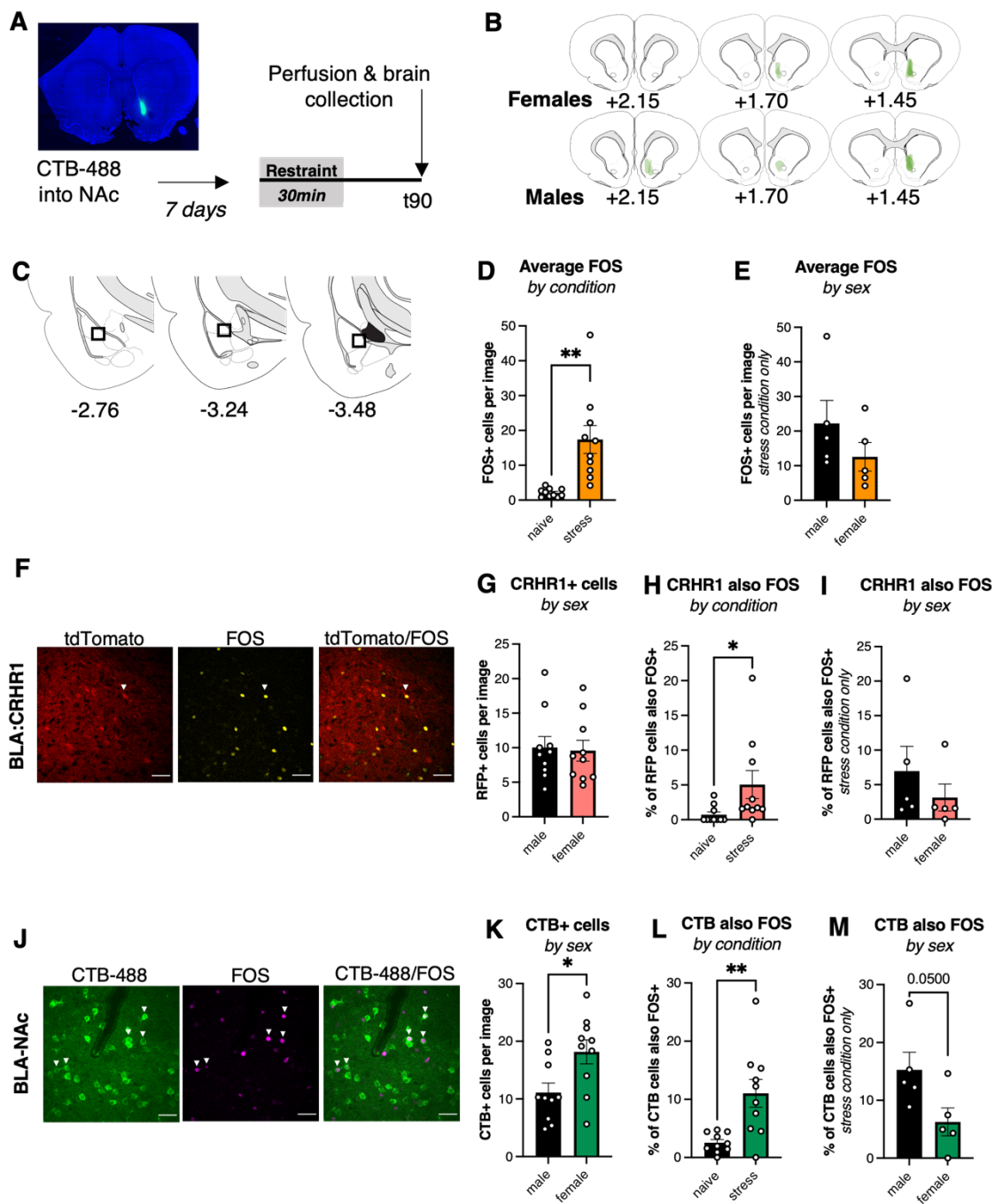


Figure 4.2. CRHR1 and BLA-NAc projection neurons are activated by restraint stress

(A) Overview of experimental procedures.

(B) Representative images of location of CTB (green) at AP +2.15, AP +1.70, and AP +1.45

(C) Region of interest in the BLA that CTB, FOS, and CRHR1-tdTomato neurons were counted.

(D) Group means (naïve=10; stress=10) of average number of FOS+ neurons per image ($t_{18}=3.805$, $p=0.0013$). Data includes both sexes

(E) Group means (stress condition only: male=5; female=5) of average number of FOS+ neurons per image ($t_{18}=0.2137$, $p=0.8332$)

(F) Representative images of CRHR1-tdTomato (left), FOS (middle), and tdTomato/FOS co-expression (right). White triangle indicates cells that are co-localized

(G) Group means (male=10; female=10) of average CRHR1-tdTomato+ neurons per image ($t_8=1.244$, $p=0.2486$).

(H) Group means (naïve=10; stress=10) of average percentage of CRHR1-tdTomato+ neurons also expressing FOS ($t_{18}=2.109$, $p=0.0492$). Data includes both sexes.

(I) Group means (stress condition only: male=5; female=5) of average percentage of CRHR1-tdTomato+ neurons also expressing FOS ($t_8=0.9424$, $p=0.3736$)

(J) Representative images of CTB (left), FOS (middle), and CTB/FOS co-expression (right). White triangle indicates cells that are co-localized

(K) Group means (male=10; female=10) of average number of CTB+ neurons per image ($t_{18}=2.661$, $p=0.0159$).

(L) Group means (naïve=10; stress=10) of average percentage of CTB+ neurons also expressing FOS ($t_{18}=3.457$, $p=0.0028$). Data includes both sexes.

(M) Group means (stress condition only: male=5; female=5) of average percentage of CTB+ neurons also expressing FOS ($t_8=2.306$, $p=0.0500$).

Finally, we tested if CRHR1+ neurons project to the NAc, and if these neurons are activated by restraint stress (Figure 4.2N). Independent-samples t-tests revealed that there was a significantly greater percentage of CRHR1-tdTomato+ neurons also expressing CTB-488 in females than males (Figure 4.2O; $t_{18}=2.548$, $p=0.0202$). On average, 5.87% of CRHR1-tdTomato+ neurons expressed CTB-488 in males, while 12.05% of CRHR1-tdTomato+ neurons expressed CTB-488 in females (Figure 4.2P). Given these sex differences, we performed a 2Way ANOVA to test an interaction between sex and condition on percentage of CRHR1+ cells expressing both FOS and CTB (Figure 4.2Q). There were no significant group differences between sex ($F_{1,16}=0.2$, $p=0.6525$) or condition ($F_{1,16}=2.7$, $p=0.1151$), and no significant interaction ($F_{1,16}=0.2$, $p=0.6525$).

Figure 4.2

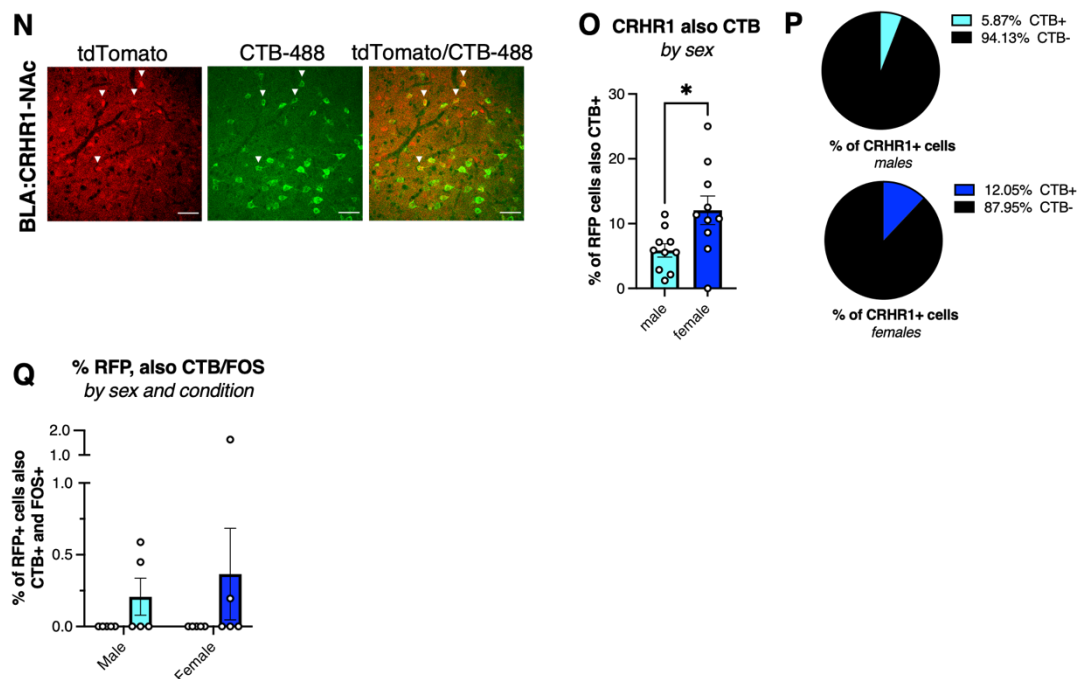


Figure 4.2. CRHR1 and BLA-NAc projection neurons are activated by restraint stress

(N) Representative images of CRHR1-tdTomato (left), CTB (middle), and tdTomato/CTB co-expression (right). White triangle indicates cells that are co-localized

(O) Group means (male=10; female=10) of average percentage of CRHR1-tdTomato+ neurons also expressing CTB ($t_{18}=2.548$, $p=0.0202$).

(P) Pie chart representing group means of percentage of total CRHR1-tdTomato+ neurons also expressing CTB in males (R; 5.87%) and females (S; 12.05%)

(Q) Group means (naïve=5 male and 5 female; stress=5 male and 5 female) of average percentage of CRHR1-tdTomato+ neurons also expressing CTB and FOS (2Way ANOVA of Sex: $F_{1,16}=0.2$, $p=0.6525$; Condition: $F_{1,16}=2.7$, $p=0.1151$; Interaction: $F_{1,16}=0.2$, $p=0.6525$).

Within-subjects data were analyzed using a paired t-test, and between-subjects data were analyzed using an independent samples t-test. Error bands represent mean \pm SEM. * $p<0.05$, ** $p<0.01$, *** $p<0.001$, **** $p<0.0001$.

Overall, these data suggest that restraint stress activates both CRHR1+ neurons and BLA-NAc projection neurons. Additionally, we found that CRHR1+ is expressed on a subset of BLA-NAc projection neurons, although only a very small proportion are activated by restraint stress. Finally, we identified several sex differences, with females exhibiting a greater proportion of BLA-NAc neurons also expressing CRHR1, and a greater proportion of BLA-NAc neurons activated by restraint stress.

Functional contribution of BLA:CRHR1 neurons.

We next tested the functional contribution of CRHR1 neurons by using an inhibitory chemogenetic approach to inhibit BLA:CRHR1 neurons prior to three separate tests: stress-induced CORT release, anxiety-like behaviour, and fear conditioning. We restricted expression of the inhibitory DREADD (hM4Di) to BLA:CRHR1 neurons by injecting AAV-DIO-hM4Di-mCherry into the BLA of adult male CRHR1-iCre-tdTomato rats and exposed animals to each test a

minimum of 4 weeks later. Animals were sequentially exposed to restraint stress, light dark test, and then fear conditioning. Stress and light-dark test was separated by 5 days, and light-dark test and fear conditioning was separated by 9-21 days (Figure 4.3A). Animals were randomly assigned to drug condition prior to each test but underwent the same treatment as their cage-mate. hM4Di-mCherry expression was largely restricted to the BLA, although in some cases there was expression also observed in the CeA (Figure 4.3B).

We first tested the effect of inhibiting BLA:CRHR1 neurons prior to restraint stress on the release of plasma CORT. Previously, we have shown that CNO does not influence stress-induced CORT in animals lacking a functional DREADD receptor (Chapter 2, Chapter 3). We administered VEH (n=7) or CNO (n=8; 3mg/kg/ml *i.p.*) 30min prior to restraint stress and serially collected blood 0, 30, 60, and 90min following stress onset (Figure 4.3C). 2Way RM ANOVA revealed a main effect of time ($F_{2.377,30.90}=60.98$, $p<0.0001$) but no significant group differences (Figure 4.3D; $F_{1,13}=0.5232$, $p=0.4823$). An independent-samples t-test revealed no significant differences in area-under-the-curve (Figure 4.3E; $t_{13}=0.5650$, $p=0.5817$).

We next tested the effect of inhibiting BLA:CRHR1 neurons on anxiety-like behaviour using the light-dark test. We administered VEH (n=8) or CNO (n=9; 3mg/kg/ml *i.p.*) 30-40min prior to the light-dark test (Figure 4.3F). Independent samples t-tests revealed no significant differences between conditions in percentage of time spent in the light compartment (Figure 4.3G; $t_{15}=0.3244$, $p=0.750$), number of transitions between compartments (Figure 4.3H; $t_{15}=0.01838$, $p=0.9856$), or latency to first enter the light compartment (Figure 4.3I; $t_{15}=0.2410$, $p=0.8128$).

Figure 4.3

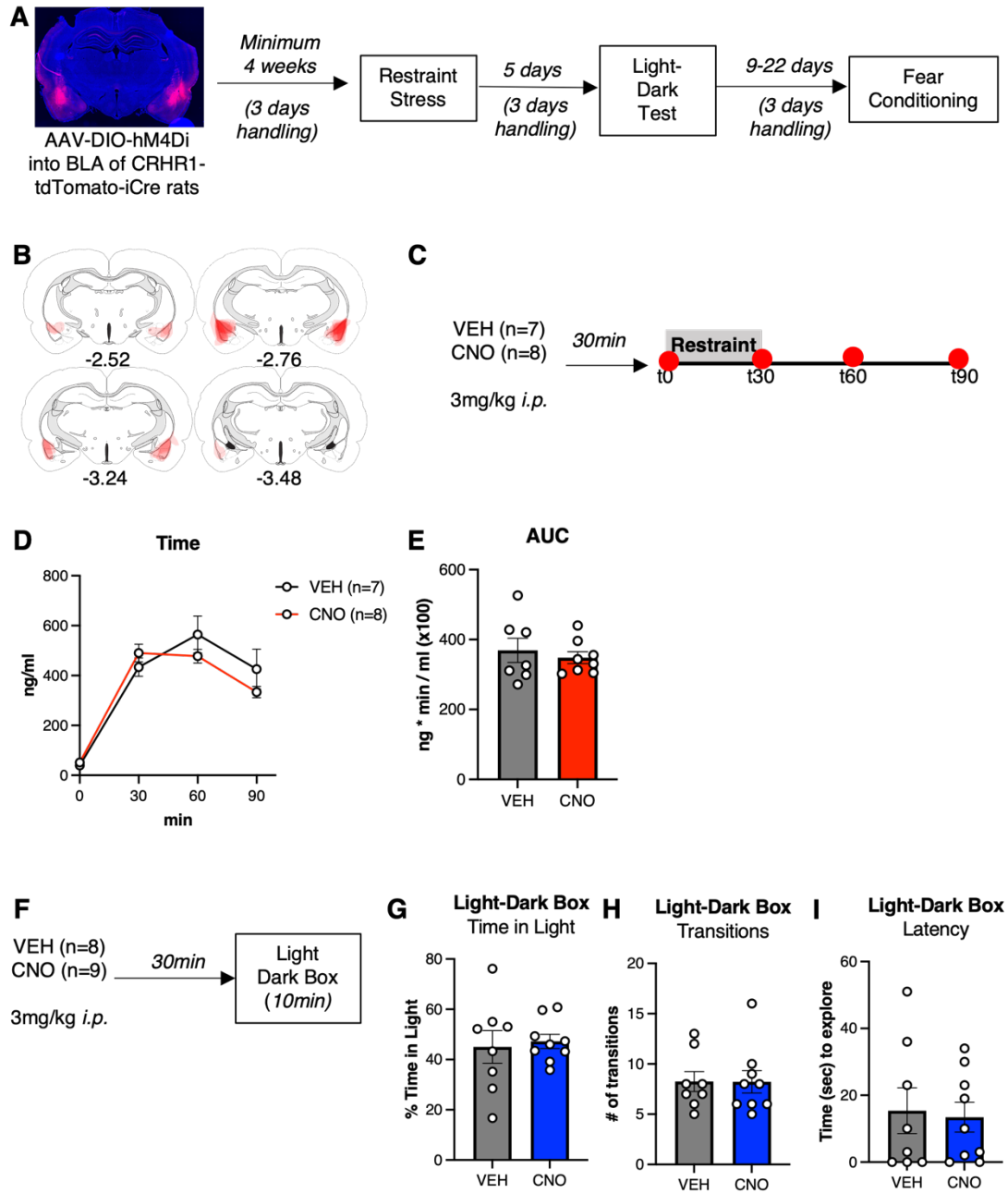


Figure 4.3. Functional contribution of BLA:CRHR1 neurons

(A) Overview of experimental procedures.

(B) Representative images of location of DIO-hM4Di-mCherry expression at AP -2.52, AP -2.76, AP -3.24, and AP -3.48

(C) Overview of restraint stress test day. Red circles indicate time of blood collection.

(D) Plasma CORT over time (VEH=7, CNO=8). Main effect of time ($F_{2,377,30,90}=60.98$, $p<0.0001$) but not group ($F_{1,13}=0.5232$, $p=0.4823$).

(E) Group means (VEH=7, CNO=8) of area-under-the-curve (AUC; $t_{13}=0.5650$, $p=0.5817$)

(F) Overview of light-dark box test day.

(G) Group means (VEH=8, CNO=9) of percentage time spent in light compartment, entire test ($t_{15}=0.3244$, $p=0.7501$)

(H) Group means (VEH=8, CNO=9) of number of transitions into the light compartment, entire test ($t_{15}=0.01838$, $p=0.9856$)

(I) Group means (VEH=8, CNO=9) of latency to enter the light compartment ($t_{15}=0.2410$, $p=0.8128$)

Between-subjects data were analyzed using an independent samples t-test, and within-subjects data between groups were analyzed using a RM 2Way ANOVA. Error bands represent mean \pm SEM.

* $p<0.05$, ** $p<0.01$, *** $p<0.001$, **** $p<0.0001$.

Finally, we tested the effect of inhibiting BLA:CRHR1 neurons on fear memory using auditory fear conditioning. We administered VEH ($n=8$) or CNO ($n=10$; 3mg/kg/ml *i.p.*) to animals 30min prior to undergoing auditory fear conditioning (7 CS-US pairings in context A). The following day, animals were tested for fear recall and extinction training on Day 2 (20 CS presentations in context B; Figure 4.3J). 2Way RM ANOVA revealed a main effect of CS presentation ($F_{6,96}=4.937$, $p=0.0002$) but not condition ($F_{1,16}=2.883$, $p=0.5549$) during auditory fear conditioning (Figure 4.3K). 2Way RM ANOVA revealed no significant differences of CS presentation ($F_{3,51}=1.532$, $p=0.2174$) or condition ($F_{1,16}=1.648$, $p=0.2176$) on fear recall or extinction training the following day (Figure 4.3L). An independent-samples t-test revealed no significant differences in percent time spent freezing on Day 2 ($t_{16}=1.284$, $p=0.2176$; Figure 4.3M).

Figure 4.3

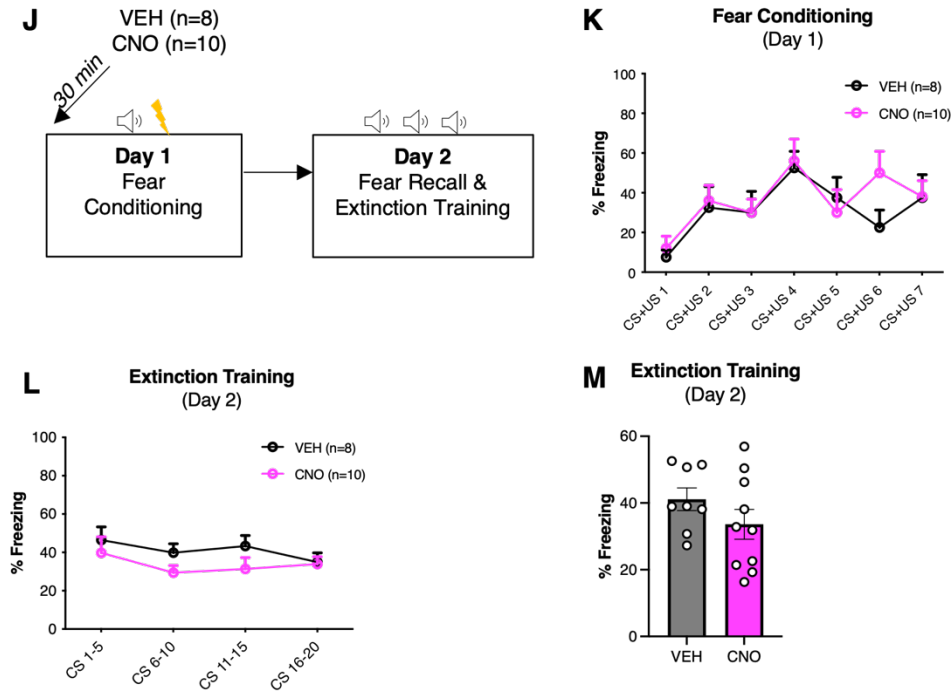


Figure 4.3. Functional contribution of BLA:CRHR1 neurons

(J) Overview of experimental procedures.

(K) Percent time spent freezing over time. Main effect of CS presentation ($F_{6,96}=4.937$, $p=0.0002$) but not condition ($F_{1,16}=2.883$, $p=0.5549$)

(L) Percent time spent freezing over time. No main effect of CS presentation ($F_{3,51}=1.532$, $p=0.2174$) or condition ($F_{1,16}=1.648$, $p=0.2176$)

(M) Group means (VEH=8, CNO=10) of percent time spent freezing during extinction training, all time points ($t_{16}=1.284$, $p=0.2176$).

Between-subjects data were analyzed using an independent samples t-test, and within-subjects data between groups were analyzed using a RM 2Way ANOVA. Error bands represent mean \pm SEM.

* $p<0.05$, ** $p<0.01$, *** $p<0.001$, **** $p<0.0001$.

Collectively, this suggests that inhibiting BLA:CRHR1 neurons does not influence stress-induced CORT, anxiety-like behaviour, or fear memory. However, we recognize that sample sizes are smaller than those typically employed for these types of behavioural experiments.

4.5 DISCUSSION

Although CRHR1 is central to the stress response, its anatomical specificity has previously been difficult to characterize at a high resolution (Refojo et al., 2011). Here, we employed a recently developed transgenic CRHR1-Cre-tdTomato rat (Weera et al., 2022) to topographically map the distribution of BLA:CRHR1+ neurons and test their functional contribution to stress-related behaviours. Additionally, we used the BLA-NAc projection neuron population as an example to test circuit-specific expression of CRHR1 in the BLA. As a result, we established four central findings: (1) CRHR1 exhibits strongest expression in the LA and in the caudal BLA; (2) BLA:CRHR1 neurons are activated by exposure to restraint stress; (3) CRHR1 is expressed on a subset of BLA-NAc projection neurons; (4) chemogenetic inhibition of BLA:CRHR1 neurons does not influence stress-induced CORT release, anxiety-like behaviour, or fear learning or recall.

Our topographical findings demonstrated a heterogenous pattern of CRHR1 expression in the BLA. The vast majority of CRHR1+ cells were expressed in the caudal regions of the BLA (AP -3.14 to AP -3.60) and particularly in the LA subregion. Although the LA is larger than other BLA subregions, particularly caudally, we observed both a significantly greater percentage of total CRHR1+ in the LA as well as a greater density and can therefore be confident on a topographical bias. Although expression of CRHR1 in the BLA is well-known (Agoglia et al., 2020; Van Pett et al., 2000), to our knowledge this is the first paper to systematically investigate regional specificity of expression within the BLA

These findings agree with our functional and anatomical understanding of the BLA. The majority of sensory input arrives into the amygdala via the LA (Sah, Faber, Lopez De Armentia, et al., 2003), and this subregion is highly involved in learning tasks (H. T. Blair et al., 2001; Maren & Quirk, 2004). Thus, high expression of CRHR1 in the LA may mediate the “gain” of salient stimuli to facilitate learning, particularly during stress. Indeed, CRH delivered directly into the LA enhances excitability of neurons to afferent signals (Rainnie et al., 1992; Ugolini et al., 2008), and intra-BLA CRHR1 antagonists impair consolidation of aversive contextual memory (Hubbard et al., 2007; Roozendaal et al., 2002).

Our mapping also revealed a caudal bias of CRHR1 expression in the BLA. This was surprising, as others have shown a caudal bias in BLA responsivity to rewarding stimuli (J. Kim et al., 2016), which doesn't agree with the putative importance of CRHR1 in responding to stress. However, we and others (Beyeler et al., 2018; Chapter 2) have not observed a rostral-caudal bias in responsivity to aversive stimuli, and therefore CRHR1+ neurons may be a particular subset of caudal neurons that preferentially respond to aversive states. Conversely, a proportion of caudal CRHR1+ neurons may be involved in reward learning. Indeed, BLA:CRHR1 signaling is implicated in regulating the strength of cocaine-memory (Ritchie et al., 2021), and comparable levels of CRH release has been observed in the CeA following food intake as well as following restraint stress (Merali et al., 1998). This may similarly be the case in the BLA. Alternatively, the role of CRHR1 in both appetitive and aversive states may be important, as it may enhance the salience of important signals in general. Indeed, intra-BLA CRH enhances excitability of neurons to other afferent signals (Rainnie et al., 1992; Ugolini et al., 2008). It will be essential, then, to test if BLA:CRHR1 neurons are activated during exposure to rewarding stimuli, and if activation occurs in the same anatomical regions of the BLA and on the same circuits as those activated during stress.

Our findings demonstrate that CRHR1+ neurons exhibit increased FOS expression following exposure to stress. This agrees with previous work demonstrating that CRH is released during restraint stress and leads to activation of BLA projection neurons (Merlo Pich et al., 1995; Rostkowski et al., 2013), and specifically demonstrates that this effect is occurring on neurons expressing CRHR1, as CRHR2 is also known to be moderately expressed in the BLA (Van Pett et al., 2000). Although not surprising given the known role of CRHR1 in stress and anxiety-like behaviour, our findings are important as there is little understanding on the molecular identity of stress-responsive cells in the BLA. Apart from recent work that has identified BLA projection populations expressing *Ppp1r1b* (J. Kim et al., 2016; X. Zhang et al., 2020) or *Thy1* (Jasnow et al., 2013; McCullough, Choi, et al., 2016) as fear-inhibiting, and projection populations expressing *Rspo2* (J. Kim et al., 2016) or CCK (Shen et al., 2019) as anxiety-promoting, there are few molecular markers for BLA neurons involved in aversive or rewarding states. As a result, the findings from this work can now include BLA:CRHR1 projection neurons to those involved in aversive states such as stress. Our findings also replicated previous work (Chapter 3) that restraint stress leads to activation of BLA-NAc projection neurons, although we expanded these findings to include both sexes. Notably, however, only a very small proportion of triple-labelled (CRHR1+/FOS+/CTB+) neurons were evident following stress and were apparent in only 4 of 10 stressed animals. Thus, it is possible that although BLA-NAc projectors express CRHR1, they may not play an important role in the stress response or may be more tightly regulated during stress exposure. As such, expression of CRHR1 on other projection neuron populations should be investigated with respect to their activation in response to stress.

BLA projection populations targeting the CeA and PrL, for example, may be especially rich in CRHR1. We have previously demonstrated that BLA projection neuron populations targeting the CeA are highly expressed in the LA (as well as the LBA) and are activated by restraint stress (Chapter 3). Given the importance of this projection in expression of learned fear (S. A. Jimenez

& Maren, 2009) and the role of BLA:CRHR1 in aversive learning (Roozendaal et al., 2002, 2008), CRHR1 may be expressed on this projection population and activated during aversive states. Additionally, other circuits such as those projecting to the prelimbic cortex are also activated by restraint stress (Chapter 3), and CRH has been shown to modulate the activity of BLA-mPFC circuits (Orozco-Cabal et al., 2008).

We observed notable sex differences that should be pursued further. First, although we did not see a significant difference between sexes in overall number of CRHR1+ neurons in both our anatomical mapping and our colocalization experiments, we did observe a significantly greater proportion of CRHR1+ neurons that project to the NAc in females. Further, we also observed greater numbers of BLA-NAc neurons in females overall, suggesting this may be a more abundant circuit in general. Given the difficulty in consistently restricting the spread of CTB injections to the same target site, these findings must be replicated in other experiments. Interestingly, Huckleberry and colleagues (2023) have found a greater number of VH-BLA projection neurons in females, suggesting sexual dimorphism in circuitry of BLA inputs. As well, Vantrease and colleagues (2022) have found that BLA-BST neurons exhibit lower excitability in females. In the context of NAc circuitry specifically, sex differences in synaptic connectivity have also been identified, with greater density and size of dendritic spines of NAc neurons (Forlano & Woolley, 2010). This may have particular consequence in models of reward learning, as CRHR1 signaling has sexually dimorphic effects in cocaine-memory learning, with stronger effects observed in females (Ritchie et al., 2021). Collectively, this suggests that the BLA:CRHR1-NAc circuit may be especially impactful in females during learning.

There is strong evidence that BLA:CRHR1 interacts with other signaling molecules such as anandamide (J. M. Gray et al., 2015) and glucocorticoids (Roozendaal et al., 2008). Thus, manipulation of CRHR1 signaling in tandem with additional systems may induce a synergistic effect. Given the evolutionary importance of an intact and appropriately regulated stress and fear-

response system, it is likely there are multiple redundant and interactive processes mediating this network. Indeed, we have previously demonstrated that although inhibition of BLA:CaMKII α projection neurons reduces stress-induced CORT, inhibition of discrete projection populations in isolation has no effect on HPA axis activation (Chapter 2, Chapter 3). This may contribute to our null findings that chemogenetic inhibition of CRHR1 neurons does not significantly influence stress-induced CORT release, anxiety-like behaviour, or fear memory, as an effect might only be unmasked with manipulations of other, parallel systems. Indeed, we found that CNO prior to fear conditioning appeared to reduce freezing during fear recall and extinction training the following day, although not significantly. This effect is partially supported by work from others demonstrating that bilateral microinfusions of a CRHR1 antagonist into the BLA had no effect on acquisition of fear but reduced freezing during re-exposure to the same context 48h later (Hubbard et al., 2007). As such, this effect may be amplified if tested in conjunction with other pharmacological manipulations. It is also possible that CRH action may be mediating effects apart from (or in tandem with) CRHR1 receptors, including CRHR2, which is also moderately expressed in the BLA (Van Pett et al., 2000).

Although we have previously demonstrated no differences in stress-induced CORT from vehicle-treated animals when CNO is administered in the absence of the functional hM4Di receptor (Chapter 2, 2023, p. 1; Chapter 3, 2023, p. 1), we did not explicitly test off-target effects of CNO in the light-dark box or fear conditioning. However, others have shown that CNO has no effect in rats in the absence of a functional DREADD receptor in various behavioural tests, including light-dark test, von Frey test, Hargreaves test, and fear learning (K. E. Cole et al., 2019; Eacret et al., 2019; Weera et al., 2022). Further, we did not observe any significant differences between groups on any behavioural test, and as such, it is unlikely that CNO exerted any substantial off-target effects on our measures.

In summary, we have demonstrated that CRHR1 is topographically distributed in the BLA, with greatest expression caudally and in the LA, and that BLA:CRHR1 neurons are activated by acute stress. These neurons may work in tandem with other populations to drive functional effects, as chemogenetic inhibition of this population prior to stress did not influence anxiety-like behaviour, fear expression, or stress-induced HPA activation. We have also expanded on previous work examining the anatomical distribution of the BLA-NAc projection population. Specifically, we identified that the BLA-NAc projection is activated by stress in both males and females, with potentially lower activation in females, and that CRHR1 is expressed on BLA-NAc projectors of both sexes (and more in females). Collectively, this improves our understanding of the anatomical organization of the BLA and its functional contribution to stress, by providing insight into the circuit-specific and molecular-specific identity of stress-responsive neurons in the BLA.

4.6 ACKNOWLEDGEMENTS

This research was performed at the University of Calgary which is located on the unceded traditional territories of the people of the Treaty 7 region in Southern Alberta, which includes the Blackfoot Confederacy (including the Siksika, Piikuni, Kainai First Nations), the Tsuut'ina, and the Stoney Nakoda (including the Chiniki, Bearspaw, and Wesley First Nations). The City of Calgary is also home to Metis Nation of Alberta, Region III. We would like to acknowledge the Hotchkiss Brain Institute advanced microscopy facility for their technical support, and Min Qiao for her technical lab support. We also acknowledge the University of Calgary Health Sciences Animal Research Centre, specifically Vincent, Krista Jensen, and Brittany Munro. AAV8-hSyn-DIO-hM4D(Gi)-mCherry (Addgene #44362) was a gift from Bryan Roth.

4.7 FUNDING

This research was supported by operating funds to MNH from the Canadian Institutes of Health Research (CIHR). RJA received salary support from the Mathison Centre for Mental Health Research & Education and the Cumming School of Medicine. GNP received salary support from BranchOut Neurological Foundation, CIHR, and the Cumming School of Medicine. AS received salary support from a Vanier Scholarship from CIHR.

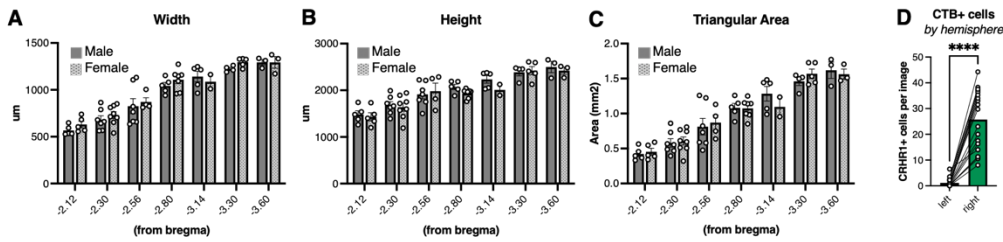
4.8 AUTHOR CONTRIBUTIONS

List of authors: Aukema RJ, Nastase AS, Petrie GN, Baglot SL, Gilpin N, Hill MN.

Contributions: RJA designed and conducted experiments, analyzed data, prepared figures, and wrote the manuscript. ANS designed, conducted, and analyzed experiments. GNP conducted experiments. SB conducted experiments and provided technical advice. NG provided animals and technical advice. MNH developed and supervised the project and wrote the manuscript.

4.9 SUPPLEMENTARY DATA

Supplementary Figure 4.1



Supplementary Figure 4.1.

- A.** Average slice width at each AP position; Data are unpaired and were analyzed between sex ($F_{1,56}=1.451$, $p=0.2335$)
- B.** Average slice height at each AP position; Data are unpaired and were analyzed between sex ($F_{1,56}=1.375$, $p=0.2459$)
- C.** Average slice triangular area at each AP position [(width*height)/2]; Data are unpaired and were analyzed between sex ($F_{1,56}=0.007270$, $p=0.9324$)
- D.** Paired group means (n=19) of CTB+ cells in the left vs. right hemisphere ($t_{18}=9.310$, $p<0.0001$)

For A-C, data points represent a single slice. For D, data points represent mean count of an individual animal. Between-subjects data were analyzed as unpaired values using an ordinary 2Way ANOVA. Within-subjects data were analyzed using an independent samples t-test. Error bands represent mean +/- SEM. ****p<0.0001.

Chapter 5. Discussion

5.1 SUMMARY OF MAIN FINDINGS.

Overview. The overarching aim of this thesis was to conduct a systematic investigation of the spatial, temporal, and circuit-specific activation patterns of BLA projection neurons during exposure to acute stress. Additionally, we wanted to clarify the role of the BLA in activation of the HPA axis, as this remains a poorly understood process. The overarching hypothesis was that stress uniquely activates discrete BLA subregions, circuits, and molecularly-defined projection populations to drive stress-related increases in HPA axis activation.

In Chapter 2, we used a combination of FOS mapping and fiber photometry in male rats to identify that CaMKII α neurons in the mBA subregion of the BLA are robustly activated by a range of different stressors. Focusing on restraint exposure as a model for stress, we then found that systemic administration of propranolol, a β -adrenoceptor antagonist, reduced the magnitude of calcium-related response in the BLA to restraint stress. Finally, we demonstrated that chemogenetic inhibition of mBA projection neurons dampened stress-induced HPA axis activity, while optogenetic stimulation of mBA projection neurons drove HPA axis activity even in non-stress conditions. This collectively demonstrated that the mBA is a critical subregion of the BLA that is highly responsive to exposure to stress and contributes to stress-induced activation of the HPA axis.

In Chapter 3, we used retrograde tracing to map the topographical distribution of six different BLA projection populations targeting the CeA, PrL, NAc, BST, LH, and VH. We observed a heterogenous distribution of projection populations, although co-expression with FOS

demonstrated that all projection populations were activated during exposure to restraint stress. Surprisingly, chemogenetic inhibition of discrete projection populations targeting the CeA, NAc, and BST had no effect on stress-induced CORT release, while inhibition of the BLA-PrL projection enhanced stress-induced CORT. Collectively, this suggests that BLA circuits are heterogeneously distributed throughout the BLA but widely activated by stress exposure, and individual circuits do not appear to contribute to driving an HPA axis response to stress in isolation.

In Chapter 4, we used transgenic CRHR1-Cre-tdTomato to map topographical and circuit-specific expression of CRHR1+ neurons in the BLA and test their functional role in the acute stress response. Topographically, CRHR1 had the strongest expression in the LA and was expressed on a subset of BLA-NAc projection neurons. Functionally CRHR1+ cells exhibited a significant increase in FOS expression following exposure to restraint stress, but chemogenetic inhibition of CRHR1+ neurons did not significantly influence stress-induced CORT, anxiety-like behaviour, or fear memory. This suggests that, although their functional role remains unclear, CRHR1+ neurons in the BLA are activated by exposure to acute stress.

Collectively, our work demonstrates the stark anatomical heterogeneity of the BLA, with a topographically heterogeneous distribution of discrete projection populations and receptors. Importantly, we identified a common spatial activation pattern in response to stress; the mBA subregion was particularly responsive to a range of stressors, although it exhibited different temporal patterns. We also provided strong evidence for the role of the BLA in the HPA response, as optogenetic stimulation or chemogenetic inhibition of projection neurons within the mBA subregion bidirectionally influenced CORT levels. Despite this global effect of targeting the mBA, chemogenetic inhibition of isolated projection neuron populations from the BLA or BLA:CRHR1 neurons did not reduce stress-induced CORT release, indicating that multiple cell types and circuits likely contribute to this response. Collectively, this work emphasizes the anatomical

heterogeneity of the BLA, and provides a framework for the mechanistic contribution of the BLA to the stress response.

5.2 MODELS OF ACUTE STRESS.

Overview and rationale for different stimuli. The BLA is implicated in many characteristic behavioural and endocrine responses to stress (i.e., anxiety-like behaviour (Tye et al., 2011) and release of CORT (Bhatnagar et al., 2004)). Thus, we hypothesized that a variety of different psychological stressors would similarly lead to activation of common spatial and temporal patterns of activity, likely triggering and coordinating common effector circuits that subsequently drive a general response to stress. As expected, shock, restraint, swim, and bobcat odour all activated a similar spatial activation pattern in the BLA, and specifically, led to robust activation of the mBA (Chapter 2, Figure 1). Interestingly, however, we observed different temporal patterns of activation to different stressors. All stressors increased initial activity of BLA projection neurons, although, this initial response was much larger in magnitude in animals exposed to swim and restraint but seemed to persist longer in animals exposed to bobcat odour, and became sensitized in animals exposed to shock.

Considerations. We did not use any stimuli that are inherently rewarding. Although crackers are highly palatable and were readily consumed during experiments (data not shown), animals are inherently neophobic (Modlinska et al., 2015). Thus, although some of the FOS+ neurons following exposure to crackers may respond to rewarding stimuli, many likely react to novelty, which can itself be aversive. This may explain why the spatial pattern of activation in response to novel food is similar to that seen in animals exposed to the novel, neutral citral odour. Likewise, this may also explain why the activation pattern is only subtly different from animals exposed to

stress; it is possible that a large proportion of neurons respond simply to salience, which is common among all types of novel stimuli.

Indeed, single-unit recordings from animals exposed to novel punishment (e.g., air puff) or reward (e.g., water) have shown that 20-25% of stimulus-responsive neurons in the LA respond to both punishment and reward (Shabel & Janak, 2009; X. Zhang & Li, 2018), and even those responsive to distinct stimuli are located in spatially intermingled populations (Gore et al., 2015). Likewise, we observed similar activation in the LA for all stimuli (both in magnitude and topography), also suggesting an intermingled or overlapping activity pattern. Notably, previous recordings were all done in the LA and no recordings were conducted in the BA (Gore et al., 2015; X. Zhang & Li, 2018). Thus, anatomical separation between aversive and novel stimuli may only be apparent in the basal amygdala, as we have observed. Alternatively, segregation may also become apparent only after learning or repeated exposure (Beyeler et al., 2018; J. Kim et al., 2016), as novelty is no longer a factor.

All the stressors we employed were acute, as we wanted to test how the BLA responds in non-pathological or normative conditions. However, there is growing evidence that the BLA responds differently to stress with repeated exposure. For example, repeated exposure to the same stressor (homotypic stress) leads to a reduction in stress-induced CORT with each subsequent experience (Girotti et al., 2006), and that this phenomenon is highly dependent on the BLA (Bhatnagar et al., 2004). In particular, intra-BLA β -adrenergic (N. M. Grissom & Bhatnagar, 2011) and CB1 receptor signaling (Hill, McLaughlin, et al., 2010) may be particularly important. Further, along with many other regions, repeated homotypic stress leads to a reduction in overall FOS expression in the amygdala (Campeau et al., 2002; Melia et al., 1994). Conversely, exposure to a novel stressor in chronically stressed animals potentiates stress-induced CORT (Bhatnagar & Vining, 2003) and BLA FOS expression (Bhatnagar & Dallman, 1998). This process may particularly involve CRHR1 signaling (Vining et al., 2007).

It is unclear if these changes involve broad or non-specific changes in sensitivity of BLA projection neurons or if they are specific to discrete projection populations. There is some evidence that homotypic stress alters dendritic structure in some BLA projection populations but not others (J.-Y. Zhang et al., 2019a), and that habituation of BLA FOS response may occur especially in populations targeting the medial prefrontal cortex (W.-H. Zhang et al., 2019). It remains to be tested using a projection-specific approach such as ours whether this is similarly observed for other populations.

Finally, temporal and spatial patterns of activation are only one measure of change. Indeed, different stress conditions lead to distinct gene expression profiles in the brain (Flati et al., 2020). For example, there is greater divergence of gene regulation in the hippocampus in response to three different acute stressors than common between stressors (Floriou-Servou et al., 2018). More specifically, distinct psychological stressors can lead to divergent biochemical changes in the BLA, with swim stress and foot shock exerting opposing influences on BLA AEA levels in rats (Vecchiarelli et al., 2022). Thus, just because a common spatial activation pattern is occurring in response to different stressors does not mean that the BLA is being impacted the same way.

5.3 FOS MAPPING

Overview of FOS. Expression of *c-fos* and its protein product FOS is induced by activation of second messenger systems (Sheng et al., 1990), and in particular via increased intracellular calcium concentration following cellular depolarization and influx of voltage-gated calcium channels (Luckman et al., 1994; Murphy et al., 1991). The exact threshold of calcium influx is unclear, however it has been demonstrated that the stimulation thresholds for induction of *c-fos* are much higher than those required to induce expression of other immediate early-genes such

as *zif268* (Worley et al., 1993). Indeed, acute stress can lead to expression of *zif268* in areas where expression of *c-fos* is absent (Cullinan et al., 1995).

We employed this tool heavily throughout the thesis, specifically for identifying and mapping spatial, circuit-specific, and molecular-specific activation of BLA projection neurons following stress. In Chapter 2, we identified the spatial location of stress-activated cells. In Chapter 3, we refined this for identifying the activation of discrete populations targeting the NAc, PrL, BST, LH, and CeA. In Chapter 4, we identified the activation of discrete populations expressing CRHR1.

This is a highly useful tool for several reasons (K. J. Kovács, 2008). First, FOS is expressed at very low levels under basal conditions (Chan et al., 1993; Hughes et al., 1992), including in the BLA (L. Á. Kovács et al., 2018). As such, this low baseline increases our likelihood of detecting a signal in response to various stimuli. Second, FOS protein is relatively short-lived, and therefore reflects only recent activity (K. J. Kovács, 2008). Third, it has high reliability and ease of detection, including within our own laboratory (e.g., Petrie et al., 2022). Finally, it can be easily used in conjunction with labels used for anatomical tracing (Jin & Maren, 2015) or protein identification (Petrovich et al., 2012; Weera et al., 2022), as we did with CTB, hM4Di-mCherry, ChR2-mCherry, and CRHR1-iCre-tdTomato.

Considerations. Despite the clear advantages of using FOS to identify spatial distribution, there are several limitations, including poor temporal resolution, expression on non-neuronal populations, and inability to detect decreases in activity.

FOS has relatively poor temporal resolution in two respects: (1) it has a broad temporal window for detection, and (2) it has an inability to detect discrete patterns of activity. Expression of FOS protein is broad, peaking 60-180min following stimulus onset and returning to basal levels within 4-6 hours (McReynolds et al., 2018). Resolution can be improved by using techniques such as cellular compartment analysis of temporal activity by fluorescent in-situ hybridization (catFISH).

This takes advantage of the early accumulation of the immediate early gene *Arc* in the nucleus, and later accumulation in the cytoplasm, thus improving temporal resolution by identifying the cellular location of RNA (Guzowski et al., 1999). However, this makes colocalization experiments with CTB more complicated and more importantly, requires *in situ* hybridization, a technique our lab does not routinely employ. Secondly, quantification of FOS is binary (i.e., simply detecting the presence or absence of), and thus it is impossible to understand duration of activation of a given FOS+ neuron. Specifically, both a short burst of calcium influx and a long or repeated pattern of calcium influx are likely sufficient to induce a similarly detectable level of FOS. Thus, it is unclear the duration of activity or precise timing relative to stimulus-onset that led to expression of FOS.

A second caveat is that FOS is expressed in both glia and astrocytes (McReynolds et al., 2018), and therefore we cannot conclusively say that observed FOS expression is restricted to neuronal populations. However, non-neuronal expression typically occurs following injury (Dragunow et al., 1990). Given that quantification of FOS occurred in brain regions far away from surgical sites, and typically collected brains several weeks following surgery, it is unlikely that astrocytic FOS was a large contribution to the overall signal we observed. Additionally, several of our experiments quantified FOS on cells labelled with CaMKIIa-dependent protein expression or CTB, neither of which typically get expressed on astrocytes (Lai et al., 2015; Vallano et al., 2000).

Finally, FOS is only able to detect increases in activity. Given that neuronal inhibition may be equally important in shaping neural circuits (Tye, 2018), this is an important caveat. To date, there have been no reliable markers of neural inhibition analogous to FOS. However, phosphorylation of pyruvate dehydrogenase (pPDH) has recently been proposed as an *in vivo* marker of neural inhibition (Yang et al., 2023). In our context, it would thus be fascinating to map expression of pPDH in the BLA in response to different stimuli. In chapter 2 we demonstrated low stress-induced FOS expression in the LBA; this could result from strong inhibitory input to this region, as would be reflected by a spatial bias of pPDH towards the LBA. Conversely, pPDH may

be especially high in the same regions as those expressing stress-induced FOS, as intermingled, competing projection populations may bias activation towards “stress-responsive” cells via collateral inputs to local inhibitory interneurons subsequently targeting neighbouring “reward” neurons (Beyeler et al., 2018; J. Kim et al., 2016).

5.4 FIBER PHOTOMETRY.

Overview. Given the poor temporal resolution of FOS described above, we used fiber photometry to detect temporal patterns of activity in BLA:CaMKIIa neurons upon exposure to novel, stressful stimuli (shock, swim, restraint, bobcat odour) or novel, neutral stimuli (citral odour and goldfish crackers). This tool allows for recording of neuronal Ca^{2+} transients specifically in excitatory CaMKIIa+ projection neurons in real time (Gunaydin et al., 2014).

We demonstrated that, unlike common spatial patterns, distinct aversive stimuli evoke different temporal patterns of activity (Chapter 2, Figure 2). Specifically, all stressors increased activity within BLA:CaMKIIa neurons in the initial 5min of stress exposure. While activity returned to baseline after 5min in animals exposed to swim or restraint, this activity seemed to persist in animals exposed to bobcat odour and even sensitize in animals exposed to shock. Notably, there was a significantly greater initial GCaMP6s response to swim and restraint than all other stimuli. As GCaMP6s reflects coordinated neural activity (Gunaydin et al., 2014), this likely reflects a larger simultaneous recruitment of neurons. Thus, a more modest, but prolonged GCaMP6s response as that observed during exposure to bobcat urine may instead reflect interchangeable activation of different populations of cells. This persistence of activity across a broad population of neurons from bobcat odour and shock may explain why these two stimuli induce such robust response in the BLA, relative to swim and restraint. Our results are particularly notable when recognizing that restraint and swim stress also evoked the largest CORT response, suggesting

that coordinated activity at stress onset (i.e., magnitude of GCaMP6s response) may be more relevant for HPA axis activation than total number of neurons activated throughout exposure (i.e., number of FOS+ cells). This prediction is supported by the fact that broad inhibition of projection neurons in the mBA attenuated stress-induced CORT, but individual projection neuron populations did not recapitulate this effect, as perhaps a large, diverse population of BLA projection neurons requires coordinated activation to promote HPA axis activation.

Considerations. Although GCaMP6s gives excellent temporal resolution of the bulk signal of CaMKIIa neurons in the BLA, we are unable to attribute activation to any discrete inputs or identify differences in temporal activation patterns of discrete projection populations.

We hypothesized that β -noradrenergic signaling may play an important role in activation of BLA neurons following stress, as norepinephrine, the main receptor ligand, is readily released in the BLA during stress exposure (Galvez et al., 1996) and is known to drive stress-related processes such as increased anxiety-like behaviour and memory enhancement (LaLumiere et al., 2003; McCall et al., 2017). Indeed, systemically blocking β -noradrenergic signaling reduced the average magnitude of BLA activity during restraint stress (Chapter 2, Figure 3). These effects are likely a direct result of receptor antagonism in the amygdala, as the BLA strongly expresses β -adrenergic receptors (Qu et al., 2008). However, given that propranolol is known to dampen the sympathetic system (Andrews & Pruessner, 2013; LeWinter et al., 1975; Rodriguez-Romaguera et al., 2009), this could also be an indirect result of reduced interoceptive stress signals, such as those terminating in the BLA from the insular cortex (Hsueh et al., 2023; Ju et al., 2020).

Greater specificity can be achieved using strategies such as G-protein-coupled receptor-activation based (GRAB) sensors, which allow for rapid detection of fluctuations in dopamine (Sun et al., 2020), CB1R signaling (A. Dong et al., 2022), norepinephrine (Feng et al., 2019), or acetylcholine (Mineur et al., 2022). These have a particular advantage over other techniques such

as microdialysis or fast-scan cyclic voltammetry, as GRAB sensors have vastly greater temporal resolution, molecular specificity, and are significantly less invasive (Sun et al., 2020).

Indeed, use of endocannabinoid sensors (GRAB_{eCB}2.0) demonstrate that BLA endocannabinoid activity significantly, and transiently, increases upon presentation of a mild foot shock in mice (A. Dong et al., 2022). Further, acetylcholine sensors (GRAB_{ACH}3.0) demonstrate that acetylcholine release in the BLA modulates active coping behaviours by altering activity of BLA:CaMKIIa neurons through complex GABAergic interactions (Mineur et al., 2022). It would therefore be interesting to compare temporal dynamics of these sensors across various stressors as we have done with CaMKIIa:GCaMP6s, to assess general roles of each modulator during stress.

5.5 DREADDS AND OPTOGENETICS.

Overview. The functional impact of BLA activity on HPA activity is unclear, likely due to the fact that the BLA does not send any direct projections to the PVN (Petrovich et al., 1996) and heterogeneity of BLA projection neurons in responding to both rewarding and stressful stimuli (Herman et al., 2020; Janak & Tye, 2015). Notably, the impact of electrical stimulation of the BLA is highly dependent on which subregions are targeted (Dunn & Whitener, 1986; Feldman et al., 1982; Matheson et al., 1971; Rubin et al., 1966; Slusher & Hyde, 1961; Vouimba & Richter-Levin, 2013). We had hypothesized that manipulations focused on stress-responsive subregions of the BLA may have a more reliable effect on HPA axis activity. Thus, we used optogenetics to restrict stimulation only to CaMKIIa projection neurons and focally targeted the mBA, as this is the region we had identified as particularly responsive to stress (Chapter 2). Indeed, we observed a significant increase in CORT following optogenetic stimulation of this region.

To inhibit discrete projection neurons, we expressed the inhibitory Gi DREADD, hM4Di (Armbruster et al., 2007), in BLA:CaMKIIa neurons (Chapter 2), discrete BLA circuits (Chapter 3), or CRHR1+ cells (Chapter 4). We demonstrated that chemogenetic inhibition of BLA:CaMKIIa neurons reduces stress-induced CORT but, to our surprise, inhibition of isolated projection neuron populations or BLA:CRHR1 cells did not have individual effects. There are several possible explanations for this discrepancy. First, it is possible that a BLA circuit we did not explicitly test may individually drive the HPA axis, such as projection from the medial amygdala (Ulrich-Lai & Herman, 2009). Second, given that restraint stress reliably induces a very strong HPA response compared to other psychological stressors (Bowers et al., 2008, Chapter 2), it is possible that an effect would only be apparent using more subtle stressors such as exposure to a novel environment. Given the critical importance of the stress response to survival, multiple redundant pathways may collectively facilitate activation of the HPA response to stress, perhaps including circuits outside of the BLA such as those going through the nucleus of the solitary tract or paraventricular thalamus (Ulrich-Lai & Herman, 2009). Finally, parallel circuits within the BLA may collectively play a role in HPA axis regulation, and an effect may only be unmasked when they are all manipulated in tandem. This was observed, for instance, when we previously restricted hM4Di broadly to CaMKIIa+ neurons (Chapter 2), which non-specifically targets all projection neurons in the BLA. Thus, inhibiting a discrete projection may be compensated for by activation of other stress-activated projections in the BLA. As such, this may be why broad pharmacological approaches such as those targeting the endocannabinoid system may be particularly effective in modulating the HPA response to stress (J. M. Gray et al., 2015; Hill et al., 2009), as the endocannabinoid system is widely expressed throughout the entire BLA (Katona et al., 2001) and may be capable of influencing multiple projection populations at once. It will be important to continue to identify molecular markers of stress-responsive neurons, which may be expressed

broadly on multiple projection neuron populations and therefore facilitate coordination of a diverse population of projection neurons.

Considerations. Although viral expression of ChR2 extended beyond the mBA, our ferrule tips were reliably localized to the mBA (Chapter 2, Supplementary Figure 2.4J-L). Given that light penetrates locally and conically away from the ferrule tip (Aravanis et al., 2007; Yona et al., 2016), and that the LA has limited dendritic branching extending into the BA (McDonald, 1984), our effect was likely localized to the BA subregion. However, many LA axons extend into the BA (Pitkänen et al., 1997). As it is likely that ChR2 is expressed on axon terminals from the LA to BA, we cannot completely exclude the possibility of antidromic propagation (Yizhar et al., 2011), although this has not been observed using similar stimulation parameters in mice (Tye et al., 2011).

We demonstrated *in vivo* that systemic administration of CNO reliably reduces expression of FOS on hM4Di+ cells. This supports our *in vitro* data showing that CNO reduces activity of cells expressing the functional DREADD. However, we and others (Anderson & Petrovich, 2018) have shown, surprisingly, that CNO administration in BLA:hM4Di+ animals leads to an overall increase in FOS+ neurons throughout the BLA (Chapter 2, Supplementary Figure 4; Chapter 3, Figure 5). This suggests that Gi DREADDs are not acting in the BLA to suppress overall activity *per se*, but rather causing a shift in activity away from neurons normally activated. This is likely a result of disinhibition of neurons receiving inhibitory inputs from the hM4Di infected neurons (Anderson & Petrovich, 2018). Indeed, competing BLA projection neurons inhibit nearby projection populations of opposing valence through collaterals to local inhibitory interneurons (Beyeler et al., 2018).

There is recent evidence that CNO can back-metabolize into the biologically active compound clozapine (Gomez et al., 2017), which has known off target effects at 5-HT receptors and could therefore influence HPA axis responses to stress (Bærentzen et al., 2019). Thus, we extensively validated hM4Di both *in vivo* and *in vitro*, demonstrating that CNO leads to inhibition

of hM4Di+ but not mCherry+ cells, and that CNO has no off-target effects on CORT in the absence of a functional hM4Di. However, we are missing controls for our DREADD experiments in Chapter 4 (inhibition of CRHR1+ cells). Although we had previously demonstrated no differences in stress-induced CORT from vehicle-treated animals when CNO is administered in the absence of the functional hM4Di receptor in Chapter 2 and 2, we did not explicitly test off-target effects of CNO in the light-dark box or fear conditioning. However, others have shown that CNO has no effect in rats in the absence of a functional DREADD receptor in various behavioural tests, including light-dark test, von Frey test, Hargreaves test, and fear learning (K. E. Cole et al., 2019; Eacret et al., 2019; Weera et al., 2022). It will be essential to directly confirm the lack of these effects in our own model.

We found that optogenetic stimulation of CaMKIIa+ neurons in the BLA increased plasma CORT (Chapter 2). Only one stimulation parameter was used: 10mW (5ms long pulses) of 20Hz light for 15min. These parameters were selected as they lead to excellent fidelity of action potentials in BLA projection neurons (Servonnet et al., 2020) and increase anxiety-like behaviour in mice expressing ChR2 in BLA neurons (Felix-Ortiz et al., 2016; Tye et al., 2011). As 15min stimulation is longer than typically employed, there was concern for seizure activity (Servonnet et al., 2020) or unintentional neural changes induced by tissue heating (Cardozo Pinto & Lammel, 2019; Owen et al., 2019). However, no animals in any condition exhibited seizures, and we did not see any significant difference in BLA FOS expression between mCherry-expressing animals receiving 473nm light and non-stimulated ChR2 controls (data not shown), confirming the absence of heating effects.

We used 15min of persistent stimulation to replicate broad BLA activity patterns in response to stressful stimuli that elicited CORT release (shock, swim, and restraint (Chapter 2, Figure 1), as our photometry recordings revealed BLA activation at different periods throughout 15min stress exposure depending on the stressor (Chapter 2, Figure 2). However, given that swim

and restraint had the greatest magnitude of GCaMP6s response in the first 5min of stress exposure and were also the stimuli that exhibited the greatest CORT response to stress, it is possible that 5min of optogenetic stimulation may have been sufficient to drive an HPA response. On the other hand, given that shock readily induces contextual fear conditioning, which strongly involves the BLA (Paré, 2003), it's possible that a more dynamic and persistent activity pattern such as that observed with shock may be important for memory consolidation. Indeed, others have also shown a prolonged increase in BLA activity following exposure to shock, and that blunting this activity such as by administering β -noradrenergic antagonists enhances immediate extinction learning (Giustino et al., 2020).

5.6 ANATOMICAL MAPPING OF PROJECTION POPULATIONS AND CRHR1+ CELLS

Overview. We mapped the topographical distribution of 6 different projection populations in the BLA targeting the NAc, PrL, LH, VH, CeA, and BST using the fluorescently conjugated retrograde tracers CTB-488 and CTB-555. We selected this tracer due to its low toxicity, rapid transport, and high signal strength (Conte et al., 2009; Saleeba et al., 2019). Further, fluorophore-conjugated CTB is readily used for co-labeling with various markers such as CTB (Jin & Maren, 2015) and tdTomato (Singh et al., 2022).

Many classical anatomical work has mapped circuitry using case studies, where injection site and expression of anatomical site are plotted separately for individual animals (for example: (McDonald, 1991)). This has a significant advantage in precision, as it is possible to pair a discrete injection site with tracer expression in a connected region. However, it is more difficult to make broad conclusions about topography of circuits, as it is extremely difficult to reliably target identical surgical locations and with similar tracer uptake and spread in multiple animals. This is particularly

important when performing DREADD, optogenetic, or fiber photometry experiments, which require use of large numbers of animals and repeated injections.

We had hypothesized that projection neuron populations are heterogeneously distributed throughout the BLA, as expressed by differences in subregion-specific density. Our anatomical mapping largely agrees with recent work from other groups that the BLA is a topographically heterogeneous structure (Beyeler et al., 2018; McGarry & Carter, 2017; O’Leary et al., 2020; Reppucci & Petrovich, 2016). There is one notable discrepancy in anatomical distribution, however. Beyeler and colleagues (2018) demonstrated a ventral bias in expression of BLA-VH projectors in mice, while we observed a dorsal bias of BLA-VH projectors towards the LA subregion in rats. However, their injection site was much more dorsal in the VH than ours. Thus, there may be either species differences or heterogeneity in anatomical targeting even within a given projection, especially to target a structure such as the hippocampus which is quite expansive and likely has heterogeneity in its inputs across its dorsal-ventral and rostral-caudal axis. A parallel topographic projection has similarly been observed in the BLA-NAc projection, where the lateral BLA preferentially targets the lateral NAc, and the medial BLA preferentially targets the medial NAc (G. Chen et al., 2023). Additionally, as injections in mice may also cover a larger proportion of the VH than in rats, due to the much smaller size of a mouse brain, it’s quite likely that retrograde studies in mice likely capture a larger proportion of the projection inputs than in rats.

Notably, we are one of the only groups to have systematically mapped topography of BLA projection populations in multiple circuits. Given variability in representation and normalization procedures between groups, this is a significant strength of our work as it allows us to directly compare projection populations relative to one another. Our work strongly emphasizes the heterogeneity of projection populations. Notably, the CeA and LH projectors are biased towards

the LBA, the PrL, NAc, and BST projectors are biased towards the mBA, and the VH projectors are biased to the mBA and LA (Chapter 3, Figure 3).

Considerations. Although we routinely injected two different coloured tracers into BLA targets (e.g., CTB-488 into the CeA, and CTB-555 into the NAc), we did not quantify co-localization of different coloured CTB in the BLA and therefore cannot explicitly assess extent of collateralization. However, others have shown mixed findings depending on the specific projection populations being investigated and the anatomical tracing technique being used (Beyeler et al., 2016, 2018; Klavir et al., 2017; Lichtenberg et al., 2021; Senn et al., 2014; Shinonaga et al., 1994). Although occasionally present in our hands, colocalized expression of CTB-488 and CTB-555 was overall rare. This remains an important question that warrants further characterization, as optogenetic or chemogenetic manipulation of a discrete projection population may inadvertently influence activity of other regions via downstream collaterals.

The bulk of our functional anatomical work focused on stress-induced activation of discrete circuits. Further studies should identify specific molecular markers of stress-responsive neurons. Indeed, neurons possessing distinct molecular markers have been shown to promote (Shen et al., 2019; Q. Zhang et al., 2022) or counteract (Jasnow et al., 2013; McCullough, Choi, et al., 2016; X. Zhang et al., 2020) anxiety-like behaviour and learned fear. It will be worth investigating if these cell types are activated during exposure to novel stimuli and, along with behavioural changes, if they influence HPA activity.

We investigated three different molecular markers, although only one (CRHR1) is reported in this thesis. CRHR1 is expressed in BLA glutamatergic projection neurons (Agoglia et al., 2020; Y. Chen et al., 2000; Van Pett et al., 2000), and CRH release during stress (Merlo Pich et al., 1995) leads to activation of CaMKII α projection neurons and drives memory consolidation, anxiety-like behaviour, and HPA axis response to stress (J. M. Gray et al., 2015; Liang & Lee,

1988; Roozendaal et al., 2002; Rostkowski et al., 2013). It is predictable, then, that in Chapter 3 we confirmed that this population exhibits increased FOS following exposure to acute restraint. Further, our findings revealed a topographical bias towards the LA. This was also unsurprising, as both CRHR1 (Roozendaal et al., 2002) and the LA (Maren & Quirk, 2004) are heavily implicated in memory consolidation.

Endocannabinoids and their hydrolyzing enzymes such as fatty acid amide hydrolase (FAAH) have a strong regulatory influence on activation of stress circuits (Hill, Patel, et al., 2010; Morena et al., 2016; Petrie et al., 2021; Steiner & Wotjak, 2008). In particular, intra-BLA pharmacological manipulations demonstrate that endocannabinoids largely act in the BLA to constrain both HPA axis activity (J. M. Gray et al., 2015; Hill et al., 2009; Hill, McLaughlin, et al., 2010) as well as fear and anxiety-like behaviour (Gunduz-Cinar et al., 2013; Petrie et al., 2021). In a few animals, we tested if either CB1R or FAAH are more heavily expressed in stress-responsive subregions of the BLA. As others have shown, both CB1R (Katona et al., 2001; Lazarini-Lopes et al., 2020) and FAAH (Gulyas et al., 2004) appeared uniformly distributed throughout the BLA.

Third, *Ppp1r1b* has been identified as a selective marker for parvicellular BLA pyramidal neurons (J. Kim et al., 2016; Uemura et al., 2022) and is particularly involved in reward learning and fear extinction (X. Zhang et al., 2020) via projections to the CeA, NAc, and infralimbic cortex (J. Kim et al., 2016). In several animals, we performed immunohistochemistry to reveal *Ppp1r1b* expression heavily in the LBA. This is notable, as this subregion reveals a stark lack of stress-induced FOS expression. However, the only available, reliable antibody is not compatible with our current FOS antibody, and as such we did not move forward with any colocalization experiments. This remains a significant marker of interest for us.

5.7 SEX AS A BIOLOGICAL VARIABLE

Overview. Except for anatomical mapping in Chapter 4, we only performed experiments in male rats. This is an important limitation, as in both rodents and humans, activation of the HPA axis and subsequent release of CORT is strongly influenced by sex of the subject (Rincón-Cortés et al., 2019). Sex differences also extend to behavioural responses to stress, as females generally display greater exploratory behaviour in the open field test and elevated plus maze (Knight et al., 2021), although this could largely be attributed to increased locomotor activity, and not lower anxiety-like behaviour (Börchers et al., 2022). Additionally, while male rats reliably exhibit a freezing response as an expression of fear, a subset of female rats display darting responses (Gruene et al., 2015). Thus, interpretation of both endocrine and behavioural effects is dependent on sex.

Considerations. As basal and stress-induced CORT levels are significantly greater in females (Drossopoulou et al., 2004; Goel et al., 2014), it is challenging to run experiments using both sexes without the robust baseline and stress-induced differences in CORT between males and females masking any changes produced by our manipulations. Thus, given that CORT was our primary functional readout in Chapter 2 and 2, we restricted most of our work to only one sex. However, we have conducted experiments on sex differences in BLA FOS reactivity to different stressors, although data analyses have not been completed and therefore is not included in the thesis. Preliminary findings suggest that the topographical pattern in response to various stressors is highly similar between males and females (data not shown).

Unlike other areas of the brain, there are low levels of estrogen receptor and no sex differences in volume or number of neurons (Rubinow & Juraska, 2009). This suggests there may not be substantial sexual dimorphism in BLA anatomy. However, there is evidence for sexual dimorphism in spine density (Rubinow et al., 2009) and number of GABAergic neurons

(Stefanova, 1998), suggesting altered neural excitability between sexes. In particular, discrete projection populations targeting the BST demonstrate lower excitability in females (Vantrease et al., 2022).

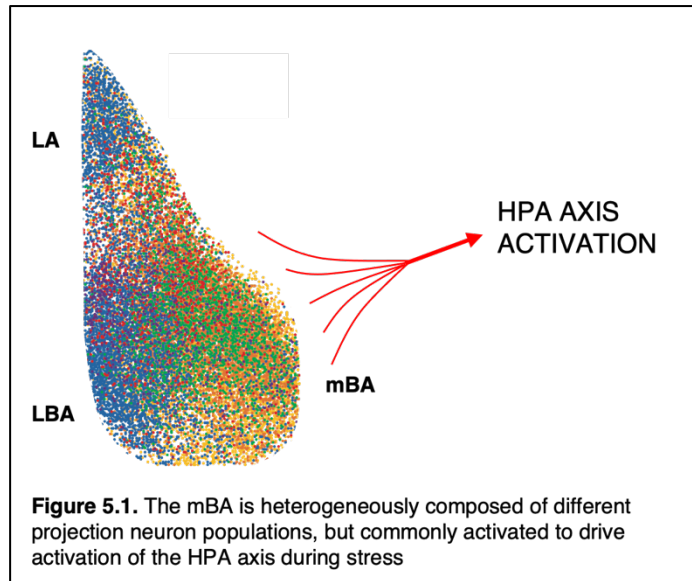
For these reasons, we explicitly addressed sex differences in Chapter 4. This was especially important, as there is strong evidence for sexual dimorphism of the CRH/CRHR1 system in the BLA (Bangasser, 2013). For instance, others have found greater expression of BLA CRHR1 mRNA in females (Georgiou et al., 2018), although we did not identify any sex differences in number of BLA CRHR1+ neurons. Given that Georgiou *et al* (2018) assessed mRNA levels, and we assessed number of CRHR1+ cells this discrepancy could be that females exhibit the same number of CRHR1+ cells but with greater density of receptors on each cell.

5.8 FUTURE DIRECTIONS AND CONCLUSION

Summary. The overarching aim of this thesis was to conduct a systematic investigation of the spatial, temporal, and circuit-specific activation patterns of BLA projection neurons during exposure to acute stress. Additionally, we wanted to explicitly test the role of the BLA in activation of the HPA axis, as this remains a poorly understood process.

We first demonstrated that projection populations are heterogeneously distributed throughout the BLA. Secondly, we established that a wide range of stressors induce a common spatial pattern of activation, with a bias towards the mBA subregion, although different stressors evoked different temporal patterns of activation. Thirdly, we demonstrated that many different projection populations were activated by exposure to stress, including those targeting the PrL, NAc, BST, CeA, VH, and LH. We then provided strong evidence for the role of the BLA in the HPA axis response to stress, as optogenetic stimulation or chemogenetic inhibition of CaMKIIa projection neurons bidirectionally influenced CORT levels. However, chemogenetic inhibition of

isolated projection neuron populations targeting the PrL, NAc, CeA, or BST did not reduce stress-induced CORT release. Likewise, chemogenetic inhibition of BLA projection neurons expressing CRHR1 also has no effect on stress-induced CORT, despite exhibiting increased FOS expression following exposure to stress. As such, perhaps a large, diverse population of



BLA projection neurons requires coordinated activation to drive changes in HPA axis activity (Figure 5.1).

Future Directions. Many important questions remain. For example, we established that various acute stressors induce a common spatial pattern of activation in the BLA, with a particular bias towards activation of the LA and the mBA. However, what stimuli lead to activation of the LBA? There is some evidence, although limited, of a discrete population of reward-encoding and fear-inhibiting neurons localized to this subregion (J. Kim et al., 2016; X. Zhang et al., 2020), and thus it is unsurprising that this region would be less activated during stress exposure. It is also possible that this region may be particularly involved in fear learning, as many CeA-projecting neurons are localized in the LBA (Beyeler et al., 2018), a circuit that is strongly implicated in expression of fear (S. A. Jimenez & Maren, 2009). As a result, activation may become more apparent with repeated exposure to aversive stimuli. Both these hypotheses could easily be tested by mapping FOS expression upon re-exposure to a learned environment, such as in contextual fear conditioning or extinction training. Along a similar line of thought, anatomical work suggests that the LBA receives particularly strong inputs from the insular cortex (McDonald, 1998) and sends dense

projections to the CeA (Beyeler et al., 2018). Given the importance of the insular cortex, BLA, and CeA in processing aversive taste (Beyeler et al., 2018; Kayyal et al., 2019; Schafe & Bernstein, 1996, 1998), learning of conditioned taste aversion may particularly involve this subregion (A. W. Johnson et al., 2009).

Secondly, we demonstrated that a wide range of BLA projection neuron populations in the mBA are activated in response to psychological stress. Do different populations have different temporal activation patterns? It is possible to record activity during exposure to acute stress by using projection-specific fiber photometry (Muir et al., 2020). Perhaps some populations contribute to the initial response to stress, while other populations are activated throughout to drive distinct behavioural responses. In a similar vein, the use of GRAB sensors could identify the temporal dynamics of neuromodulatory inputs such as dopamine, acetylcholine, norepinephrine, or endocannabinoids. For example, (Mineur et al., 2022) demonstrated that cholinergic signaling in the BLA accompanied transitions in behavioural state towards active coping, suggesting that this signal may play an important role in modulating behavioural state. As such, identifying activity of discrete signals in relation to stress responsivity may provide further insight into the potential role of discrete BLA cell types or inputs during stress.

Most importantly, what are the molecular markers of stress-responsive neurons? The BLA exhibits wide heterogeneity in molecular expression (O’Leary et al., 2020). However, there are very few known molecular markers for BLA neurons that drive stress-related behaviours. While we demonstrated that a wide range of different projection populations were activated by stress, it is possible that a distinct molecular marker may be specific to stress-responsive neurons, and thus be expressed widely in multiple projection populations. This could be addressed using various molecular approaches such as fluorescence-activated cell sorting (FACS) in combination with activity-dependent tagging of neuronal populations (McCullough, Morrison, et al., 2016). Identification of molecular signatures within discrete circuits emanating from the BLA may in turn

allow for pharmacological manipulation of these circuit to influence behavior or hormonal outcomes. Indeed, a similar approach to this has revealed the importance of neurotensin expression within neurons promoting reward and reducing fear (Li et al., 2022; McCullough, Choi, et al., 2016), suggesting that discrete neural circuits can be targeted for therapeutic benefit in stress-related psychiatric conditions. This is therefore an important avenue to continue exploring.

References

- Abraham, N. M., Guerin, D., Bhaukaurally, K., & Carleton, A. (2012). Similar Odor Discrimination Behavior in Head-Restrained and Freely Moving Mice. *PLoS ONE*, 7(12), e51789. <https://doi.org/10.1371/journal.pone.0051789>
- Agoglia, A. E., Zhu, M., Ying, R., Sidhu, H., Natividad, L. A., Wolfe, S. A., Buczynski, M. W., Contet, C., Parsons, L. H., Roberto, M., & Herman, M. A. (2020). Corticotropin-Releasing Factor Receptor-1 Neurons in the Lateral Amygdala Display Selective Sensitivity to Acute and Chronic Ethanol Exposure. *Eneuro*, 7(2), ENEURO.0420-19.2020. <https://doi.org/10.1523/ENEURO.0420-19.2020>
- Aitta-aho, T., Hay, Y. A., Phillips, B. U., Saksida, L. M., Bussey, T. J., Paulsen, O., & Apergis-Schoute, J. (2018). Basal Forebrain and Brainstem Cholinergic Neurons Differentially Impact Amygdala Circuits and Learning-Related Behavior. *Current Biology*, 28(16), 2557-2569.e4. <https://doi.org/10.1016/j.cub.2018.06.064>
- Aizenberg, M., Rolón-Martínez, S., Pham, T., Rao, W., Haas, J. S., & Geffen, M. N. (2019). Projection from the Amygdala to the Thalamic Reticular Nucleus Amplifies Cortical Sound Responses. *Cell Reports*, 28(3), 605-615.e4. <https://doi.org/10.1016/j.celrep.2019.06.050>
- Al-Hasani, R., McCall, J. G., Shin, G., Gomez, A. M., Schmitz, G. P., Bernardi, J. M., Pyo, C.-O., Park, S. I., Marcinkiewicz, C. M., Crowley, N. A., Krashes, M. J., Lowell, B. B., Kash, T. L., Rogers, J. A., & Bruchas, M. R. (2015). Distinct Subpopulations of Nucleus Accumbens Dynorphin Neurons Drive Aversion and Reward. *Neuron*, 87(5), 1063–1077. <https://doi.org/10.1016/j.neuron.2015.08.019>
- Alvarez-Crespo, M., Skibicka, K. P., Farkas, I., Molnár, C. S., Egecioglu, E., Hrabovszky, E., Liposits, Z., & Dickson, S. L. (2012). The Amygdala as a Neurobiological Target for Ghrelin in Rats: Neuroanatomical, Electrophysiological and Behavioral Evidence. *PLoS ONE*, 7(10), e46321. <https://doi.org/10.1371/journal.pone.0046321>
- Anderson, L. C., & Petrovich, G. D. (2018). Ventromedial prefrontal cortex mediates sex differences in persistent cognitive drive for food. *Scientific Reports*, 8(1), 2230. <https://doi.org/10.1038/s41598-018-20553-4>
- Andolina, D., Maran, D., Valzania, A., Conversi, D., & Puglisi-Allegra, S. (2013). Prefrontal/amygdalar system determines stress coping behavior through 5-HT/GABA connection. *Neuropsychopharmacology: Official Publication of the American College of Neuropsychopharmacology*, 38(10), 2057–2067. <https://doi.org/10.1038/npp.2013.107>
- Andrews, J., & Pruessner, J. C. (2013). The Combined Propranolol/TSST Paradigm – A New Method for Psychoneuroendocrinology. *PLoS ONE*, 8(2), e57567. <https://doi.org/10.1371/journal.pone.0057567>
- Aravanis, A. M., Wang, L.-P., Zhang, F., Meltzer, L. A., Mogri, M. Z., Schneider, M. B., & Deisseroth, K. (2007). An optical neural interface: *In vivo* control of rodent motor cortex with integrated fiberoptic

- and optogenetic technology. *Journal of Neural Engineering*, 4(3), S143–S156.
<https://doi.org/10.1088/1741-2560/4/3/S02>
- Armario, A., Montero, J. L., & Balasch, J. (1986). Sensitivity of corticosterone and some metabolic variables to graded levels of low intensity stresses in adult male rats. *Physiology & Behavior*, 37(4), 559–561. [https://doi.org/10.1016/0031-9384\(86\)90285-4](https://doi.org/10.1016/0031-9384(86)90285-4)
- Armbruster, B. N., Li, X., Pausch, M. H., Herlitze, S., & Roth, B. L. (2007). Evolving the lock to fit the key to create a family of G protein-coupled receptors potentially activated by an inert ligand. *Proceedings of the National Academy of Sciences*, 104(12), 5163–5168.
<https://doi.org/10.1073/pnas.0700293104>
- Asan, E. (1997). Ultrastructural features of tyrosine-hydroxylase-immunoreactive afferents and their targets in the rat amygdala. *Cell and Tissue Research*, 288(3), 449–469.
<https://doi.org/10.1007/s004410050832>
- Asan, E., Steinke, M., & Lesch, K.-P. (2013). Serotonergic innervation of the amygdala: Targets, receptors, and implications for stress and anxiety. *Histochemistry and Cell Biology*, 139(6), 785–813. <https://doi.org/10.1007/s00418-013-1081-1>
- Asede, D., Bosch, D., Lüthi, A., Ferraguti, F., & Ehrlich, I. (2015). Sensory Inputs to Intercalated Cells Provide Fear-Learning Modulated Inhibition to the Basolateral Amygdala. *Neuron*, 86(2), 541–554. <https://doi.org/10.1016/j.neuron.2015.03.008>
- Bærentzen, S., Casado-Sainz, A., Lange, D., Shalgunov, V., Tejada, I. M., Xiong, M., L'Estrade, E. T., Edgar, F. G., Lee, H., Herth, M. M., & Palner, M. (2019). The Chemogenetic Receptor Ligand Clozapine N-Oxide Induces in vivo Neuroreceptor Occupancy and Reduces Striatal Glutamate Levels. *Frontiers in Neuroscience*, 13, 187. <https://doi.org/10.3389/fnins.2019.00187>
- Bagot, R. C., Parise, E. M., Peña, C. J., Zhang, H.-X., Maze, I., Chaudhury, D., Persaud, B., Cachope, R., Bolaños-Guzmán, C. A., Cheer, J. F., Deisseroth, K., Han, M.-H., & Nestler, E. J. (2015). Ventral hippocampal afferents to the nucleus accumbens regulate susceptibility to depression. *Nature Communications*, 6(1), 7062. <https://doi.org/10.1038/ncomms8062>
- Bangasser, D. A. (2013). Sex differences in stress-related receptors: "micro" differences with "macro" implications for mood and anxiety disorders. *Biology of Sex Differences*, 4(1), 2.
<https://doi.org/10.1186/2042-6410-4-2>
- Bannerman, D. M., Grubb, M., Deacon, R. M. J., Yee, B. K., Feldon, J., & Rawlins, J. N. P. (2003). Ventral hippocampal lesions affect anxiety but not spatial learning. *Behavioural Brain Research*, 139(1–2), 197–213. [https://doi.org/10.1016/s0166-4328\(02\)00268-1](https://doi.org/10.1016/s0166-4328(02)00268-1)
- Ben-Ari, Y., Zigmond, R. E., Shute, C. C. D., & Lewis, P. R. (1977). Regional distribution of choline acetyltransferase and acetylcholinesterase within the amygdaloid complex and stria terminalis system. *Brain Research*, 120(3), 435–445. [https://doi.org/10.1016/0006-8993\(77\)90397-3](https://doi.org/10.1016/0006-8993(77)90397-3)

- Beyeler, A., Chang, C.-J., Silvestre, M., L  v  que, C., Namburi, P., Wildes, C. P., & Tye, K. M. (2018). Organization of Valence-Encoding and Projection-Defined Neurons in the Basolateral Amygdala. *Cell Reports*, 22(4), 905–918. <https://doi.org/10.1016/j.celrep.2017.12.097>
- Beyeler, A., Namburi, P., Glover, G. F., Simonnet, C., Calhoon, G. G., Conyers, G. F., Luck, R., Wildes, C. P., & Tye, K. M. (2016). Divergent Routing of Positive and Negative Information from the Amygdala during Memory Retrieval. *Neuron*, 90(2), 348–361. <https://doi.org/10.1016/j.neuron.2016.03.004>
- Bhatnagar, S., & Dallman, M. (1998). Neuroanatomical basis for facilitation of hypothalamic-pituitary-adrenal responses to a novel stressor after chronic stress. *Neuroscience*, 84(4), 1025–1039. [https://doi.org/10.1016/S0306-4522\(97\)00577-0](https://doi.org/10.1016/S0306-4522(97)00577-0)
- Bhatnagar, S., & Vining, C. (2003). Facilitation of hypothalamic–pituitary–adrenal responses to novel stress following repeated social stress using the resident/intruder paradigm. *Hormones and Behavior*, 43(1), 158–165. [https://doi.org/10.1016/S0018-506X\(02\)00011-9](https://doi.org/10.1016/S0018-506X(02)00011-9)
- Bhatnagar, S., Vining, C., & Denski, K. (2004). Regulation of chronic stress-induced changes in hypothalamic-pituitary-adrenal activity by the basolateral amygdala. *Annals of the New York Academy of Sciences*, 1032, 315–319. <https://doi.org/10.1196/annals.1314.050>
- Birnie, M. T., Short, A. K., De Carvalho, G. B., Taniguchi, L., Gunn, B. G., Pham, A. L., Itoga, C. A., Xu, X., Chen, L. Y., Mahler, S. V., Chen, Y., & Baram, T. Z. (2023). Stress-induced plasticity of a CRH/GABA projection disrupts reward behaviors in mice. *Nature Communications*, 14(1), 1088. <https://doi.org/10.1038/s41467-023-36780-x>
- Blair, H. T., Schafe, G. E., Bauer, E. P., Rodrigues, S. M., & LeDoux, J. E. (2001). Synaptic Plasticity in the Lateral Amygdala: A Cellular Hypothesis of Fear Conditioning. *Learning & Memory*, 8(5), 229–242. <https://doi.org/10.1101/lm.30901>
- Blair, K. S., Otero, M., Teng, C., Geraci, M., Lewis, E., Hollon, N., Blair, R. J. R., Ernst, M., Grillon, C., & Pine, D. S. (2016). Learning from other people’s fear: Amygdala-based social reference learning in social anxiety disorder. *Psychological Medicine*, 46(14), 2943–2953. <https://doi.org/10.1017/S0033291716001537>
- Bloodgood, D. W., Sugam, J. A., Holmes, A., & Kash, T. L. (2018). Fear extinction requires infralimbic cortex projections to the basolateral amygdala. *Translational Psychiatry*, 8(1), 60. <https://doi.org/10.1038/s41398-018-0106-x>
- Blum, S., Hebert, A. E., & Dash, P. K. (2006). A role for the prefrontal cortex in recall of recent and remote memories. *NeuroReport*, 17(3), 341–344. <https://doi.org/10.1097/01.wnr.0000201509.53750.bc>
- B  rchers, S., Krieger, J.-P., Asker, M., Maric, I., & Skibicka, K. P. (2022). Commonly-used rodent tests of anxiety-like behavior lack predictive validity for human sex differences. *Psychoneuroendocrinology*, 141, 105733. <https://doi.org/10.1016/j.psyneuen.2022.105733>

- Bowers, S. L., Bilbo, S. D., Dhabhar, F. S., & Nelson, R. J. (2008). Stressor-specific alterations in corticosterone and immune responses in mice. *Brain, Behavior, and Immunity*, 22(1), 105–113. <https://doi.org/10.1016/j.bbi.2007.07.012>
- Boyden, E. S., Zhang, F., Bamberg, E., Nagel, G., & Deisseroth, K. (2005). Millisecond-timescale, genetically targeted optical control of neural activity. *Nature Neuroscience*, 8(9), 1263–1268. <https://doi.org/10.1038/nn1525>
- Brake, W. G., Flores, G., Francis, D., Meaney, M. J., Srivastava, L. K., & Gratton, A. (2000). Enhanced nucleus accumbens dopamine and plasma corticosterone stress responses in adult rats with neonatal excitotoxic lesions to the medial prefrontal cortex. *Neuroscience*, 96(4), 687–695. [https://doi.org/10.1016/S0306-4522\(00\)00002-6](https://doi.org/10.1016/S0306-4522(00)00002-6)
- Brog, J. S., Salyapongse, A., Deutch, A. Y., & Zahm, D. S. (1993). The patterns of afferent innervation of the core and shell in the ?Accumbens? Part of the rat ventral striatum: Immunohistochemical detection of retrogradely transported fluoro-gold. *The Journal of Comparative Neurology*, 338(2), 255–278. <https://doi.org/10.1002/cne.903380209>
- Bruzsik, B., Biro, L., Zelena, D., Sipos, E., Szezik, H., Sarosdi, K. R., Horvath, O., Farkas, I., Csillag, V., Finszter, C. K., Mikics, E., & Toth, M. (2021). Somatostatin Neurons of the Bed Nucleus of Stria Terminalis Enhance Associative Fear Memory Consolidation in Mice. *The Journal of Neuroscience*, 41(9), 1982–1995. <https://doi.org/10.1523/JNEUROSCI.1944-20.2020>
- Bucy, P. C., & Klüver, H. (1955). An anatomical investigation of the temporal lobe in the monkey (*Macaca mulatta*): TEMPORAL LOBE OF MONKEY. *Journal of Comparative Neurology*, 103(2), 151–251. <https://doi.org/10.1002/cne.901030202>
- Butler, M. P., Karatsoreos, I. N., LeSauter, J., & Silver, R. (2012). Dose-dependent effects of androgens on the circadian timing system and its response to light. *Endocrinology*, 153(5), 2344–2352. <https://doi.org/10.1210/en.2011-1842>
- Calhoon, G. G., & Tye, K. M. (2015). Resolving the neural circuits of anxiety. *Nature Neuroscience*, 18(10), 1394–1404. <https://doi.org/10.1038/nn.4101>
- Campbell, E. J., Mitchell, C. S., Adams, C. D., Yeoh, J. W., Hodgson, D. M., Graham, B. A., & Dayas, C. V. (2017). Chemogenetic activation of the lateral hypothalamus reverses early life stress-induced deficits in motivational drive. *European Journal of Neuroscience*, 46(7), 2285–2296. <https://doi.org/10.1111/ejn.13674>
- Campeau, S., Dolan, D., Akil, H., & Watson, S. J. (2002). c-fos mRNA induction in acute and chronic audiogenic stress: Possible role of the orbitofrontal cortex in habituation. *Stress (Amsterdam, Netherlands)*, 5(2), 121–130. <https://doi.org/10.1080/10253890290027895>
- Canteras, N. S., & Swanson, L. W. (1992). Projections of the ventral subiculum to the amygdala, septum, and hypothalamus: A PHAL anterograde tract-tracing study in the rat. *The Journal of Comparative Neurology*, 324(2), 180–194. <https://doi.org/10.1002/cne.903240204>

- Cardozo Pinto, D. F., & Lammel, S. (2019). Hot topic in optogenetics: New implications of in vivo tissue heating. *Nature Neuroscience*, 22(7), 1039–1041. <https://doi.org/10.1038/s41593-019-0426-z>
- Carlsen, J., & Heimer, L. (1988). The basolateral amygdaloid complex as a cortical-like structure. *Brain Research*, 441(1–2), 377–380. [https://doi.org/10.1016/0006-8993\(88\)91418-7](https://doi.org/10.1016/0006-8993(88)91418-7)
- Casada, J. H., & Dafny, N. (1991). Restraint and stimulation of bed nucleus of the stria terminalis produce similar stress-like behaviors. *Brain Research Bulletin*, 27(2), 207–212. [https://doi.org/10.1016/0361-9230\(91\)90069-V](https://doi.org/10.1016/0361-9230(91)90069-V)
- Cedarbaum, J. M., & Aghajanian, G. K. (1978). Afferent projections to the rat locus coeruleus as determined by a retrograde tracing technique. *The Journal of Comparative Neurology*, 178(1), 1–15. <https://doi.org/10.1002/cne.901780102>
- Cenci, M. A., Kalén, P., Mandel, R. J., & Björklund, A. (1992). Regional differences in the regulation of dopamine and noradrenaline release in medial frontal cortex, nucleus accumbens and caudate-putamen: A microdialysis study in the rat. *Brain Research*, 581(2), 217–228. [https://doi.org/10.1016/0006-8993\(92\)90711-H](https://doi.org/10.1016/0006-8993(92)90711-H)
- Chaaya, N., Jacques, A., Belmer, A., Richard, D. J., Bartlett, S. E., Battle, A. R., & Johnson, L. R. (2019). Localization of Contextual and Context Removed Auditory Fear Memory within the Basolateral Amygdala Complex. *Neuroscience*, 398, 231–251. <https://doi.org/10.1016/j.neuroscience.2018.12.004>
- Chan, R. K., Brown, E. R., Ericsson, A., Kovács, K. J., & Sawchenko, P. E. (1993). A comparison of two immediate-early genes, c-fos and NGFI-B, as markers for functional activation in stress-related neuroendocrine circuitry. *The Journal of Neuroscience: The Official Journal of the Society for Neuroscience*, 13(12), 5126–5138. <https://doi.org/10.1523/JNEUROSCI.13-12-05126.1993>
- Chaouloff, F., Durand, M., & Mormède, P. (1997). Anxiety- and activity-related effects of diazepam and chlordiazepoxide in the rat light/dark and dark/light tests. *Behavioural Brain Research*, 85(1), 27–35. [https://doi.org/10.1016/s0166-4328\(96\)00160-x](https://doi.org/10.1016/s0166-4328(96)00160-x)
- Chapter 1. (2023).
- Chapter 2. (2023).
- Chen, G., Lai, S., Bao, G., Ke, J., Meng, X., Lu, S., Wu, X., Xu, H., Wu, F., Xu, Y., Xu, F., Bi, G.-Q., Peng, G., Zhou, K., & Zhu, Y. (2023). Distinct reward processing by subregions of the nucleus accumbens. *Cell Reports*, 42(2), 112069. <https://doi.org/10.1016/j.celrep.2023.112069>
- Chen, Y., Brunson, K. L., Müller, M. B., Cariaga, W., & Baram, T. Z. (2000). Immunocytochemical distribution of corticotropin-releasing hormone receptor type-1 (CRF(1))-like immunoreactivity in the mouse brain: Light microscopy analysis using an antibody directed against the C-terminus. *The Journal of Comparative Neurology*, 420(3), 305–323. [https://doi.org/10.1002/\(sici\)1096-9861\(20000508\)420:3<305::aid-cne3>3.0.co;2-8](https://doi.org/10.1002/(sici)1096-9861(20000508)420:3<305::aid-cne3>3.0.co;2-8)

- Ch'ng, S., Fu, J., Brown, R. M., McDougall, S. J., & Lawrence, A. J. (2018). The intersection of stress and reward: BNST modulation of aversive and appetitive states. *Progress in Neuro-Psychopharmacology and Biological Psychiatry*, 87, 108–125.
<https://doi.org/10.1016/j.pnpbp.2018.01.005>
- Choi, D. C., Furay, A. R., Evanson, N. K., Ostrander, M. M., Ulrich-Lai, Y. M., & Herman, J. P. (2007). Bed nucleus of the stria terminalis subregions differentially regulate hypothalamic-pituitary-adrenal axis activity: Implications for the integration of limbic inputs. *The Journal of Neuroscience: The Official Journal of the Society for Neuroscience*, 27(8), 2025–2034.
<https://doi.org/10.1523/JNEUROSCI.4301-06.2007>
- Choleris, E., Thomas, A. W., Kavaliers, M., & Prato, F. S. (2001). A detailed ethological analysis of the mouse open field test: Effects of diazepam, chlordiazepoxide and an extremely low frequency pulsed magnetic field. *Neuroscience and Biobehavioral Reviews*, 25(3), 235–260.
[https://doi.org/10.1016/s0149-7634\(01\)00011-2](https://doi.org/10.1016/s0149-7634(01)00011-2)
- Cohen, H., Vainer, E., Zeev, K., Zohar, J., & Mathé, A. A. (2018). Neuropeptide S in the basolateral amygdala mediates an adaptive behavioral stress response in a rat model of posttraumatic stress disorder by increasing the expression of BDNF and the neuropeptide YY1 receptor. *European Neuropsychopharmacology*, 28(1), 159–170. <https://doi.org/10.1016/j.euroneuro.2017.11.006>
- Cole, K. E., Lee, J., Davis, M., & Parsons, R. G. (2019). Subthreshold Fear Conditioning Produces a Rapidly Developing Neural Mechanism that Primes Subsequent Learning. *ENeuro*, 6(3), ENEURO.0113-19.2019. <https://doi.org/10.1523/ENeuro.0113-19.2019>
- Cole, S., Powell, D. J., & Petrovich, G. D. (2013). Differential recruitment of distinct amygdalar nuclei across appetitive associative learning. *Learning & Memory (Cold Spring Harbor, N. Y.)*, 20(6), 295–299. <https://doi.org/10.1101/lm.031070.113>
- Conte, W. L., Kamishina, H., & Reep, R. L. (2009). Multiple neuroanatomical tract-tracing using fluorescent Alexa Fluor conjugates of cholera toxin subunit B in rats. *Nature Protocols*, 4(8), 1157–1166. <https://doi.org/10.1038/nprot.2009.93>
- Coover, G., Ursin, H., & Levine, S. (1973). Corticosterone and avoidance in rats with basolateral amygdala lesions. *Journal of Comparative and Physiological Psychology*, 85(1), 111–122.
<https://doi.org/10.1037/h0034858>
- Corcoran, K. A., & Quirk, G. J. (2007). Activity in Prelimbic Cortex Is Necessary for the Expression of Learned, But Not Innate, Fears. *The Journal of Neuroscience*, 27(4), 840–844.
<https://doi.org/10.1523/JNEUROSCI.5327-06.2007>
- Crestani, C., Alves, F., Gomes, F., Resstel, L., Correa, F., & Herman, J. (2013). Mechanisms in the Bed Nucleus of the Stria Terminalis Involved in Control of Autonomic and Neuroendocrine Functions: A Review. *Current Neuropharmacology*, 11(2), 141–159.
<https://doi.org/10.2174/1570159X11311020002>

- Crowley, N. A., Bloodgood, D. W., Hardaway, J. A., Kendra, A. M., McCall, J. G., Al-Hasani, R., McCall, N. M., Yu, W., Schools, Z. L., Krashes, M. J., Lowell, B. B., Whistler, J. L., Bruchas, M. R., & Kash, T. L. (2016). Dynorphin Controls the Gain of an Amygdalar Anxiety Circuit. *Cell Reports*, 14(12), 2774–2783. <https://doi.org/10.1016/j.celrep.2016.02.069>
- Cullinan, W. E., Herman, J. P., Battaglia, D. F., Akil, H., & Watson, S. J. (1995). Pattern and time course of immediate early gene expression in rat brain following acute stress. *Neuroscience*, 64(2), 477–505. [https://doi.org/10.1016/0306-4522\(94\)00355-9](https://doi.org/10.1016/0306-4522(94)00355-9)
- Cullinan, W. E., Herman, J. P., & Watson, S. J. (1993). Ventral subicular interaction with the hypothalamic paraventricular nucleus: Evidence for a relay in the bed nucleus of the stria terminalis. *The Journal of Comparative Neurology*, 332(1), 1–20. <https://doi.org/10.1002/cne.903320102>
- Davis, M. (1992). The Role of the Amygdala in Fear and Anxiety. *Annual Review of Neuroscience*, 15(1), 353–375. <https://doi.org/10.1146/annurev.ne.15.030192.002033>
- Davis, M., Walker, D. L., Miles, L., & Grillon, C. (2010). Phasic vs sustained fear in rats and humans: Role of the extended amygdala in fear vs anxiety. *Neuropsychopharmacology: Official Publication of the American College of Neuropsychopharmacology*, 35(1), 105–135. <https://doi.org/10.1038/npp.2009.109>
- Daviu, N., Bruchas, M. R., Moghaddam, B., Sandi, C., & Beyeler, A. (2019). Neurobiological links between stress and anxiety. *Neurobiology of Stress*, 11, 100191. <https://doi.org/10.1016/j.ynstr.2019.100191>
- Daviu, N., Füzesi, T., Rosenegger, D. G., Rasiah, N. P., Sterley, T.-L., Peringod, G., & Bains, J. S. (2020). Paraventricular nucleus CRH neurons encode stress controllability and regulate defensive behavior selection. *Nature Neuroscience*, 23(3), 398–410. <https://doi.org/10.1038/s41593-020-0591-0>
- de Oliveira, A. R., Reimer, A. E., Reis, F. M. C. V., & Brandão, M. L. (2017). Dopamine D2-like receptors modulate freezing response, but not the activation of HPA axis, during the expression of conditioned fear. *Experimental Brain Research*, 235(2), 429–436. <https://doi.org/10.1007/s00221-016-4805-3>
- Deacon, R. M. J., Bannerman, D. M., & Rawlins, J. N. P. (2002). Anxiolytic effects of cytotoxic hippocampal lesions in rats. *Behavioral Neuroscience*, 116(3), 494–497. <https://doi.org/10.1037//0735-7044.116.3.494>
- Deolindo, M. V., Reis, D. G., Crestani, C. C., Tavares, R. F., Resstel, L. B. M., & Corrêa, F. M. A. (2013). NMDA receptors in the lateral hypothalamus have an inhibitory influence on the tachycardiac response to acute restraint stress in rats. *European Journal of Neuroscience*, 38(3), 2374–2381. <https://doi.org/10.1111/ejn.12246>
- DeVuono, M. V., Hrelja, K. M., Petrie, G. N., Limebeer, C. L., Rock, E. M., Hill, M. N., & Parker, L. A. (2020). Nausea-Induced Conditioned Gaping Reactions in Rats Produced by High-Dose

- Synthetic Cannabinoid, JWH-018. *Cannabis and Cannabinoid Research*, 5(4), 298–304.
<https://doi.org/10.1089/can.2019.0103>
- Di, S., Itoga, C. A., Fisher, M. O., Solomonow, J., Roltsch, E. A., Gilpin, N. W., & Tasker, J. G. (2016). Acute Stress Suppresses Synaptic Inhibition and Increases Anxiety via Endocannabinoid Release in the Basolateral Amygdala. *The Journal of Neuroscience: The Official Journal of the Society for Neuroscience*, 36(32), 8461–8470. <https://doi.org/10.1523/JNEUROSCI.2279-15.2016>
- Dickie, E. W., Brunet, A., Akerib, V., & Armony, J. L. (2011). Neural correlates of recovery from post-traumatic stress disorder: A longitudinal fMRI investigation of memory encoding. *Neuropsychologia*, 49(7), 1771–1778. <https://doi.org/10.1016/j.neuropsychologia.2011.02.055>
- Diorio, D., Viau, V., & Meaney, M. (1993). The role of the medial prefrontal cortex (cingulate gyrus) in the regulation of hypothalamic-pituitary-adrenal responses to stress. *The Journal of Neuroscience*, 13(9), 3839–3847. <https://doi.org/10.1523/JNEUROSCI.13-09-03839.1993>
- Dong, A., He, K., Dudok, B., Farrell, J. S., Guan, W., Liput, D. J., Puhl, H. L., Cai, R., Wang, H., Duan, J., Albarran, E., Ding, J., Lovinger, D. M., Li, B., Soltesz, I., & Li, Y. (2022). A fluorescent sensor for spatiotemporally resolved imaging of endocannabinoid dynamics in vivo. *Nature Biotechnology*, 40(5), 787–798. <https://doi.org/10.1038/s41587-021-01074-4>
- Dong, H.-W., Petrovich, G. D., & Swanson, L. W. (2001). Topography of projections from amygdala to bed nuclei of the stria terminalis. *Brain Research Reviews*, 38(1–2), 192–246.
[https://doi.org/10.1016/S0165-0173\(01\)00079-0](https://doi.org/10.1016/S0165-0173(01)00079-0)
- Dragunow, M., De Castro, D., & Faull, R. L. M. (1990). Induction of Fos in glia-like cells after focal brain injury but not during wallerian degeneration. *Brain Research*, 527(1), 41–54.
[https://doi.org/10.1016/0006-8993\(90\)91058-O](https://doi.org/10.1016/0006-8993(90)91058-O)
- Drossopoulou, G., Antoniou, K., Kitraki, E., Papathanasiou, G., Papalexi, E., Dalla, C., & Papadopoulou-Daifoti, Z. (2004). Sex differences in behavioral, neurochemical and neuroendocrine effects induced by the forced swim test in rats. *Neuroscience*, 126(4), 849–857.
<https://doi.org/10.1016/j.neuroscience.2004.04.044>
- Dunn, J. D., & Whitener, J. (1986). Plasma Corticosterone Responses to Electrical Stimulation of the Amygdaloid Complex: Cytoarchitectural Specificity. *Neuroendocrinology*, 42(3), 211–217.
<https://doi.org/10.1159/000124442>
- Eacret, D., Grafe, L. A., Dobkin, J., Gotter, A. L., Renger, J. J., Winrow, C. J., & Bhatnagar, S. (2019). Orexin signaling during social defeat stress influences subsequent social interaction behaviour and recognition memory. *Behavioural Brain Research*, 356, 444–452.
<https://doi.org/10.1016/j.bbr.2018.05.032>
- Ehrlich, I., Humeau, Y., Grenier, F., Ciocchi, S., Herry, C., & Lüthi, A. (2009). Amygdala Inhibitory Circuits and the Control of Fear Memory. *Neuron*, 62(6), 757–771.
<https://doi.org/10.1016/j.neuron.2009.05.026>

- Emmert, M. H., & Herman, J. P. (1999). Differential forebrain c-fos mRNA induction by ether inhalation and novelty: Evidence for distinctive stress pathways. *Brain Research*, 845(1), 60–67. [https://doi.org/10.1016/S0006-8993\(99\)01931-9](https://doi.org/10.1016/S0006-8993(99)01931-9)
- Engel, K., Bandelow, B., Gruber, O., & Wedekind, D. (2009). Neuroimaging in anxiety disorders. *Journal of Neural Transmission*, 116(6), 703–716. <https://doi.org/10.1007/s00702-008-0077-9>
- Etkin, A., & Wager, T. D. (2007). Functional Neuroimaging of Anxiety: A Meta-Analysis of Emotional Processing in PTSD, Social Anxiety Disorder, and Specific Phobia. *American Journal of Psychiatry*, 164(10), 1476–1488. <https://doi.org/10.1176/appi.ajp.2007.07030504>
- Fadok, J. P., Markovic, M., Tovote, P., & Lüthi, A. (2018). New perspectives on central amygdala function. *Current Opinion in Neurobiology*, 49, 141–147. <https://doi.org/10.1016/j.conb.2018.02.009>
- Fallon, J. H., Koziell, D. A., & Moore, R. Y. (1978). Catecholamine innervation of the basal forebrain II. Amygdala, suprarhinal cortex and entorhinal cortex. *The Journal of Comparative Neurology*, 180(3), 509–531. <https://doi.org/10.1002/cne.901800308>
- Fanselow, M. S., & Dong, H.-W. (2010). Are the Dorsal and Ventral Hippocampus Functionally Distinct Structures? *Neuron*, 65(1), 7–19. <https://doi.org/10.1016/j.neuron.2009.11.031>
- Feldman, S., Conforti, N., & Saphier, D. (1990). The preoptic area and bed nucleus of the stria terminalis are involved in the effects of the amygdala on adrenocortical secretion. *Neuroscience*, 37(3), 775–779. [https://doi.org/10.1016/0306-4522\(90\)90107-F](https://doi.org/10.1016/0306-4522(90)90107-F)
- Feldman, S., Conforti, N., & Siegel, R. A. (1982). Adrenocortical Responses following Limbic Stimulation in Rats with Hypothalamic Deafferentations. *Neuroendocrinology*, 35(3), 205–211. <https://doi.org/10.1159/000123382>
- Felix-Ortiz, A. C., Beyeler, A., Seo, C., Leppla, C. A., Wildes, C. P., & Tye, K. M. (2013). BLA to vHPC inputs modulate anxiety-related behaviors. *Neuron*, 79(4), 658–664. <https://doi.org/10.1016/j.neuron.2013.06.016>
- Felix-Ortiz, A. C., Burgos-Robles, A., Bhagat, N. D., Leppla, C. A., & Tye, K. M. (2016). Bidirectional modulation of anxiety-related and social behaviors by amygdala projections to the medial prefrontal cortex. *Neuroscience*, 321, 197–209. <https://doi.org/10.1016/j.neuroscience.2015.07.041>
- Felix-Ortiz, A. C., & Tye, K. M. (2014). Amygdala inputs to the ventral hippocampus bidirectionally modulate social behavior. *The Journal of Neuroscience: The Official Journal of the Society for Neuroscience*, 34(2), 586–595. <https://doi.org/10.1523/JNEUROSCI.4257-13.2014>
- Fendt, M., Endres, T., & Apfelbach, R. (2003). Temporary Inactivation of the Bed Nucleus of the Stria Terminalis But Not of the Amygdala Blocks Freezing Induced by Trimethylthiazoline, a Component of Fox Feces. *The Journal of Neuroscience*, 23(1), 23–28. <https://doi.org/10.1523/JNEUROSCI.23-01-00023.2003>

- Feng, J., Zhang, C., Lischinsky, J. E., Jing, M., Zhou, J., Wang, H., Zhang, Y., Dong, A., Wu, Z., Wu, H., Chen, W., Zhang, P., Zou, J., Hires, S. A., Zhu, J. J., Cui, G., Lin, D., Du, J., & Li, Y. (2019). A Genetically Encoded Fluorescent Sensor for Rapid and Specific In Vivo Detection of Norepinephrine. *Neuron*, 102(4), 745–761.e8. <https://doi.org/10.1016/j.neuron.2019.02.037>
- Fillinger, C., Yalcin, I., Barrot, M., & Veinante, P. (2017). Afferents to anterior cingulate areas 24a and 24b and midcingulate areas 24a' and 24b' in the mouse. *Brain Structure and Function*, 222(3), 1509–1532. <https://doi.org/10.1007/s00429-016-1290-1>
- Flati, T., Gioiosa, S., Chillemi, G., Mele, A., Oliverio, A., Mannironi, C., Rinaldi, A., & Castrignanò, T. (2020). A gene expression atlas for different kinds of stress in the mouse brain. *Scientific Data*, 7(1), 437. <https://doi.org/10.1038/s41597-020-00772-z>
- Flores, Á., Herry, C., Maldonado, R., & Berrendero, F. (2017). Facilitation of Contextual Fear Extinction by Orexin-1 Receptor Antagonism Is Associated with the Activation of Specific Amygdala Cell Subpopulations. *International Journal of Neuropsychopharmacology*, 20(8), 654–659. <https://doi.org/10.1093/ijnp/pyx029>
- Floresco, S. B. (2015). The Nucleus Accumbens: An Interface Between Cognition, Emotion, and Action. *Annual Review of Psychology*, 66(1), 25–52. <https://doi.org/10.1146/annurev-psych-010213-115159>
- Floriou-Servou, A., Von Ziegler, L., Stalder, L., Sturman, O., Privitera, M., Rassi, A., Cremonesi, A., Thöny, B., & Bohacek, J. (2018). Distinct Proteomic, Transcriptomic, and Epigenetic Stress Responses in Dorsal and Ventral Hippocampus. *Biological Psychiatry*, 84(7), 531–541. <https://doi.org/10.1016/j.biopsych.2018.02.003>
- Folkes, O. M., Báldi, R., Kondev, V., Marcus, D. J., Hartley, N. D., Turner, B. D., Ayers, J. K., Baechle, J. J., Misra, M. P., Altemus, M., Grueter, C. A., Grueter, B. A., & Patel, S. (2020). An endocannabinoid-regulated basolateral amygdala-nucleus accumbens circuit modulates sociability. *The Journal of Clinical Investigation*, 130(4), 1728–1742. <https://doi.org/10.1172/JCI131752>
- Forlano, P. M., & Woolley, C. S. (2010). Quantitative analysis of pre- and postsynaptic sex differences in the nucleus accumbens. *The Journal of Comparative Neurology*, 518(8), 1330–1348. <https://doi.org/10.1002/cne.22279>
- Galvez, R., Mesches, M. H., & McGaugh, J. L. (1996). Norepinephrine Release in the Amygdala in Response to Footshock Stimulation. *Neurobiology of Learning and Memory*, 66(3), 253–257. <https://doi.org/10.1006/nlme.1996.0067>
- Gehrlach, D. A., Weiland, C., Gaitanos, T. N., Cho, E., Klein, A. S., Hennrich, A. A., Conzelmann, K.-K., & Gogolla, N. (2020). A whole-brain connectivity map of mouse insular cortex. *ELife*, 9, e55585. <https://doi.org/10.7554/eLife.55585>

- Georgiou, P., Zanos, P., Bhat, S., Tracy, J. K., Merchenthaler, I. J., McCarthy, M. M., & Gould, T. D. (2018). Dopamine and Stress System Modulation of Sex Differences in Decision Making. *Neuropsychopharmacology*, 43(2), 313–324. <https://doi.org/10.1038/npp.2017.161>
- Gilman, T. L., Dutta, S., Adkins, J. M., Cecil, C. A., & Jasnow, A. M. (2018). Basolateral amygdala Thy1-expressing neurons facilitate the inhibition of contextual fear during consolidation, reconsolidation, and extinction. *Neurobiology of Learning and Memory*, 155, 498–507. <https://doi.org/10.1016/j.nlm.2018.09.010>
- Gilpin, N. W., Herman, M. A., & Roberto, M. (2015). The central amygdala as an integrative hub for anxiety and alcohol use disorders. *Biological Psychiatry*, 77(10), 859–869. <https://doi.org/10.1016/j.biopsych.2014.09.008>
- Girgis, M. (1980). Acetylcholinesterase enzyme localization in the amygdala: A comparative histochemical and ultrastructural study. *Cells Tissues Organs*, 106(2), 192–202. <https://doi.org/10.1159/000145181>
- Girotti, M., Pace, T. W. W., Gaylord, R. I., Rubin, B. A., Herman, J. P., & Spencer, R. L. (2006). Habituation to repeated restraint stress is associated with lack of stress-induced c-fos expression in primary sensory processing areas of the rat brain. *Neuroscience*, 138(4), 1067–1081. <https://doi.org/10.1016/j.neuroscience.2005.12.002>
- Giustino, T. F., Ramanathan, K. R., Totty, M. S., Miles, O. W., & Maren, S. (2020). Locus Coeruleus Norepinephrine Drives Stress-Induced Increases in Basolateral Amygdala Firing and Impairs Extinction Learning. *The Journal of Neuroscience: The Official Journal of the Society for Neuroscience*, 40(4), 907–916. <https://doi.org/10.1523/JNEUROSCI.1092-19.2019>
- Goel, N., Workman, J. L., Lee, T. T., Innala, L., & Viau, V. (2014). Sex Differences in the HPA Axis. In R. Terjung (Ed.), *Comprehensive Physiology* (1st ed., pp. 1121–1155). Wiley. <https://doi.org/10.1002/cphy.c130054>
- Goldstein, L. E., Rasmusson, A. M., Bunney, B. S., & Roth, R. H. (1996). Role of the Amygdala in the Coordination of Behavioral, Neuroendocrine, and Prefrontal Cortical Monoamine Responses to Psychological Stress in the Rat. *The Journal of Neuroscience*, 16(15), 4787–4798. <https://doi.org/10.1523/JNEUROSCI.16-15-04787.1996>
- Gomes-de-Souza, L., Costa-Ferreira, W., Mendonça, M. M., Xavier, C. H., & Crestani, C. C. (2021). Lateral hypothalamus involvement in control of stress response by bed nucleus of the stria terminalis endocannabinoid neurotransmission in male rats. *Scientific Reports*, 11(1), 16133. <https://doi.org/10.1038/s41598-021-95401-z>
- Gomez, J. L., Bonaventura, J., Lesniak, W., Mathews, W. B., Sysa-Shah, P., Rodriguez, L. A., Ellis, R. J., Richie, C. T., Harvey, B. K., Dannals, R. F., Pomper, M. G., Bonci, A., & Michaelides, M. (2017). Chemogenetics revealed: DREADD occupancy and activation via converted clozapine. *Science*, 357(6350), 503–507. <https://doi.org/10.1126/science.aan2475>

- Goode, T. D., Ressler, R. L., Acca, G. M., Miles, O. W., & Maren, S. (2019). Bed nucleus of the stria terminalis regulates fear to unpredictable threat signals. *ELife*, 8, e46525. <https://doi.org/10.7554/eLife.46525>
- Gore, F., Schwartz, E. C., Brangers, B. C., Aladi, S., Stujenske, J. M., Likhtik, E., Russo, M. J., Gordon, J. A., Salzman, C. D., & Axel, R. (2015). Neural Representations of Unconditioned Stimuli in Basolateral Amygdala Mediate Innate and Learned Responses. *Cell*, 162(1), 134–145. <https://doi.org/10.1016/j.cell.2015.06.027>
- Gray, J. M., Vecchiarelli, H. A., Morena, M., Lee, T. T. Y., Hermanson, D. J., Kim, A. B., McLaughlin, R. J., Hassan, K. I., Kuhne, C., Wotjak, C. T., Deussing, J. M., Patel, S., & Hill, M. N. (2015). Corticotropin-Releasing Hormone Drives Anandamide Hydrolysis in the Amygdala to Promote Anxiety. *Journal of Neuroscience*, 35(9), 3879–3892. <https://doi.org/10.1523/JNEUROSCI.2737-14.2015>
- Gray, T. S., Carney, M. E., & Magnuson, D. J. (1989). Direct Projections from the Central Amygdaloid Nucleus to the Hypothalamic Paraventricular Nucleus: Possible Role in Stress-Induced Adrenocorticotropin Release. *Neuroendocrinology*, 50(4), 433–446. <https://doi.org/10.1159/000125260>
- Gray, T. S., Piechowski, R. A., Yracheta, J. M., Rittenhouse, P. A., Bethea, C. L., & Van De Kar, L. D. (1993). Ibotenic Acid Lesions in the Bed Nucleus of the Stria terminalis Attenuate Conditioned Stress-Induced Increases in Prolactin, ACTH and Corticosterone. *Neuroendocrinology*, 57(3), 517–524. <https://doi.org/10.1159/000126400>
- Griebel, G., & Holmes, A. (2013). 50 years of hurdles and hope in anxiolytic drug discovery. *Nature Reviews. Drug Discovery*, 12(9), 667–687. <https://doi.org/10.1038/nrd4075>
- Grissom, N., Kerr, W., & Bhatnagar, S. (2008). Struggling behavior during restraint is regulated by stress experience. *Behavioural Brain Research*, 191(2), 219–226. <https://doi.org/10.1016/j.bbr.2008.03.030>
- Grissom, N. M., & Bhatnagar, S. (2011). The basolateral amygdala regulates adaptation to stress via β -adrenergic receptor-mediated reductions in phosphorylated extracellular signal-regulated kinase. *Neuroscience*, 178, 108–122. <https://doi.org/10.1016/j.neuroscience.2010.12.049>
- Gruene, T. M., Flick, K., Stefano, A., Shea, S. D., & Shansky, R. M. (2015). Sexually divergent expression of active and passive conditioned fear responses in rats. *ELife*, 4, e11352. <https://doi.org/10.7554/eLife.11352>
- Gulyas, A. I., Cravatt, B. F., Bracey, M. H., Dinh, T. P., Piomelli, D., Boscia, F., & Freund, T. F. (2004). Segregation of two endocannabinoid-hydrolyzing enzymes into pre- and postsynaptic compartments in the rat hippocampus, cerebellum and amygdala. *European Journal of Neuroscience*, 20(2), 441–458. <https://doi.org/10.1111/j.1460-9568.2004.03428.x>

- Gunaydin, L. A., Grosenick, L., Finkelstein, J. C., Kauvar, I. V., Fenno, L. E., Adhikari, A., Lammel, S., Mirzabekov, J. J., Airan, R. D., Zalocusky, K. A., Tye, K. M., Anikeeva, P., Malenka, R. C., & Deisseroth, K. (2014). Natural neural projection dynamics underlying social behavior. *Cell*, 157(7), 1535–1551. <https://doi.org/10.1016/j.cell.2014.05.017>
- Gunduz-Cinar, O., Hill, M. N., McEwen, B. S., & Holmes, A. (2013). Amygdala FAAH and anandamide: Mediating protection and recovery from stress. *Trends in Pharmacological Sciences*, 34(11), 637–644. <https://doi.org/10.1016/j.tips.2013.08.008>
- Gungor, N. Z., & Pare, D. (2016). Functional Heterogeneity in the Bed Nucleus of the Stria Terminalis. *Journal of Neuroscience*, 36(31), 8038–8049. <https://doi.org/10.1523/JNEUROSCI.0856-16.2016>
- Guzowski, J. F., McNaughton, B. L., Barnes, C. A., & Worley, P. F. (1999). Environment-specific expression of the immediate-early gene Arc in hippocampal neuronal ensembles. *Nature Neuroscience*, 2(12), 1120–1124. <https://doi.org/10.1038/16046>
- Habib, K. E., Weld, K. P., Rice, K. C., Pushkas, J., Champoux, M., Listwak, S., Webster, E. L., Atkinson, A. J., Schulkin, J., Contoreggi, C., Chrousos, G. P., McCann, S. M., Suomi, S. J., Higley, J. D., & Gold, P. W. (2000a). Oral administration of a corticotropin-releasing hormone receptor antagonist significantly attenuates behavioral, neuroendocrine, and autonomic responses to stress in primates. *Proceedings of the National Academy of Sciences of the United States of America*, 97(11), 6079–6084. <https://doi.org/10.1073/pnas.97.11.6079>
- Habib, K. E., Weld, K. P., Rice, K. C., Pushkas, J., Champoux, M., Listwak, S., Webster, E. L., Atkinson, A. J., Schulkin, J., Contoreggi, C., Chrousos, G. P., McCann, S. M., Suomi, S. J., Higley, J. D., & Gold, P. W. (2000b). Oral administration of a corticotropin-releasing hormone receptor antagonist significantly attenuates behavioral, neuroendocrine, and autonomic responses to stress in primates. *Proceedings of the National Academy of Sciences of the United States of America*, 97(11), 6079–6084. <https://doi.org/10.1073/pnas.97.11.6079>
- Hájos, N. (2021). Interneuron Types and Their Circuits in the Basolateral Amygdala. *Frontiers in Neural Circuits*, 15, 687257. <https://doi.org/10.3389/fncir.2021.687257>
- Han, W., Tellez, L. A., Rangel, M. J., Motta, S. C., Zhang, X., Perez, I. O., Canteras, N. S., Shammah-Lagnado, S. J., van den Pol, A. N., & de Araujo, I. E. (2017). Integrated Control of Predatory Hunting by the Central Nucleus of the Amygdala. *Cell*, 168(1–2), 311–324.e18. <https://doi.org/10.1016/j.cell.2016.12.027>
- Han, Z. (2003). Leptin receptor expression in the basolateral nucleus of amygdala of conditioned taste aversion rats. *World Journal of Gastroenterology*, 9(5), 1034. <https://doi.org/10.3748/wjg.v9.i5.1034>
- Haralambous, T., & Westbrook, R. F. (1999). An infusion of bupivacaine into the nucleus accumbens disrupts the acquisition but not the expression of contextual fear conditioning. *Behavioral Neuroscience*, 113(5), 925–940. <https://doi.org/10.1037/0735-7044.113.5.925>

- Hardaway, J. A., Halladay, L. R., Mazzone, C. M., Pati, D., Bloodgood, D. W., Kim, M., Jensen, J., DiBerto, J. F., Boyt, K. M., Shiddapur, A., Erfani, A., Hon, O. J., Neira, S., Stanhope, C. M., Sugam, J. A., Saddoris, M. P., Tipton, G., McElligott, Z., Jhou, T. C., ... Kash, T. L. (2019). Central Amygdala Prepronociceptin-Expressing Neurons Mediate Palatable Food Consumption and Reward. *Neuron*, 102(5), 1037-1052.e7. <https://doi.org/10.1016/j.neuron.2019.03.037>
- Hasegawa, E., Miyasaka, A., Sakurai, K., Cherasse, Y., Li, Y., & Sakurai, T. (2022). Rapid eye movement sleep is initiated by basolateral amygdala dopamine signaling in mice. *Science*, 375(6584), 994–1000. <https://doi.org/10.1126/science.abl6618>
- Herman, J. P., & Cullinan, W. E. (1997). Neurocircuitry of stress: Central control of the hypothalamo–pituitary–adrenocortical axis. *Trends in Neurosciences*, 20(2), 78–84. [https://doi.org/10.1016/S0166-2236\(96\)10069-2](https://doi.org/10.1016/S0166-2236(96)10069-2)
- Herman, J. P., Figueiredo, H., Mueller, N. K., Ulrich-Lai, Y., Ostrander, M. M., Choi, D. C., & Cullinan, W. E. (2003). Central mechanisms of stress integration: Hierarchical circuitry controlling hypothalamo–pituitary–adrenocortical responsiveness. *Frontiers in Neuroendocrinology*, 24(3), 151–180. <https://doi.org/10.1016/j.yfrne.2003.07.001>
- Herman, J. P., McKlveen, J. M., Ghosal, S., Kopp, B., Wulsin, A., Makinson, R., Scheimann, J., & Myers, B. (2016). Regulation of the Hypothalamic-Pituitary-Adrenocortical Stress Response. *Comprehensive Physiology*, 6(2), 603–621. <https://doi.org/10.1002/cphy.c150015>
- Herman, J. P., Nawreen, N., Smail, M. A., & Cotella, E. M. (2020). Brain mechanisms of HPA axis regulation: Neurocircuitry and feedback in context Richard Kvetnansky lecture. *Stress (Amsterdam, Netherlands)*, 23(6), 617–632. <https://doi.org/10.1080/10253890.2020.1859475>
- Herman, J. P., Ostrander, M. M., Mueller, N. K., & Figueiredo, H. (2005). Limbic system mechanisms of stress regulation: Hypothalamo-pituitary-adrenocortical axis. *Progress in Neuro-Psychopharmacology and Biological Psychiatry*, 29(8), 1201–1213. <https://doi.org/10.1016/j.pnpbp.2005.08.006>
- Herry, C., Ciocchi, S., Senn, V., Demmou, L., Müller, C., & Lüthi, A. (2008). Switching on and off fear by distinct neuronal circuits. *Nature*, 454(7204), 600–606. <https://doi.org/10.1038/nature07166>
- Hill, M. N., McLaughlin, R. J., Bingham, B., Shrestha, L., Lee, T. T. Y., Gray, J. M., Hillard, C. J., Gorzalka, B. B., & Viau, V. (2010). Endogenous cannabinoid signaling is essential for stress adaptation. *Proceedings of the National Academy of Sciences of the United States of America*, 107(20), 9406–9411. <https://doi.org/10.1073/pnas.0914661107>
- Hill, M. N., McLaughlin, R. J., Morrish, A. C., Viau, V., Floresco, S. B., Hillard, C. J., & Gorzalka, B. B. (2009). Suppression of Amygdalar Endocannabinoid Signaling by Stress Contributes to Activation of the Hypothalamic–Pituitary–Adrenal Axis. *Neuropsychopharmacology*, 34(13), 2733–2745. <https://doi.org/10.1038/npp.2009.114>

- Hill, M. N., Patel, S., Campolongo, P., Tasker, J. G., Wotjak, C. T., & Bains, J. S. (2010). Functional Interactions between Stress and the Endocannabinoid System: From Synaptic Signaling to Behavioral Output. *The Journal of Neuroscience*, 30(45), 14980–14986. <https://doi.org/10.1523/JNEUROSCI.4283-10.2010>
- Hintiryan, H., Bowman, I., Johnson, D. L., Korobkova, L., Zhu, M., Khanjani, N., Gou, L., Gao, L., Yamashita, S., Bienkowski, M. S., Garcia, L., Foster, N. N., Benavidez, N. L., Song, M. Y., Lo, D., Cotter, K. R., Becerra, M., Aquino, S., Cao, C., ... Dong, H.-W. (2021). Connectivity characterization of the mouse basolateral amygdalar complex. *Nature Communications*, 12(1), 2859. <https://doi.org/10.1038/s41467-021-22915-5>
- Hoover, W. B., & Vertes, R. P. (2007). Anatomical analysis of afferent projections to the medial prefrontal cortex in the rat. *Brain Structure and Function*, 212(2), 149–179. <https://doi.org/10.1007/s00429-007-0150-4>
- Horvitz, J. C. (2000). Mesolimbocortical and nigrostriatal dopamine responses to salient non-reward events. *Neuroscience*, 96(4), 651–656. [https://doi.org/10.1016/S0306-4522\(00\)00019-1](https://doi.org/10.1016/S0306-4522(00)00019-1)
- Hsueh, B., Chen, R., Jo, Y., Tang, D., Raffiee, M., Kim, Y. S., Inoue, M., Randles, S., Ramakrishnan, C., Patel, S., Kim, D. K., Liu, T. X., Kim, S. H., Tan, L., Mortazavi, L., Cordero, A., Shi, J., Zhao, M., Ho, T. T., ... Deisseroth, K. (2023). Cardiogenic control of affective behavioural state. *Nature*. <https://doi.org/10.1038/s41586-023-05748-8>
- Huang, L., Chen, Y., Jin, S., Lin, L., Duan, S., Si, K., Gong, W., & Julius Zhu, J. (2021). Organizational principles of amygdalar input-output neuronal circuits. *Molecular Psychiatry*, 26(12), 7118–7129. <https://doi.org/10.1038/s41380-021-01262-3>
- Huang, T.-N., Hsu, T.-T., Lin, M.-H., Chuang, H.-C., Hu, H.-T., Sun, C.-P., Tao, M.-H., Lin, J. Y., & Hsueh, Y.-P. (2019). Interhemispheric Connectivity Potentiates the Basolateral Amygdalae and Regulates Social Interaction and Memory. *Cell Reports*, 29(1), 34-48.e4. <https://doi.org/10.1016/j.celrep.2019.08.082>
- Hubbard, D. T., Nakashima, B. R., Lee, I., & Takahashi, L. K. (2007). Activation of basolateral amygdala corticotropin-releasing factor 1 receptors modulates the consolidation of contextual fear. *Neuroscience*, 150(4), 818–828. <https://doi.org/10.1016/j.neuroscience.2007.10.001>
- Huckleberry, K. A., Calitri, R., Li, A. J., Mejdell, M., Singh, A., Bhutani, V., Laine, M. A., Nastase, A. S., Morena, M., Hill, M. N., & Shansky, R. M. (2023). *CB1R blockade unmasks TRPV1-mediated contextual fear generalization in female, but not male rats* [Preprint]. *Neuroscience*. <https://doi.org/10.1101/2023.04.12.536625>
- Huff, M. L., Emmons, E. B., Narayanan, N. S., & LaLumiere, R. T. (2016). Basolateral amygdala projections to ventral hippocampus modulate the consolidation of footshock, but not contextual, learning in rats. *Learning & Memory*, 23(2), 51–60. <https://doi.org/10.1101/lm.039909.115>

- Hughes, P., Lawlor, P., & Dragunow, M. (1992). Basal expression of Fos, Fos-related, Jun, and Krox 24 proteins in rat hippocampus. *Molecular Brain Research*, 13(4), 355–357.
[https://doi.org/10.1016/0169-328X\(92\)90219-2](https://doi.org/10.1016/0169-328X(92)90219-2)
- Ikegame, S., Yoshimoto, M., & Miki, K. (2022). Simultaneous measurement of central amygdala neuronal activity and sympathetic nerve activity during daily activities in rats. *Experimental Physiology*, 107(9), 1071–1080. <https://doi.org/10.1113/EP090538>
- Ipser, J. C., Singh, L., & Stein, D. J. (2013). Meta-analysis of functional brain imaging in specific phobia: Imaging meta-analysis of specific phobia. *Psychiatry and Clinical Neurosciences*, 67(5), 311–322.
<https://doi.org/10.1111/pcn.12055>
- Iwata, J., Ledoux, J. E., & Reis, D. J. (1986). Destruction of intrinsic neurons in the lateral hypothalamus disrupts the classical conditioning of autonomic but not behavioral emotional responses in the rat. *Brain Research*, 368(1), 161–166. [https://doi.org/10.1016/0006-8993\(86\)91055-3](https://doi.org/10.1016/0006-8993(86)91055-3)
- Jacobson, L., & Sapolsky, R. (1991). The Role of the Hippocampus in Feedback Regulation of the Hypothalamic-Pituitary-Adrenocortical Axis*. *Endocrine Reviews*, 12(2), 118–134.
<https://doi.org/10.1210/edrv-12-2-118>
- Jacques, A., Chaaya, N., Hettiarachchi, C., Carmody, M.-L., Beecher, K., Belmer, A., Chehrehasa, F., Bartlett, S., Battle, A. R., & Johnson, L. R. (2019). Microtopography of fear memory consolidation and extinction retrieval within prefrontal cortex and amygdala. *Psychopharmacology*, 236(1), 383–397. <https://doi.org/10.1007/s00213-018-5068-4>
- Janak, P. H., & Tye, K. M. (2015). From circuits to behaviour in the amygdala. *Nature*, 517(7534), 284–292. <https://doi.org/10.1038/nature14188>
- Jasnow, A. M., Ehrlich, D. E., Choi, D. C., Dabrowska, J., Bowers, M. E., McCullough, K. M., Rainnie, D. G., & Ressler, K. J. (2013). Thy1-expressing neurons in the basolateral amygdala may mediate fear inhibition. *The Journal of Neuroscience: The Official Journal of the Society for Neuroscience*, 33(25), 10396–10404. <https://doi.org/10.1523/JNEUROSCI.5539-12.2013>
- Jensen, J., McIntosh, A. R., Crawley, A. P., Mikulis, D. J., Remington, G., & Kapur, S. (2003). Direct Activation of the Ventral Striatum in Anticipation of Aversive Stimuli. *Neuron*, 40(6), 1251–1257.
[https://doi.org/10.1016/S0896-6273\(03\)00724-4](https://doi.org/10.1016/S0896-6273(03)00724-4)
- Jensen, M., Ratner, C., Rudenko, O., Christiansen, S. H., Skov, L. J., Hundahl, C., Woldbye, D. P. D., & Holst, B. (2016). Anxiolytic-Like Effects of Increased Ghrelin Receptor Signaling in the Amygdala. *International Journal of Neuropsychopharmacology*, 19(5), pyv123.
<https://doi.org/10.1093/ijnp/pyv123>
- Jimenez, J. C., Su, K., Goldberg, A. R., Luna, V. M., Biane, J. S., Ordek, G., Zhou, P., Ong, S. K., Wright, M. A., Zweifel, L., Paninski, L., Hen, R., & Kheirbek, M. A. (2018). Anxiety Cells in a Hippocampal-Hypothalamic Circuit. *Neuron*, 97(3), 670-683.e6.
<https://doi.org/10.1016/j.neuron.2018.01.016>

- Jimenez, S. A., & Maren, S. (2009). Nuclear disconnection within the amygdala reveals a direct pathway to fear. *Learning & Memory*, 16(12), 766–768. <https://doi.org/10.1101/lm.1607109>
- Jin, J., & Maren, S. (2015). Fear renewal preferentially activates ventral hippocampal neurons projecting to both amygdala and prefrontal cortex in rats. *Scientific Reports*, 5(1), 8388. <https://doi.org/10.1038/srep08388>
- Jochman, K. A., Newman, S. M., Kalin, N. H., & Bakshi, V. P. (2005). Corticotropin-releasing factor-1 receptors in the basolateral amygdala mediate stress-induced anorexia. *Behavioral Neuroscience*, 119(6), 1448–1458. <https://doi.org/10.1037/0735-7044.119.6.1448>
- Johnson, A. W., Gallagher, M., & Holland, P. C. (2009). The Basolateral Amygdala Is Critical to the Expression of Pavlovian and Instrumental Outcome-Specific Reinforcer Devaluation Effects. *The Journal of Neuroscience*, 29(3), 696–704. <https://doi.org/10.1523/JNEUROSCI.3758-08.2009>
- Johnson, S. B., Emmons, E. B., Lingg, R. T., Anderson, R. M., Romig-Martin, S. A., LaLumiere, R. T., Narayanan, N. S., Viau, V., & Radley, J. J. (2019). Prefrontal–Bed Nucleus Circuit Modulation of a Passive Coping Response Set. *The Journal of Neuroscience*, 39(8), 1405–1419. <https://doi.org/10.1523/JNEUROSCI.1421-18.2018>
- Ju, A., Fernandez-Arroyo, B., Wu, Y., Jacky, D., & Beyeler, A. (2020). Expression of serotonin 1A and 2A receptors in molecular- and projection-defined neurons of the mouse insular cortex. *Molecular Brain*, 13(1), 99. <https://doi.org/10.1186/s13041-020-00605-5>
- Kant, G. J., Mougey, E. H., Pennington, L. L., & Meyerhoff, J. L. (1983). Graded footshock stress elevates pituitary cyclic AMP and plasma beta-endorphin, beta-LPH corticosterone and prolactin. *Life Sciences*, 33(26), 2657–2663. [https://doi.org/10.1016/0024-3205\(83\)90350-8](https://doi.org/10.1016/0024-3205(83)90350-8)
- Katona, I., Rancz, E. A., Acsady, L., Ledent, C., Mackie, K., Hajos, N., & Freund, T. F. (2001). Distribution of CB1 cannabinoid receptors in the amygdala and their role in the control of GABAergic transmission. *The Journal of Neuroscience: The Official Journal of the Society for Neuroscience*, 21(23), 9506–9518.
- Kayyal, H., Yiannakas, A., Kolatt Chandran, S., Khamaisy, M., Sharma, V., & Rosenblum, K. (2019). Activity of Insula to Basolateral Amygdala Projecting Neurons is Necessary and Sufficient for Taste Valence Representation. *The Journal of Neuroscience*, 39(47), 9369–9382. <https://doi.org/10.1523/JNEUROSCI.0752-19.2019>
- Kim, J., Pignatelli, M., Xu, S., Itohara, S., & Tonegawa, S. (2016). Antagonistic negative and positive neurons of the basolateral amygdala. *Nature Neuroscience*, 19(12), 1636–1646. <https://doi.org/10.1038/nn.4414>
- Kim, S.-Y., Adhikari, A., Lee, S. Y., Marshel, J. H., Kim, C. K., Mallory, C. S., Lo, M., Pak, S., Mattis, J., Lim, B. K., Malenka, R. C., Warden, M. R., Neve, R., Tye, K. M., & Deisseroth, K. (2013). Diverging neural pathways assemble a behavioural state from separable features in anxiety. *Nature*, 496(7444), 219–223. <https://doi.org/10.1038/nature12018>

- Kjelstrup, K. G., Tuvnes, F. A., Steffenach, H.-A., Murison, R., Moser, E. I., & Moser, M.-B. (2002). Reduced fear expression after lesions of the ventral hippocampus. *Proceedings of the National Academy of Sciences of the United States of America*, 99(16), 10825–10830. <https://doi.org/10.1073/pnas.152112399>
- Klavir, O., Prigge, M., Sarel, A., Paz, R., & Yizhar, O. (2017). Manipulating fear associations via optogenetic modulation of amygdala inputs to prefrontal cortex. *Nature Neuroscience*, 20(6), 836–844. <https://doi.org/10.1038/nn.4523>
- Knight, P., Chellian, R., Wilson, R., Behnood-Rod, A., Panunzio, S., & Bruijnzeel, A. W. (2021). Sex differences in the elevated plus-maze test and large open field test in adult Wistar rats. *Pharmacology Biochemistry and Behavior*, 204, 173168. <https://doi.org/10.1016/j.pbb.2021.173168>
- Kovács, K. J. (2008). Measurement of Immediate-Early Gene Activation- *c-fos* and Beyond. *Journal of Neuroendocrinology*, 20(6), 665–672. <https://doi.org/10.1111/j.1365-2826.2008.01734.x>
- Kovács, L. Á., Schiessl, J. A., Nafz, A. E., Csernus, V., & Gaszner, B. (2018). Both Basal and Acute Restraint Stress-Induced c-Fos Expression Is Influenced by Age in the Extended Amygdala and Brainstem Stress Centers in Male Rats. *Frontiers in Aging Neuroscience*, 10, 248. <https://doi.org/10.3389/fnagi.2018.00248>
- Krabbe, S., Gründemann, J., & Lüthi, A. (2018). Amygdala Inhibitory Circuits Regulate Associative Fear Conditioning. *Biological Psychiatry*, 83(10), 800–809. <https://doi.org/10.1016/j.biopsych.2017.10.006>
- Krettek, J. E., & Price, J. L. (1977). Projections from the amygdaloid complex to the cerebral cortex and thalamus in the rat and cat. *The Journal of Comparative Neurology*, 172(4), 687–722. <https://doi.org/10.1002/cne.901720408>
- Krettek, J. E., & Price, J. L. (1978). A description of the amygdaloid complex in the rat and cat with observations on intra-amygdaloid axonal connections. *The Journal of Comparative Neurology*, 178(2), 255–279. <https://doi.org/10.1002/cne.901780205>
- Kyriazi, P., Headley, D. B., & Paré, D. (2020). Different Multidimensional Representations across the Amygdalo-Prefrontal Network during an Approach-Avoidance Task. *Neuron*, 107(4), 717-730.e5. <https://doi.org/10.1016/j.neuron.2020.05.039>
- Lai, B.-Q., Qiu, X.-C., Zhang, K., Zhang, R.-Y., Jin, H., Li, G., Shen, H.-Y., Wu, J.-L., Ling, E.-A., & Zeng, Y.-S. (2015). Cholera Toxin B Subunit Shows Transneuronal Tracing after Injection in an Injured Sciatic Nerve. *PloS One*, 10(12), e0144030. <https://doi.org/10.1371/journal.pone.0144030>
- LaLumiere, R. T., Buen, T.-V., & McGaugh, J. L. (2003). Post-Training Intra-Basolateral Amygdala Infusions of Norepinephrine Enhance Consolidation of Memory for Contextual Fear Conditioning. *The Journal of Neuroscience*, 23(17), 6754–6758. <https://doi.org/10.1523/JNEUROSCI.23-17-06754.2003>

- Lang, P. J., Davis, M., & Ohman, A. (2000). Fear and anxiety: Animal models and human cognitive psychophysiology. *Journal of Affective Disorders*, 61(3), 137–159. [https://doi.org/10.1016/s0165-0327\(00\)00343-8](https://doi.org/10.1016/s0165-0327(00)00343-8)
- Lazarini-Lopes, W., Da Silva-Júnior, R. M. P., Servilha-Menezes, G., Do Val-da Silva, R. A., & Garcia-Cairasco, N. (2020). Cannabinoid Receptor Type 1 (CB1R) Expression in Limbic Brain Structures After Acute and Chronic Seizures in a Genetic Model of Epilepsy. *Frontiers in Behavioral Neuroscience*, 14, 602258. <https://doi.org/10.3389/fnbeh.2020.602258>
- Leake, J., Zinn, R., Corbit, L. H., Fanselow, M. S., & Vissel, B. (2021). Engram Size Varies with Learning and Reflects Memory Content and Precision. *The Journal of Neuroscience: The Official Journal of the Society for Neuroscience*, 41(18), 4120–4130. <https://doi.org/10.1523/JNEUROSCI.2786-20.2021>
- Lebow, M. A., & Chen, A. (2016). Overshadowed by the amygdala: The bed nucleus of the stria terminalis emerges as key to psychiatric disorders. *Molecular Psychiatry*, 21(4), 450–463. <https://doi.org/10.1038/mp.2016.1>
- LeDoux, J. (2007). The amygdala. *Current Biology*, 17(20), R868–R874. <https://doi.org/10.1016/j.cub.2007.08.005>
- LeDoux, J., Cicchetti, P., Xagoraris, A., & Romanski, L. (1990). The lateral amygdaloid nucleus: Sensory interface of the amygdala in fear conditioning. *The Journal of Neuroscience*, 10(4), 1062–1069. <https://doi.org/10.1523/JNEUROSCI.10-04-01062.1990>
- Lee, Y., Fitz, S., Johnson, P. L., & Shekhar, A. (2008). Repeated stimulation of CRF receptors in the BNST of rats selectively induces social but not panic-like anxiety. *Neuropsychopharmacology: Official Publication of the American College of Neuropsychopharmacology*, 33(11), 2586–2594. <https://doi.org/10.1038/sj.npp.1301674>
- LeWinter, M. M., Crawford, M. H., Karliner, J. S., & O'Rourke, R. A. (1975). Effects of oral propranolol in normal subjects. *Clinical Pharmacology & Therapeutics*, 17(6), 709–712. <https://doi.org/10.1002/cpt1975176709>
- Li, H., Namburi, P., Olson, J. M., Borio, M., Lemieux, M. E., Beyeler, A., Calhoon, G. G., Hitora-Imamura, N., Coley, A. A., Libster, A., Bal, A., Jin, X., Wang, H., Jia, C., Choudhury, S. R., Shi, X., Felix-Ortiz, A. C., de la Fuente, V., Barth, V. P., ... Tye, K. M. (2022). Neurotensin orchestrates valence assignment in the amygdala. *Nature*, 608(7923), 586–592. <https://doi.org/10.1038/s41586-022-04964-y>
- Liang, K. C., & Lee, E. M. Y. (1988). Intra-amygdala injections of corticotropin releasing factor facilitate inhibitory avoidance learning and reduce exploratory behavior in rats. *Psychopharmacology*, 96(2). <https://doi.org/10.1007/BF00177566>
- Lichtenberg, N. T., Sepe-Forrest, L., Pennington, Z. T., Lamparelli, A. C., Greenfield, V. Y., & Wassum, K. M. (2021). The Medial Orbitofrontal Cortex–Basolateral Amygdala Circuit Regulates the Influence

- of Reward Cues on Adaptive Behavior and Choice. *The Journal of Neuroscience*, 41(34), 7267–7277. <https://doi.org/10.1523/JNEUROSCI.0901-21.2021>
- Lingg, R. T., Johnson, S. B., Emmons, E. B., Anderson, R. M., Romig-Martin, S. A., Narayanan, N. S., McGaugh, J. L., LaLumiere, R. T., & Radley, J. J. (2020). Bed nuclei of the stria terminalis modulate memory consolidation via glucocorticoid-dependent and -independent circuits. *Proceedings of the National Academy of Sciences*, 117(14), 8104–8114. <https://doi.org/10.1073/pnas.1915501117>
- Little, J. P., & Carter, A. G. (2013). Synaptic Mechanisms Underlying Strong Reciprocal Connectivity between the Medial Prefrontal Cortex and Basolateral Amygdala. *The Journal of Neuroscience*, 33(39), 15333–15342. <https://doi.org/10.1523/JNEUROSCI.2385-13.2013>
- Lowery-Gionta, E. G., Crowley, N. A., Bukalo, O., Silverstein, S., Holmes, A., & Kash, T. L. (2018). Chronic stress dysregulates amygdalar output to the prefrontal cortex. *Neuropharmacology*, 139, 68–75. <https://doi.org/10.1016/j.neuropharm.2018.06.032>
- Luckman, S., Dyball, R., & Leng, G. (1994). Induction of c-fos expression in hypothalamic magnocellular neurons requires synaptic activation and not simply increased spike activity. *The Journal of Neuroscience*, 14(8), 4825–4830. <https://doi.org/10.1523/JNEUROSCI.14-08-04825.1994>
- Lungwitz, E. A., Molosh, A., Johnson, P. L., Harvey, B. P., Dirks, R. C., Dietrich, A., Minick, P., Shekhar, A., & Truitt, W. A. (2012). Orexin-A induces anxiety-like behavior through interactions with glutamatergic receptors in the bed nucleus of the stria terminalis of rats. *Physiology & Behavior*, 107(5), 726–732. <https://doi.org/10.1016/j.physbeh.2012.05.019>
- Machida, M., Sweeten, B. L. W., Adkins, A. M., Wellman, L. L., & Sanford, L. D. (2021). Basolateral Amygdala Regulates EEG Theta-activity During Rapid Eye Movement Sleep. *Neuroscience*, 468, 176–185. <https://doi.org/10.1016/j.neuroscience.2021.06.018>
- Maeng, L. Y., Waddell, J., & Shors, T. J. (2010). The Prefrontal Cortex Communicates with the Amygdala to Impair Learning after Acute Stress in Females but Not in Males. *The Journal of Neuroscience*, 30(48), 16188–16196. <https://doi.org/10.1523/JNEUROSCI.2265-10.2010>
- Manoocheri, K., & Carter, A. G. (2022). Rostral and caudal basolateral amygdala engage distinct circuits in the prelimbic and infralimbic prefrontal cortex. *ELife*, 11, e82688. <https://doi.org/10.7554/eLife.82688>
- Marcus, D. J., Bedse, G., Gaulden, A. D., Ryan, J. D., Kondev, V., Winters, N. D., Rosas-Vidal, L. E., Altemus, M., Mackie, K., Lee, F. S., Delpire, E., & Patel, S. (2020). Endocannabinoid Signaling Collapse Mediates Stress-Induced Amygdalo-Cortical Strengthening. *Neuron*, 105(6), 1062–1076.e6. <https://doi.org/10.1016/j.neuron.2019.12.024>
- Maren, S., & Quirk, G. J. (2004). Neuronal signalling of fear memory. *Nature Reviews Neuroscience*, 5(11), 844–852. <https://doi.org/10.1038/nrn1535>

- Martianova, E., Aronson, S., & Proulx, C. D. (2019). Multi-Fiber Photometry to Record Neural Activity in Freely-Moving Animals. *Journal of Visualized Experiments*, 152, 60278. <https://doi.org/10.3791/60278>
- Masaki, T., & Nakajima, S. (2005). Further evidence for conditioned taste aversion induced by forced swimming. *Physiology & Behavior*, 84(1), 9–15. <https://doi.org/10.1016/j.physbeh.2004.09.022>
- Masneuf, S., Lowery-Gionta, E., Colacicco, G., Pleil, K. E., Li, C., Crowley, N., Flynn, S., Holmes, A., & Kash, T. (2014). Glutamatergic mechanisms associated with stress-induced amygdala excitability and anxiety-related behavior. *Neuropharmacology*, 85, 190–197. <https://doi.org/10.1016/j.neuropharm.2014.04.015>
- Matheson, G. K., Branch, B. J., & Taylor, A. N. (1971). Effects of amygdaloid stimulation on pituitary-adrenal activity in conscious cats. *Brain Research*, 32(1), 151–167. [https://doi.org/10.1016/0006-8993\(71\)90160-0](https://doi.org/10.1016/0006-8993(71)90160-0)
- Mazzone, C. M., Pati, D., Michaelides, M., DiBerto, J., Fox, J. H., Tipton, G., Anderson, C., Duffy, K., McKlveen, J. M., Hardaway, J. A., Magness, S. T., Falls, W. A., Hammack, S. E., McElligott, Z. A., Hurd, Y. L., & Kash, T. L. (2018). Acute engagement of Gq-mediated signaling in the bed nucleus of the stria terminalis induces anxiety-like behavior. *Molecular Psychiatry*, 23(1), 143–153. <https://doi.org/10.1038/mp.2016.218>
- McCall, J. G., Siuda, E. R., Bhatti, D. L., Lawson, L. A., McElligott, Z. A., Stuber, G. D., & Bruchas, M. R. (2017). Locus coeruleus to basolateral amygdala noradrenergic projections promote anxiety-like behavior. *ELife*, 6, e18247. <https://doi.org/10.7554/eLife.18247>
- McCullough, K. M., Choi, D., Guo, J., Zimmerman, K., Walton, J., Rainnie, D. G., & Ressler, K. J. (2016). Molecular characterization of Thy1 expressing fear-inhibiting neurons within the basolateral amygdala. *Nature Communications*, 7, 13149. <https://doi.org/10.1038/ncomms13149>
- McCullough, K. M., Morrison, F. G., & Ressler, K. J. (2016). Bridging the Gap: Towards a cell-type specific understanding of neural circuits underlying fear behaviors. *Neurobiology of Learning and Memory*, 135, 27–39. <https://doi.org/10.1016/j.nlm.2016.07.025>
- McDonald, A. J. (1982). Neurons of the lateral and basolateral amygdaloid nuclei: A golgi study in the rat. *The Journal of Comparative Neurology*, 212(3), 293–312. <https://doi.org/10.1002/cne.902120307>
- McDonald, A. J. (1984). Neuronal organization of the lateral and basolateral amygdaloid nuclei in the rat. *The Journal of Comparative Neurology*, 222(4), 589–606. <https://doi.org/10.1002/cne.902220410>
- McDonald, A. J. (1991). Topographical organization of amygdaloid projections to the caudatoputamen, nucleus accumbens, and related striatal-like areas of the rat brain. *Neuroscience*, 44(1), 15–33. [https://doi.org/10.1016/0306-4522\(91\)90248-M](https://doi.org/10.1016/0306-4522(91)90248-M)
- McDonald, A. J. (1998). Cortical pathways to the mammalian amygdala. *Progress in Neurobiology*, 55(3), 257–332. [https://doi.org/10.1016/S0301-0082\(98\)00003-3](https://doi.org/10.1016/S0301-0082(98)00003-3)

- McDonald, A. J. (2020). Functional neuroanatomy of the basolateral amygdala: Neurons, neurotransmitters, and circuits. In *Handbook of Behavioral Neuroscience* (Vol. 26, pp. 1–38). Elsevier. <https://doi.org/10.1016/B978-0-12-815134-1.00001-5>
- McDonald, A. J., Beitz, A. J., Kuriyama, R., Sllitg, C., & Madl, J. E. (1989). Colocalization of glutamate and tubuline in putative excitatory neurons of the hippocampus and amygdala: An immunohistochemical study using monoclonal antibodies. *Neurosci.Lett.*, *30*(2), 405–421.
- McDonald, A. J., & Mascagni, F. (1997). Projections of the lateral entorhinal cortex to the amygdala: A Phaseolus vulgaris leucoagglutinin study in the rat. *Neuroscience*, *77*(2), 445–459. [https://doi.org/10.1016/S0306-4522\(96\)00478-2](https://doi.org/10.1016/S0306-4522(96)00478-2)
- McDonald, A. J., & Mascagni, F. (2007). Neuronal localization of 5-HT type 2A receptor immunoreactivity in the rat basolateral amygdala. *Neuroscience*, *146*(1), 306–320. <https://doi.org/10.1016/j.neuroscience.2007.01.047>
- McDonald, A. J., Mascagni, F., & Guo, L. (1996). Projections of the medial and lateral prefrontal cortices to the amygdala: A Phaseolus vulgaris leucoagglutinin study in the rat. *Neuroscience*, *71*(1), 55–75. [https://doi.org/10.1016/0306-4522\(95\)00417-3](https://doi.org/10.1016/0306-4522(95)00417-3)
- McDonald, A. J., & Mott, D. D. (2017). Functional neuroanatomy of amygdalohippocampal interconnections and their role in learning and memory: Amygdalohippocampal Interconnections. *Journal of Neuroscience Research*, *95*(3), 797–820. <https://doi.org/10.1002/jnr.23709>
- McDonald, A. J., Muller, J. F., & Mascagni, F. (2002). GABAergic innervation of alpha type II calcium/calmodulin-dependent protein kinase immunoreactive pyramidal neurons in the rat basolateral amygdala. *The Journal of Comparative Neurology*, *446*(3), 199–218. <https://doi.org/10.1002/cne.10204>
- McEwen, B. S. (1998). Stress, Adaptation, and Disease: Allostasis and Allostatic Load. *Annals of the New York Academy of Sciences*, *840*(1), 33–44. <https://doi.org/10.1111/j.1749-6632.1998.tb09546.x>
- McEwen, B. S. (2006). Protective and damaging effects of stress mediators: Central role of the brain. *Dialogues in Clinical Neuroscience*, *8*(4), 367–381. <https://doi.org/10.31887/DCNS.2006.8.4/bmcewen>
- McEwen, B. S. (2007). Physiology and Neurobiology of Stress and Adaptation: Central Role of the Brain. *Physiological Reviews*, *87*(3), 873–904. <https://doi.org/10.1152/physrev.00041.2006>
- McEwen, B. S., Nasca, C., & Gray, J. D. (2016). Stress Effects on Neuronal Structure: Hippocampus, Amygdala, and Prefrontal Cortex. *Neuropsychopharmacology*, *41*(1), 3–23. <https://doi.org/10.1038/npp.2015.171>
- McGarry, L. M., & Carter, A. G. (2017). Prefrontal Cortex Drives Distinct Projection Neurons in the Basolateral Amygdala. *Cell Reports*, *21*(6), 1426–1433. <https://doi.org/10.1016/j.celrep.2017.10.046>

- McGregor, A., & Herbert, J. (1992). Differential effects of excitotoxic basolateral and corticomedial lesions of the amygdala on the behavioural and endocrine responses to either sexual or aggression-promoting stimuli in the male rat. *Brain Research*, 574(1–2), 9–20. [https://doi.org/10.1016/0006-8993\(92\)90793-9](https://doi.org/10.1016/0006-8993(92)90793-9)
- McHugh, S. B., Deacon, R. M. J., Rawlins, J. N. P., & Bannerman, D. M. (2004). Amygdala and ventral hippocampus contribute differentially to mechanisms of fear and anxiety. *Behavioral Neuroscience*, 118(1), 63–78. <https://doi.org/10.1037/0735-7044.118.1.63>
- McReynolds, J. R., Christianson, J. P., Blacktop, J. M., & Mantsch, J. R. (2018). What does the Fos say? Using Fos-based approaches to understand the contribution of stress to substance use disorders. *Neurobiology of Stress*, 9, 271–285. <https://doi.org/10.1016/j.ynstr.2018.05.004>
- Melia, K. R., Ryabinin, A. E., Schroeder, R., Bloom, F. E., & Wilson, M. C. (1994). Induction and habituation of immediate early gene expression in rat brain by acute and repeated restraint stress. *The Journal of Neuroscience: The Official Journal of the Society for Neuroscience*, 14(10), 5929–5938. <https://doi.org/10.1523/JNEUROSCI.14-10-05929.1994>
- Merali, Z., McIntosh, J., Kent, P., Michaud, D., & Anisman, H. (1998). Aversive and appetitive events evoke the release of corticotropin-releasing hormone and bombesin-like peptides at the central nucleus of the amygdala. *The Journal of Neuroscience: The Official Journal of the Society for Neuroscience*, 18(12), 4758–4766. <https://doi.org/10.1523/JNEUROSCI.18-12-04758.1998>
- Merlo Pich, E., Lorang, M., Yeganeh, M., Rodriguez de Fonseca, F., Raber, J., Koob, G. F., & Weiss, F. (1995). Increase of extracellular corticotropin-releasing factor-like immunoreactivity levels in the amygdala of awake rats during restraint stress and ethanol withdrawal as measured by microdialysis. *The Journal of Neuroscience: The Official Journal of the Society for Neuroscience*, 15(8), 5439–5447. <https://doi.org/10.1523/JNEUROSCI.15-08-05439.1995>
- Millhouse, O. E., & DeOlmos, J. (1983). Neuronal configurations in lateral and basolateral amygdala. *Neuroscience*, 10(4), 1269–1300. [https://doi.org/10.1016/0306-4522\(83\)90112-4](https://doi.org/10.1016/0306-4522(83)90112-4)
- Mineur, Y. S., Mose, T. N., Maibom, K. L., Pittenger, S. T., Soares, A. R., Wu, H., Taylor, S. R., Huang, Y., & Picciotto, M. R. (2022). ACh signaling modulates activity of the GABAergic signaling network in the basolateral amygdala and behavior in stress-relevant paradigms. *Molecular Psychiatry*, 27(12), 4918–4927. <https://doi.org/10.1038/s41380-022-01749-7>
- Mirenowicz, J., & Schultz, W. (1996). Preferential activation of midbrain dopamine neurons by appetitive rather than aversive stimuli. *Nature*, 379(6564), 449–451. <https://doi.org/10.1038/379449a0>
- Mobbs, D., Headley, D. B., Ding, W., & Dayan, P. (2020). Space, Time, and Fear: Survival Computations along Defensive Circuits. *Trends in Cognitive Sciences*, 24(3), 228–241. <https://doi.org/10.1016/j.tics.2019.12.016>
- Modlinska, K., Stryjek, R., & Pisula, W. (2015). Food neophobia in wild and laboratory rats (multi-strain comparison). *Behavioural Processes*, 113, 41–50. <https://doi.org/10.1016/j.beproc.2014.12.005>

- Moghaddam, B. (1993). Stress Preferentially Increases Extraneuronal Levels of Excitatory Amino Acids in the Prefrontal Cortex: Comparison to Hippocampus and Basal Ganglia. *Journal of Neurochemistry*, 60(5), 1650–1657. <https://doi.org/10.1111/j.1471-4159.1993.tb13387.x>
- Morena, M., Aukema, R. J., Leidl, K. D., Rashid, A. J., Vecchiarelli, H. A., Josselyn, S. A., & Hill, M. N. (2019). Upregulation of Anandamide Hydrolysis in the Basolateral Complex of Amygdala Reduces Fear Memory Expression and Indices of Stress and Anxiety. *The Journal of Neuroscience*, 39(7), 1275–1292. <https://doi.org/10.1523/JNEUROSCI.2251-18.2018>
- Morena, M., Nastase, A. S., Santori, A., Cravatt, B. F., Shansky, R. M., & Hill, M. N. (2021). Sex-dependent effects of endocannabinoid modulation of conditioned fear extinction in rats. *British Journal of Pharmacology*, 178(4), 983–996. <https://doi.org/10.1111/bph.15341>
- Morena, M., Patel, S., Bains, J. S., & Hill, M. N. (2016). Neurobiological Interactions Between Stress and the Endocannabinoid System. *Neuropsychopharmacology*, 41(1), 80–102. <https://doi.org/10.1038/npp.2015.166>
- Morimoto, M., Morita, N., Ozawa, H., Yokoyama, K., & Kawata, M. (1996). Distribution of glucocorticoid receptor immunoreactivity and mRNA in the rat brain: An immunohistochemical and in situ hybridization study. *Neuroscience Research*, 26(3), 235–269. [https://doi.org/10.1016/S0168-0102\(96\)01105-4](https://doi.org/10.1016/S0168-0102(96)01105-4)
- Morrison, S. E., & Salzman, C. D. (2010). Re-valuing the amygdala. *Current Opinion in Neurobiology*, 20(2), 221–230. <https://doi.org/10.1016/j.conb.2010.02.007>
- Morrow, B. A., Elsworth, J. D., & Roth, R. H. (2002). Fear-like biochemical and behavioral responses in rats to the predator odor, TMT, are dependent on the exposure environment. *Synapse*, 46(1), 11–18. <https://doi.org/10.1002/syn.10109>
- Muir, J., Tse, Y. C., Iyer, E. S., Biris, J., Cvetkovska, V., Lopez, J., & Bagot, R. C. (2020). Ventral Hippocampal Afferents to Nucleus Accumbens Encode Both Latent Vulnerability and Stress-Induced Susceptibility. *Biological Psychiatry*, 88(11), 843–854. <https://doi.org/10.1016/j.biopsych.2020.05.021>
- Muller, J. F., Mascagni, F., & McDonald, A. J. (2003). Synaptic connections of distinct interneuronal subpopulations in the rat basolateral amygdalar nucleus. *The Journal of Comparative Neurology*, 456(3), 217–236. <https://doi.org/10.1002/cne.10435>
- Muller, J. F., Mascagni, F., & McDonald, A. J. (2005). Coupled Networks of Parvalbumin-Immunoreactive Interneurons in the Rat Basolateral Amygdala. *The Journal of Neuroscience*, 25(32), 7366–7376. <https://doi.org/10.1523/JNEUROSCI.0899-05.2005>
- Muller, J. F., Mascagni, F., & McDonald, A. J. (2011). Cholinergic innervation of pyramidal cells and parvalbumin-immunoreactive interneurons in the rat basolateral amygdala. *The Journal of Comparative Neurology*, 519(4), 790–805. <https://doi.org/10.1002/cne.22550>

- Müller, M. B., Zimmermann, S., Sillaber, I., Hagemeyer, T. P., Deussing, J. M., Timpl, P., Kormann, M. S. D., Droste, S. K., Kühn, R., Reul, J. M. H. M., Holsboer, F., & Wurst, W. (2003). Limbic corticotropin-releasing hormone receptor 1 mediates anxiety-related behavior and hormonal adaptation to stress. *Nature Neuroscience*, 6(10), 1100–1107. <https://doi.org/10.1038/nn1123>
- Murphy, T. H., Worley, P. F., & Baraban, J. M. (1991). L-type voltage-sensitive calcium channels mediate synaptic activation of immediate early genes. *Neuron*, 7(4), 625–635. [https://doi.org/10.1016/0896-6273\(91\)90375-A](https://doi.org/10.1016/0896-6273(91)90375-A)
- Namburi, P., Beyeler, A., Yorozu, S., Calhoon, G. G., Halbert, S. A., Wichmann, R., Holden, S. S., Mertens, K. L., Anahtar, M., Felix-Ortiz, A. C., Wickersham, I. R., Gray, J. M., & Tye, K. M. (2015). A circuit mechanism for differentiating positive and negative associations. *Nature*, 520(7549), 675–678. <https://doi.org/10.1038/nature14366>
- Nikolenko, V. N., Oganessian, M. V., Rizaeva, N. A., Kudryashova, V. A., Nikitina, A. T., Pavliv, M. P., Shchedrina, M. A., Giller, D. B., Bulygin, K. V., & Sinelnikov, M. Y. (2020). Amygdala: Neuroanatomical and Morphophysiological Features in Terms of Neurological and Neurodegenerative Diseases. *Brain Sciences*, 10(8), 502. <https://doi.org/10.3390/brainsci10080502>
- Niu, M., Kasai, A., Tanuma, M., Seiriki, K., Igarashi, H., Kuwaki, T., Nagayasu, K., Miyaji, K., Ueno, H., Tanabe, W., Seo, K., Yokoyama, R., Ohkubo, J., Ago, Y., Hayashida, M., Inoue, K.-I., Takada, M., Yamaguchi, S., Nakazawa, T., ... Hashimoto, H. (2022). Claustrum mediates bidirectional and reversible control of stress-induced anxiety responses. *Science Advances*, 8(11), eabi6375. <https://doi.org/10.1126/sciadv.abi6375>
- O’Leary, T. P., Sullivan, K. E., Wang, L., Clements, J., Lemire, A. L., & Cembrowski, M. S. (2020). Extensive and spatially variable within-cell-type heterogeneity across the basolateral amygdala. *ELife*, 9, e59003. <https://doi.org/10.7554/eLife.59003>
- Ong, L. K., Guan, L., Damanhuri, H., Goodchild, A. K., Bobrovskaya, L., Dickson, P. W., & Dunkley, P. R. (2014). Neurobiological consequences of acute footshock stress: Effects on tyrosine hydroxylase phosphorylation and activation in the rat brain and adrenal medulla. *Journal of Neurochemistry*, 128(4), 547–560. <https://doi.org/10.1111/jnc.12482>
- Orozco-Cabal, L., Liu, J., Pollandt, S., Schmidt, K., Shinnick-Gallagher, P., & Gallagher, J. P. (2008). Dopamine and Corticotropin-Releasing Factor Synergistically Alter Basolateral Amygdala-to-Medial Prefrontal Cortex Synaptic Transmission: Functional Switch after Chronic Cocaine Administration. *The Journal of Neuroscience*, 28(2), 529–542. <https://doi.org/10.1523/JNEUROSCI.2666-07.2008>
- Orsini, C. A., Trotta, R. T., Bizon, J. L., & Setlow, B. (2015). Dissociable Roles for the Basolateral Amygdala and Orbitofrontal Cortex in Decision-Making under Risk of Punishment. *The Journal of Neuroscience*, 35(4), 1368–1379. <https://doi.org/10.1523/JNEUROSCI.3586-14.2015>

- Owen, S. F., Liu, M. H., & Kreitzer, A. C. (2019). Thermal constraints on in vivo optogenetic manipulations. *Nature Neuroscience*, 22(7), 1061–1065. <https://doi.org/10.1038/s41593-019-0422-3>
- Paré, D. (2003). Role of the basolateral amygdala in memory consolidation. *Progress in Neurobiology*, 70(5), 409–420. [https://doi.org/10.1016/S0301-0082\(03\)00104-7](https://doi.org/10.1016/S0301-0082(03)00104-7)
- Parfitt, G. M., Nguyen, R., Bang, J. Y., Aqrabawi, A. J., Tran, M. M., Seo, D. K., Richards, B. A., & Kim, J. C. (2017). Bidirectional Control of Anxiety-Related Behaviors in Mice: Role of Inputs Arising from the Ventral Hippocampus to the Lateral Septum and Medial Prefrontal Cortex. *Neuropsychopharmacology*, 42(8), 1715–1728. <https://doi.org/10.1038/npp.2017.56>
- Paxinos, G., & Watson, C. (2007). *The rat brain in stereotaxic coordinates* (6th ed). Elsevier.
- Pellow, S., Chopin, P., File, S. E., & Briley, M. (1985). Validation of open:closed arm entries in an elevated plus-maze as a measure of anxiety in the rat. *Journal of Neuroscience Methods*, 14(3), 149–167. [https://doi.org/10.1016/0165-0270\(85\)90031-7](https://doi.org/10.1016/0165-0270(85)90031-7)
- Perrotti, L. I., Hadeishi, Y., Ulery, P. G., Barrot, M., Monteggia, L., Duman, R. S., & Nestler, E. J. (2004). Induction of deltaFosB in reward-related brain structures after chronic stress. *The Journal of Neuroscience: The Official Journal of the Society for Neuroscience*, 24(47), 10594–10602. <https://doi.org/10.1523/JNEUROSCI.2542-04.2004>
- Petrie, G. N., Balsevich, G., Füzesi, T., Aukema, R. J., Driever, W. P. F., Van Der Stelt, M., Bainsand, J. S., & Hill, M. N. (2022). *Disruption of Tonic Endocannabinoid Signaling Triggers the Generation of a Stress Response* [Preprint]. Neuroscience. <https://doi.org/10.1101/2022.09.27.509585>
- Petrie, G. N., Nastase, A. S., Aukema, R. J., & Hill, M. N. (2021). Endocannabinoids, cannabinoids and the regulation of anxiety. *Neuropharmacology*, 195, 108626. <https://doi.org/10.1016/j.neuropharm.2021.108626>
- Petrovich, G. D., Canteras, N. S., & Swanson, L. W. (2001). Combinatorial amygdalar inputs to hippocampal domains and hypothalamic behavior systems. *Brain Research Reviews*, 38(1–2), 247–289. [https://doi.org/10.1016/S0165-0173\(01\)00080-7](https://doi.org/10.1016/S0165-0173(01)00080-7)
- Petrovich, G. D., Hobin, M. P., & Reppucci, C. J. (2012). Selective Fos induction in hypothalamic orexin/hypocretin, but not melanin-concentrating hormone neurons, by a learned food-cue that stimulates feeding in sated rats. *Neuroscience*, 224, 70–80. <https://doi.org/10.1016/j.neuroscience.2012.08.036>
- Petrovich, G. D., Risold, P. Y., & Swanson, L. W. (1996). Organization of projections from the basomedial nucleus of the amygdala: A PHAL study in the rat. *The Journal of Comparative Neurology*, 374(3), 387–420. [https://doi.org/10.1002/\(SICI\)1096-9861\(19961021\)374:3<387::AID-CNE6>3.0.CO;2-Y](https://doi.org/10.1002/(SICI)1096-9861(19961021)374:3<387::AID-CNE6>3.0.CO;2-Y)

- Petrovich, G. D., Ross, C. A., Mody, P., Holland, P. C., & Gallagher, M. (2009). Central, But Not Basolateral, Amygdala Is Critical for Control of Feeding by Aversive Learned Cues. *The Journal of Neuroscience*, 29(48), 15205–15212. <https://doi.org/10.1523/JNEUROSCI.3656-09.2009>
- Petrovich, G. D., Setlow, B., Holland, P. C., & Gallagher, M. (2002). Amygdalo-Hypothalamic Circuit Allows Learned Cues to Override Satiety and Promote Eating. *The Journal of Neuroscience*, 22(19), 8748–8753. <https://doi.org/10.1523/JNEUROSCI.22-19-08748.2002>
- Piazza, P. V., Cota, D., & Marsicano, G. (2017). The CB1 Receptor as the Cornerstone of Exostasis. *Neuron*, 93(6), 1252–1274. <https://doi.org/10.1016/j.neuron.2017.02.002>
- Pickel, V. M., Colago, E. E., Mania, I., Molosh, A. I., & Rainnie, D. G. (2006). Dopamine D1 receptors co-distribute with N-methyl-d-aspartic acid type-1 subunits and modulate synaptically-evoked N-methyl-d-aspartic acid currents in rat basolateral amygdala. *Neuroscience*, 142(3), 671–690. <https://doi.org/10.1016/j.neuroscience.2006.06.059>
- Pinard, C. R., Muller, J. F., Mascagni, F., & McDonald, A. J. (2008). Dopaminergic innervation of interneurons in the rat basolateral amygdala. *Neuroscience*, 157(4), 850–863. <https://doi.org/10.1016/j.neuroscience.2008.09.043>
- Pitkänen, A., Kelly, J. L., & Amaral, D. G. (2002). Projections from the lateral, basal, and accessory basal nuclei of the amygdala to the entorhinal cortex in the macaque monkey: Amygdalo-Entorhinal Connections. *Hippocampus*, 12(2), 186–205. <https://doi.org/10.1002/hipo.1099>
- Pitkänen, A., Savander, V., & LeDoux, J. E. (1997). Organization of intra-amygdaloid circuitries in the rat: An emerging framework for understanding functions of the amygdala. *Trends in Neurosciences*, 20(11), 517–523. [https://doi.org/10.1016/S0166-2236\(97\)01125-9](https://doi.org/10.1016/S0166-2236(97)01125-9)
- Prewitt, C. M. F., & Herman, J. P. (1998). Anatomical interactions between the central amygdaloid nucleus and the hypothalamic paraventricular nucleus of the rat: A dual tract-tracing analysis. *Journal of Chemical Neuroanatomy*, 15(3), 173–186. [https://doi.org/10.1016/S0891-0618\(98\)00045-3](https://doi.org/10.1016/S0891-0618(98)00045-3)
- Pruessner, J. C., Kirschbaum, C., Meinlschmid, G., & Hellhammer, D. H. (2003). Two formulas for computation of the area under the curve represent measures of total hormone concentration versus time-dependent change. *Psychoneuroendocrinology*, 28(7), 916–931. [https://doi.org/10.1016/S0306-4530\(02\)00108-7](https://doi.org/10.1016/S0306-4530(02)00108-7)
- Pugliesi, G. P., & De Aguiar Corrêa, F. M. (2004). Cardiovascular responses to the injection of l-glutamate in the lateral hypothalamus of unanesthetized or anesthetized rats. *Autonomic Neuroscience*, 116(1–2), 19–29. <https://doi.org/10.1016/j.autneu.2004.08.010>
- Qin, X., Pan, H.-Q., Huang, S.-H., Zou, J.-X., Zheng, Z.-H., Liu, X.-X., You, W.-J., Liu, Z.-P., Cao, J.-L., Zhang, W.-H., & Pan, B.-X. (2022). GABAA(δ) receptor hypofunction in the amygdala-hippocampal circuit underlies stress-induced anxiety. *Science Bulletin*, 67(1), 97–110. <https://doi.org/10.1016/j.scib.2021.09.007>

- Qu, L.-L., Guo, N.-N., & Li, B.-M. (2008). B1- and β 2-Adrenoceptors in basolateral nucleus of amygdala and their roles in consolidation of fear memory in rats. *Hippocampus*, 18(11), 1131–1139. <https://doi.org/10.1002/hipo.20478>
- Quirk, G. J., Repa, J. C., & LeDoux, J. E. (1995). Fear conditioning enhances short-latency auditory responses of lateral amygdala neurons: Parallel recordings in the freely behaving rat. *Neuron*, 15(5), 1029–1039. [https://doi.org/10.1016/0896-6273\(95\)90092-6](https://doi.org/10.1016/0896-6273(95)90092-6)
- Rabasa, C., & Dickson, S. L. (2016). Impact of stress on metabolism and energy balance. *Current Opinion in Behavioral Sciences*, 9, 71–77. <https://doi.org/10.1016/j.cobeha.2016.01.011>
- Radke, A. K. (2009). The role of the bed nucleus of the stria terminalis in learning to fear. *The Journal of Neuroscience: The Official Journal of the Society for Neuroscience*, 29(49), 15351–15352. <https://doi.org/10.1523/JNEUROSCI.5194-09.2009>
- Radley, J. J., Gosselink, K. L., & Sawchenko, P. E. (2009). A discrete GABAergic relay mediates medial prefrontal cortical inhibition of the neuroendocrine stress response. *The Journal of Neuroscience: The Official Journal of the Society for Neuroscience*, 29(22), 7330–7340. <https://doi.org/10.1523/JNEUROSCI.5924-08.2009>
- Radley, J. J., & Sawchenko, P. E. (2011). A common substrate for prefrontal and hippocampal inhibition of the neuroendocrine stress response. *The Journal of Neuroscience: The Official Journal of the Society for Neuroscience*, 31(26), 9683–9695. <https://doi.org/10.1523/JNEUROSCI.6040-10.2011>
- Rainnie, D. G., Fernhout, B. J., & Shinnick-Gallagher, P. (1992). Differential actions of corticotropin releasing factor on basolateral and central amygdaloid neurones, in vitro. *The Journal of Pharmacology and Experimental Therapeutics*, 263(2), 846–858.
- Rau, A. R., Chappell, A. M., Butler, T. R., Ariwodola, O. J., & Weiner, J. L. (2015). Increased Basolateral Amygdala Pyramidal Cell Excitability May Contribute to the Anxiogenic Phenotype Induced by Chronic Early-Life Stress. *Journal of Neuroscience*, 35(26), 9730–9740. <https://doi.org/10.1523/JNEUROSCI.0384-15.2015>
- Rauch, S. L., Whalen, P. J., Shin, L. M., McNerney, S. C., Macklin, M. L., Lasko, N. B., Orr, S. P., & Pitman, R. K. (2000). Exaggerated amygdala response to masked facial stimuli in posttraumatic stress disorder: A functional MRI study. *Biological Psychiatry*, 47(9), 769–776. [https://doi.org/10.1016/S0006-3223\(00\)00828-3](https://doi.org/10.1016/S0006-3223(00)00828-3)
- Ray, M. H., Russ, A. N., Walker, R. A., & McDannald, M. A. (2020). The Nucleus Accumbens Core is Necessary to Scale Fear to Degree of Threat. *The Journal of Neuroscience*, 40(24), 4750–4760. <https://doi.org/10.1523/JNEUROSCI.0299-20.2020>
- Reed, S. J., Lafferty, C. K., Mendoza, J. A., Yang, A. K., Davidson, T. J., Grosenick, L., Deisseroth, K., & Britt, J. P. (2018). Coordinated Reductions in Excitatory Input to the Nucleus Accumbens Underlie Food Consumption. *Neuron*, 99(6), 1260–1273.e4. <https://doi.org/10.1016/j.neuron.2018.07.051>

- Refojo, D., Schweizer, M., Kuehne, C., Ehrenberg, S., Thoeringer, C., Vogl, A. M., Dedic, N., Schumacher, M., Von Wolff, G., Avrabos, C., Touma, C., Engblom, D., Schütz, G., Nave, K.-A., Eder, M., Wotjak, C. T., Sillaber, I., Holsboer, F., Wurst, W., & Deussing, J. M. (2011). Glutamatergic and Dopaminergic Neurons Mediate Anxiogenic and Anxiolytic Effects of CRHR1. *Science*, 333(6051), 1903–1907. <https://doi.org/10.1126/science.1202107>
- Reppucci, C. J., & Petrovich, G. D. (2016). Organization of connections between the amygdala, medial prefrontal cortex, and lateral hypothalamus: A single and double retrograde tracing study in rats. *Brain Structure and Function*, 221(6), 2937–2962. <https://doi.org/10.1007/s00429-015-1081-0>
- Reznikov, L. R., Reagan, L. P., & Fadel, J. R. (2008). Activation of phenotypically distinct neuronal subpopulations in the anterior subdivision of the rat basolateral amygdala following acute and repeated stress. *The Journal of Comparative Neurology*, 508(3), 458–472. <https://doi.org/10.1002/cne.21687>
- Rincón-Cortés, M., Herman, J. P., Lupien, S., Maguire, J., & Shansky, R. M. (2019). Stress: Influence of sex, reproductive status and gender. *Neurobiology of Stress*, 10, 100155. <https://doi.org/10.1016/j.ynstr.2019.100155>
- Ritchie, J. L., Walters, J. L., Galliou, J. M. C., Christian, R. J., Qi, S., Savenkova, M. I., Ibarra, C. K., Grogan, S. R., & Fuchs, R. A. (2021). Basolateral amygdala corticotropin-releasing factor receptor type 1 regulates context-cocaine memory strength during reconsolidation in a sex-dependent manner. *Neuropharmacology*, 200, 108819. <https://doi.org/10.1016/j.neuropharm.2021.108819>
- Rodriguez-Romaguera, J., Sotres-Bayon, F., Mueller, D., & Quirk, G. J. (2009). Systemic propranolol acts centrally to reduce conditioned fear in rats without impairing extinction. *Biological Psychiatry*, 65(10), 887–892. <https://doi.org/10.1016/j.biopsych.2009.01.009>
- Roozendaal, B., Brunson, K. L., Holloway, B. L., McGaugh, J. L., & Baram, T. Z. (2002). Involvement of stress-released corticotropin-releasing hormone in the basolateral amygdala in regulating memory consolidation. *Proceedings of the National Academy of Sciences of the United States of America*, 99(21), 13908–13913. <https://doi.org/10.1073/pnas.212504599>
- Roozendaal, B., de Quervain, D. J.-F., Ferry, B., Setlow, B., & McGaugh, J. L. (2001). Basolateral Amygdala–Nucleus Accumbens Interactions in Mediating Glucocorticoid Enhancement of Memory Consolidation. *The Journal of Neuroscience*, 21(7), 2518–2525. <https://doi.org/10.1523/JNEUROSCI.21-07-02518.2001>
- Roozendaal, B., McEwen, B. S., & Chattarji, S. (2009). Stress, memory and the amygdala. *Nature Reviews Neuroscience*, 10(6), 423–433. <https://doi.org/10.1038/nrn2651>
- Roozendaal, B., & McGaugh, J. L. (2011). Memory modulation. *Behavioral Neuroscience*, 125(6), 797–824. <https://doi.org/10.1037/a0026187>

- Rooszendaal, B., Nguyen, B. T., Power, A. E., & McGaugh, J. L. (1999). Basolateral amygdala noradrenergic influence enables enhancement of memory consolidation induced by hippocampal glucocorticoid receptor activation. *Proceedings of the National Academy of Sciences*, 96(20), 11642–11647. <https://doi.org/10.1073/pnas.96.20.11642>
- Rooszendaal, B., Schelling, G., & McGaugh, J. L. (2008). Corticotropin-Releasing Factor in the Basolateral Amygdala Enhances Memory Consolidation via an Interaction with the -Adrenoceptor-cAMP Pathway: Dependence on Glucocorticoid Receptor Activation. *Journal of Neuroscience*, 28(26), 6642–6651. <https://doi.org/10.1523/JNEUROSCI.1336-08.2008>
- Rosenkranz, J. A., Venheim, E. R., & Padival, M. (2010). Chronic Stress Causes Amygdala Hyperexcitability in Rodents. *Biological Psychiatry*, 67(12), 1128–1136. <https://doi.org/10.1016/j.biopsych.2010.02.008>
- Ross, S. E., Lehmann Levin, E., Itoga, C. A., Schoen, C. B., Selmane, R., & Aldridge, J. W. (2016). Deep brain stimulation in the central nucleus of the amygdala decreases ‘wanting’ and ‘liking’ of food rewards. *European Journal of Neuroscience*, 44(7), 2431–2445. <https://doi.org/10.1111/ejn.13342>
- Rostkowski, A. B., Leitermann, R. J., & Urban, J. H. (2013). Differential activation of neuronal cell types in the basolateral amygdala by corticotropin releasing factor. *Neuropeptides*, 47(4), 273–280. <https://doi.org/10.1016/j.npep.2012.12.004>
- Rubin, R. T., Mandell, A. J., & Crandall, P. H. (1966). Corticosteroid Responses to Limbic Stimulation in Man: Localization of Stimulus Sites. *Science*, 153(3737), 767–768. <https://doi.org/10.1126/science.153.3737.767>
- Rubinow, M. J., Drogos, L. L., & Juraska, J. M. (2009). Age-related dendritic hypertrophy and sexual dimorphism in rat basolateral amygdala. *Neurobiology of Aging*, 30(1), 137–146. <https://doi.org/10.1016/j.neurobiolaging.2007.05.006>
- Rubinow, M. J., & Juraska, J. M. (2009). Neuron and glia numbers in the basolateral nucleus of the amygdala from preweaning through old age in male and female rats: A stereological study. *The Journal of Comparative Neurology*, 512(6), 717–725. <https://doi.org/10.1002/cne.21924>
- Russchen, F. T., Amaral, D. G., & Price, J. L. (1985). The afferent connections of the substantia innominata in the monkey, *Macaca fascicularis*. *The Journal of Comparative Neurology*, 242(1), 1–27. <https://doi.org/10.1002/cne.902420102>
- Sah, P., Faber, E. S. L., Armentia, M. L. D. E., & Power, J. (2003). The Amygdaloid Complex: Anatomy and Physiology. *Physiol Rev*, 83, 803–834.
- Sah, P., Faber, E. S. L., Lopez De Armentia, M., & Power, J. (2003). The amygdaloid complex: Anatomy and physiology. *Physiological Reviews*, 83(3), 803–834. <https://doi.org/10.1152/physrev.00002.2003>
- Saha, S., Batten, T. F. C., & Henderson, Z. (2000). A GABAergic projection from the central nucleus of the amygdala to the nucleus of the solitary tract: A combined anterograde tracing and electron

- microscopic immunohistochemical study. *Neuroscience*, 99(4), 613–626.
[https://doi.org/10.1016/S0306-4522\(00\)00240-2](https://doi.org/10.1016/S0306-4522(00)00240-2)
- Saitoh, A., Ohashi, M., Suzuki, S., Tsukagoshi, M., Sugiyama, A., Yamada, M., Oka, J.-I., Inagaki, M., & Yamada, M. (2014). Activation of the prelimbic medial prefrontal cortex induces anxiety-like behaviors via N-Methyl-D-aspartate receptor-mediated glutamatergic neurotransmission in mice: Prelimbic-mPFC and Anxiety-Like Behavior. *Journal of Neuroscience Research*, 92(8), 1044–1053. <https://doi.org/10.1002/jnr.23391>
- Sajdyk, T. J., Johnson, P. L., Leitermann, R. J., Fitz, S. D., Dietrich, A., Morin, M., Gehlert, D. R., Urban, J. H., & Shekhar, A. (2008). Neuropeptide Y in the Amygdala Induces Long-Term Resilience to Stress-Induced Reductions in Social Responses But Not Hypothalamic–Adrenal–Pituitary Axis Activity or Hyperthermia. *The Journal of Neuroscience*, 28(4), 893–903.
<https://doi.org/10.1523/JNEUROSCI.0659-07.2008>
- Sajdyk, T. J., & Shekhar, A. (1997). Excitatory amino acid receptor antagonists block the cardiovascular and anxiety responses elicited by gamma-aminobutyric acidA receptor blockade in the basolateral amygdala of rats. *The Journal of Pharmacology and Experimental Therapeutics*, 283(2), 969–977.
- Sajdyk, T., Johnson, P., Fitz, S., & Shekhar, A. (2008). Chronic inhibition of GABA synthesis in the bed nucleus of the stria terminalis elicits anxiety-like behavior. *Journal of Psychopharmacology*, 22(6), 633–641. <https://doi.org/10.1177/0269881107082902>
- Saleeba, C., Dempsey, B., Le, S., Goodchild, A., & McMullan, S. (2019). A Student’s Guide to Neural Circuit Tracing. *Frontiers in Neuroscience*, 13, 897. <https://doi.org/10.3389/fnins.2019.00897>
- Sanders, J. I., & Kepecs, A. (2014). A low-cost programmable pulse generator for physiology and behavior. *Frontiers in Neuroengineering*, 7. <https://doi.org/10.3389/fneng.2014.00043>
- Sanders, S. K., & Shekhar, A. (1991). Blockade of GABAA receptors in the region of the anterior basolateral amygdala of rats elicits increases in heart rate and blood pressure. *Brain Research*, 567(1), 101–110. [https://doi.org/10.1016/0006-8993\(91\)91441-3](https://doi.org/10.1016/0006-8993(91)91441-3)
- Sangha, S., Chadick, J. Z., & Janak, P. H. (2013). Safety encoding in the basal amygdala. *The Journal of Neuroscience: The Official Journal of the Society for Neuroscience*, 33(9), 3744–3751.
<https://doi.org/10.1523/JNEUROSCI.3302-12.2013>
- Saraiva, L. R., Kondoh, K., Ye, X., Yoon, K., Hernandez, M., & Buck, L. B. (2016). Combinatorial effects of odorants on mouse behavior. *Proceedings of the National Academy of Sciences*, 113(23).
<https://doi.org/10.1073/pnas.1605973113>
- Savander, V., Go, C.-G., Ledoux, J. E., & Pitkänen, A. (1995). Intrinsic connections of the rat amygdaloid complex: Projections originating in the basal nucleus: INTRINSIC CONNECTIONS OF THE RAT AMYGDALA. *Journal of Comparative Neurology*, 361(2), 345–368.
<https://doi.org/10.1002/cne.903610211>

- Savander, V., Miettinen, R., LeDoux, J. E., & Pitkänen, A. (1997). Lateral nucleus of the rat amygdala is reciprocally connected with basal and accessory basal nuclei: A light and electron microscopic study. *Neuroscience*, 77(3), 767–781. [https://doi.org/10.1016/S0306-4522\(96\)00513-1](https://doi.org/10.1016/S0306-4522(96)00513-1)
- Schafe, G. E., & Bernstein, I. L. (1996). Forebrain contribution to the induction of a brainstem correlate of conditioned taste aversion: I. The amygdala. *Brain Research*, 741(1–2), 109–116. [https://doi.org/10.1016/S0006-8993\(96\)00906-7](https://doi.org/10.1016/S0006-8993(96)00906-7)
- Schafe, G. E., & Bernstein, I. L. (1998). Forebrain contribution to the induction of a brainstem correlate of conditioned taste aversion. *Brain Research*, 800(1), 40–47. [https://doi.org/10.1016/S0006-8993\(98\)00492-2](https://doi.org/10.1016/S0006-8993(98)00492-2)
- Schneiderman, N., Ironson, G., & Siegel, S. D. (2005). Stress and Health: Psychological, Behavioral, and Biological Determinants. *Annual Review of Clinical Psychology*, 1(1), 607–628. <https://doi.org/10.1146/annurev.clinpsy.1.102803.144141>
- Schwabe, L., Hermans, E. J., Joëls, M., & Roozendaal, B. (2022). Mechanisms of memory under stress. *Neuron*, 110(9), 1450–1467. <https://doi.org/10.1016/j.neuron.2022.02.020>
- Seabrook, L. T., & Borgland, S. L. (2020). The orbitofrontal cortex, food intake and obesity. *Journal of Psychiatry and Neuroscience*, 45(5), 304–312. <https://doi.org/10.1503/jpn.190163>
- Seggie, J. (1987). Differential responsivity of corticosterone and prolactin to stress following lesions of the septum or amygdala: Implications for psychoneuroendocrinology. *Progress in Neuro-Psychopharmacology and Biological Psychiatry*, 11(2–3), 315–324. [https://doi.org/10.1016/0278-5846\(87\)90076-5](https://doi.org/10.1016/0278-5846(87)90076-5)
- Senn, V., Wolff, S. B. E., Herry, C., Grenier, F., Ehrlich, I., Gründemann, J., Fadok, J. P., Müller, C., Letzkus, J. J., & Lüthi, A. (2014). Long-Range Connectivity Defines Behavioral Specificity of Amygdala Neurons. *Neuron*, 81(2), 428–437. <https://doi.org/10.1016/j.neuron.2013.11.006>
- Servonnet, A., Hernandez, G., El Hage, C., Rompré, P.-P., & Samaha, A.-N. (2020). Optogenetic Activation of the Basolateral Amygdala Promotes Both Appetitive Conditioning and the Instrumental Pursuit of Reward Cues. *The Journal of Neuroscience: The Official Journal of the Society for Neuroscience*, 40(8), 1732–1743. <https://doi.org/10.1523/JNEUROSCI.2196-19.2020>
- Shabel, S. J., & Janak, P. H. (2009). Substantial similarity in amygdala neuronal activity during conditioned appetitive and aversive emotional arousal. *Proceedings of the National Academy of Sciences*, 106(35), 15031–15036. <https://doi.org/10.1073/pnas.0905580106>
- Shen, C.-J., Zheng, D., Li, K.-X., Yang, J.-M., Pan, H.-Q., Yu, X.-D., Fu, J.-Y., Zhu, Y., Sun, Q.-X., Tang, M.-Y., Zhang, Y., Sun, P., Xie, Y., Duan, S., Hu, H., & Li, X.-M. (2019). Cannabinoid CB1 receptors in the amygdalar cholecystinin glutamatergic afferents to nucleus accumbens modulate depressive-like behavior. *Nature Medicine*, 25(2), 337–349. <https://doi.org/10.1038/s41591-018-0299-9>

- Sheng, M., McFadden, G., & Greenberg, M. E. (1990). Membrane depolarization and calcium induce c-fos transcription via phosphorylation of transcription factor CREB. *Neuron*, 4(4), 571–582. [https://doi.org/10.1016/0896-6273\(90\)90115-V](https://doi.org/10.1016/0896-6273(90)90115-V)
- Shi, C. -j., & Cassell, M. D. (1999). Perirhinal cortex projections to the amygdaloid complex and hippocampal formation in the rat. *The Journal of Comparative Neurology*, 406(3), 299–328. [https://doi.org/10.1002/\(SICI\)1096-9861\(19990412\)406:3<299::AID-CNE2>3.0.CO;2-9](https://doi.org/10.1002/(SICI)1096-9861(19990412)406:3<299::AID-CNE2>3.0.CO;2-9)
- Shinonaga, Y., Takada, M., & Mizuno, N. (1994). Topographic organization of collateral projections from the basolateral amygdaloid nucleus to both the prefrontal cortex and nucleus accumbens in the rat. *Neuroscience*, 58(2), 389–397. [https://doi.org/10.1016/0306-4522\(94\)90045-0](https://doi.org/10.1016/0306-4522(94)90045-0)
- Singh, S., Wilson, T. D., Valdivia, S., Benowitz, B., Chaudhry, S., Ma, J., Adke, A. P., Soler-Cedeño, O., Velasquez, D., Penzo, M. A., & Carrasquillo, Y. (2022). An inhibitory circuit from central amygdala to zona incerta drives pain-related behaviors in mice. *ELife*, 11, e68760. <https://doi.org/10.7554/eLife.68760>
- Slotnick, B. (2004). Olfaction in Olfactory Bulbectomized Rats. *Journal of Neuroscience*, 24(41), 9195–9200. <https://doi.org/10.1523/JNEUROSCI.1936-04.2004>
- Slusher, M. A., & Hyde, J. E. (1961). EFFECT OF LIMBIC STIMULATION ON RELEASE OF CORTICOSTEROIDS INTO THE ADRENAL VENOUS EFFLUENT OF THE CAT 1. *Endocrinology*, 69(6), 1080–1084. <https://doi.org/10.1210/endo-69-6-1080>
- Smith, G. W., Aubry, J.-M., Dellu, F., Contarino, A., Bilezikjian, L. M., Gold, L. H., Chen, R., Marchuk, Y., Hauser, C., Bentley, C. A., Sawchenko, P. E., Koob, G. F., Vale, W., & Lee, K.-F. (1998). Corticotropin Releasing Factor Receptor 1–Deficient Mice Display Decreased Anxiety, Impaired Stress Response, and Aberrant Neuroendocrine Development. *Neuron*, 20(6), 1093–1102. [https://doi.org/10.1016/S0896-6273\(00\)80491-2](https://doi.org/10.1016/S0896-6273(00)80491-2)
- Smith, Y., & Paré, D. (1994). Intra-amygdaloid projections of the lateral nucleus in the cat: PHA-L anterograde labeling combined with postembedding GABA and glutamate immunocytochemistry. *Journal of Comparative Neurology*, 342(2), 232–248. <https://doi.org/10.1002/cne.903420207>
- Soltis, R. P., Cook, J. C., Gregg, A. E., & Sanders, B. J. (1997). Interaction of GABA and Excitatory Amino Acids in the Basolateral Amygdala: Role in Cardiovascular Regulation. *The Journal of Neuroscience*, 17(23), 9367–9374. <https://doi.org/10.1523/JNEUROSCI.17-23-09367.1997>
- Sorg, B. A., & Kalivas, P. W. (1991). Effects of cocaine and footshock stress on extracellular dopamine levels in the ventral striatum. *Brain Research*, 559(1), 29–36. [https://doi.org/10.1016/0006-8993\(91\)90283-2](https://doi.org/10.1016/0006-8993(91)90283-2)
- Spencer, S. J., Buller, K. M., & Day, T. A. (2005). Medial prefrontal cortex control of the paraventricular hypothalamic nucleus response to psychological stress: Possible role of the bed nucleus of the stria terminalis. *The Journal of Comparative Neurology*, 481(4), 363–376. <https://doi.org/10.1002/cne.20376>

- Stefanova, N. (1998). γ -Aminobutyric acid-immunoreactive neurons in the amygdala of the rat – sex differences and effect of early postnatal castration. *Neuroscience Letters*, 255(3), 175–177. [https://doi.org/10.1016/S0304-3940\(98\)00735-6](https://doi.org/10.1016/S0304-3940(98)00735-6)
- Steiner, M., & Wotjak, C. (2008). Role of the endocannabinoid system in regulation of the hypothalamic-pituitary-adrenocortical axis. In *Progress in Brain Research* (Vol. 170, pp. 397–432). Elsevier. [https://doi.org/10.1016/S0079-6123\(08\)00433-0](https://doi.org/10.1016/S0079-6123(08)00433-0)
- Stuber, G. D., Sparta, D. R., Stamatakis, A. M., van Leeuwen, W. A., Hardjoprajitno, J. E., Cho, S., Tye, K. M., Kempadoo, K. A., Zhang, F., Deisseroth, K., & Bonci, A. (2011). Excitatory transmission from the amygdala to nucleus accumbens facilitates reward seeking. *Nature*, 475(7356), 377–380. <https://doi.org/10.1038/nature10194>
- Sugita, T., Kanamaru, M., Iizuka, M., Sato, K., Tsukada, S., Kawamura, M., Homma, I., & Izumizaki, M. (2015). Breathing is affected by dopamine D2-like receptors in the basolateral amygdala. *Respiratory Physiology & Neurobiology*, 209, 23–27. <https://doi.org/10.1016/j.resp.2014.09.020>
- Sullivan, G. M., Apergis, J., Bush, D. E. A., Johnson, L. R., Hou, M., & Ledoux, J. E. (2004). Lesions in the bed nucleus of the stria terminalis disrupt corticosterone and freezing responses elicited by a contextual but not by a specific cue-conditioned fear stimulus. *Neuroscience*, 128(1), 7–14. <https://doi.org/10.1016/j.neuroscience.2004.06.015>
- Sun, F., Zhou, J., Dai, B., Qian, T., Zeng, J., Li, X., Zhuo, Y., Zhang, Y., Wang, Y., Qian, C., Tan, K., Feng, J., Dong, H., Lin, D., Cui, G., & Li, Y. (2020). Next-generation GRAB sensors for monitoring dopaminergic activity in vivo. *Nature Methods*, 17(11), 1156–1166. <https://doi.org/10.1038/s41592-020-00981-9>
- Swanson, L. W. (2004). *Brain maps III: Structure of the rat brain: an atlas with printed and electronic templates for data, models, and schematics* (3rd rev. ed). Elsevier, Academic Press.
- Tank, W. A., & Wong, D. L. (2014). Peripheral and Central Effects of Circulating Catecholamines. In R. Terjung (Ed.), *Comprehensive Physiology* (1st ed., pp. 1–15). Wiley. <https://doi.org/10.1002/cphy.c140007>
- Tavares, R. F., Corrêa, F. M. A., & Resstel, L. B. M. (2009). Opposite role of infralimbic and prelimbic cortex in the tachycardiac response evoked by acute restraint stress in rats. *Journal of Neuroscience Research*, 87(11), 2601–2607. <https://doi.org/10.1002/jnr.22070>
- Taylor, S. R., Badurek, S., Dileone, R. J., Nashmi, R., Minichiello, L., & Picciotto, M. R. (2014). GABAergic and glutamatergic efferents of the mouse ventral tegmental area. *The Journal of Comparative Neurology*, 522(14), 3308–3334. <https://doi.org/10.1002/cne.23603>
- Tovote, P., Fadok, J. P., & Lüthi, A. (2015). Neuronal circuits for fear and anxiety. *Nature Reviews. Neuroscience*, 16(6), 317–331. <https://doi.org/10.1038/nrn3945>
- Tye, K. M. (2018). Neural Circuit Motifs in Valence Processing. *Neuron*, 100(2), 436–452. <https://doi.org/10.1016/j.neuron.2018.10.001>

- Tye, K. M., Prakash, R., Kim, S.-Y., Fenno, L. E., Grosenick, L., Zarabi, H., Thompson, K. R., Gradinaru, V., Ramakrishnan, C., & Deisseroth, K. (2011). Amygdala circuitry mediating reversible and bidirectional control of anxiety. *Nature*, 471(7338), 358–362. <https://doi.org/10.1038/nature09820>
- Úbeda-Contreras, J., Marín-Blasco, I., Nadal, R., & Armario, A. (2018). Brain c-fos expression patterns induced by emotional stressors differing in nature and intensity. *Brain Structure and Function*, 223(5), 2213–2227. <https://doi.org/10.1007/s00429-018-1624-2>
- Uemura, M., Furuse, T., Yamada, I., Kushida, T., Abe, T., Imai, K., Nagao, S., Kudoh, M., Yoshizawa, K., Tamura, M., Kiyonari, H., Wakana, S., & Hirano, S. (2022). Deficiency of protocadherin 9 leads to reduction in positive emotional behaviour. *Scientific Reports*, 12(1), 11933. <https://doi.org/10.1038/s41598-022-16106-5>
- Ugolini, A., Sokal, D. M., Arban, R., & Large, C. H. (2008). CRF1 receptor activation increases the response of neurons in the basolateral nucleus of the amygdala to afferent stimulation. *Frontiers in Behavioral Neuroscience*, 2, 2. <https://doi.org/10.3389/neuro.08.002.2008>
- Ulrich-Lai, Y. M., & Herman, J. P. (2009). Neural regulation of endocrine and autonomic stress responses. *Nature Reviews Neuroscience*, 10(6), 397–409. <https://doi.org/10.1038/nrn2647>
- Unal, C. T., Pare, D., & Zaborszky, L. (2015). Impact of Basal Forebrain Cholinergic Inputs on Basolateral Amygdala Neurons. *The Journal of Neuroscience*, 35(2), 853–863. <https://doi.org/10.1523/JNEUROSCI.2706-14.2015>
- Vallano, M. L., Beaman-Hall, C. M., Mathur, A., & Chen, Q. (2000). Astrocytes express specific variants of CaM KII ? And ?, but not ? and ?, that determine their cellular localizations. *Glia*, 30(2), 154–164. [https://doi.org/10.1002/\(SICI\)1098-1136\(200004\)30:2<154::AID-GLIA5>3.0.CO;2-S](https://doi.org/10.1002/(SICI)1098-1136(200004)30:2<154::AID-GLIA5>3.0.CO;2-S)
- van Marle, H. J. F., Hermans, E. J., Qin, S., & Fernández, G. (2009). From Specificity to Sensitivity: How Acute Stress Affects Amygdala Processing of Biologically Salient Stimuli. *Biological Psychiatry*, 66(7), 649–655. <https://doi.org/10.1016/j.biopsych.2009.05.014>
- Van Pett, K., Viau, V., Bittencourt, J. C., Chan, R. K. W., Li, H.-Y., Arias, C., Prins, G. S., Perrin, M., Vale, W., & Sawchenko, P. E. (2000). Distribution of mRNAs encoding CRF receptors in brain and pituitary of rat and mouse. *The Journal of Comparative Neurology*, 428(2), 191–212. [https://doi.org/10.1002/1096-9861\(20001211\)428:2<191::AID-CNE1>3.0.CO;2-U](https://doi.org/10.1002/1096-9861(20001211)428:2<191::AID-CNE1>3.0.CO;2-U)
- Vantrease, J. E., Avonts, B., Padival, M., DeJoseph, M. R., Urban, J. H., & Rosenkranz, J. A. (2022). Sex Differences in the Activity of Basolateral Amygdalar Neurons That Project to the Bed Nucleus of the Stria Terminalis and Their Role in Anticipatory Anxiety. *The Journal of Neuroscience*, 42(22), 4488–4504. <https://doi.org/10.1523/JNEUROSCI.1499-21.2022>
- Vecchiarelli, H. A., Morena, M., Lee, T. T. Y., Nastase, A. S., Aukema, R. J., Leidl, K. D., Gray, J. M., Petrie, G. N., Tellez-Monnery, K. J., & Hill, M. N. (2022). Sex and stressor modality influence acute stress-induced dynamic changes in corticolimbic endocannabinoid levels in adult Sprague Dawley rats. *Neurobiology of Stress*, 20, 100470. <https://doi.org/10.1016/j.ynstr.2022.100470>

- Vining, C., Iyer, V., & Bhatnagar, S. (2007). Intracerebroventricular Administration of Corticotrophin-Releasing Hormone Receptor Antagonists Produces Different Effects on Hypothalamic Pituitary Adrenal Responses to Novel Restraint Depending on the Stress History of the Animal. *Journal of Neuroendocrinology*, 19(3), 198–207. <https://doi.org/10.1111/j.1365-2826.2006.01522.x>
- Vouimba, R.-M., & Richter-Levin, G. (2013). Different patterns of amygdala priming differentially affect dentate gyrus plasticity and corticosterone, but not CA1 plasticity. *Frontiers in Neural Circuits*, 7. <https://doi.org/10.3389/fncir.2013.00080>
- Wadenberg, M.-L., Ericson, E., Magnusson, O., & Ahlenius, S. (1990). Suppression of conditioned avoidance behavior by the local application of (–)sulpiride into the ventral, but not the dorsal, striatum of the rat. *Biological Psychiatry*, 28(4), 297–307. [https://doi.org/10.1016/0006-3223\(90\)90657-N](https://doi.org/10.1016/0006-3223(90)90657-N)
- Walker, D. L., & Davis, M. (1997). Double Dissociation between the Involvement of the Bed Nucleus of the Stria Terminalis and the Central Nucleus of the Amygdala in Startle Increases Produced by Conditioned versus Unconditioned Fear. *The Journal of Neuroscience*, 17(23), 9375–9383. <https://doi.org/10.1523/JNEUROSCI.17-23-09375.1997>
- Wang, G.-W., Liu, J., & Wang, X.-Q. (2017). Post-training reversible disconnection of the ventral hippocampal–basolateral amygdaloid circuits impairs consolidation of inhibitory avoidance memory in rats. *Learning & Memory*, 24(11), 602–606. <https://doi.org/10.1101/lm.044701.116>
- Wassum, K. M., & Izquierdo, A. (2015). The basolateral amygdala in reward learning and addiction. *Neuroscience & Biobehavioral Reviews*, 57, 271–283. <https://doi.org/10.1016/j.neubiorev.2015.08.017>
- Wassum, K. M., Ostlund, S. B., Maidment, N. T., & Balleine, B. W. (2009). Distinct opioid circuits determine the palatability and the desirability of rewarding events. *Proceedings of the National Academy of Sciences*, 106(30), 12512–12517. <https://doi.org/10.1073/pnas.0905874106>
- Weera, M. M., Agoglia, A. E., Douglass, E., Jiang, Z., Rajamanickam, S., Shackett, R. S., Herman, M. A., Justice, N. J., & Gilpin, N. W. (2022). Generation of a CRF1-Cre transgenic rat and the role of central amygdala CRF1 cells in nociception and anxiety-like behavior. *eLife*, 11, e67822. <https://doi.org/10.7554/eLife.67822>
- Wei, J., Zhong, P., Qin, L., Tan, T., & Yan, Z. (2018). Chemicogenetic Restoration of the Prefrontal Cortex to Amygdala Pathway Ameliorates Stress-Induced Deficits. *Cerebral Cortex*, 28(6), 1980–1990. <https://doi.org/10.1093/cercor/bhx104>
- Weinberg, M. S., Johnson, D. C., Bhatt, A. P., & Spencer, R. L. (2010). Medial prefrontal cortex activity can disrupt the expression of stress response habituation. *Neuroscience*, 168(3), 744–756. <https://doi.org/10.1016/j.neuroscience.2010.04.006>

- Weiskrantz, L. (1956). Behavioral changes associated with ablation of the amygdaloid complex in monkeys. *Journal of Comparative and Physiological Psychology*, 49(4), 381–391.
<https://doi.org/10.1037/h0088009>
- Wellman, C. L., Bollinger, J. L., & Moench, K. M. (2020). Effects of stress on the structure and function of the medial prefrontal cortex: Insights from animal models. In *International Review of Neurobiology* (Vol. 150, pp. 129–153). Elsevier. <https://doi.org/10.1016/bs.irn.2019.11.007>
- Wellman, L. L., Forcelli, P. A., Aguilar, B. L., & Malkova, L. (2016). Bidirectional Control of Social Behavior by Activity within Basolateral and Central Amygdala of Primates. *The Journal of Neuroscience: The Official Journal of the Society for Neuroscience*, 36(33), 8746–8756.
<https://doi.org/10.1523/JNEUROSCI.0333-16.2016>
- Wen, Z., Raio, C. M., Pace-Schott, E. F., Lazar, S. W., LeDoux, J. E., Phelps, E. A., & Milad, M. R. (2022). Temporally and anatomically specific contributions of the human amygdala to threat and safety learning. *Proceedings of the National Academy of Sciences*, 119(26), e2204066119.
<https://doi.org/10.1073/pnas.2204066119>
- Wendler, E., Gaspar, J. C. C., Ferreira, T. L., Barbiero, J. K., Andreatini, R., Vital, M. A. B. F., Blaha, C. D., Winn, P., & Da Cunha, C. (2014). The roles of the nucleus accumbens core, dorsomedial striatum, and dorsolateral striatum in learning: Performance and extinction of Pavlovian fear-conditioned responses and instrumental avoidance responses. *Neurobiology of Learning and Memory*, 109, 27–36. <https://doi.org/10.1016/j.nlm.2013.11.009>
- Whitaker, A. M., & Gilpin, N. W. (2015). Blunted hypothalamo-pituitary adrenal axis response to predator odor predicts high stress reactivity. *Physiology & Behavior*, 147, 16–22.
<https://doi.org/10.1016/j.physbeh.2015.03.033>
- Wilson, M. A., & Fadel, J. R. (2017). Cholinergic regulation of fear learning and extinction: Cholinergic Regulation of Fear Learning and Extinction. *Journal of Neuroscience Research*, 95(3), 836–852.
<https://doi.org/10.1002/jnr.23840>
- Winstanley, C. A., Theobald, D. E. H., Cardinal, R. N., & Robbins, T. W. (2004). Contrasting roles of basolateral amygdala and orbitofrontal cortex in impulsive choice. *The Journal of Neuroscience: The Official Journal of the Society for Neuroscience*, 24(20), 4718–4722.
<https://doi.org/10.1523/JNEUROSCI.5606-03.2004>
- Wolff, S. B. E., Gründemann, J., Tovote, P., Krabbe, S., Jacobson, G. A., Müller, C., Herry, C., Ehrlich, I., Friedrich, R. W., Letzkus, J. J., & Lüthi, A. (2014). Amygdala interneuron subtypes control fear learning through disinhibition. *Nature*, 509(7501), 453–458. <https://doi.org/10.1038/nature13258>
- Woodruff, A. R., & Sah, P. (2007). Inhibition and Synchronization of Basal Amygdala Principal Neuron Spiking by Parvalbumin-Positive Interneurons. *Journal of Neurophysiology*, 98(5), 2956–2961.
<https://doi.org/10.1152/jn.00739.2007>

- Worley, P. F., Bhat, R. V., Baraban, J. M., Erickson, C. A., McNaughton, B. L., & Barnes, C. A. (1993). Thresholds for synaptic activation of transcription factors in hippocampus: Correlation with long-term enhancement. *The Journal of Neuroscience: The Official Journal of the Society for Neuroscience*, 13(11), 4776–4786. <https://doi.org/10.1523/JNEUROSCI.13-11-04776.1993>
- Xiao, Q., Xu, X., & Tu, J. (2020). Chronic optogenetic manipulation of basolateral amygdala astrocytes rescues stress-induced anxiety. *Biochemical and Biophysical Research Communications*, 533(4), 657–664. <https://doi.org/10.1016/j.bbrc.2020.09.106>
- Yaeger, J. D. W., Krupp, K. T., Jacobs, B. M., Onserio, B. O., Meyerink, B. L., Cain, J. T., Ronan, P. J., Renner, K. J., DiLeone, R. J., & Summers, C. H. (2022). Orexin 1 Receptor Antagonism in the Basolateral Amygdala Shifts the Balance From Pro- to Antistress Signaling and Behavior. *Biological Psychiatry*, 91(9), 841–852. <https://doi.org/10.1016/j.biopsych.2021.12.019>
- Yang, D., Wang, Y., Qi, T., Zhang, X., Shen, L., Ma, J., Pang, Z., Lal, N. K., McClatchy, D. B., Wang, K., Xie, Y., Polli, F., Maximov, A., Augustine, V., Cline, H. T., Yates, J. R., & Ye, L. (2023). *Phosphorylation of pyruvate dehydrogenase marks the inhibition of in vivo neuronal activity* [Preprint]. Neuroscience. <https://doi.org/10.1101/2023.03.13.532494>
- Yin, F., Guo, H., Cui, J., Shi, Y., Su, R., Xie, Q., Chang, J., Wang, Y., & Lai, J. (2019). The basolateral amygdala regulation of complex cognitive behaviours in the five-choice serial reaction time task. *Psychopharmacology*, 236(11), 3135–3146. <https://doi.org/10.1007/s00213-019-05260-w>
- Yizhar, O., Fenno, L. E., Davidson, T. J., Mogri, M., & Deisseroth, K. (2011). Optogenetics in Neural Systems. *Neuron*, 71(1), 9–34. <https://doi.org/10.1016/j.neuron.2011.06.004>
- Yona, G., Meitav, N., Kahn, I., & Shoham, S. (2016). Realistic Numerical and Analytical Modeling of Light Scattering in Brain Tissue for Optogenetic Applications(1,2,3). *ENeuro*, 3(1), ENEURO.0059-15.2015. <https://doi.org/10.1523/ENeuro.0059-15.2015>
- Yu, G., & Sharp, B. M. (2015). Basolateral amygdala and ventral hippocampus in stress-induced amplification of nicotine self-administration during reacquisition in rat. *Psychopharmacology*, 232(15), 2741–2749. <https://doi.org/10.1007/s00213-015-3911-4>
- Yu, X., Liu, L., Chen, W., Cao, Q., Zepf, F. D., Ji, G., Wu, Z., An, L., Wang, P., Qian, Q., Zang, Y., Sun, L., & Wang, Y. (2020). Integrity of Amygdala Subregion-Based Functional Networks and Emotional Lability in Drug-Naïve Boys With ADHD. *Journal of Attention Disorders*, 24(12), 1661–1673. <https://doi.org/10.1177/1087054716661419>
- Zhang, J.-Y., Liu, T.-H., He, Y., Pan, H.-Q., Zhang, W.-H., Yin, X.-P., Tian, X.-L., Li, B.-M., Wang, X.-D., Holmes, A., Yuan, T.-F., & Pan, B.-X. (2019a). Chronic Stress Remodels Synapses in an Amygdala Circuit-Specific Manner. *Biological Psychiatry*, 85(3), 189–201. <https://doi.org/10.1016/j.biopsych.2018.06.019>
- Zhang, J.-Y., Liu, T.-H., He, Y., Pan, H.-Q., Zhang, W.-H., Yin, X.-P., Tian, X.-L., Li, B.-M., Wang, X.-D., Holmes, A., Yuan, T.-F., & Pan, B.-X. (2019b). Chronic Stress Remodels Synapses in an

- Amygdala Circuit–Specific Manner. *Biological Psychiatry*, 85(3), 189–201.
<https://doi.org/10.1016/j.biopsych.2018.06.019>
- Zhang, Q., Gao, S.-H., Shen, Z.-S., Wang, Y., Hu, S.-W., Duan, G.-B., Liu, Y., Zhong, D.-Y., Liu, J., Sun, M.-H., Zhang, X., Cao, T.-Y., Cao, J.-L., Tang, Q.-Y., & Zhang, Z. (2022). The Slack Channel Regulates Anxiety-Like Behaviors via Basolateral Amygdala Glutamatergic Projections to Ventral Hippocampus. *The Journal of Neuroscience*, 42(14), 3049–3064.
<https://doi.org/10.1523/JNEUROSCI.2027-21.2022>
- Zhang, W.-H., Liu, W.-Z., He, Y., You, W.-J., Zhang, J.-Y., Xu, H., Tian, X.-L., Li, B.-M., Mei, L., Holmes, A., & Pan, B.-X. (2019). Chronic Stress Causes Projection-Specific Adaptation of Amygdala Neurons via Small-Conductance Calcium-Activated Potassium Channel Downregulation. *Biological Psychiatry*, 85(10), 812–828. <https://doi.org/10.1016/j.biopsych.2018.12.010>
- Zhang, X., Kim, J., & Tonegawa, S. (2020). Amygdala Reward Neurons Form and Store Fear Extinction Memory. *Neuron*, 105(6), 1077–1093.e7. <https://doi.org/10.1016/j.neuron.2019.12.025>
- Zhang, X., & Li, B. (2018). Population coding of valence in the basolateral amygdala. *Nature Communications*, 9(1), 5195. <https://doi.org/10.1038/s41467-018-07679-9>
- Zhu, W., Umegaki, H., Suzuki, Y., Miura, H., & Iguchi, A. (2001). Involvement of the bed nucleus of the stria terminalis in hippocampal cholinergic system-mediated activation of the hypothalamo–pituitary–adrenocortical axis in rats. *Brain Research*, 916(1–2), 101–106.
[https://doi.org/10.1016/S0006-8993\(01\)02871-2](https://doi.org/10.1016/S0006-8993(01)02871-2)